DOCTORAL DISSERTATION

Application of Evolutionary Algorithms and the Boundary Element Method in the optimization of noise barrier profiles

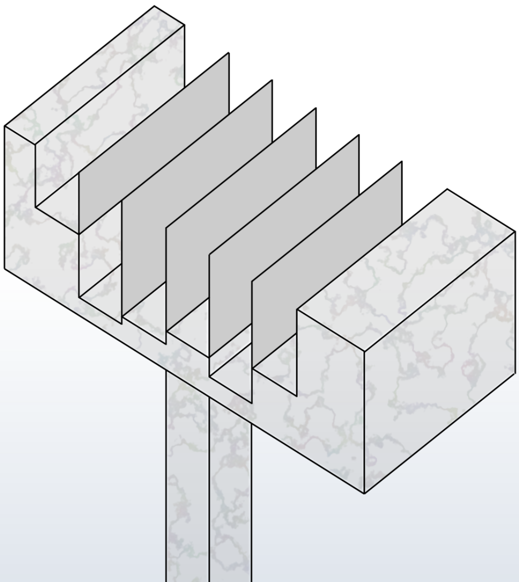

Rayco Toledo Quintana

Continuum Mechanics and Structures Division

Las Palmas de Gran Canaria • November 2015

INSTITUTO UNIVERSITARIO SIANI INGENIERIA COMPUTACIONAL

UNIVERSIDAD DE LAS PALMAS DE GRAN CANARIA

UNIVERSIDAD DE LAS PALMAS DE GRAN CANARIA
Instituto Universitario de Sistemas Inteligentes
y Aplicaciones Numéricas en Ingeniería

EDUARDO RODRÍGUEZ BARRERA, SECRETARIO DEL INSTITUTO UNIVERSITARIO DE SISTEMAS INTELIGENTES Y APLICACIONES NUMÉRICAS EN INGENIERÍA (SIANI) DE LA UNIVERSIDAD DE LAS PALMAS DE GRAN CANARIA,

CERTIFICA

Que el Consejo de Doctores del Instituto Universitario de Sistemas Inteligentes y Aplicaciones Numéricas en Ingeniería (SIANI), en su sesión de fecha 11 de noviembre de 2015, tomó el acuerdo de dar el consentimiento para la tramitación de la Tesis Doctoral titulada 'Aplicación de los Algoritmos Evolutivos y el Método de los Elementos de Contorno en la Optimización de Perfiles de Pantallas Acústicas (Application of Evolutionary Algorithms and the Boundary Element Method in the Optimization of Noise Barrier Profiles)", presentada por el doctorando **D. Rayco Toledo Quintana**, dirigida por el Dr. D. Orlando Francisco Maeso Fortuny, el Dr. D. Juan José Aznárez González y el Dr. D. David Juan Greiner Sánchez, a la vista de la idoneidad y calidad de su contenido, interés y relevancia del tema.

Para que así conste, y a los efectos oportunos se expide el correspondiente certificado a 11 de noviembre de 2015.

Application of Evolutionary Algorithms and the Boundary Element Method in the Optimization of Noise Barrier Profiles

Rayco Toledo Quintana

Programa de doctorado:
Sistemas Inteligentes y Aplicaciones Numéricas en Ingeniería
Instituto Universitario SIANI

Director:	Director:	Director:
Orlando Maeso Fortuny	Juan J. Aznárez González	David Greiner Sánchez

Las Palmas de Gran Canaria, noviembre 2015

“It would be possible to describe everything scientifically, but it would make no sense; it would be without meaning, as if you described a Beethoven symphony as a variation of wave pressure”

Albert Einstein

To my nearest and
dearest one. To Cristina.

Acknowledgments

It is fair that my fullest gratitude is expressed for those people who, despite not having had a direct involvement on this work, deserve each and every kind gesture from my part. My big notes to appreciation are for my parents, my sister, my niece, my nephew and those who were and sadly no longer are. But mainly and above all to Cristina, who has taught me, unintentionally, that purest lights never go out.

Following, I would like to acknowledge the supervisors and *intellectual fathers* of this thesis, Prof. Orlando Maeso, Prof. Juan J. Aznárez and Prof. David Greiner, whom without their knowledge and expertise this work would never have happened.

I owe a lot to my colleagues of the Continuum Mechanics and Structures Division of the Institute of Intelligent Systems and Numerical Applications in Engineering. Special thanks to Cristina for being *through the thick and thin*, and to Fernando, Ariel, Chema, Jacob, Guillermo and Lorenzo for being always willing to lend a helping hand. It has been such a pleasure to work with you guys. I would also like to express my appreciation to Prof. Fidel García and Prof. Luis Padrón for being generous with their time and gestures.

I am deeply grateful to Juan Ignacio González for being far more than the technical engineering of the institute. It became very enjoyable and fulfilling to share insights, ideas and talk time with such a nice person. You are definitely a *dark horse*. Most of the layout of this document bears his stamp.

Last but not least, I would also like to extend a word of thanks to those whose memory still lingers in my mind, especially as soon as I set foot at the facilities of the University of Las Palmas de Gran Canaria.

This work was supported by the Ministerio de Economía y Competitividad (MINECO) of Spain and FEDER through research project BIA2010-21399-C02-01. The author is a recipient of a fellowship from the Subprogram of Predoctoral Fellowships of Research Personnel in Training (FPI-MINECO) and wishes to acknowledge this financial support.

Las Palmas de Gran Canaria, November 2015

Rayco Toledo Quintana

Application of Evolutionary Algorithms and the Boundary Element Method in the Optimization of Noise Barrier Profiles

---

Abstract. My original contribution to knowledge is to develop a general, robust methodology that may cover any type of 2D acoustic optimization problem. A procedure involving the coupling of Boundary Elements (BE) and Evolutionary Algorithms is proposed for systematic geometric modifications of road barriers that lead to designs with ever-increasing screening performance. With the exclusive implementation of the classical BE formulation, the assessment of certain configurations are, in most cases, unaffordable in terms of both the evaluation of the topological feasibility of designs of diverse geometric nature and the faithful representation of the shielding efficiency of barriers that often reveal fictitious natural frequencies. In this respect, the Dual BE approach proposed in this work is the most appropriate strategy involving BE that allows the methodology 1) to assume a simplification of reality by idealizing very thin elements (widely present in diverse barrier designs) as null-thickness type and 2) to mitigate the fictitious eigenfrequencies associated with the inner domain of barriers with real dimensions. The solution to these challenges, especially the null-thickness idealization, enables an easier, more general procedure in obtaining barrier designs that normally cover a large range of possible geometries along the optimum search process. Numerical simulations involving single- and multi-objective optimizations of noise barriers of varied nature have been included in this document, considering the influence of both surface treatments and barrier locations on the screening behavior. Results disclosed justify the implementation of this methodology by leading to optimal solutions of previously defined topologies that, in general, greatly outperform the acoustic efficiency of classical, widely used barrier designs normally erected near roads.

Keywords: Noise barriers; Very thin bodies; Shape optimization; Evolutionary Algorithms; Dual Boundary Element Formulation

PACS numbers: 43.28.Js, 43.50.Gf, 47.11.Hj

Aplicación de Algoritmos Evolutivos y el Método de los Elementos de Contorno en la Optimización de Perfiles de Pantallas Acústicas

Resumen. La contribución original de este trabajo se encuentra en el desarrollo de un procedimiento general, robusto y versátil que permite el estudio de cualquier problema de optimización acústica en 2D. Mediante el uso acoplado de Elementos de Contorno (EC) y Algoritmos Evolutivos se realiza una búsqueda guiada de geometrías basadas en modelos topológicos de pantallas anti-ruido que conduce a diseños cada vez más eficientes. El análisis de ciertas configuraciones desde la formulación clásica de los EC supone, a menudo, un problema inabordable en términos tanto de la determinación de la validez topológica de los diseños como de la correcta evaluación de la eficacia acústica de pantallas que menudo manifiestan falsas frecuencias de resonancia. En este sentido, la formulación Dual de EC propuesta es la estrategia más apropiada desde los EC, al permitir 1) adoptar simplificaciones geométricas sobre el diseño real de la pantalla mediante la idealización de elementos muy delgados (muy presentes en muchos diseños) como cuerpos sin espesor y 2) evitar las frecuencias espurias asociadas al dominio interior de la barrera. La solución a estos planteamientos, sobre todo la idealización de elementos muy delgados, permite un procedimiento más general y sencillo en la mejora sistemática de modelos que, a menudo, gozan de completa libertad geométrica de acuerdo a su patrón topológico. Se presentan simulaciones numéricas sobre la base de optimizaciones mono- y multi-objetivo de pantallas de distinta naturaleza, considerando la influencia de tratamientos superficiales y la localización de la pantalla en su eficacia. Los resultados mostrados justifican la necesidad de implementar metodologías como la que aquí se presenta para mejorar la calidad de apantallamiento de diseños clásicos de pantallas que normalmente se erigen en el entorno de carreteras.

Palabras clave: Pantallas acústicas; Elementos con y sin espesor; Optimización de la eficacia acústica; Algoritmos Evolutivos, Formulación Dual de los Elementos de Contorno

Referencias PACS: 43.28.Js, 43.50.Gf, 47.11.Hj

Contents

List of Figures

List of Tables

1. INTRODUCTION AND BACKGROUND

Among the byproducts derived from the industrial and technological development the environmental degradation arises, undoubtedly, as one of the most damaging. Unfortunately, this deterioration has increased considerably over the recent years with the rapid growth of cities and the associated activities of urban areas. The disruptive effects of these activities may have serious consequences on people health by affecting them both physically and psychologically [1, 2], which has ultimately contributed to raise awareness on citizens engagement.

Although increasingly omnipresent form of pollution, noise is yet underestimated in some cases. For the sake of greater precision, according to the Organization for Economic Cooperation and Development (OECD), noise pollution is defined as *sound at excessive levels that may be detrimental to human health*. In other words, it is either excessive amount of noise or an unpleasant sound that causes temporary disruption in the natural balance. This definition is usually applicable to sounds or noises that are unnatural in either their volume or their production.

Roadway traffic is, by far, the most common source of noise pollution in cities and urban areas by representing 80% of the overall noise pollution. An estimated 80 million people suffer unacceptable levels of continuous outdoor transport noise within the European Union (EU). Consequently, one of the issues citizens usually complain most in opinion surveys is the noise associated with motor vehicles.

Urban noise management is a major concern for politicians, urban planners and municipal officials. In this line, the tasks involved in managing noise include solving noise complaints, noise mapping and policing noise limits as well as noise abatement and zoning. This has also been a matter of concern for International Organizations, such as the OECD, the EU and the World Health Organization (WHO), among others, which have been establishing and promoting diverse directives, guidelines and recommendations for the noise mitigation over the recent years, especially for the minimization of noise impact derived from existing and new transport infrastructures.

Fortunately, proactive steps are being taken toward silencing existing noise problems and preventing new ones before lives are disrupted. Once noise levels are known (either by measurement or prediction) today's planners can minimize the effects of noise on surrounding areas by introducing, when possible, corrective measures. In this respect, it is important to underline that planners are often reminded during detailed design stage that sufficient space should be allowed for the erection of noise barriers. It is therefore not surprising the prominent role that sound barriers have gained lately, particularly in scenarios in which the desired degree of noise reduction cannot be achieved by *at-source* measures. In such cases, these elements (normally termed as Direct Technical Remedies) are considered the most reasonable noise mitigation measures available.

The primary function of noise barriers is to shield receivers from excessive noise generated by road traffic, generating a *shadow* region in the intended protected area. An adequate design should contemplate aspects of varying nature. Acoustical design considerations include barrier material, barrier locations, dimensions and shapes. They are not the only requirements leading to an acceptable design, though. As is often the case, the solution of one problem (noise attenuation in this case) may cause other problems, such as unsafe conditions, visual blight, maintenance difficulties and lack of maintenance access due to improper barrier design, among others. The consideration of these non-acoustical related factors is also advisable prior the erection of the barrier. It is for these reasons that the research and development of all types of road barriers is currently on the rise. In this sense, companies continuously endeavor in the development and patent of their own commercial designs and surface treatment products.

But unfortunately, noise nature highly differs from light's. Due to sound diffraction noise can easily surpass the top of the barrier (the lower the frequency the easier), so the shadow region is generally far from perfect. Despite progress in this area, further steps should be taken on the research and development on the top edge of road barriers, the weakest point in the shielding efficiency due to diffraction. It is precisely in the mitigation of the negative effects of this phenomenon that efforts should focus with the challenge of achieving acceptable levels of background noise.

1.1 Literature review

Among all of the different numerical methods available concerning the issue, the Boundary Element Method (BEM) is one of the broadly used. Remarkable works using BEM for assessing the acoustic efficiency of noise barriers have been carried out to date. As a brief background, Seznec [3] implements this methodology to assess the diffracted sound field behind a barrier. Hothersall et al. [4] perform 2D numerical calculations to predict the sound pressure level in the region of balconies of a tall building near a road with different absorbing treatment scenarios, concluding that reflections from ceilings and rear wall of balconies affect adversely the shielding efficiency. However, the application of sound absorbing materials to the aforementioned walls is found to be the best strategy in terms of noise reduction. Watts et al. [5] use the method to predict the leakage of sound through louvred road barriers featuring different gaps, angles and sets of absorbing treatments. Martin and Hothersall [6] conduct a study to predict the ground attenuation effects using coherent and incoherent line source models in scenarios with both roadside and median barriers. Hothersall et al. [7, 8] make use of this technique to study the performance of a vertical screen and compare it with different types of barriers with diffusive elements on their top. Within the same research line, Ishizuka et al. [9] assess the performance of reflectors installed at balconies of tall buildings, concluding that a noise reduction by up to 10 dB(A) may be achieved when compared with ordinary balconies. The study is complemented with 3D scale-model experiments. Watts and Morgan [10] predict the acoustic behavior of a sound-interference-type device added on the top of an existing straight barrier, yielding a significant improvement in the screening performance. Crombie et al. [11] study the performance of multiple-edge barriers, concluding that the addition of side-panels leads to a significant increase in acoustic efficiency over a simple vertical screen. Fujiwara et al. [12] assess the shielding efficiency of thin, volumetric, T-shaped and cylindrical edge barriers featuring rigid, absorbing and soft boundary surfaces. This latter condition (a surface with a null sound pressure level) is achieved by considering a plane surface of varying impedance which is ideally equivalent to the performance of real wells with different depths installed on the top edge of such a surface. Monazzam and Lam [13] carry out a comparison study between T-, Y-, cylindrical- and arrow-shaped barriers and the same designs simulated with different quadratic residue diffuser (QRD) sequences on their tops, for both rigid and with absorptive coverage. In the same line, Ishizuka and Fujiwara [14] conclude that providing the top of noise barriers with soft edges significantly improves their efficiency. Configuration modifications provide only a slight improvement, though. Okubo and Fujiwara [15] assess the acoustic efficiency of the so-called *waterwheel cylinder* installed on the top-edge of noise barriers to produce an approximate soft surface, concluding that these designs are strongly frequency dependent. Jean et al. [16] study the influence of both source and ground type on the assessment of the efficiency of a straight, a T-shaped and a cylindrical top barrier. Jean and Gabillet [17] study the interaction between train and very thin, small screens placed very close to rails in addition to a 2 m height vertical roadside barrier. The highest levels in noise reduction were found for absorbing treatments of both the screens and under the train, for the considered sources-receivers scheme. To supplement this compendium, other notable works for assessing the acoustic efficiency of noise barriers conducted by Maeso and Aznárez can be consulted in [18]. Other interesting works concerning the use of BEM in outdoor acoustic problems are presented in the bibliography [19–39].

From a broader point of view, there are some noteworthy works involving Dual BEM formulations in the literature. This approach has been proposed in the study of crack problems in elasticity by Hong and Chen [40] and Portela et al. [41]. Afterwards, other interesting works involving the use of this strategy were developed by Krishnasamy et al. [42], Chen and Chen [43] and Wu [44]. A comprehensive, detailed review of the use of this approach, with special consideration on the regularization techniques for hyper-singular integrals, is reflected in Chen and Hong [45]. More recently, Chen et al. [46] make use of a Dual BEM formulation in water wave problems to suppress the fictitious frequencies that arise when handling with non-thin elements. Particularly in outdoor acoustics, de Lacerda et al. [47] present a 2D Dual BEM formulation for the treatment of non-thickness configurations and applied it to the assessment of a vertical and a T-shaped noise barrier, modeled as thin bodies over an absorbing ground. Tadeu et al. [48] propose a coupled BEM-TBEM (Traction BEM) formulation to model the propagation of sound in the presence of very thin elements. Other noteworthy works involving Dual BEM formulations can be consulted in [49–56].

Concerning experimental research works, May and Osman [57] conduct a study concerning acoustic measurements of scale-model tests on various barriers in different highway scenarios, highlighting the benefits of T-profile models and the effectiveness of sound absorptive materials, depending on the case. In [58–60] the study of the incidence of traffic noise on buildings in the vicinity of roads is performed. Again May and Osman [61] test the acoustic behavior of a 4 m height vertical screen with first an absorptive side and then with a reflective side, and compare it with a T-shaped barrier of the same height to finally show that this latter configuration outperforms the shielding efficiency of the simple screen. Jung et al. [62] perform reduced-scale model tests to measure the screening behavior of simple and T-shaped barriers with reactive surfaces near a high-speed train track. Watts et al. [63] carry out full scale tests of 2-m height T-shaped, multiple edge and double barriers featuring different set of dimensions and surface treatments, concluding that the proposed designs perform better than a simple vertical screen of the same height. Hothersall et al. [64] address scale model tests of diverse railway noise barriers considering different surface conditions of both the barrier and the ground, highlighting the importance of considering rigid ground and absorptive surfaces (especially on the track-facing side of the barrier) to increase the screening performance. Watts [65, 66] experiment with the shielding efficiency of both parallel and multiple edge traffic noise barriers. With the intention of faithfully determining the effect of sound absorptive materials in noise reduction, Watts and Godfrey [67] study two sites where noise barriers had already been erected, concluding that differences in noise reduction less than a decibel were observed when changed from sound absorptive to reflective barrier surface.

Among the different metaheuristic / bioinspired / swarm intelligence optimization methods (e.g., Evolution Strategies, Particle Swarm Optimization, etc.), Genetic Algorithms (GAs) are chosen in this thesis as representatives of the Evolutionary Algorithms paradigm. Generally speaking, any of the previously mentioned optimization algorithms may provide a satisfactory solution within the proposed framework of this work. However, the proven suitability of GAs for the application here described, largely present in the literature, supports its use in this study. Some remarkable works combining the use of BEM and GA in shape design optimization have been carried out in the past decade and are referenced in the bibliography. For instance, Duhamel [68] starts off with a rectangular volumetric structure built of equally-sized bricks to lead to the final optimized shapes with non-inner holes and fillings. Baulac et al. [69] carry out a multi-criteria optimization of multiple edge barriers. Later on, the same authors [70] assess the performance of T-shaped barriers with a reactive surface on the top. Greiner et al. [71, 72] conduct the study of a single- and a multi-objective design optimization of a Y-shaped noise barrier; the consideration of uncertainties in the optimum designs have also been handled in [73]. Grubeša et al. [74] address a 3D optimization of both acoustic performance and economical feasibility of a noise barrier built from different modules with varying cross-sections. A more recent research also covers the inclusion of an *innovization* procedure for multi-objective noise barrier optimum design in Deb et al. [75].

1.2 Background

The approach of this dissertation is conceived as a part of an ongoing research line within the Institute of Intelligent Systems and Numerical Applications in Engineering (SIANI institute), involving the shape design optimization of road acoustic barriers by coupling Boundary Elements with Evolutionary Algorithms.

As a background, Prof. Orlando Maeso and Prof. Juan J. Aznárez (both supervisors of this thesis) have been working in previous years on the development and application of numerical methods for solving wave propagation problems in elastic media. The codes developed so far, based principally on BEM, have successfully allowed addressing diverse, complex issues. In this regard, it is worth mentioning the research works implementing either the multi-region BEM or the coupled use of this technique with Finite Elements (BEM-FEM) for solving structural dynamics problems (seismic response of embedded and pilled foundations [76–83] and of arch dams [84–90], soil - structure interaction by substructure methods [91, 92], soil - foundation - structure interaction [93, 94], fluid - structure interaction [95], fluid - soil - structure interaction [96] and structure - soil - structure interaction [97]). Prior the research work presented in this thesis, a numerical model for the realistic simulation of outdoor sound propagation problems induced by any type of noise source had been continuously developed and improved over years. This bi-dimensional model was coded according to the Standard Boundary Integral Equation (SBIE) of the Method and was initially intended for the study of a practical, contemporary issue: the assessment of the shielding efficiency of road acoustic barriers. Based on this code, some studies for the assessment of the screening behavior on various barrier designs in different scenarios are collected in [18]. Another interesting work entirely on the basis of this code is found [98].

Later on, the scope of this research line was extended to the systematic improvement of the screening performance of commonly used barrier configurations. In this respect, these studies were complemented with the knowledge of Prof. David Greiner (also supervisor of this document), contributor in some prior works concerning the use of Evolutionary Algorithms (EAs) and, in particular, Genetic Algorithms (GAs) applied to different optimization problems in engineering. These include works in structural optimum design [99–104] and in other engineering fields [105–107]. In this regard, prior this document, the supervisors of this thesis had successfully developed and implemented a general, systematic procedure coupling BEM with EA for the shape design optimization of road barriers. As a result, the first joint application of both numerical approaches within the Research Group where this thesis is developed is found in [71]. In such work, the maximization of the acoustic efficiency of Y-shaped barriers with respect to a reference barrier featuring the same topology is conducted. Following, the shape design optimization of volumetric M-shaped barriers with constrained effective height is proposed in [108]. Differently from former work, the optimization is performed on the base of the minimization of differences in shielding efficiency between the considered M model and reference simple screens featuring higher effective height. In [73] a robust multi-objective optimization is presented. Concretely, the procedure focused on the search of Y-shaped designs with top absorbing surface that better fit the acoustic behavior of a reference Y configuration for each barrier length value, first including the consideration of multiple receiver points. The minimization of both conflicting objectives is intended. Finally, a single- and multi-objective optimization of Y models with different surface treatments, on the same line of previous works, is carried out in [72].

1.3 Aims and objectives

Until this thesis, the methodology developed had successfully addressed the systematic improvement of the acoustic efficiency of noise barriers. However, the assessment of certain types of barrier geometries were challenging and, in most cases, just seen as unaffordable in terms of 1) the evaluation of the feasibility of complex designs proposed by the optimizer and 2) the faithful representation of the shielding behavior. This lack of versatility and adaptability raises the need of implementing a more robust, general methodology that may cover any type of 2D acoustic optimization problem. In accordance with this, the aim of this PhD thesis is twofold:

- To develop and implement more adequate BE formulations that allows us to address the shape optimization of any type of 2D road barrier in a more robust, flexible way than that from formulations developed so far.

- To design and implement a methodology involving the coupled use of BEM and EA that leads to road barrier designs with ever-increasing acoustic efficiency.

For the sake of a more detailed description, this dissertation aims to search for the best shielding solutions that help minimize the acoustic impact of road traffic near residential areas. The introduced methodology leads to optimal solutions of previously defined noise barrier topologies that, in general, greatly outperform the acoustic efficiency of classical, widely used designs normally erected near roads.

Along this document, the assessment of both innovative and existing designs largely studied in the literature is proposed. By means of systematic geometric modifications, barrier configurations with ever higher screening performance are obtained. The complexity normally associated with such designs raises the need to consider some simplifications in order to ease the optimization processes. In this sense, there are often elements in the barrier design (if not the whole barrier design itself) eligible of both mathematical and geometric simplification that allows the consideration of very thin elements as null-section bodies, for acoustic performance evaluation distant from the barrier boundary. In this context, the barrier typologies that can be addressed by the procedure here presented are categorized as follows: i) volumetric barrier designs. It is the case of real barriers featuring thick elements, such as M-shaped barriers; ii) very thin barriers. The assessment of these types of barriers is performed by idealizing the whole design as a *single-wire* configuration; iii) volumetric barriers featuring very thin elements. It is a mixed case. The general configuration remains its real geometry while the very thin elements are idealized and studied as null-thickness type.

1.4 Numerical approaches implemented in this thesis

The laws governing natural phenomena are normally expressed in terms of differential equations. Unfortunately, the large majority of problems facing engineering applications cannot be solved directly, as just few differential equations have solution in terms of elemental functions (the differential equations that could be solved explicitly until the second half of 20th century were limited) or, simply, systems described by differential equations are so complex or large that a purely analytical solution to such equations is not tractable. It is in these complex systems where computer simulations and numerical methods are useful.

The numerical approach of these phenomena allows us both to obtain the approximate solution easily, in the case of unknown exact solutions, and to help reduce costs derived from real experimentation. Despite the fact that these techniques were developed before programmable computation existed, the significant development of computers in the last decades has enabled the easy and fast implementation of these methods based on numerical approximations of the real solution.

The Boundary Element Method (BEM), also known as the Boundary Integral Equation Method or Boundary Integral Method, is a numerical approach for solving linear partial differential equations which have been formulated as integral equations. During the last few decades, BEM has gradually evolved to become one of the few widely used numerical techniques for solving boundary value problems in engineering and physical sciences. Due to this inherent ability to address infinite domains or free field problems (in implementing the method, just the boundary of the solution domain has to be discretized into elements. The solution at any arbitrary point of the domain can be found after determining the unknown boundary data, though), BEM arises as the most suitable technique in the study of outdoor sound propagation prediction. However, the implementation of the standard formulation of the Method leads to insurmountable obstacles in most cases of the problems studied in this work.

The accomplishment of the aims and purposes of this work (stated in the previous section) demands a specific BE formulation that allows the problem to be solved. Such a formulation combines the standard singular integral equality of the Method with a hyper-singular variant which is obtained by derivation of the former, to finally get the so-called Dual BEM formulation. The coupled use of both approaches in this Dual formulation allows us to avoid drawbacks associated with the exclusive implementation of the standard BEM formulation. In this respect, the Dual approach arises as the most appropriate strategy involving BE to address the proposed problems numerically, by allowing us 1) to assume a simplification of reality by idealizing very thin elements as null-thickness type, greatly facilitating the geometric definition of complex configurations with no substantial influence on the acoustic performance for the considered thickness of very thin sections [47] (widely present in diverse barrier designs), 2) to mitigate the fictitious eigenfrequencies associated with the inner domain of the barrier that may adversely affect to the assessment of the screening efficiency. In dealing with these issues with BE often results, according to the individual case, in serious numerical drawbacks if not to a singular system of equations when dealing with the idealization of very thin elements. Both problems are properly addressed in the methodology presented in this work. The solution to these challenges, especially the null-thickness idealization, enables an easier, more general procedure in obtaining barrier designs that normally cover a large range of possible configurations along the optimum search process.

Under this proposal, the real barrier can be then modeled, depending on the case, as either a *single-wire* configuration, as representative of a very thin barrier - Figure 1.1(a) -, or as a volumetric structure featuring very thin sections idealized as null-thickness type - Figure 1.1(b) -. Based on a frame of free geometric constraints, the definition of the barrier profile is then easily accomplished. This approach results in faster computational times within a cumbersome process where every possible design is assessed along the whole spectrum of frequencies.

The need of the implementation of the Dual BEM formulation in this work is clarified in Figure 6.2. The strategy of the application of both formulations varies depending of the nature of the element under consideration. This way, with the purpose of mitigating the effects of the fictitious eigenfrequencies when dealing with non-thin bodies, a Dual BEM formulation based on the combined use of the standard boundary integral equation (SBIE) and the hyper-singular boundary integral equation (HBIE) coupled by means of a frequency-related complex value is proposed [109]. The nature of the issue is different when dealing with very thin bodies. In this case, numerical integration problems may appear affecting to the barrier performance. As shown in Figure 6.2(b), the boundaries at both sides of elements with null sections (featuring different values of sound

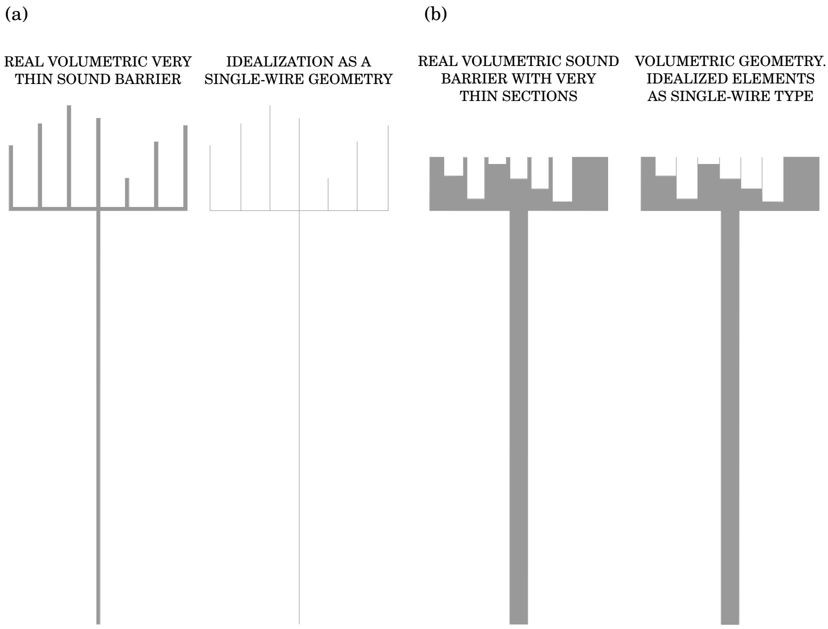

FIGURE 1.1: Examples of complex designs eligible for geometric idealizations. (a) Fork-shaped barrier. The very thin cross-section along the overall configuration suggests its modeling as a single-wire geometry. (b) Quadratic Residue Diffuser (QRD)-based barrier with very thin elements idealized as null-thickness bodies.

pressure and flux) are represented by the discretization itself. The application of the SBIE on both sides of nodes yields a singular system of equations that does not allow the solution to be obtained. However, the joint implementation of the SBIE and its derivative on the collocation node (HBIE) provides a compatible system of equation that allows us to know the solution at both sides of the barrier. With this aim, the SBIE and the HBIE are then applied separately. As a result, this formulation enables the idealization of very thin elements as single-wire bodies. Such a simplification of reality is a real asset, especially when compared with the case of the faithful, detailed definition of real complex volumetric.

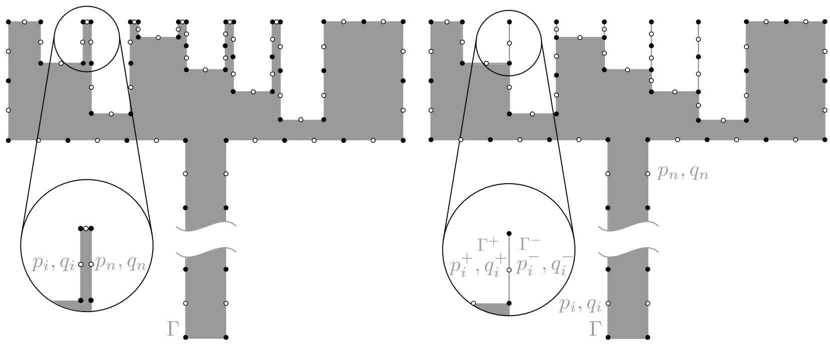

FIGURE 1.2: Example of the discretization with parabolic elements (3 nodes) for f=500 Hz of a QRD-based design. (a) Discretization of the real geometry. (b) Discretization after idealization of very thin bodies as null-width elements.

Optimization methods arise as a worthwhile strategy that help us reach our goals in accordance with the stated objectives. Generally speaking, any of the optimization methods available may provide a satisfactory solution within the proposed framework of this thesis. Howeve, as previously stated, Evolutionary Algorithms have been chosen in this work in pursuit of barrier designs with increasingly higher efficiency. These are relatively new, but very powerful techniques used to find solutions to many real-world search and optimization problems. Many of these problems have multiple objectives, which leads to the need to obtain a set of optimal solutions known as *non-dominated* solutions. In this line, the implementation of EAs has been found to be a highly effective way of finding multiple effective solutions in a single simulation run [110, 111].

With the aim of benefiting the existing research line in the Group concerning shape optimization, Genetic Algorithms are chosen in this work as representatives of the evolutionary algorithms paradigm. Among EAs, GAs have largely proven suitability in problems and methodologies similar to the ones introduced here [68–75].

Results concerning single- and multi-objective frame optimization of different noise barriers are included in this document. The EA software used in the single-objective optimization of the shielding efficiency of such road barriers applies the GAlib package [112], a collection of C++ genetic algorithm components from which it is possible to quickly construct GA's to deal with a wide variety of problems.

The increasing relevance and utility of evolutionary multi-objective optimization (EMO) [110, 111] in recent years can be attributed to its role in successfully solving an important number of science and engineering problems and applications [113]. EMO algorithms are very practical and efficient tools when the optimization of two or more conflicting objectives is required. This is what occurs in the multi-objective optimization performed in this work. One of the criterion involves maximization of the noise attenuation efficiency, while the remaining one deals with the minimization of the total length of the barrier, as representative of manufacturing costs. It is easy to see that no one objective can be improved without degrading performance on the other. In other words, in this case, reduction in length of barriers is associated, in the vast majority of cases, with lower shielding efficiency. The code used in this multi-objective optimization is an own implementation of the NSGA-II algorithm [114], widely used in research works by the SIANI institute (e.g., [72, 73, 103, 108]).

1.5 Structure of the dissertation

After these introductory remarks, Chapter 2 focuses on the fundamental aspects of acoustics. More precisely, a brief introduction on the basis of the physics of the problem and the notation of the most common acoustic variables used along the chapter are provided at first, followed by a detailed description of the assumptions taken into consideration and the presentation of the governing equations. The definition of the boundary conditions applicable on sound wave propagation problems is also handled, with emphasis on partially absorbing boundaries (Robin condition) and the determination of its acoustic impedance by means of the Delany and Bazley model [115]. This chapter concludes with the definition of the most common acoustic magnitudes and the characterization of noise by its frequency content and related information.

The main issue of this work is the Dual BEM formulation for the analysis of any type of 2D acoustic problem. Chapter 3 is devoted to this BE approach. Firstly, the bases of both the standard formulation (SBIE) and the hyper-singular boundary integral equation (HBIE) of the Method is introduced as a previous step to the presentation of the Dual formulation in its different variants for the problems addressed here. In this sense, a detailed description of the approach for 1) avoiding the fictitious eigen-frequencies that may appear when dealing with barriers featuring real dimensions, 2) the idealization of very thin elements as single-wire bodies and 3) dealing with volumetric barriers featuring elements with small sections that can be idealized as null-thickness type is provided. Validation examples for the aforementioned approaches are found at the end of this chapter.

Chapter 4 deals with the theoretical bases of Evolutionary Algorithms and, in particular, of Genetic Algorithms and the convenience of this optimization method in the framework of this thesis. After the overview of these paradigms, a contextualized description of the GA applied in the single-objective optimization performed in this work is provided. Following a brief introduction to the evolutionary multi-objective optimization, the description of the chosen EMO algorithm closes off this chapter.

Chapters 5 through 7 are devoted to results. More specifically, Chapter 5 collects the results on the numerical shape optimization of two studies involving very thin barriers idealized as single-wire configurations. Different barrier topologies of practical interest are presented in the first study, covering overall shape and top edge configurations; spline curves- and polynomial-shaped designs; rigid and noise absorbing boundaries materials. Given the strong theoretical nature of the presented topologies, easier-to-build designs are proposed based on slight geometric modifications from optimal barriers. While results are achieved by using a specific receivers' scheme, the influence of the receivers' distribution on the acoustic performance is also addressed. It is precisely on this latter point, but with a broader perspective, where the second study focuses: the influence of the screening performance through distance. In this case, two different barrier models are proposed in the analysis, for two different receivers configurations and three clearly distinguishable regions in terms of closeness to the barrier. The most remarkable insights of both studies are also found in this chapter.

Still within the framework of single optimization, Chapter 6 presents numerical results on the basis of three well-based barrier topologies defined by a general volumetric structure featuring very thin top elements eligible of geometric simplification as null-thickness bodies. With the intention of both determining how important the role of wells at the top is in the shielding behavior and leading to more practical designs, similarly to previous chapter, some geometric modifications are performed on the optimal designs of one of the proposed models. This chapter ends with the partial conclusions derived from the analysis of the presented results.

Results on the multi-objective optimization are shown in Chapter 7. The analysis performed in this chapter focuses on the simultaneous optimization of two objectives in conflict: the maximization of noise attenuation and the minimization of the costs of all barrier material used, represented by the overall length of the boundaries. The topologies to be optimized are those presented and described in the first study of Chapter 5, with the same 2D configuration but just considering perfectly reflecting barrier surfaces. Under this scenario, two simulation cases are considered for the optimization: 1) when starting off with a random initial population and 2) when including the best single-objective optimal design obtained in Chapter 5 in the initial population. In the analysis of the results, the benefits of this latter case in the improvement of the best found solutions is discussed.

Chapter 8 summarizes the most outstanding achievements and the most remarkable conclusions derived from this Study. Specific recommendations for future research directions and developments that may shortly follow this work are also suggested.

Following the main content of the text, Appendix A includes the numerical aspects concerning the hyper-singular integrals involved in the Dual BEM formulation presented in Chapter 3. In addition, a long summary in Spanish covering information relating to Chapters 1, 3, 6 and Chapter 8 is provided at the end of the presented document.

Finally, this document concludes with the bibliographic references arranged by order of appearance.

1.6 Published works derived from this thesis

The findings derived from the development of this dissertation over the past four years have resulted in publications and presentations in different events. To end with this chapter, details concerning this scientific production are presented below.

1.6.1 Conference contributions

- R. Toledo, J. J. Aznárez, O. Maeso and D. Greiner (2013). Optimización de diseños de pantallas acústicas de pequeño espesor mediante la implementación de la formulación dual del MEC. *Congreso de Métodos Numéricos en Ingeniería, SEMNI, Bilbao, Spain*.

- R. Toledo, J. J. Aznárez, O. Maeso and D. Greiner (2013). A comparative study in design optimization of polygonal and Bézier curve shaped-thin noise barriers using dual BEM formulation. *International Conference on Evolutionary and Deterministic Methods for Design, Optimization and Control with Applications to Industrial and Societal Problems, EUROGEN, Las Palmas de G. C., Spain*.

- R. Toledo, J. J. Aznárez, O. Maeso and D. Greiner (2014). Une méthodologie por l'optimisation d'écrans anti-bruit routiers de faible épaisseur et forme géométrique complexe en utilizant des algorithmes évolutionnaires et la méthode des éléments de frontière. *12éme Congrès Français d'Acoustique, CFA, Poitiers, France,* pp. 337-343.

- R. Toledo, J. J. Aznárez, O. Maeso and D. Greiner. A procedure for the top geometry optimization of thin acoustic barriers (2014). *E. Oñate et al. (Eds.), 11th World Congress on Computational Methods, WCCM XI, Barcelona, Spain*. ISBN.: 978-84-942844-7-2.

- R. Toledo, J. J. Aznárez, O. Maeso and D. Greiner (2015). Procedimiento para la optimización de forma de dispositivos de coronación para mejora de la eficacia de pantallas acústicas. *Congress on Numerical Methods in Engineering, Lisbon, Portugal*.

1.6.2 Book chapter contributions

- R. Toledo, J. J. Aznárez, O. Maeso and D. Greiner (2015). A comparative study on design optimization of polygonal and Bézier curve-shaped thin noise barriers using Dual BEM formulation. In: D. Greiner et al. (eds), *Advances in Evolutionary and Deterministic Methods for Design, Optimization and Control in Engineering and Sciences, Computational Methods in Applied Sciences,* vol. 36, pp. 335-349. Springer International Publishing Switzerland.

- R. Toledo, J. J. Aznárez, O. Maeso and D. Greiner (2015). A procedure for improving the acoustic efficiency of top-edge devices on noise barriers: an application of genetic algorithms and boundary elements. In: J. Magalhaes-Mendes, D. Greiner (eds.), *Evolutionary Algorithms and Metaheuristics in Civil Engineering and Construction Management, Computational Methods in Applied Sciences,* vol. 39, pp. 105-125. Springer.

1.6.3 Contributions in indexed (ISI-JCR) journals

- R. Toledo, J. J. Aznárez, O. Maeso and D. Greiner (2015). Optimization of thin noise barrier designs using Evolutionary Algorithms and a Dual BEM formulation. *Journal of Sound and Vibration,* **334**, 219-238.

- R. Toledo, J. J. Aznárez, D. Greiner and O. Maeso (2015). Shape design optimization of road acoustic barriers featuring top-edge devices by using Genetic Algorithms and Boundary Elements. *Engineering Analysis with Boundary Elements*. Accepted for publication.

1.6.4 Contributions in other journals

- R. Toledo, J. J. Aznárez, O. Maeso and D. Greiner (2015). Un procedimiento basado en el uso de algoritmos genéticos y elementos de contorno para el diseño óptimo de la geometría de pantallas acústicas de pequeño espesor. *Revista de Acústica, SEA,* **46(1,2)**, 13-21.

2. FUNDAMENTALS OF ACOUSTICS

Noise can be defined as *disagreeable* or *undesired* sound or any other kind of sound disturbance. Acoustically speaking, the phenomenon underlying both noise and sound is the same: the distortion of the propagation medium (the air in exterior acoustic problems) with respect to its at-rest state. More precisely, both terms are the result of pressure variations or oscillations in an elastic medium (e.g., air, water, solids, etc.), generated by a vibrating surface or a turbulent fluid flow. These changes in medium obey to an energy propagation mechanism denominated *wave*. Sound waves are perceived by the auditory system and transformed into electric impulses whose information is properly interpreted in the brain to finally get this perception that we call *sound*. How wished a particular sound seems to one person sets the limit between sound and noise. In other words, what is sound and what is noise is determined by the attitude toward the noise source. The differentiation between them is indeed purely subjective.

The human being is able to detect just sounds within a specific range of both amplitudes and frequencies. However, the range to which the human auditory system responds is quite remarkable. Although this capacity may vary between individuals and is adversely influenced by many factors (age, auditory disorders, temporary or permanent loss hearing by exposure to high noise levels, etc.), the frequency range associated with a healthy human varies from approximately 20 to 20 000 Hz, meaning more than nine octaves (each octave representing a doubling of frequency). Sound waves below and above these limits are known as *infrasound* and *ultrasound*, respectively. Human vision is also quite remarkable, but far from comparison with human hearing. The frequency range of vision is a little less than one octave (about $4{\times}10^{14} - 7{\times}10^{14}$ Hz). Within this one octave range we can identify more than 7 million colors. Making a parallel with auditory system and recalling that the frequency range of the ear is nine times greater, one can imagine how many sound *colors* might be possible. The sensitivity of the auditory system is frequency depending, though. Furthermore, two sounds with identical pressure levels may be perceived differently in intensity, according to its spectral content. As an essential role throughout evolution, it is not surprising that human hearing is most sensitive over the frequency range covered by human speech (between 2 000 and 5 000 Hz) [116].

The characterization of noise demands, however, a proper definition of its related waves. As a starting point, an overview of the sound propagation phenomenon in terms of physical and mathematical aspects when the sound disturbances are, in some sense, small are presented in this chapter. As essential in the precise definition of the road acoustic problem and in the following assessment of screening strategies, a general, necessary background covering basic definitions and magnitudes related to the physics of sound and noise are also introduced.

2.1 Introduction

Assuming that the viscosity of the propagation medium (air) is considered negligible, sound waves can be modeled as elastic waves, that is, that particles feature both forward and backward lineal movements according to direction of propagation around their initial position (the so-called undisturbed or at-rest position), leading to overpressure and subpressure regions in the vicinity of each particle. These changes in pressure, caused when the fluid expands or shrinks, give rise to internal recovery forces responsible for the pressure wave propagation.

In this way, the term *fluid particle* has been introduced. Such a particle is represented by a volume element that is large enough to enclose a large number of molecules but, at the same time, small enough to enable the consideration of the acoustic variables as constant along this elemental volume. In other words, the acoustic variables are properly defined as an average of the corresponding values of the molecules of air (continuum medium model). These molecules enter and leave the volume element while the overall number of them is considered, on average, constant. Therefore, the macroscopic properties of the fluid particle are uniform, so we can speak of *particle velocity*, *particle acceleration*, etc., when dealing with acoustic waves in fluids, similarly to the study of elastic waves in solids.

Below, the notation of the most common acoustic variables used along this chapter is provided:

t: time variable.
$\mathbf{x} = x\,\mathbf{i} + y\,\mathbf{j} + z\,\mathbf{k}$: vector that defines the particle position in the undisturbed condition. $\mathbf{i}$, $\mathbf{j}$, $\mathbf{k}$ are the unit vectors corresponding to the coordinates directions.

$\mathbf{u} = \mathbf{u}(\mathbf{x}, t) = u_x\ \mathbf{i} + u_y\ \mathbf{j} + u_z\ \mathbf{k}$: particle displacement from the equilibrium state.
$\mathbf{v} = \mathbf{v}(\mathbf{x}, t) = v_x\ \mathbf{i} + v_y\ \mathbf{j} + v_z\ \mathbf{k}$: particle velocity.
$\rho_0(\mathbf{x})$: constant representing the fluid density in the undisturbed state.
$\rho(\mathbf{x}) = \rho(\mathbf{x}, t)$: instant density.
$p_0(\mathbf{x})$: fluid pressure field in the undisturbed state.
$p_T = p_T(\mathbf{x}, t)$: instant pressure at any point.
$p(\mathbf{x},t) = p_T - p_0$: acoustic pressure at any point.
c: wave propagation or phase-wave velocity.

2.2 Assumptions and governing equations

The derivative formulation to be obtained can be understood as equivalent to the derivative approach seen in the elastic problem in solids (or, in general, in any continuum medium), with the same basic relations and meaning: 1) kinematic equations, 2) constitutive equations and 3) equilibrium equations.

Before dealing with the governing equations approach, the fundamental assumptions taking into consideration in the framework of the intended formulation are introduced:

- As the viscosity of the medium (air) is negligible, dissipative effects involving this condition are neglected.

- In all the studies addressed we consider the case of propagation of sound waves through the air and in the vicinity of the noise source. This allows us to neglect the influence of the gravity, so we assume that pressure and density are uniform in the domain. This means assuming that the medium is homogeneous.

- The air is considered as a perfectly elastic, isotropic medium. This means neglecting some effects, such as thermal gradients, on the sound propagation.

- It is assumed that distortions in the medium due to sound waves are small enough, so changes in density and pressure are equally small in comparison with their values when at rest. Under this assumption, changes in both density and pressure levels around a particle are well mathematically represented by considering just linear terms of the series.

- It is accepted that the air is initially at rest, with no wind effects.

With these assumptions, the simplest formulation involving the wave propagation in fluids is obtained. Fortunately, results disclosed from this model are largely supported by experimental evidence for a wide variety of acoustic problems. It should be recalled, however, that there are scenarios of great interest where such assumptions are unacceptable.

2.2.1 Continuity equation

Let us imagine a volume element $d\Omega$ that, for the sake of simplicity, it is considered as a parallelepiped of volume $d\Omega = dx\,dy\,dz$. The continuity relation establishes that for a continuum medium with neither source nor sink of matter, the net quantity of fluid that enters $d\Omega$ has to be the same than the mass increment in $d\Omega$. This condition relates the fluid movement to its dilation and compression. Assuming a lineal variation of the velocity around the origin, the total amount of matter that enters $d\Omega$ in x direction is equal to:

$$-\frac{\partial(\rho\, v_x)}{\partial x}\,dx(dydz) = -\frac{\partial(\rho\, v_x)}{\partial x}\,d\Omega \tag{2.1}$$

Thus, the total amount that enters $d\Omega$ due to the flow in the three coordinate directions is:

$$-\left[\frac{\partial(\rho\, v_x)}{\partial x} + \frac{\partial(\rho\, v_y)}{\partial y} + \frac{\partial(\rho\, v_z)}{\partial z}\right] d\Omega = -\nabla(\rho\,\mathbf{v})\,d\Omega \tag{2.2}$$

where the divergence operator is applied $\nabla = \frac{\partial}{\partial x}\mathbf{i}+\frac{\partial}{\partial y}\mathbf{j}+\frac{\partial}{\partial z}\mathbf{k}$. As previously stated, the total amount from (2.2) must be equal to the mass increment in $d\Omega$. Thus:

$$\frac{\partial\rho}{\partial t}\,d\Omega = -\nabla(\rho\,\mathbf{v})\,d\Omega \tag{2.3}$$

so, finally, the continuity equation is obtained:

$$\frac{\partial\rho}{\partial t}\,d\Omega + \nabla(\rho\,\mathbf{v})\,d\Omega = 0 \tag{2.4}$$

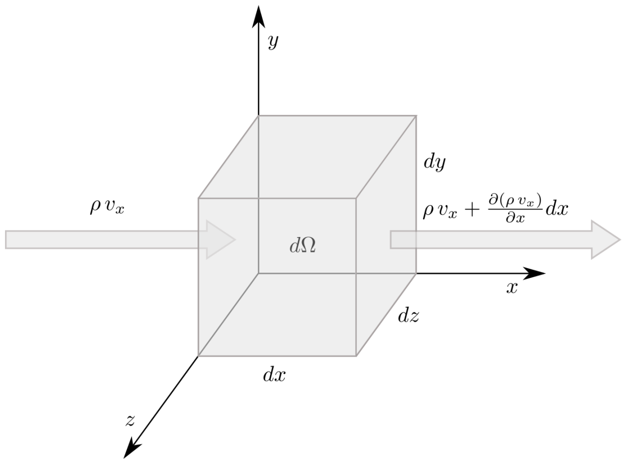

FIGURE 2.1: Fluid flow through elemental volume $d\Omega$ in x direction.

As usual, the density increment around a particle is expressed in terms of its at-rest value, by means of the so-called *condensation* (s) variable:

$$s = \frac{\rho - \rho_0}{\rho_0} \tag{2.5}$$

thus:

$$\rho = \rho_0(1 + s) \tag{2.6}$$

Therefore, (2.4) can be re-written (ρ_0 is constant) as follows:

$$\frac{\partial s}{\partial t} + \nabla \left[\mathbf{v}(1 + s) \right] = 0 \tag{2.7}$$

With the assumed hypothesis of small disturbances $|s| << 1$, the previous equation can be then linearized:

$$\frac{\partial s}{\partial t} + \nabla \mathbf{v} + \nabla (s\mathbf{v}) = 0 \tag{2.8}$$

The last term is negligible, as corresponds to a high-order infinitesimal term:

$$\frac{\partial s}{\partial t} + \nabla \mathbf{v} = 0 \tag{2.9}$$

that corresponds to the **linearized continuity equation**. The integration of (2.9) along time must be null (a constant with value different from zero would mean that the acoustic variables present non-null values when at rest). This way:

$$\int \left(\frac{\partial s}{\partial t} + \nabla \mathbf{v} \right) dt = 0 \tag{2.10}$$

so:

$$\int \left(\frac{\partial s}{\partial t} \right) dt = -\int (\nabla \mathbf{v}) \, dt = -\nabla \int \mathbf{v} \, dt = -\nabla \mathbf{u} \tag{2.11}$$

and finally:

$$s = -\nabla \mathbf{u} \tag{2.12}$$

This final expression relates unit density fluctuations (and therefore, the occupied volume) with particle position variations.

2.2.2 Constitutive or state equation

This equation relates the deformations in the fluid medium to the internal recovery forces, in terms of changes in density (or condensation). Given its inherent nature, this equation must be defined by any constant characterizing the properties of the considered continuum medium. Once assumed both the isotropy of the medium and the absence of shear waves, the fluid medium is clearly well determined by knowing the value of just a constant.

At this point it is worth emphasizing that it is the medium behavior what determines the kind of formal expression for the state equation. In this sense, experimental evidence allows one to deduce that the acoustic propagation is governed by a slightly adiabatic process. That is to say, heat exchanges between nearby particles are negligible. Considering the assumed elastic behavior of the fluid, with small values of disturbance in comparison with their values when at rest, we conclude that the fluid behavior is, additionally, reversible.

As a perfect gas, the usual form to obtain the isentropic relation between pressure and changes in density in air can be expressed by means of a Taylor's series expansion:

$$p_T = p_0 + \left(\frac{\partial p_T}{\partial \rho}\right)_{\rho_0} (\rho - \rho_0) + \frac{1}{2}\left(\frac{\partial^2 p_T}{\partial \rho^2}\right)_{\rho_0} (\rho - \rho_0)^2 + \ldots \tag{2.13}$$

where the partial derivatives are constants for the determination of both expansion and compression of the fluid around its density when at rest. Within a state with small disturbances the high-order terms can be neglected. This way, a linearized expression is obtained:

$$p_T = p_0 + \left(\frac{\partial p_T}{\partial \rho}\right)_{\rho_0} (\rho - \rho_0) \tag{2.14}$$

Defining the *adiabatic compression module* (K):

$$K = \rho_0 + \left(\frac{\partial p_T}{\partial \rho}\right)_{\rho_0} \tag{2.15}$$

the isentropic state equation for small disturbances ($|s| << 1$) can be written as:

$$p = K\, s \tag{2.16}$$

that, as intended, relates changes in pressure to changes in relative density by means of a medium-dependent constant. Finally, combining (2.12) and (2.16) we get:

$$p = -K\, \nabla \mathbf{u} \tag{2.17}$$

that it can be considered as a **behavior** or **compatibility equation**.

2.2.3 Equilibrium equation

Under the framework of the assumptions considered (the viscosity and the adiabatic behavior of the medium is negligible, as well as gravitational effects), the equilibrium equations are immediately achieved after the application of the Newton law on a volume element $d\Omega = dx\, dy\, dz$ which flows with the fluid.

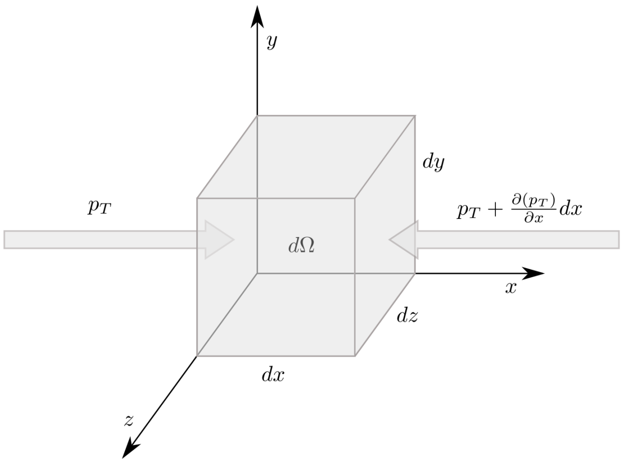

FIGURE 2.2: Elemental forces on $d\Omega$ in x direction.

In the absence of volume forces, the equilibrium condition along x direction is established as follows:

$$df_x = dm \frac{\partial v_x}{\partial t} \tag{2.18}$$

with dm being the fluid mass within $d\Omega$. In the remaining coordinate directions similar expressions are obtained. Considering, as before, a state featuring small disturbances, a lineal variation of the pressure can be admitted:

$$-\frac{\partial p}{\partial x} dx(dydz) = \rho_0 \, d\Omega \frac{\partial v_x}{\partial t} \tag{2.19}$$

$$-\frac{\partial p}{\partial x} = \rho_0 \frac{\partial v_x}{\partial t} \tag{2.20}$$

and finally in three coordinate directions:

$$-\nabla p = \rho_0 \frac{\partial \mathbf{v}}{\partial t} \tag{2.21}$$

that corresponds to the intended **linearized equilibrium equation**.

In the light of expression (2.21), it is worth noting that the internal forces involved in the process to make particles back to their at-rest position (the internal recovery forces) are not conditioned by the pressure values but by their spatial variation.

2.2.4 Wave equation

The continuity (2.9), state (2.16) and equilibrium (2.21) equations, along with initial boundary conditions (issue discussed in detail in the next section), mathematically define the approach of the problem. However, it is also straightforward to obtain a more simple derivative formulation, involving just an equation and a variable. While this equation can be expressed in terms of any acoustic variable (pressure, density, displacement/velocity, etc.), it is decided to express it using pressure as dependent variable, the most common way to do so. Applying divergence on equilibrium equation:

$$-\nabla^2 p = \rho_0 \nabla \frac{\partial \mathbf{v}}{\partial t} \tag{2.22}$$

Deriving continuity equation with respect to time:

$$\frac{\partial^2 s}{\partial t^2} + \frac{\partial}{\partial t}\nabla \mathbf{v} = \frac{\partial^2 s}{\partial t^2} + \nabla \frac{\partial \mathbf{v}}{\partial t} = 0 \tag{2.23}$$

Thus, from both latter expressions:

$$\nabla^2 p = \rho_0 \frac{\partial^2 s}{\partial t^2} \tag{2.24}$$

Using the state equation, we obtain:

$$\nabla^2 p = \frac{\rho_0}{K}\frac{\partial^2 p}{\partial t^2} \tag{2.25}$$

Introducing the following constant:

$$c = \sqrt{\frac{K}{\rho_0}} \tag{2.26}$$

with dimensions of velocity, we finally obtain:

$$\nabla^2 p = \frac{1}{c^2}\frac{\partial^2 p}{\partial t^2} \tag{2.27}$$

that corresponds to the so-called **wave equation**. This expression governs the acoustic propagation in non-viscous fluids and in lineal range of small disturbances.

The c constant represents the *velocity of propagation* of waves or *phase velocity*. As it can be seen, it is independent from the frequency of the disturbance what implies that it is assumed that the considered medium is non-dispersive. c defines the elastic properties of the fluid and depends on the thermodynamic characteristics of the medium (temperature, pressure and density). In dry air conditions at 20°C the value of this constant, that is, the speed of sound in air, can be taken as 343 m/s.

In the presence of either sources/sinks of matter or internal sources of pressure, expression (2.27) is no longer homogeneous. In both cases, the continuity and the equilibrium equations are modified. It is possible in these scenarios, however, to obtain a more general expression of the wave equation. This generalist wave equation can be conveniently written as follows:

$$\nabla^2 p + \frac{1}{c^2} b(\mathbf{x}, t) = \frac{1}{c^2}\frac{\partial^2 p}{\partial t^2} \tag{2.28}$$

2.2.5 Plane harmonic waves

In the cases when the spatial variation of any acoustic variable is dependent exclusively on just a coordinate direction (so that all points contained in a plane perpendicular to the propagation direction vibrate in phase) we are dealing with a plane harmonic wave problem. If, in addition, the boundary conditions and the possible internal sources of pressure feature a harmonic temporal variation with pulse ω, all acoustic variables also feature the same harmonic variation with the same pulse. Choosing a coordinate system coincident with the wave propagation along the x coordinate, the following can be written:

$$p(x,t) = p(x;\omega)e^{i\omega t} \tag{2.29}$$

$$b(x,t) = b(x;\omega)e^{i\omega t} \tag{2.30}$$

Substituting these latter expressions into (2.28) leads immediately to the **wave equation in frequency domain**:

$$\frac{d^2p}{dx^2} + k^2p + \frac{1}{c^2}b = 0 \tag{2.31}$$

where $p = p(x;\, \omega)$ is the complex response function and the *wave number* $k = \omega/c$ has been introduced. In absence of volume forces (internal forces), the homogeneous equation to be solved is the so-called **Helmholtz equation**:

$$\frac{d^2p}{dx^2} + k^2p = 0 \tag{2.32}$$

The dynamic equilibrium equation (2.21) allows us to obtain the following:

$$-\nabla p = i\rho_0\omega\mathbf{v} \tag{2.33}$$

For a determined direction η, the associated displacement u_η can be then written:

$$\frac{\partial p}{\partial \eta} = -i\rho_0\omega v_\eta \tag{2.34}$$

$$v_\eta = i\omega u_\eta \tag{2.35}$$

The general solution of equation (2.32) is a complex expression of type:

$$p(x;\, \omega) = Ae^{i(\omega t - kx)} + Be^{i(\omega t + kx)} \tag{2.36}$$

That is to say, it is the contribution of two plane waves featuring, in general, complex amplitudes. In other words, a forward and a backward wave, respectively, according to the x propagation direction:

$$x^+ :\ p^+ = Ae^{i(\omega t - kx)} \tag{2.37}$$

$$x^- :\ p^- = Be^{i(\omega t + kx)} \tag{2.38}$$

$$\tag{2.39}$$

The particle velocity is obtained by derivation:

$$\mathbf{v} = v(x;\,\omega)\mathbf{i} = -\frac{1}{i\omega\rho_0}\frac{\partial p}{\partial x} = \left[\frac{A}{\rho_0 c}e^{i(\omega t - kx)} - \frac{B}{\rho_0 c}e^{i(\omega t + kx)}\right]\mathbf{i} \tag{2.40}$$

Both the forward and the backward wave can be then expressed in the form:

$$v^+ = \frac{p^+}{\rho_0 c} \tag{2.41}$$

$$v^- = -\frac{p^-}{\rho_0 c} \tag{2.42}$$

The constant value $\rho_0 c$ corresponds to the *characteristic impedance*, a property of the medium represented by a real number. It therefore follows that pressure and velocity are in phase for plane waves.

The generalization of the plane harmonic wave in an arbitrary spatial direction yields the derivative form of the expression:

$$\nabla^2 p + k^2 p = 0 \tag{2.43}$$

with solutions of type:

$$p(\mathbf{x};\,\omega) = Pe^{i(\omega t - \mathbf{kx})} \tag{2.44}$$

with $\mathbf{x}$ being the position vector and $\mathbf{k}$ a vector representing the propagation direction:

$$|\mathbf{k}| = \frac{\omega}{c} \tag{2.45}$$

This way, the constant value $\mathbf{kx}$ corresponds to constant phase planes, that is, parallel planes to the wave front.

2.3 Boundary conditions

The integration of the wave equation (2.43) requires the consideration of the boundary conditions. In other words, the solution involving any sound propagation problem in frequency domain must comply with both this expression and the conditions imposed at the boundaries of the domain under study. Three types of boundary conditions are applicable:

- **Dirichlet condition ($p = \overline{p}$).** The sound pressure is known on the boundary. This is the case of a radiant boundary, that is, a boundary pulsing with a particular wave amplitude.

- **Neumann condition ($\frac{\partial p}{\partial n} = q$).** The flux is known on the boundary. The most characteristic example corresponds to a completely reflective boundary, which features a null flux.

- **Robin condition ($\frac{\partial p}{\partial n} = -ik\beta p$).** Partially absorbing boundary (mixed condition). This is the most commonly presented condition and represents boundaries with capacity of absorbing a portion of the incident acoustic wave.

The sound pressure and the pressure flux in absorbing boundaries (Robin condition) are related, in the case of normal wave incidence, by an absorbing boundary coefficient β. The next lines are devoted to the obtainment of such coefficient.

2.3.1 One-dimensional fluid interaction problem

Let us consider two fluid mediums separated by a plane inter-phase. In one of them (medium 1) a harmonic wave plane propagates with a frequency ω towards the medium 2 perpendicularly to the inter-phase (normal incidence) as seen in Figure 2.3. The acoustic properties of the mediums are characterized by their corresponding acoustic impedances: $r_1 = \rho_0 c$ for medium 1 (the air in this case) and $r_2 = \rho_2 c_2$ for medium 2. After reaching the inter-phase, the incident wave is divided into a reflected wave (that propagates along medium 1) and a transmitted wave (that propagates along medium 2). Under conditions described above, both the reflected and the transmitted waves are also logically plane waves propagating perpendicularly to the inter-phase. Therefore, the problem under investigation is monodimensional.

In permanent state, the overall wave pressure in medium 1 is the sum of the incident p_i and the reflected wave p_r. In the frequency domain, using complex notation and omitting the temporal variation $e^{i\omega t}$ the following can be written:

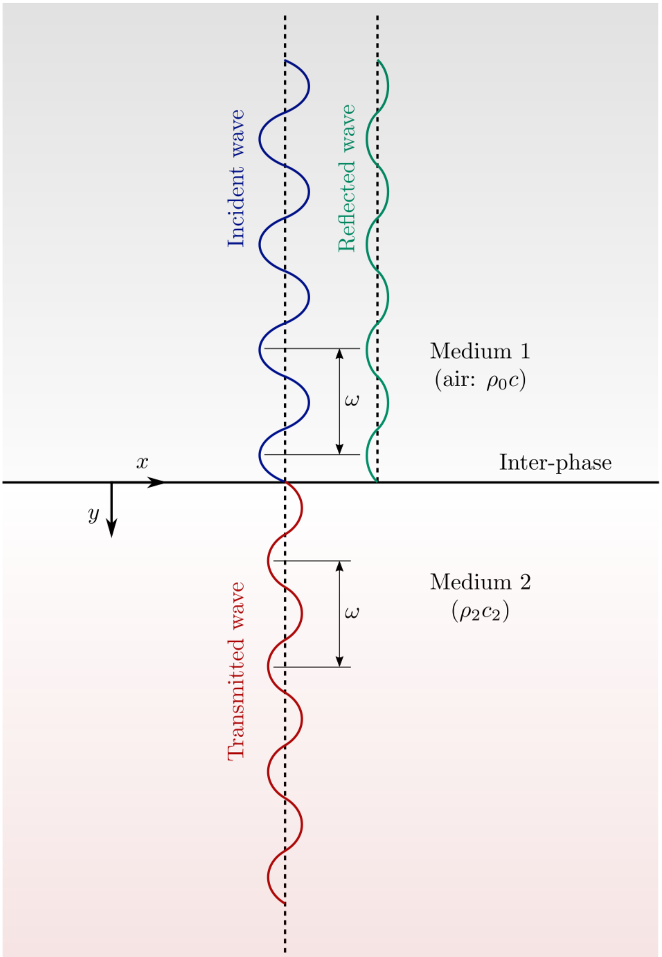

FIGURE 2.3: Transmission and reflection of plane waves (normal incidence) after changing mediums.

$$p_i(y;\omega) = P_i(\omega)e^{-ik_1 y} \tag{2.46}$$
$$p_r(y;\omega) = P_r(\omega)e^{ik_1 y} \tag{2.47}$$
$$p(y;\omega) = p_i(y;\omega) + p_r(y;\omega) \tag{2.48}$$

with $k_1 = \omega/c$ being the wave number in the medium 1. In the medium 2 just the transmitted wave is considered:

$$p_t(y;\omega) = P_t(\omega)e^{-iky} \tag{2.49}$$

with $k_2 = \omega/c_2$ being the wave number in the medium 2, with the exponent signs being properly chosen according to the wave propagation sense. The plane nature of these waves permits to establish the *stiffness* of the mediums as follows:

$$\frac{p_i}{v_i} = r_1 \; ; \; \frac{p_r}{v_r} = -r_1 \; ; \; \frac{p_t}{v_t} = r_2 \tag{2.50}$$

Note that the transmitted and the incident waves propagate with the same frequency ω but with different wave numbers, as a consequence of being in mediums with different wave propagation speed. In the inter-phase, the following conditions must be satisfied for every point and at every moment ($\forall x$, $\forall t$):

- **Equilibrium.** It demands that sound pressure at both sides of the inter-phase is the same:

$$p_i(0;\omega) + p_r(0;\omega) = p_t(0;\omega) \tag{2.51}$$

- **Continuity of velocities.** This ensures the contact between fluids:

$$v_i(0;\omega) + v_r(0;\omega) = v_t(0;\omega) \tag{2.52}$$

Dividing both latter expressions, the continuity of the *acoustic impedance* normal to the inter-phase ($y = 0$) is obtained:

$$\frac{p_i + p_r}{v_i + v_r} = \frac{p_t}{v_t} \tag{2.53}$$

and the substitution of (2.50) into (2.53) leads to:

$$r_1 \frac{p_i + p_r}{p_i - p_r} = r_2 \tag{2.54}$$

It is possible to obtain a relation between sound pressure and sound flux in the inter-phase by applying relations (2.34), (2.50) and (2.53):

$$\frac{dp}{dy} = -i\rho_0 \omega v = -ikr_1 v \tag{2.55}$$

$$\frac{p(0;\omega)}{v(0;\omega)} = -\frac{p(0;\omega)ikr_1}{\frac{dp}{dy}(0;\omega)} = \frac{p_t(0;\omega)}{v_t(0;\omega)} = r_2 \tag{2.56}$$

and finally:

$$\left(\frac{dp}{dy} = -ik\frac{r_1}{r_2}p\right)_{y=0} \tag{2.57}$$

and, in general, for any η direction perpendicular to the inter-phase:

$$\frac{dp}{d\eta} = -ik\beta p \tag{2.58}$$

where the boundary *admittance* $\beta = \frac{r_1}{r_2}$ has been introduced.

Expression (2.58) corresponds to the previously seen Robin boundary condition. It relates both the sound pressure and the flux pressure for partially absorbing boundaries and is of application when the medium 2 is a porous solid instead of a fluid. In this case, the specific acoustic impedance r_2 and, therefore, the admittance are normally complex numbers [115].

2.4 Determination of the acoustic impedance of partially absorbing boundaries. Delany and Bazley model [115]

The application of expression (2.58) as boundary condition on absorbing boundaries involves an estimation of the admittance β of the considered boundary. To do so, the model developed by Delany and Bazley [115], widely and successfully used over years in many works, arises as an adequate solution. These researchers propose an empiric relation to determine the boundary admittance for porous materials, typically used as absorbing materials. This relation is expressed below:

$$\frac{1}{\beta} = 1 + 9.08\left(10^3\frac{f}{\sigma}\right)^{-0.75} - i \cdot 11.9\left(10^3\frac{f}{\sigma}\right)^{-0.73} \tag{2.59}$$

where f represents the excitation frequency, in hertzs, and σ is the *air flow resistivity* of the porous material (the inverse to the medium permeability), expressed in Nsm^{-4} in SI units. This latter parameter only depends on the characteristics of absorbing material. The relationship (2.59) is intended for absorbing materials with considerable thickness and featuring values of σ ranging from 10^3 to $5x10^5$ Nsm^{-4}. However, very thin absorbing materials are normally used in many applications, particularly in coatings of reflective surfaces. In theses cases, the admittance of the boundary corresponds to the expression:

$$\beta_e = \beta \tanh(\gamma e) \tag{2.60}$$

being β the admittance value obtained from (2.59), e the thickness of the coating, in meters, and γ the wave number associated with the wave propagation across the absorbing medium. This latter variable responds to the following relationship:

$$\frac{\gamma}{k} = 10.3\left(10^3\frac{f}{\sigma}\right)^{-0.59} + i \cdot \left[1 + 10.8\left(10^3\frac{f}{\sigma}\right)^{-0.70}\right] \tag{2.61}$$

with k being the wave number of the wave propagation in air.

2.5 Acoustic magnitudes of interest

2.5.1 Sound pressure level

The acoustic pressure is an easily assessable variable. However, human ear does not respond linearly to the acoustic pressure but does it approximately linear to the received energy, with the acoustic energy being proportional to the square of the acoustic pressure.

The lowest acoustic pressure that can be detected by human ear corresponds to 20 μPa, while the highest bearable value before reaching pain tolerance is about 60 Pa. The pressure range is, as may be seen, fairly wide. The marked dynamic range of human ear suggests to use a compressed scale to properly represent it. Logarithmic scale fits more adequately than linear scale with the subjective response of human ear, by expressing the acoustic energy in units that better adapt to the ear nature. To avoid a too compressed scale, a multiplying factor of 10 is applied. By doing this, the *decibel* (dB) is defined.

The acoustic pressure level p is $\mathrm{L_p}$ decibels higher or lower than a specific reference pressure p_{ref} according to the following expression:

$$\mathrm{L_p} = 10 \log_{10} \frac{< p^2 >}{< p^2_{ref} >} \quad [\mathrm{dB}] \tag{2.62}$$

with $< p^2 >$ being the quadratic temporal mean value.

When absolute values (no relative ones) of the acoustic pressure are intended, the lowest acoustic pressure detected by human ear is used as reference. The obtained value is defined as *sound pressure level* (SPL):

$$\mathrm{SPL} = 10 \log_{10} \frac{< p^2 >}{(20 \cdot 10^{-6})^2} \tag{2.63}$$

$$\mathrm{SPL} = 10 \log_{10} < p^2 > +94 \quad [\mathrm{dB}] \tag{2.64}$$

As a reference, Table 2.1 enables one to have a notion about the acoustic annoyance levels associated with every SPL.

Table 2.1: Sonorous sensations and their corresponding sound pressure levels (SPL).

SPL (dB)	Noise source description	Sonorous sensation
0	Absolute threshold of hearing	-
20	Recording studio	Quite noiseless
40	Quite conversation	Noiseless
60	Restaurant, mall	Noisy
80	Scream, nearby highway	Noisy
100	Textile industrial chain	Very noisy
120	Ship engine room	Unbearable
140	Artillery fire at shoot location	Unbearable

2.5.2 Insertion loss coefficient

With the intention of impeding the natural propagation of the sound wave in the free field, road barriers are placed between the noise source and the intended protected area. This strategy leads to the attenuation of the acoustic energy behind the barrier according to the propagation direction (the so-called *shadow region*) as a consequence of the reflection of the incident wave on the obstacle (just a fraction of the incident wave is diffracted over the top of the barrier - the energy transmission across the barrier is negligible in practice -). The measurement in decibels of the referred sound loss is one of the most common strategies to assess the shielding efficiency of noise barriers. This represents the *insertion loss* (IL) by the barrier and determines the difference in acoustic pressure levels at a particular point of the domain in the situation before and after the inclusion of the screen:

$$\mathrm{IL} = \mathrm{SPL}_{\mathrm{Barrier}} - \mathrm{SPL}_{\mathrm{Half-space}} \tag{2.65}$$

$$\mathrm{IL} = 10\log_{10}\left(\frac{\mathrm{P}^2_{\mathrm{Barrier}}}{\mathrm{P}^2_{\mathrm{ref}}}\right) - 10\log_{10}\left(\frac{\mathrm{P}^2_{\mathrm{Half-space}}}{\mathrm{P}^2_{\mathrm{ref}}}\right) \tag{2.66}$$

$$\mathrm{IL} = 10\log_{10}\left(\frac{\mathrm{P}^2_{\mathrm{B}}}{\mathrm{P}^2_{\mathrm{HS}}}\right) \tag{2.67}$$

$$\mathrm{IL} = 20\log_{10}\left(\frac{\mathrm{P}_{\mathrm{B}}}{\mathrm{P}_{\mathrm{HS}}}\right) \tag{2.68}$$

with $\mathrm{P_B}$ and $\mathrm{P_{HS}}$ being the acoustic pressure assessed at a particular point in the situation with an without considering the inclusion of the barrier, respectively. As can be noted, IL values are, most of the times, negatives in the shadow region, as the sound pressure in the free field is expected to be higher with respect to the scenario with the presence of the barrier.

2.5.3 Broadband insertion loss

With the purpose of representing in a number the global efficiency of the barrier along the whole range of frequencies under study, the *broadband insertion loss* ($\mathrm{IL_{total}}$) takes into consideration the complex, subjective response of human ear in such evaluation. Thus, the assessment of this parameter for a particular point of the domain is easily accomplished once both the screening performance of the barrier and the corrections introduced (in terms of decibels) to better represent the human perception of sound levels at each frequency are known for the considered spectrum:

$$\mathrm{IL_{total}} = -10 \cdot \log_{10}\left(\frac{\sum_{\mathrm{i}=1}^{\mathrm{NF}} 10^{(\mathrm{A_i}-\mathrm{IL_i})/10}}{\sum_{\mathrm{i}=1}^{\mathrm{NF}} 10^{\mathrm{A_i}/10}}\right) [\mathrm{dB(A)}] \qquad (2.69)$$

with NF being the number of frequencies considered, $\mathrm{A_i}$ the A-weighted noise level according to the noise spectrum (see Table (2.3) and (2.4) as examples), and $\mathrm{IL_i}$ the insertion loss value for sources pulsing at every frequency, in agreement with (2.68).

2.6 Frequency noise characterization

The frequency range associated with a healthy human varies, as previously seen, from approximately 20 to 20 000 Hz. Such a quite wide range covers a large variety of *noise* that, in general, is comprised of many different acoustic components featuring different vibes according to the frequency to which they belong (within the audible frequency range). Noise characterization demands, therefore, to know the sound pressure level associated to each mono-frequency component. In practice, however, the extensive nature of the cited audible range recommends to assemble the information in *bands* of frequencies. In this way, each frequency band (of variable amplitude) represents all frequencies enclosed in such a band. The resulting noise is in practice well represented if the intensity acoustic level associated with each band of the whole audible range is known. This is what is known as *noise spectrum*. Depending on the width of the bands, these can be categorized as one-octave, one-third, one-fifteenth, etc., bands. A band has a width of one-octave when the highest frequency value, in hertzs, of such a band is twice the lowest value.

2.6.1 One-third octave bands spectrum

If the logarithmic scale band is evenly divided into three, a one-third octave band is obtained. Every band is then represented by its central frequency value. Although the definition of these frequency bands may be a quite open issue, the fact is that the International Standard Organization (ISO) recommends the harmonization of bands used in acoustics.

Table 2.2 represents the octave and one-third octave bands for a specific frequency range.

TABLE 2.2: Octave bands, one-third octave bands and their corresponding central frequencies.

Band nº	Octave band central frequency	1/3 octave band central frequency	Band limits	
			Lower	Higher
17		50	44	57
18	63	63	57	71
19		80	71	88
20		100	88	113
21	125	125	113	141
22		160	141	176
23		200	176	225
24	250	250	225	283
25		315	283	353
26		400	353	440
27	500	500	440	565
28		630	565	707
29		800	707	880
30	1 000	1 000	880	1 130
31		1 250	1 130	1 414
32		1 600	1 414	1 760
33	2 000	2 000	1 760	2 250
34		2 500	2 250	2 825
35		3 150	2 825	3 530
36	4 000	4 000	3 530	4 400
37		5 000	4 400	5 650

However, as previously mentioned, human ear does not respond equally to all audible frequencies. The marked subjective character of the sonorous sensitivity is not only dependent on the acoustic pressure but also to the frequency. Thus, a particular sound at a certain frequency may be more unpleasant than other featuring the same sound intensity but with different frequency. That is why some corrections (or weights) are introduced in frequency spectra, so that the final value may better reflect the subjective way that frequencies affect us. The A-weighting, the most common used standard weighting of the audible frequencies, has been proposed to properly reflect the response of the human ear to noise. In other words, the A-weighted value of a noise source is an approximation to how the human ear perceives the noise. Measurements made using this type of correction are expressed in terms of dB(A), to show that noise is characterized in terms of A-weighted decibels. Table 2.3 collects the corrections corresponding to the A-weighting normalized traffic noise spectrum, generating pure tones ranging from 100 to 5 000 Hz corresponding to one-third center band frequencies, used by the UNE-EN 1793 standard [117].

2.6.2 One-fifteenth octave bands spectrum

The election of one-third octave bands is normally adequate for covering the information relative to each frequency band. In cases in which the noise level along the spectrum is strongly frequency-dependent this discretization, however, may be not enough and the consideration of narrower bandwidth is advisable instead. To properly represent the noise information along the finer spectrum, the weights associated to such narrower bands must be calculated. As the *intensity sound level* (ISL) of each band remains constant (see Figure 2.5), the new corrections are obtained straightforward according to:

$$\mathrm{A_i} = \mathrm{ISL_i} + 10\log_{10} w_i \tag{2.70}$$

with w_i being the considered width of the new band. As an example, Table 2.4 collects the corrections associated to every 1/15 octave interval after expanding the normalized 1/3 octave band spectrum considered in Table 2.3.

TABLE 2.3: Corrections (A_i) for the A-weighting normalized traffic noise spectrum by the UNE-EN 1793 standard [117], bandwidth (w_i) and intensity sound level (ISL_i) of each center band frequency.

f_i [Hz]	Band limits		A_i [dB]	w_i [Hz]	ISL_i [dB]
	f_i^{upper}	f_i^{lower}			
100	88	113	-20	25	-33.98
125	113	141	-20	28	-34.47
160	141	176	-18	35	-33.44
200	176	225	-16	49	-32.90
250	225	283	-15	58	-32.63
315	283	353	-14	70	-32.45
400	353	440	-13	87	-32.40
500	440	565	12	125	-32.97
630	565	707	-11	142	-32.52
800	707	880	-9	173	-31.38
1000	880	1 130	-8	250	-31.98
1250	1 130	1 414	-9	284	-33.53
1600	1 414	1 760	-10	346	-35.39
2000	1 760	2 250	-11	490	-37.90
2500	2 250	2 825	-13	575	-40.60
3150	2 825	3 530	-15	705	-43.48
4000	3 530	4 400	-16	870	-45.40
5000	4 400	5 650	-18	1250	-48.97

Table 2.4: A-weighting one-fifteenth noise spectrum derived from the normalized one by the UNE-EN 1793 standard [117] for one-third octave bands. Corrections $\mathrm{A_i}$, bandwidth (w_i) and intensity sound level ($\mathrm{ISL_i}$) of each center band frequency.

$\mathrm{f_i}$ [Hz]	Band limits		w_i [Hz]	$\mathrm{ISL_i}$ [dB]	$\mathrm{A_i} = \mathrm{ISL_i} + 10\log_{10} w_i$ [dB]
	f_i^{upper}	f_i^{lower}			
100	97	102	5	-33.98	-27
104	102	107	5	-33.98	-27
109	107	112	5	-33.98	-27
114	112	117	5	-34.47	-27
120	117	122	5	-34.47	-27
125	122	128	5	-34.47	-27
131	128	134	6	-34.47	-27
137	134	141	7	-34.47	-26
144	140	147	7	-33.44	-25
151	147	154	7	-33.44	-25
158	154	161	7	-33.44	-25
165	161	169	8	-33.44	-25
173	169	177	8	-33.44	-24
⋮	⋮	⋮	⋮	⋮	⋮
2895	2828	2962	134	-43.48	-22
3031	2962	3102	140	-43.48	-22
3150	3102	3249	147	-43.48	-22
3325	3249	3403	154	-43.48	-22
3482	3403	3564	161	-43.48	-21
3647	3564	3732	168	-45.40	-23
3819	3732	3909	177	-45.40	-23
4000	3909	4093	184	-45.40	-23
4189	4093	4287	194	-45.40	-23
4387	4287	4490	203	-45.40	-22
4595	4490	4702	212	-48.97	-26
4812	4702	4925	223	-48.97	-25
5000	4925	5157	232	-48.97	-25

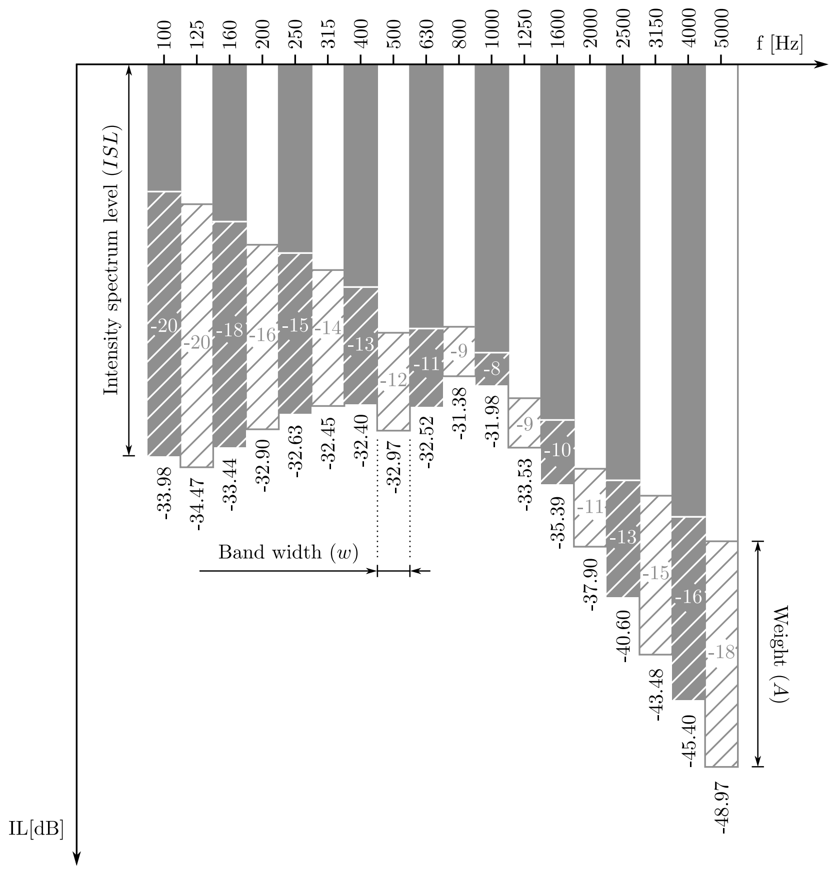

FIGURE 2.4: One-third octave bands and corresponding corrections according to the normalized traffic noise spectrum by the UNE-EN 1793 standard [117].

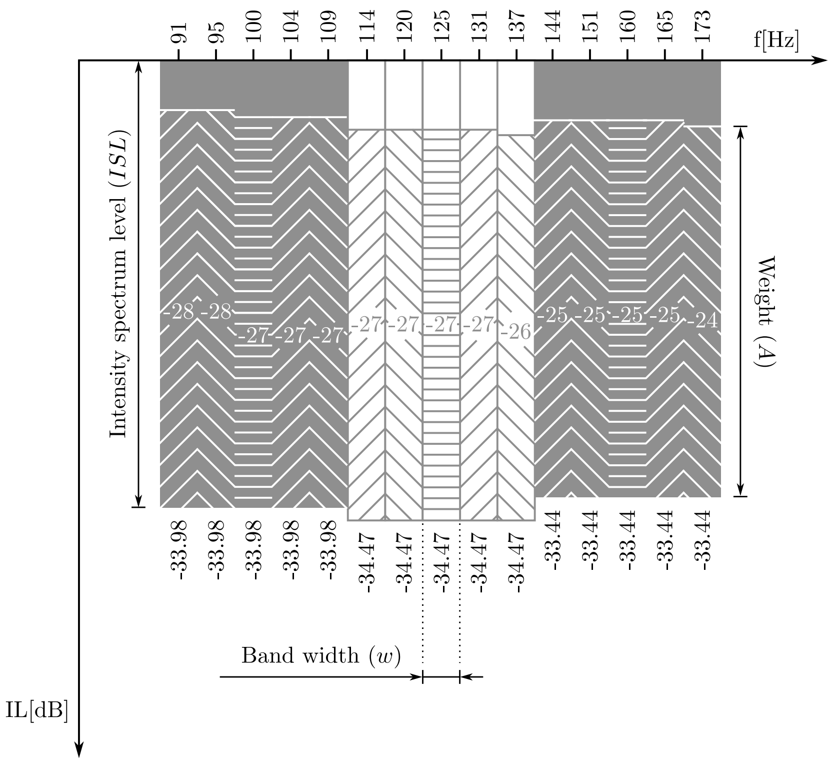

FIGURE 2.5: Some one-fifteenth octave bands and corresponding corrections after expanding the normalized traffic noise spectrum by the UNE-EN 1793 standard [117] .

3. DUAL BOUNDARY ELEMENTS FORMULATION

The improvement of the acoustic performance of standard, commonly used road barriers without increasing the effective height is a challenging task. These simplest form of noise barriers are based, very often, on a simple vertical screen. Although such configurations can perform well under particularly good conditions, the fact is that the noise reduction by diffraction associated with these highly reflective barriers is almost negligible. There is then a real need of proposing alternative shapes that raises the shielding efficiency of these regular barriers. In this direction, some designs have been proposed over the past years with varying degrees of success. Generally speaking, it was found that configurations showing higher levels of sound reduction were those presenting some kind of modification on the barrier top, e.g., tilted, multiple-edge, T-, Y-, M-, cylinder-, arrow-shaped barriers, etc. Other more complex designs have addressed the issue by considering well-based designs on the basis of sequence number series, such as Maximum Length Sequence (MLS), Quadratic Residue Diffuser (QRD), Primitive Roots Diffuser (PRD), etc.

The geometric nature of many of the aforementioned designs is diverse. Some of them are very thin barriers whose section along the overall configuration can be idealized as a *single-wire* body, for shielding efficiency unaffected by such simplification of reality. In other cases, the road barrier is comprised of a general volumetric configuration featuring very thin elements eligible of geometric simplification, as commented above, in which the section is neglected.

The appropriate treatment of these designs from Boundary Elements (BE) demands an approach that permits to overcome the main drawbacks arising from the direct application of the standard formulation of the Boundary Element Method (BEM). In this respect, the so-called Dual BEM approach arises as the most appropriate strategy involving BE to address the subject by 1) mitigating the fictitious eigenfrequencies revealed when dealing with volumetric structures and 2) permitting to consider the idealization of very thin elements as single-wire bodies. Both difficulties have strong presence in the barrier models studied in this work.

Depending on the geometric nature, this approach is applied differently. The features of the classical, the hypersingular and the Dual BEM formulations (according to the different approaches) are described in detail in the next sections.

3.1 Singular boundary integral equation (SBIE). Classical BEM formulation

The SBIE for the boundary point i to be solved by BEM can be expressed as follows:

$$c_i p_i + \fint_{\Gamma} p \frac{\partial G(k,r)}{\partial n_j} \, d\Gamma = G_0(k,r) + \int_{\Gamma} \frac{\partial p}{\partial n_j} G(k,r) \, d\Gamma \tag{3.1}$$

This integral equality just involves the boundary of the barrier under investigation. The $\fint$ symbol represents the integral along the boundary to be understood in the Cauchy principal value sense, once the singularity around the collocation point i has been extracted (c_i), as shown in Figure 3.1. In (3.1), p is the acoustic pressure field over the barrier surface and $G(k,r)$ is the half-space fundamental solution (the acoustic pressure field when the source is placed at the collocation point i over a plane with admittance β_g - ground admittance -) and c_i is the free term. As a general rule: $c_i = \theta/2\pi$, where θ represents the inner angle to the boundary measured in radians. It is easily shown that $c_i = 0.5$ for smooth boundaries.

The expressions of the fundamental solution and its derivative for a perfectly reflecting ground ($\beta_g = 0$) for bi-dimensional, harmonious problems are:

$$G(k,r) = \frac{1}{2\pi} \left[K_0(ikr) + K_0(ik\overline{r}) \right] \tag{3.2}$$

$$\frac{\partial G(k,r)}{\partial n_j} = -\frac{ik}{2\pi} \left[K_1(ikr) \frac{\partial r}{\partial n_j} + K_1(ik\overline{r}) \frac{\partial \overline{r}}{\partial n_j} \right] \tag{3.3}$$

being i the imaginary unit, k the wave number and r, $\overline{r}$ the distances to the observation point from the collocation point and its symmetric point with respect to the ground plane, respectively (see Figure 3.1). K_0 and K_1 are the Bessel modified functions of order 0 and 1, respectively.

By applying (3.1) on a node i of the boundary discretization and interpolating the variable with quadratic elements, the following can be written:

$$c_i \cdot p_i + \sum_{k=1}^{NE} \sum_{l=1}^{3} p_l^k \cdot h_l^{ik} = p_0^* + \sum_{k=1}^{NE} \sum_{l=1}^{3} q_l^k \cdot g_l^{ik} \tag{3.4}$$

with NE being the overall number of elements. The repeated application of (3.1) on each node of the boundary discretization leads to the following system of equations:

$$(\mathbf{C}^s + \mathbf{H}) \cdot \mathbf{P} = \mathbf{G} \cdot \mathbf{Q} + \mathbf{G_0} \tag{3.5}$$

where $\mathbf{C}^s$ is a diagonal matrix whose entries involve the free term values at the nodes of the discretization, $\mathbf{P}$, $\mathbf{Q}$ are the pressure and the flux (the derivative of the pressure with respect to the normal at each boundary node) vectors, $\mathbf{G_0}$ vector stores the values of the fundamental solution concerning the external noise source and $\mathbf{H}$, $\mathbf{G}$ are matrices whose entries are associated with the integration cores of the BEM formulation, involving just the variables of the problem along the barrier boundary:

$$h_l^{ik} = \int_{\Gamma_k} \frac{\partial G(k,r)}{\partial n_k} \, \phi_l \, d\Gamma_k \quad ; \quad g_l^{ik} = \int_{\Gamma_k} G(k,r) \, \phi_l \, d\Gamma_k \tag{3.6}$$

with i being the collocation point, k the element under integration and ϕ_l the shape functions with quadratic approximation of the local variable ξ along the element under integration, both to get the acoustic pressure level along the boundary (3.7) and to fit the barrier profile (isoparametric elements). The sound pressure in the element k can be then expressed as follows:

$$p^k = \sum_{l=1}^{3} \phi_l \, p_l^k = \phi_1 \, p_1^k + \phi_2 \, p_2^k + \phi_3 \, p_3^k \tag{3.7}$$

being:

$$\begin{aligned} \phi_1(\xi) &= \frac{1}{2} \xi \, (\xi - 1) \\ \phi_2(\xi) &= 1 - \xi^2 \\ \phi_3(\xi) &= \frac{1}{2} \xi \, (\xi + 1) \end{aligned} \tag{3.8}$$

3.2 Hyper-singular boundary integral equation (HBIE)

The HBIE for the boundary point i to be solved by BEM can be written as follows:

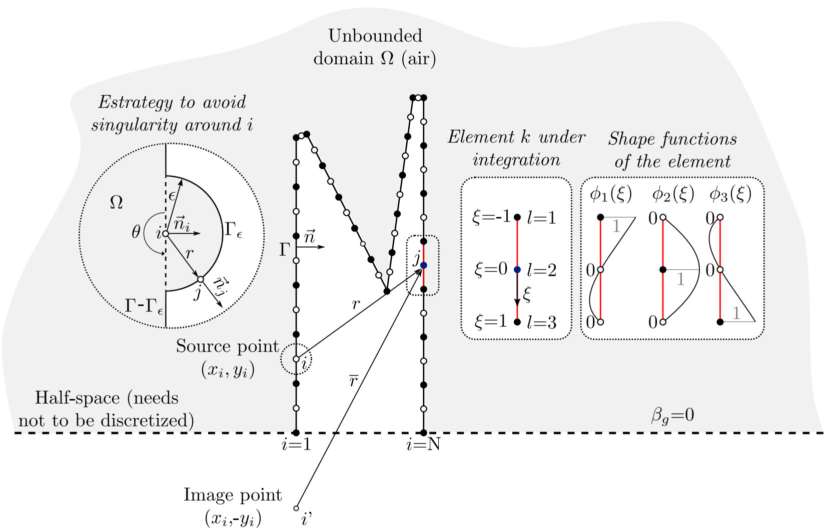

FIGURE 3.1: Source-image collocation after discretization of a M-shaped barrier with quadratic elements (3 nodes). Integration over a generic element k. The collocation point is denoted by i while the observation point in the element under integration is denoted by j (after element discretization with Gauss point distribution).

$$c_i\left(\frac{\partial p_i}{\partial n_i}\right)+\,=\!\!\!\!\!\!\int_\Gamma p\frac{\partial^2 G(k,r)}{\partial n_i \partial n_j}d\Gamma = -\!\!\!\!\!\!\int_\Gamma \frac{\partial G(k,r)}{\partial n_i}\frac{\partial p}{\partial n_j}d\Gamma + \frac{\partial G_0(k,r)}{\partial n_i} \tag{3.9}$$

where the $=\!\!\!\!\!\int$ and $-\!\!\!\!\!\int$ symbols represent the integral along the boundary to be understood in the Hadamard finite part integral and in the Cauchy principal value sense, respectively. As the Hölder condition [118] must be satisfied at the collocation point i, the numerical treatment of the hyper-singular formulation can be conducted either 1) by using discontinuous boundary elements or 2) by moving the source towards inside the element in a non-nodal point (see Figure 3.3). In both strategies and in all situations $c_i = 0.5$ in (3.9).

Expressions (3.10) and (3.11) show the values of the derivatives of the fundamental solution implied in the hyper-singular integral equation (3.9):

$$\frac{\partial G(k,r)}{\partial n_i} = -\frac{ik}{2\pi}\left[K_1(ikr)\,\frac{\partial r}{\partial n_i} + K_1(ik\overline{r})\,\frac{\partial \overline{r}}{\partial n_I}\right] \tag{3.10}$$

$$\begin{aligned}\frac{\partial^2 G(k,r)}{\partial n_i \partial n_j} = \frac{(ik)^2}{2\pi}&\left[\left(K_2(ikr)\,\frac{\partial r}{\partial n_i}\frac{\partial r}{\partial n_j} + \frac{1}{r}\,K_1(ikr)\,n_i\cdot n_j\right) + \right.\\ &\left.\left(K_2\,(ik\overline{r})\frac{\partial \overline{r}}{\partial n_I}\frac{\partial \overline{r}}{\partial n_j} + \frac{1}{\overline{r}}\,K_1(ik\overline{r})\,n_I\cdot n_j\right)\right]\end{aligned} \tag{3.11}$$

As in (3.1), i is the imaginary unit, k the wave number and r, $\overline{r}$ the distances to the observation point from the collocation point and its symmetric point with respect to the ground plane, respectively. It is worth making a distinction here regarding the normal vectors involved in the expressions above. n_j is the normal to the boundary at the integration point and n_i (n_x^i, n_y^i), n_I $(n_x^i,\text{-}n_y^i)$ represent the normal vectors to the real boundary at the collocation point (i) and at its symmetric point (I) placed on a fictitious, symmetric boundary with respect to the ground plane, respectively. K_1 and K_2 represent the Bessel modified functions of order 1 and 2, respectively.

By applying (3.9) on a node i of the boundary discretization and interpolating the variable with quadratic elements, the following can be written:

$$c_i\cdot q_i + \sum_{k=1}^{NE}\sum_{l=1}^{3} p_l^k\cdot m_l^{ik} = \frac{\partial G_0(k,r)}{\partial n_i} + \sum_{k=1}^{NE}\sum_{l=1}^{3} q_l^k\cdot l_l^{ik} \tag{3.12}$$

with NE being the overall number of elements. The repeated application of (3.9) on each node of the boundary discretization, as in the classical formulation, leads to the following system of equations:

$$\mathbf{M}\cdot\mathbf{P} = \left(\mathbf{L} - \mathbf{C}^h\right)\cdot\mathbf{Q} + \frac{\partial \mathbf{G_0}}{\partial n_i} \tag{3.13}$$

where $\mathbf{C}^h$ is a diagonal matrix with entry values of 0.5, $\mathbf{P}$, $\mathbf{Q}$ are the pressure and the flux (the derivative of the pressure with respect to normal at each boundary node) vectors, $\frac{\partial \mathbf{G_0}}{\partial n_i}$ array stores the values of the derivative of the fundamental solution concerning the external noise source, and

$\mathbf{M}$, $\mathbf{L}$ are matrices whose entries are associated with the integration cores of the hyper-singular BEM formulation involving just the variables of the problem along the barrier boundary:

$$m_l^{ik} = \int_{\Gamma_k} \frac{\partial^2 G(k,r)}{\partial n_i \, n_j} \, \phi_l \, d\Gamma_k \quad ; \quad l_l^{ik} = \int_{\Gamma_k} \frac{\partial G(k,r)}{\partial n_i} \, \phi_l \, d\Gamma_k \tag{3.14}$$

with i being the collocation point, k the element under integration and ϕ_l the shape functions with quadratic approximation, with ξ representing the local coordinate within the element with side limits (-1, 1) (see Figure 3.3).

The numerical strategies employed in the evaluation of both the singular and the hyper-singular BEM integrals have been developed and implemented in a computer code by following the patterns proposed by Sáez et al. [119].

3.3 Dual BEM formulation

Once the SBIE and the HBIE have been presented, the following subsections focus on the different approaches involving the combined use of these formulations in the so-called Dual BEM formulation. As previously stated, this variant of the BEM is the most appropriate strategy from the Method for the treatment of the road barriers assessed in this document.

3.3.1 Approach for avoiding fictitious eigenfrequencies

Some undesirable problems may arise at certain frequencies when dealing with volumetric elements in exterior problems. These mathematically-related effects reveal the eigenfrequencies of the interior acoustic problem (the eigenvalues of the classical BEM matrices) and may seriously distort the screening performance of the barrier. An appropriate solution to this problem is that derived from the formulation proposed by Burton and Miller [109] for the exterior problem featuring a fictitious resonances-free solution. This formulation is based on the combined use of both the SBIE and the HBIE coupled by a frequency-related complex value (α). In this case, the expression for the boundary point i to be solved by BEM can be written then:

$$0.5\,(p_i + \alpha\, q_i) + \sum_{j=1}^{N} (h_j + \alpha\, m_j)\; p_j = \sum_{j=1}^{N} (g_j + \alpha\, l_j)\; q_j + \left(G_0 + \alpha\,\frac{\partial G_0}{\partial n_i}\right) \tag{3.15}$$

In (3.15), p is the acoustic pressure field over the barrier surface, q is the flux (the derivative of the pressure with respect to the normal at each boundary node) and G_0 and $\frac{\partial G_0}{\partial n_i}$ the half-space fundamental solution and its derivative concerning the external noise source, respectively. Finally, h and g are the integration cores of the BEM formulation and l and m the integration cores of the hiper-singular one, involving just the variables of the problem along the barrier boundary with N nodes after the discretization process. The most commonly used value for the coupling parameter is found to be $\alpha = i/k$ [120, 121], being i the imaginary unit and k the wave number. The hyper-singular formulation of the method demands the collocation point j to be inside the element. This way, the free term is assumed as 0.5 in all cases.

The absorptive capacity of the barrier boundary is usually determined by means of the Robin boundary condition, so the pressure value and its derivative at each node are related:

$$q_j = -i\,k\,\beta_\Gamma\,p_j \tag{3.16}$$

This way, (3.15) can be written matricially:

$$[0.5\;(1+\beta)\;\mathbf{I} + \mathbf{H} + (i/k)\,\mathbf{M}\; + (i\,k\,\mathbf{G} - \mathbf{L})\;\beta] \cdot \mathbf{P} = \mathbf{G_0} - (i/k)\,\frac{\partial \mathbf{G_0}}{\partial n_i} \tag{3.17}$$

with $\mathbf{I}$ being the identity matrix.

3.3.2 Approach for the idealization of for very thin elements as single-wire bodies

The nature of the issue is different when dealing with very thin bodies. In this case, numerical integration problems may appear affecting, equally, to the barrier performance. The idealization of such boundaries as non-thickness bodies not only solves the problem but also contributes to ease their geometric representation. With this aim, the SBIE and the

HBIE are applied separately ([47, 54]). Figure 3.2 facilitates comprehension. The boundaries at both sides of the idealized null-thickness bodies are represented by the discretization, with disparate values of acoustic pressure and flux. The application of the classic formulation of the method, based on the SBIE applied at both sides of null-width elements, yields a singular system of equations that does not allow the solution of the problem to be obtained. However, the use of both the SBIE and the HBIE (hyper-singular boundary integral equation) leads to a Dual BEM formulation that offers a proper solution to address this issue.

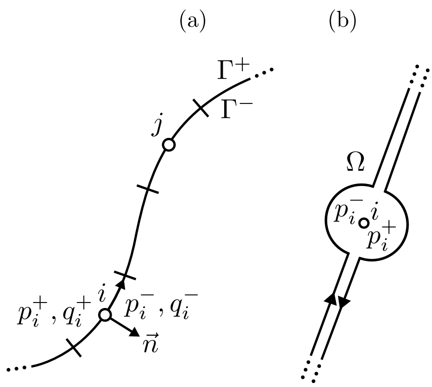

FIGURE 3.2: (a) Geometric idealization as single-wire configuration of a barrier featuring a very thin section. (b) Strategy used to avoid the singularity around the collocation point in the Dual approach for the treatment of elements idealized as null-thickness type (see e.g. [95, 122]).

Figure 3.2(a) represents an idealization of a generic thin body to be solved by the Dual BEM formulation. After a discretization process, each node holds the values of pressure and flux with respect to the boundary normal (p^+, q^+, p^-, q^- hereinafter). The strategy used to isolate the singularity of the method in this type of domains can be seen in Figure 3.2(b) [95, 122]. Thus, the BEM expression for these boundaries can be written as follows:

$$0.5\left(p_i^+ + p_i^-\right) + \sum_{j=1}^{N}\left(H_j^+ p_j^+ + H_j^- p_j^-\right) = \sum_{j=1}^{N}\left(G_j^+ q_j^+ + G_j^- q_j^-\right) + G_0(k,r) \tag{3.18}$$

being N the overall nodes number of the discretization over the boundary. Taking into account that $n^+ = -n^-$, it is easily shown that:

$$H_j^+ = -H_j^- \quad ; \quad G_j^+ = G_j^- \tag{3.19}$$

Considering the Robin boundary condition (3.16), the following matrix expression is obtained:

$$(0.5\,\mathbf{I}^* \; + \mathbf{H} + i\,k\,\beta\,\mathbf{G}) \cdot \mathbf{P} = \mathbf{G}_0 \tag{3.20}$$

being $\mathbf{I}^*$ a matrix with the following form:

$$\mathbf{I}^* = \begin{bmatrix} 1 & 1 & 0 & 0 & 0 & 0 & \cdots & 0 & 0 \\ 0 & 0 & 1 & 1 & 0 & 0 & \cdots & 0 & 0 \\ \vdots & \vdots & \vdots & \vdots & \vdots & \vdots & \vdots & \vdots & \vdots \\ 0 & 0 & 0 & 0 & 0 & 0 & \cdots & 1 & 1 \end{bmatrix} \tag{3.21}$$

that allows us to consider the contribution of the free term at both sides of the discretization nodes.

As previously mentioned, the application of the SBIE at each collocation point of the discretization (nodes) yields an incompatible system of equations (two unknowns exist for each node), making the problem intractable. However, the application of the HBIE as a complementary formulation permits us to address the subject successfully by introducing the remaining equations that allows the problem to be solved. The hypersingular expression concerning these types of geometries is then obtained:

$$0.5\left(\frac{\partial p_i^+}{\partial n_i^+} + \frac{\partial p_i^-}{\partial n_i^+}\right) + \sum_{j=1}^{N}\left(M_j^+ p_j^+ + M_j^- p_j^-\right) = \sum_{j=1}^{N}\left(L_j^+ q_j^+ + L_j^- q_j^-\right) \tag{3.22}$$

where:

$$\frac{\partial p_i^-}{\partial n_i^+} = -q_i \quad ; \quad M_j^+ = -M_j^- \quad ; \quad L_j^+ = L_j^- \tag{3.23}$$

Considering the Robin boundary condition (3.16), the following matrix expression can be written:

$$[i\,k\,\beta\,(0.5\,\mathbf{I}^{*}+\mathbf{L})+\mathbf{M}]\cdot\mathbf{P}=\frac{\partial\mathbf{G_0}}{\partial n_i} \tag{3.24}$$

Finally, gathering expressions (3.20) and (3.24) the following matritial system is obtained for the proper assessment of noise barrier configurations idealized as bodies with null section:

$$\begin{bmatrix} 0.5\,\mathbf{I}^{*}\;+\mathbf{H}+i\,k\,\beta\,\mathbf{G} \\ \\ i\,k\,\beta\,(0.5\,\mathbf{I}^{*}+\mathbf{L})+\mathbf{M} \end{bmatrix}\cdot\left\{\mathbf{P}\right\}=\left\{\begin{matrix}\mathbf{G_0} \\ \\ \dfrac{\partial\mathbf{G_0}}{\partial n_i}\end{matrix}\right\} \tag{3.25}$$

3.3.3 Approach for volumetric configurations featuring very thin bodies idealized as null sections

This general Dual BEM approach incorporates both versions of the Dual formulation, permitting us to assess the shielding efficiency of road barriers based on volumetric structures featuring very thin elements. According to some of the expressions obtained in previous sections and denoting:

$$\mathbf{A_1} = 0.5\,(1+\beta)\,\mathbf{I}+\mathbf{H}+(i/k)\,\mathbf{M}+(i\,k\,\mathbf{G}-\mathbf{L})\,\beta \tag{3.26}$$

$$\mathbf{A_2} = 0.5\,\mathbf{I}^{*}\;+\mathbf{H}+i\,k\,\beta\,\mathbf{G}\;\;;\;\;\mathbf{A_3}=i\,k\,\beta\,(0.5\,\mathbf{I}^{*}+\mathbf{L})+\mathbf{M} \tag{3.27}$$

$$\mathbf{B_1} = \mathbf{G}_0-(i/k)\,\frac{\partial\mathbf{G_0}}{\partial n_i}\;\;;\;\;\mathbf{B_2}=\mathbf{G}_0\;\;;\;\;\mathbf{B_3}=\frac{\partial\mathbf{G_0}}{\partial n_i} \tag{3.28}$$

the final Dual BEM matrix expression for barriers with thin and non-thin bodies may be written as follows:

$$\begin{bmatrix}\mathbf{A_1}\\ \mathbf{A_2}\\ \mathbf{A_3}\end{bmatrix}\cdot\left\{\mathbf{P}\right\}=\begin{Bmatrix}\mathbf{B_1}\\ \mathbf{B_2}\\ \mathbf{B_3}\end{Bmatrix} \tag{3.29}$$

In (3.29), $\mathbf{A_1}$ is a $N_{Thick}\,x\,N_{Unk}$ matrix and $\mathbf{A_2}$, $\mathbf{A_3}$ are $N_{Thin}\,x\,N_{Unk}$ ones. In this case, N_{Thick} and N_{Thin} represent the number of nodes involving the discratization of elements with real sections and those idealized as null-thickness type, respectively, while N_{Unk} is the unknowns of the problem ($N_{Thick} + 2xN_{Thin}$). In accordance with this nomenclature, $\mathbf{P}$ is a N_{Unk}-dimension array that stores the pressure values according to the barrier discretization, $\mathbf{B_1}$ is a N_{Thick}-dimension array and $\mathbf{B_2}$, $\mathbf{B_3}$ are N_{Thin}-dimension ones.

3.4 Sound pressure in the domain

Once the variables on the barrier boundary are known, the acoustic pressure values at any internal point (receiver position) can be easily obtained, as usual, by applying the standard BEM formulation:

$$p^i = G_0(k,r) - \sum_{j=1}^{N_{Unk}} (h_j + i\,k\,\beta\,g_j)\;p_j \tag{3.30}$$

3.5 Discretization criterion applied

At this point it is important to note that the discretization process is frequency-dependent. In this regard, all simulations in this work have been performed with barrier boundary discretization featuring four elements per wavelength at least. A good convergence of results by applying this meshing criterion has been observed in previous numerical experiments carried out by the researcher of this work. Furthermore, this criterion is in line with other works [7, 123].

Some special procedures to tackle both sharp-angled boundaries and sharp angles between boundaries are considered. In order to assure the convergence of the numerical integrations of nearly singular integrals, the computing code used in this work implements two strategies. One of them is based on the procedure proposed by Telles [124], consisting in the reallocation and concentration of the Gauss points around the point with the minimum r distance within the element under integration. The other strategy consists in the subdivision of the associated element from the barrier discretization into multiple sub-intervals, depending on the minimum r distance to the quasi-singular point. The final result is the overall sum of the numerical integration applied to each sub-interval of the element.

3.6 Collocation point strategy performed

As for the SBIE formulation, the code that implements this formulation for the studies of this work makes use of nodal collocation with the exception of the nodes placed at non-connected extremes of boundaries, where a non-nodal collocation strategy is employed.

Figure 3.3 represents the strategy used in the implementation of the hyper-singular BEM formulation when assessing the acoustic efficiency of the road barriers presented in this document. As previously mentioned, a non-nodal collocation is required in the extreme nodes of the elements. Extensive references concerning the choice of δ value can be found in scientific literature (e.g., [123, 125]) for discontinuous elements.

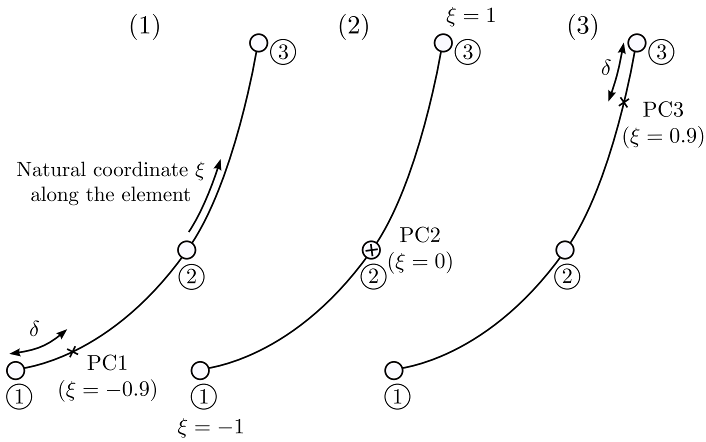

FIGURE 3.3: Non nodal collocation points at the bound limits of the element when dealing with the hyper-singular BEM formulation: (1) collocation point PC1; (2) collocation point PC2; (3) collocation point PC3.

For the cases here presented, the collocation point strategy has been carried out with a well-proven distance of $\delta = 5\%$ of the element length for the point displacement towards inside. The election of this value has been substantiated by previous numerical experiments carried out by the authors of this work. Even so, differences in results associated with the election of δ (within the framework of the ranges used in the bibliography) are not significant, particularly given the fact that sound pressure levels of interest here are those neither at the barrier boundaries nor at the barrier corners but at the receiver points.

3.7 Validation studies

This section collects the validation cases conducted of the Dual BEM approaches introduced above. Analyses are presented in terms of the acoustic behavior of road barriers when assessed both with the reference classical BEM formulation and with the corresponding Dual BEM approach.

The need of implementing the Dual BEM formulation when dealing with volumetric structures is clarified in Figure 3.4. As easily observable, the Dual BEM approach provides an efficient, adequate solution to avoid the resonance frequencies associated with the inner structure of the barrier. In spite of the problems studied here are outdoor-type, these fictitious frequencies are revealed when applying the standard formulation of the Method, greatly distorting the shielding efficiency (high peak values of IL in the graphic) of the barrier at such frequencies. The importance of the issue is undisputed, especially within an optimization process where the best individuals may be selected according to this unrealistic screening performance.

The convenience of representing very thin road barriers as single-wire bodies is highlighted in Figure 3.5. In this case, the Dual BEM approach greatly eases the geometry generation of the barrier profile when compared with the real representation. This effect is more noticeable as the topological complexity of the barrier increases. Besides, and no less important, the idealization of very thin sections as null-thickness type helps mitigate numerical integration problems that may appear when dealing with quasi-singular points. As observed in the graphic, this latter issue, however, is not of concern for this particular case.

Finally, Figure 3.6 represents the acoustic performance evolution derived from the analysis of a road barrier previously studied in the literature by Monazzam et al. [13] (the so-called Quadratic Residue Difffuser (QRD) top). In accordance with the results presented in such work, the validation is performed on the basis of 1/15 octave band center frequencies. The Dual BEM approach proposed is truly convenient when dealing with complex configurations eligible for some sort of geometric simplification, as in the presented case. For the ease of viewing, the general volumetric structure of the QRD-based barrier is represented in blue, while very thin sections are idealized as single-wire bodies and depicted in red. As observed in the graph, despite the differences observed at some frequencies, results derived from the Dual BEM formulation agree well with numerical outcomes from the aforementioned work with the standard BEM formulation.

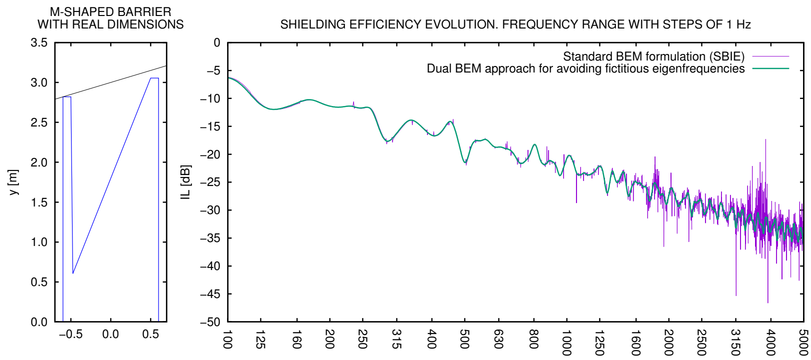

FIGURE 3.4: Validation of the Dual BEM approach in a volumetric M-shaped barrier. Noise source and receiver are located at (-10.0, 0.0) and at (50.0, 0.0), respectively.

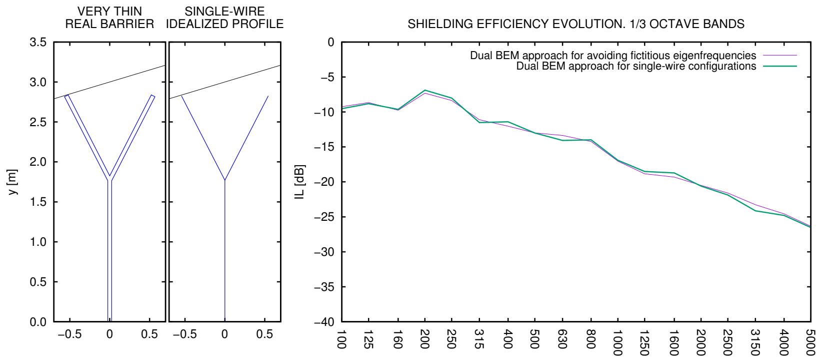

FIGURE 3.5: Validation of the formulation in a benchmark very thin Y-shaped barrier. Noise source and receiver are located at (-10.0, 0.0) and at (50.0, 0.0), respectively.

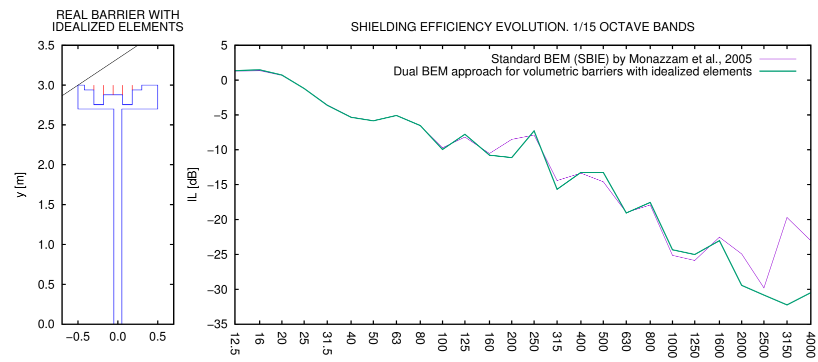

FIGURE 3.6: Validation of the presented Dual BEM formulation for volumetric barriers with very thin elements. Comparative results with those by Monazzam et al. [13]. Noise source and receiver are located at (-5.0, 0.0) and (50.0, 0.0), respectively.

4. EVOLUTIONARY OPTIMIZATION FUNDAMENTALS

In the pursuit of imitating nature, an adequate approach on the basis of natural evolution arises to both solve and optimize problems leading to results no achieved to date by any other known method. This is the case of Evolutionary Computation, currently presented as a powerful tool for Sciences and Engineering.

Under the umbrella of Search Optimization Techniques, Evolutionary Computation (or Evolutionary Algorithms) covers a wide range of problem-solving methods based on principles of biological evolution (see Figure 4.1), such as natural selection and genetic inheritance, in which the survival of the fittest along time leads to the predominance of the best individuals. In other words, Evolutionary Computation Techniques incorporates evolutionary principles into algorithms that may be used to search for optimal solutions to a given problem.

These techniques are being increasingly applied to a variety of problems according to the development of computers. This way, the high time-consuming task of resolving a problem several times can be easily addressed by computers permitting, after the proper codification of the problem, the convergence to optimal solutions within the frame of the requirements defined.

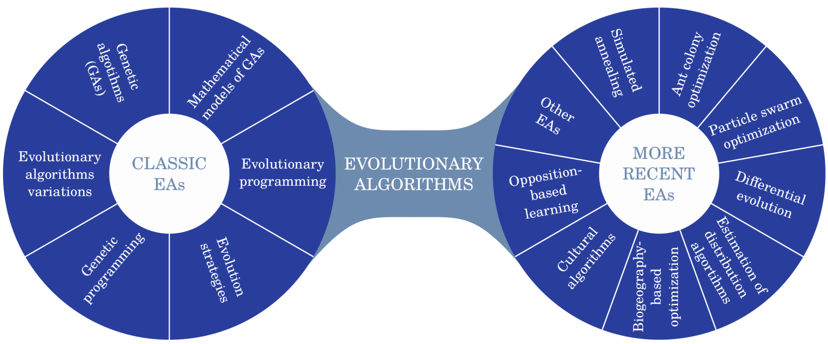

Figure 4.1: Taxonomy of Evolutionary Optimization Techniques (based on [126]).

As an essential part of the methodology developed in this document in the pursuit of improved noise barriers, this chapter presents a brief overview of Evolutionary Algorithms (EAs) and, more specifically, of Genetic Algorithms (GAs). In this line, a brief, general description of the bases of the selected GAs and the main features of the codes that implement them are detailed.

4.1 A brief introduction to Evolutionary Algorithms

Evolutionary Algorithms (EAs) are stochastic search methods that have become popular for solving many engineering problems, including search, optimization and design problems, among many others. Based on the imitation of natural biological evolution (simulated evolution), these algorithms are an excellent tool when searching for solutions to complex problems, where the mathematical functions that describe them are, very often, unknown. Broadly speaking, EAs operate on a population of potential solutions applying the principle of survival of the fittest to produce better and better approximations to a solution.

As seen in Figure 4.1, there are different types of evolutionary algorithms. Genetic algorithms (GAs) and evolution strategies are two of the most basic forms of evolutionary algorithms. GAs were developed in the United States by J. Holland and his students [127] focusing mainly on the genetic operators: selection, crossover and mutation. Evolution strategies were developed in the mid 1960's at the Technical University of Berlin under the leadership of P. Bienert, I. Rechenberg and H.-P. Schwefel. These strategies tend originally to real-valued representation [128] of optimization problems, prioritizing mutation over crossover. Population size is, in general, smaller than that normally used in genetic algorithms. While these both paradigms have been widely used for optimization, GAs have had a prominent role in search, optimization and machine learning [127, 129], while evolution strategies have focused mainly on optimization [130–132]. Later on, genetic programming was conceived as an evolutionary methodology for automatic programming and machine learning [133, 134], gaining a considerable importance in the field of Evolutionary Computation. The remaining strategy of interest in this field corresponds to evolutionary programming. These strategies were first developed in the 1960's [135] but were inactive until 1990's [136], when were redefined in a way very similar to evolution strategies. Each of this paradigms has its own strengths and weakness, though.

Evolutionary algorithms differ substantially from traditional search and optimization methods. In a traditional search algorithm, a number of possible solutions to a problem are available with the purpose of finding the optimum in a given time. When the *search space* (the space where the entire range of feasible solutions are) is reduced, the optimal solution may be obtained in a reasonable amount of time. This search greatly complicates as the search space grows in size, though. The main benefit of EAs, and that distinguishes them from traditional ones, lies in the fact that they are categorized as *population-based* search algorithms. More specifically, through the adaptation of successive generations of a large number of individuals (*population*) an EA performs an efficient directed search.

Below, by way of a summary, the most significant differences between evolutionary algorithms and more traditional search and optimization techniques are listed:

- EAs feature a search of points in parallel instead of a single point search.
- The direction of search is guided just by the objective function and the corresponding fitness levels so they do not require additional information or knowledge.
- EAs use probabilistic transition rules instead of deterministic ones.
- Their application is straightforward in the sense that no restrictions in the definition of the objective function are required (within a well defined search space of feasible solutions).
- These algorithms, when used with the proper tools, can cope with multi-modal functions so a number of equally valid potential solutions are provided for the decision-makers.

As selected strategy in the improvement of the shielding efficiency of the noise barriers studied in this thesis for their proven suitability in finding optimal solutions relatively shortly, the bases of Genetic Algorithms paradigm are briefly introduced in the next section.

4.2 Genetic Algorithms: an overview

The most popular technique in Evolutionary Computation research is the Genetic Algorithm (GA). The concept of GA was first developed by Holland and his colleagues in the 1960s and 1970s [127], inspired by the evolutionist theory explaining the origin of species. In short, in nature weak and unfit species within their environment are faced with extinction by natural selection.

These algorithms are metaheuristic, search-based global, adaptative, iterative and robust methods inspired, generally speaking, on the process of nature evolution, a scientific theory based on considering that some species are derived from others after DNA sequence alterations along time. Among all living beings result of both natural combination (crossover) and mutation, a wide variety of individuals, on which natural selection operates prioritizing the best adapted forms to the environment (survival of the fittest), is obtained. In other words, the fittest ones have greater opportunity to pass their genes to future generations via reproduction. In the long run, species carrying the best combination in their genes become dominant in their population. Sometimes, during the slow process of evolution, random changes may occur in genes. If these changes provide additional advantages in the challenge for survival, new species evolve from the old ones. Unsuccessful changes are eliminated by natural selection.

Every problem to be optimized following this paradigm must be properly defined according to the so-called *representation scheme*: the set of possible solutions that form the search space codified in arrays of bits (*chromosomes*). This way, the process starts off with the creation of the initial population, based on a certain number of individuals or possible solutions (random-based or specifically included by the user). The whole optimization process is comprised of a series of iterative steps until a solution satisfies a pre-defined termination criterion, either convergence or generation limit. Each individual of every population (of the initial population and the successive ones along the process) is evaluated according to the so-called *fitness function*, that is defined according to the intended requirements of the problems under study and determines how well an individual is adapted. Based on this parameter, a certain number of individuals are chosen (*selection*) to be *parents* and produce new individuals (*offspring*) after the information exchange (*crossover*) between them by means of their chromosomes and/or the random variation of such information (*mutation*). The fitness function of these new individuals are then determined. Finally, *survivors* (the best adapted individuals) are selected from the old population and the offspring to form the new population of the next generation. Thus, the average quality of the chromosomes (representatives of the solutions of the considered problem) of the population is progressively improved in terms of fitness. The outline of the basics of this paradigm is shown below:

1. **Start**. Generate either a random-based or a specifically included population of n individuals (chromosomes), that is, feasible solutions of the problems.

2. **Fitness**. Evaluate the fitness of each chromosome in the population.

3. **New population**. Create a new population by repeating the following steps until the new population is complete:

   (a) **Selection**. Select two parents' chromosomes from a population according to their fitness (the better the fitness, higher the chances to be selected).

   (b) **Crossover**. With certain probability, cross over the parents to form new offspring (children). If no crossover is performed, offspring is an exact copy of their parents.

   (c) **Mutation**. With certain probability, mutate new offspring by varying some information of the chromosome.

   (d) **Acceptance**. Place the modified offspring into the new population, after being assessed in terms of their fitness.

4. **New run**. Use the new generated population for a further run of the algorithm.

5. **Test**. If the end condition is satisfied, stop and return the best solution in the current population; if not, repeat the process from step 3.

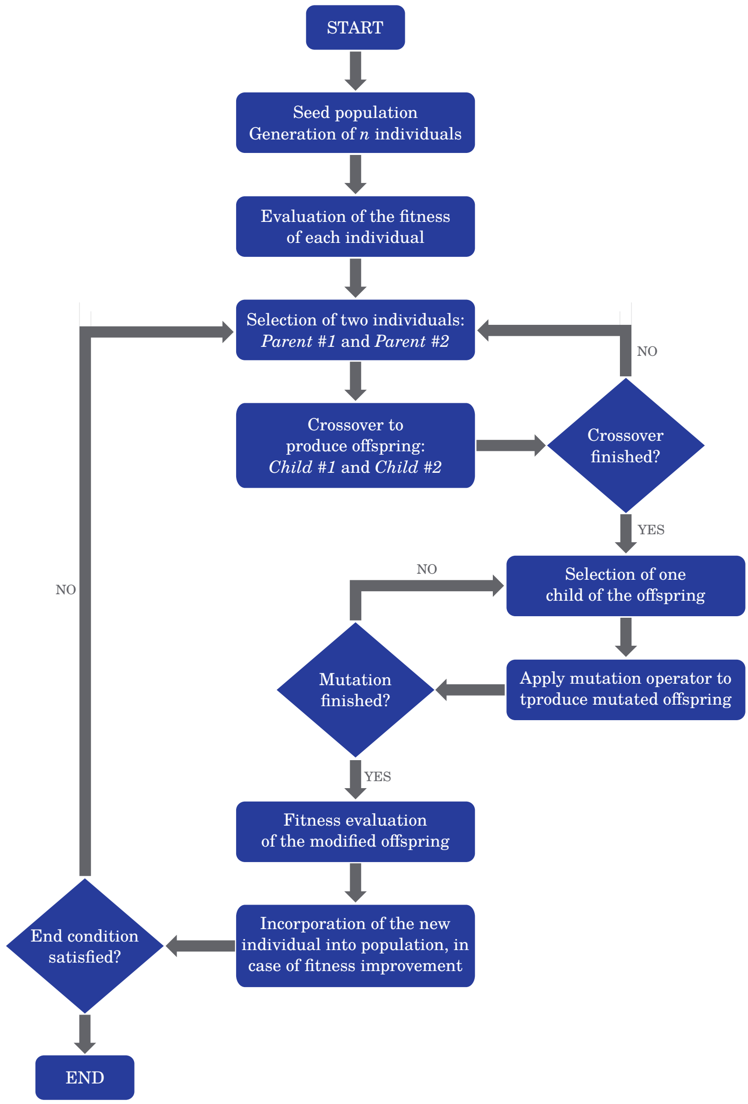

FIGURE 4.2: Generic flow diagram of the basis of a genetic algorithm.

4.3 Description of the performed genetic algorithm (GA)

The single optimization algorithm used in the studies presented in this document deals with the GAlib package [112], a collection of C++ GA components from which it is possible to quickly construct GAs to address a wide variety of problems. The main features of the algorithm and the parameters used in the GA code implemented in such studies are described below.

4.3.1 Chromosome representation

The representation of the feasible solutions to our problems (the valid geometries for a particular noise barrier model) is performed in the style of a string of binary bits that map to real numbers: *binary-to-real* representation. Each position in the string (chromosome) is assumed to represent a particular feature of an individual, called *genes* (the design variables in the case of the design optimization of noise barriers), and the value stored in that position represents how that feature is expressed in the solution (the overall geometry configuration of the barrier). GA operates with a collection of chromosomes, called *population* (set of different barrier configurations), which is normally randomly initialized. As the search evolves, the population includes fitter and fitter solutions and eventually it converges, meaning that it is dominated by a single solution.

As the number of feasible solutions is endless, the representation should be precise enough to perform a good equilibrium between the consideration of a reasonably large number of possible solutions and an adequate, fast convergence of the problem. In this line, all barrier models introduced in this document are represented by chromosomes determined by design variables coded with binary precision no longer than 8 bits.

Let us introduce an explanatory example, based on references [71, 72], to ease comprehension of the process involving the geometrical definition of the barrier designs proposed by the optimizer. Figure 5.2 represents a simple procedure to mathematically represent the barrier geometry, in this case, a Y-shaped model. The design points of this model are defined in a systematic, simple way in a reference domain - Figure 5.2(a) - as a previous step to the barrier profile generation in the real space - Figure 5.2(c) -. As shown, the characterization of this specific profile is performed on the basis of the design variables of points P_1, P_2 and P_3 that define the geometry in the GA search space of feasible solutions: ξ_1, η_1, ξ_2, η_2, ξ_3 and η_3. More specifically, the encoding of such design variables (genes) in this particular case is made by using binary variables of 8 bits precision. This way, the total length of the chromosome (n_{ch}) is 48 bits (see Figure 4.4).

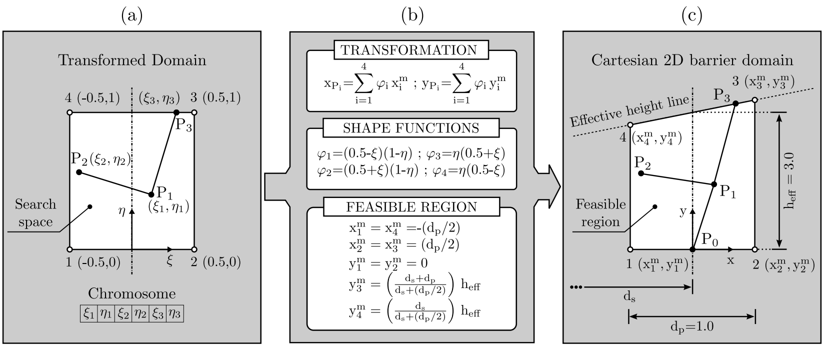

FIGURE 4.3: Bi-dimensional coordinate systems and transformation process from the transformed domain into the Cartesian domain. Example of a particular Y-shaped barrier geometry (individual) based on six design variables (genes).

The search space, according to the codification of the design variables with 8 bits, is discretized into 255 elements in both orthogonal directions of the domain, representing ξ and η ranges. Thus, the transformed domain is divided into 256 values (2^8) ranging from 0 to 255 (in representation of 00000000 and 11111111 binary numbers, respectively) in both coordinates, so the binary representation of every design variable (a particular point in the grid) has a direct (ξ, η) point image. By repeating the process for every binary representation (genes) of the chromosome, a set of real values representing the coordinates of the design variables of the barrier in the transformed domain is obtained by applying a proper transformation - see Figure 5.2(b) - of such coordinates into the 2D Cartesian domain.

Using the chromosome value from Figure 4.4 as starting point, the final Y-shaped geometry can be obtained following the steps above. Figure 4.6 shows the real barrier geometry and the corresponding values in the real space of every design variable according to seen in Figure 4.5.

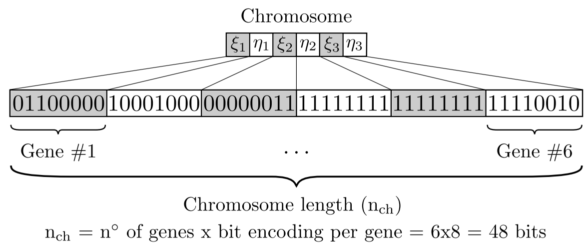

FIGURE 4.4: Example of chromosome encoding with binary variables of 8 bits precision.

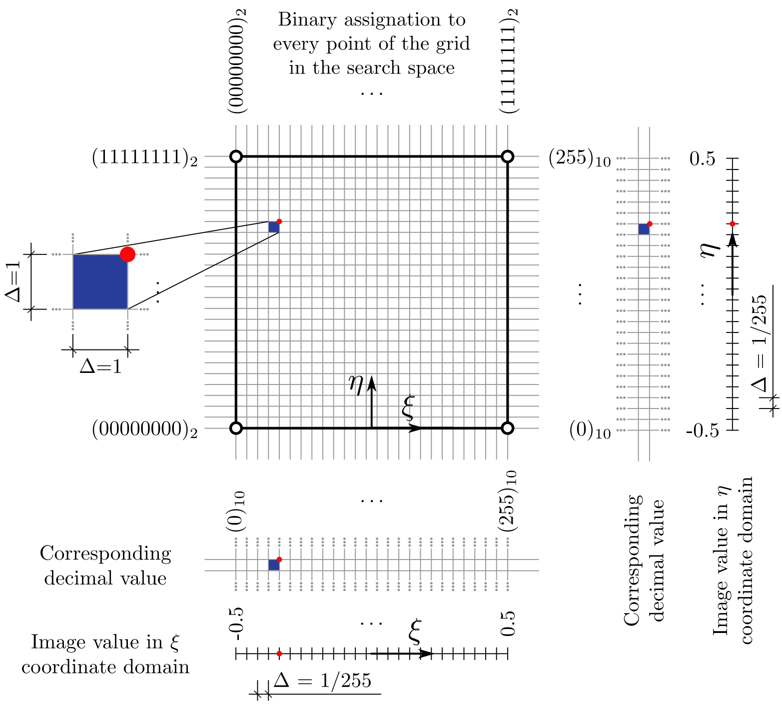

FIGURE 4.5: Mesh discretization of the GA search space into 255 elements in both orthogonal directions (design variables ξ and η coded with 8 bits). Each point of the mesh has its (ξ, η) image.

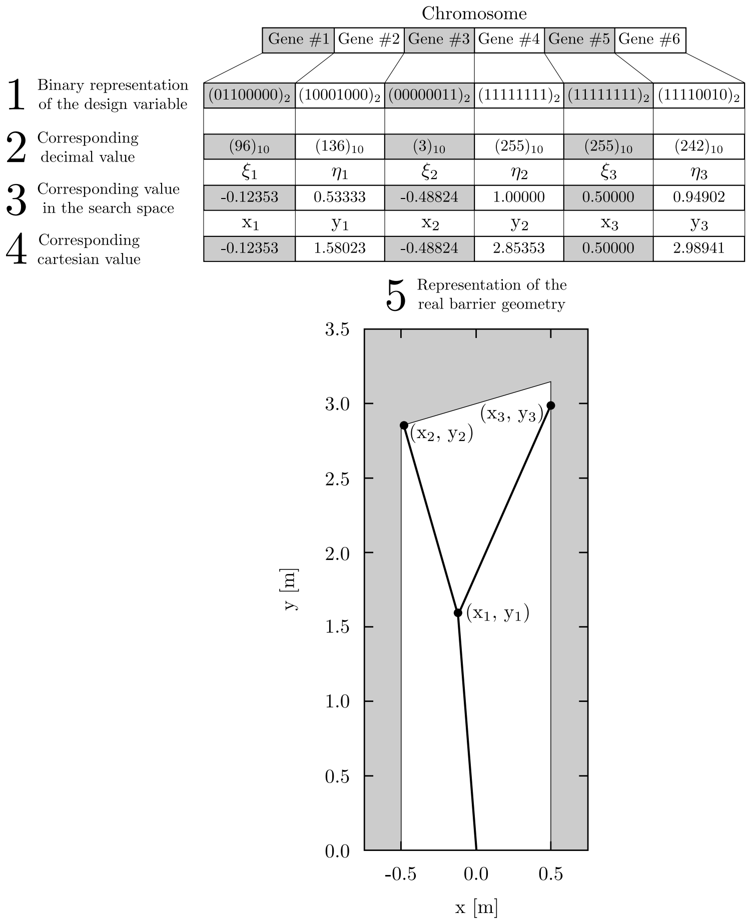

FIGURE 4.6: Chromosome encoding representation and process to obtain the final barrier geometry.

4.3.2 Overview of the GA applied

For a good balance between exploration and exploitation, a *steady-state* GA is applied in the improvement of the sound attenuation of noise barriers. This genetic algorithm uses overlapping populations with a user-specifiable amount of overlap (2% for the cases studied here). The algorithm performance roughly follows these steps:

1. **Population initialization**. The initial population P_0 of size N (overall number of individuals or feasible solutions) is created based on the problem range and constraints.

2. **Sorting of the initial population**. P_0 is sorted according to fitness criteria (objective function value of each individual of the population).

3. **Temporary population**. A temporary population T of size n is obtained, with n being a value representing either a percentage or a low number of individuals of the parent population P_t (t is the generation counter) to be replaced in the current population. Such individuals are probabilistically selected from P_t according to their fitness score (the higher the value, the higher the chance of being selected) to produce, after crossover and mutation operations, the offspring contained in T.

4. **Replacement of worse individuals**. After evaluation of population T, the offspring is added to the parent population P_t and the worst individuals are removed in order to return this latter population to its original size. In order words, the best individuals are directly selected from population T according to fitness score and replace the worse individuals from population P_t in case of fitness improvement.

5. **Test**. If the generation limit is met ($t = t_{max.}$), the algorithm stops and returns the optimum solutions in the current population. If not, $t = t + 1$ and the process continues running from step 3.

4.3.3 GA operators

The simplest form of genetic algorithm involves three types of operators: selection, crossover and mutation. Following, a brief description of the GA operators used is provided.

Selection

Selection is used to pick individuals from a population (comprised of 100 individuals in the studies performed in this document) before mating and mutation occur. The implemented code applies a useful and robust selection mechanism commonly used by genetic algorithms: *tournament* selection. This method picks two individuals randomly. Finally, the one with the higher score (the *winner*), that corresponds to the better fitness value, is selected for crossover.

Crossover

The crossover operator defines the procedure for generating a child from two parents. Depending on the study under consideration, two different crossover operators have been used for the single-objective optimization analysis presented in this document: *single-* and *two-point* crossover operators. In both cases, a crossover rate of 0.9 is applied (a probability of 90% of parents to be crossed over).

In the single-point crossover, two strings are used as parents and new individuals are formed by swapping a sub-sequence between these two strings from a crossover point selected arbitrarily - see Figure 4.7 (a) -. The two-point crossover differs from the single-point one in the fact that two crossover points are selected randomly - see Figure 4.7 (b) -.

Mutation

The mutation operator determines the patterns through which the information (bits) contained in the offspring chromosomes is mutated or varied. The studies performed in this document apply the *bit-flipping* mutation, in which a single bit in the string is flipped to form a new offspring string (see Figure 4.8).

The considered mutation rate is $1/n_{ch}$, with n_{ch} being the chromosome length of the barrier under study depending, as seen before, on both the number of design variables and the precision of the binary bits codification (see Figure 4.4).

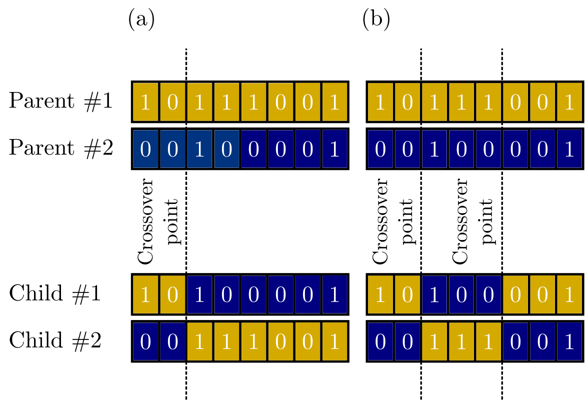

FIGURE 4.7: Scheme of the crossover operators used in the single-objective optimization of barrier models presented in this document. Bit string crossover of parent #1 and #2 to produce offspring (child #1 and #2). (a) Single-crossover. (b) Two-point crossover.

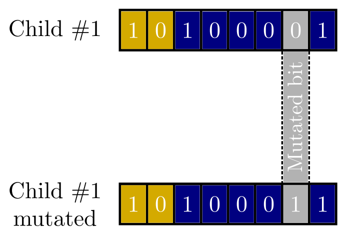

FIGURE 4.8: Scheme of the mutation operator used in the single-objective optimization of barrier models presented in this document.

4.4 Introduction to multi-objective optimization and related concepts

In optimization, the general approach can be summarized as follows: the search of the optimum through either the maximization or minimization of the considered objective function. However, such a paradigm present serious shortcomings that distances it greatly from real processes. Generally speaking, it can be said that *real* optimization is multi-objective type. More specifically, *real* problems normally involve more than just an objective simultaneously and are possibly in conflict with each other.

In the case of road barriers, the multi-objective optimum design arises as an adequate strategy that allows the decision-makers to take various relevant factors into account when selecting the final design. Firstly, undoubtedly, barriers must be acoustically adequate in terms of sound attenuation. But, focusing just in acoustical design considerations, there are other requirements leading to proper design of noise barriers. These include the height, the location and the cost of the barrier to be built, among others.

Under this proposal, after some concepts and a brief description of the bases of multi-criterion optimization, the main features of the multi-objective genetic algorithm and the code implemented for the multi-objective optimization of noise barriers presented in Chapter 7 are detailed. A comprehensive, more technical description of aspects involving this issue are provided in [110, 137], both books of reference in the EMO field.

4.4.1 Concept of dominance

The optimization of a problem from a multi-criterion point of view is a common need in Engineering. In contrast to the single-objective optimization, where the search of either a global optimum or a very close solution to that optimum is the desired aim, in the multi-objective optimization the improvement of one of the intended goals normally leads to the deterioration of the remaining objective. There is, therefore, not a unique valid solution but a set of solutions where the enhancement of one criterion yields the detriment of the other. These sets of solutions are arranged in the so-called *non-dominated fronts*, with the optimal solutions lying on the optimal Pareto front (see Figure 4.9). In this respect, these solutions are considered *non-dominated*, as it does not exist another feasible solution better than the these ones in some objective function without worsening other objective function. More precisely, it can be said that a solution *x dominates* other solution *y* if two of the following conditions are simultaneously satisfied:

- Solution x is not worse than solution y for all the considered objectives. For instance, in the case of minimization of both the sound pressure level (concept introduced in Chapter 2) and the overall boundary length, a specific barrier configuration (solution x) dominates other barrier configuration (solution y) if presents equal or lower values of both parameters.

- Solution *x* is strictly better than solution y in at least one of the objectives considered. Following the above example, solution x presents, at least, a lower value of either sound pressure level or barrier length than solution y.

If any of the above conditions is not satisfied, then solution x does not dominate solution y. Otherwise, x dominates y (mathematically $x \prec= y$) and:

- y is dominated by x or;

- x is non-dominated by y or;

- x is non-worse than y.

In this case, x is better than y in terms of multi-objective optimization.

4.4.2 Concept of Pareto optimality

The *Pareto optimality* or *Pareto efficiency* is an economic concept of application in Engineering. It is achieved when the intended objectives are optimized in the most efficient manner. In other words, it is obtained, as previously stated, when one criterion cannot be improved without making the other goal worse. This concept receives the name of the economist Vilfredo Pareto, an Italian economist of the late 19th and early 20th century, who allocated economic resources in the most efficient way.

The set of non-dominated solutions within a set of solutions P are those that are non-dominated by any member of the P set. In case that the P set consists of the feasible space as a whole, the set of non-dominated solutions is called *Pareto optimal* or *Pareto front / surface* (see Figure 4.9).

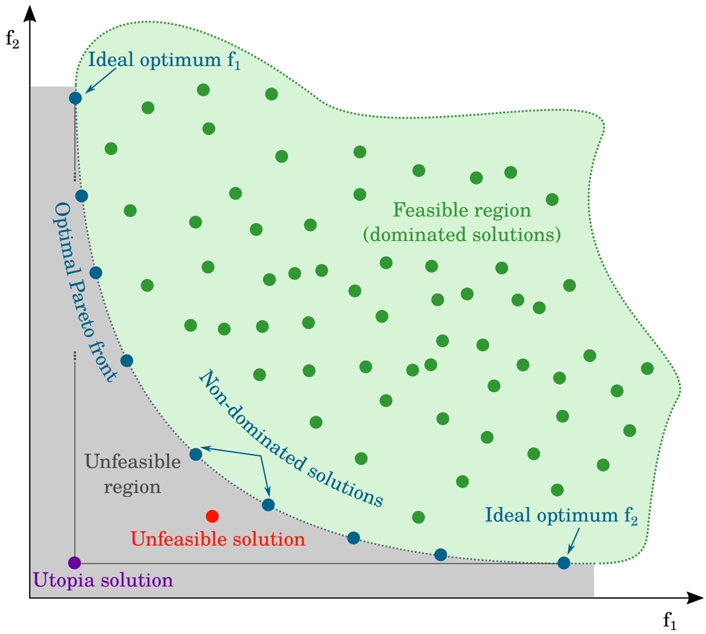

FIGURE 4.9: Generic scheme of a multi-objective optimization by minimizing both objectives.

As explanatory example of the search direction of the Pareto front in terms of minimization or maximization of two conflicting goals, the possible combinations involving bi-functional optimization processes (double minimization, double maximization, f_1 maximization and f_2 minimization and vice versa) are shown in Figure 4.10.

In contrast to single-objective optimization, in multi-objective optimization fitness assignment and selection have to take into account all the different objectives. Among the different fitness assignment strategies, the one applied in the study presented in Chapter 7 deals with *Pareto dominance* (PD). This strategy has been the most commonly adopted relation to discriminate among solutions and have been successfully applied in the optimization of bi- and three-objective problems, becoming the basis to develop most of the multi-objective evolutionary algorithms (MOEAs) proposed until recently.

Basically, the PD applied in this work is based on the division of the population into several fronts with different ranking numbers that reflects the closeness to the optimal Pareto front: the lower the ranking number, the closer to the optimal front (labeled as 0). This fitness assignment is related to the whole population, in contrast to the individual raw fitness value calculation independently of other individuals (see Figure 4.11).

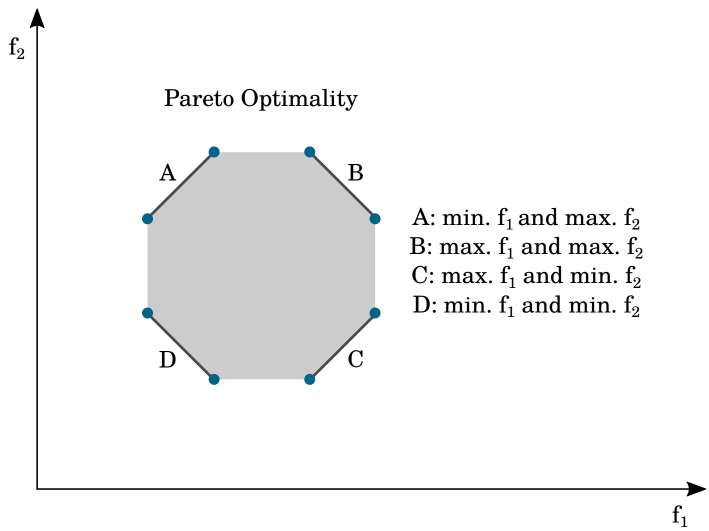

FIGURE 4.10: Simplified representation of Pareto fronts according to the optimization criterion applied to each objective.

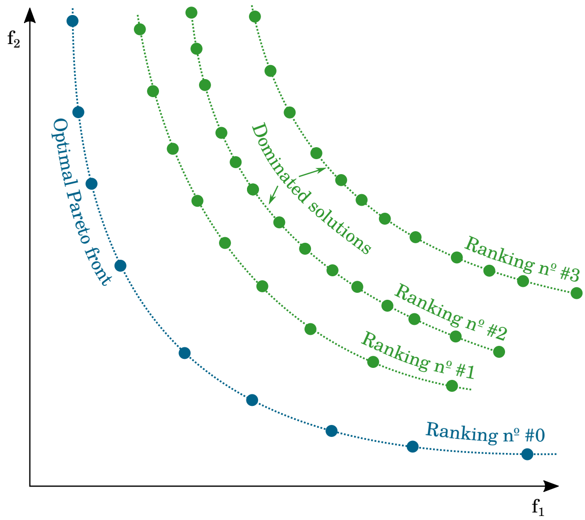

FIGURE 4.11: Fitness assignment based on Pareto dominance method with the division of population into rank-based fronts.

4.4.3 Measuring performance of an evolutionary multi-objective (EMO) algorithm

The methods for measuring performance of an EMO algorithm are numerous. In this line, different metrics have been proposed to evaluate and compare the performance of different Pareto fronts in terms of 1) how well solutions are guided towards the Pareto front and 2) how diverse, uniform and wide population is around this front. Some metrics focus on each of the aforementioned aspects independently. However, there are also metrics that intend to incorporate several of these aspects and express the performance of the algorithm in a overall scalar number. Such is the case of the so-called *hypervolume indicator*, proposed in [138, 139]. It measures the area covered by the dominated portion of the objective space (with respect to a user-specifiable reference point), as shown in Figure 4.12. The analysis carried out in the performance of the Pareto fronts of the multi-objective optimizations conducted in this document apply this measure.

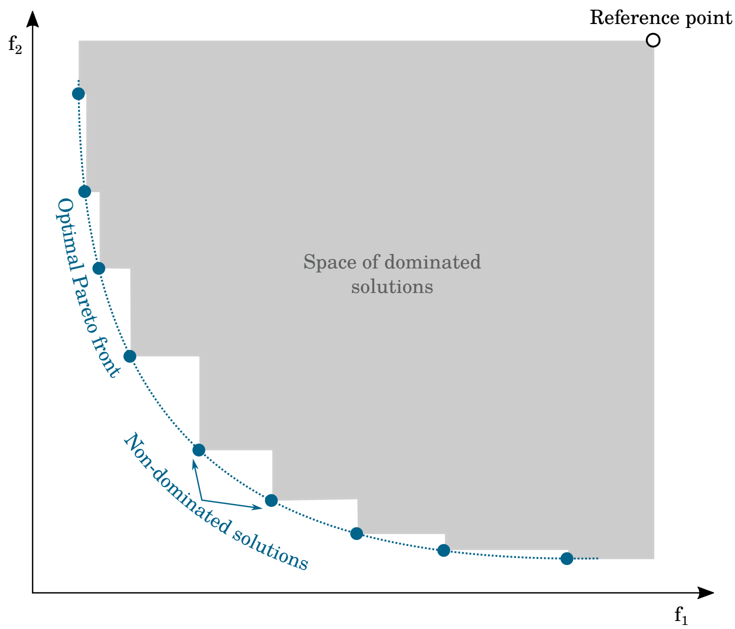

FIGURE 4.12: Illustrative representation of the comparative metric used in this work: hypervolume measure with area covered by non-dominated solutions and a user-specifiable reference point (both f_1 and f_2 are minimizing objectives).

4.4.4 Aims of an EMO algorithm

After the definition of some key concepts in EMO, the aims to be taken into consideration when designing a multi-objective genetic algorithm are finally pointed out. These should achieve the following purposes: 1) guiding the search to a set of solutions as close as possible to the optimal Pareto front, 2) keeping a diverse, homogeneous set of non-dominated solutions to prevent population from containing mostly identical solutions. In all the above aims there is an underlying characteristic that guide the whole process towards the success: *elitism* to prevent non-dominated solution from being lost.

4.5 Description of the performed multi-objective genetic algorithm (MOGA)

The MOGA used in the multi-objective optimization presented in this document applies the NSGA-II [114, 140] algorithm, the second version of the famous *Non-dominated Sorting Genetic Algorithm* (NSGA [141, 142]) based on the work of Prof. Kalyanmoy Deb.

The basis of this algorithm has been implemented in a computer code developed by Prof. David Greiner, one of the supervisors of this thesis, and successfully applied on the multi-objective optimization in many engineering research works [72, 99–103, 107] at the Institute of Intelligent Systems and Numerical Applications in Engineering (SIANI) of the Universidad de Las Palmas de Gran Canaria. The main features of the algorithm as well as the parameters used in the code implemented in such studies are described below.

4.5.1 Chromosome representation

The representation of feasible barrier configurations is performed in the style of a string of binary bits that map to real numbers, with barrier models featuring design variables coded with binary precision of 8 bits.

4.5.2 Overview of the MOGA performed

As previously stated, the MOGA used deals with the NSGA-II. The main features of the algorithm are summarized below:

- This algorithm implements *elitism*, which stores the solutions from the best non-dominated front and include them in the next generation.

- The sorting of each individual is based on the non-domination criterion, the same implemented by the NSGA algorithm. More specifically, this algorithm performs a population sorting into non-dominated fronts by means of a rank value, which is dependent on the location of each front with respect to the overall population (see Figure 4.11).

- It incorporates an adequate mechanism based on the *crowding distance* (see Figure 4.13) to guarantee diversity and spread solutions within the same non-dominated front (i.e., this operator favors solutions with lesser domination rank when two solutions lie on different fronts. When both belong to the same front, the one in a less dense region, corresponding to a higher crowding distance, is preferred, though).

- No penalty functions are considered. Constraints are applied by means of a modified definition of dominance, though (unfeasible solutions violating different constraints are classified as members of the same non-dominated front).

- It implements a fast sorting algorithm that requires just $O(mN^2)$ operations instead of $O(mN^3)$ calculus needed in the former algorithm, with m being the total number of objectives and N the size of the population.

Roughly speaking, the performance of this algorithm can be summarized in the following steps:

1. **Population initialization**. The initial population P_0 of size N (overall number of individuals or feasible solutions) is created based on the problem range and constraints.

2. **Sorting of the initial population**. P_0 is sorted according to non-domination criteria and crowding operator. A fitness value equal to its non-domination level is assigned to each individual of the population (the lower the value, the better the level).

3. **Initial offspring**. An offspring population Q_0 of size N is created through recombination based on selection of parents from P_0 and by cross over and inducing mutations to new children.

4. **Combined population**. A combined population R_t (t representing the generation counter) of size $2N$ is obtained as the result of the union of populations P_t and Q_t ($R_t = P_t \cup Q_t$). This resulting population is then sorted according to a fast non-domination procedure (population is sorted in Pareto fronts with ranking values according to non-domination criteria by means of a fast sorting algorithm).

Crowding distance operator criterion
Solution i-2 is preferred over solution i.
Solution i is preferred over solution j.
Solution j is preferred over solution k.
Solution i-2 is the most preferred solution.

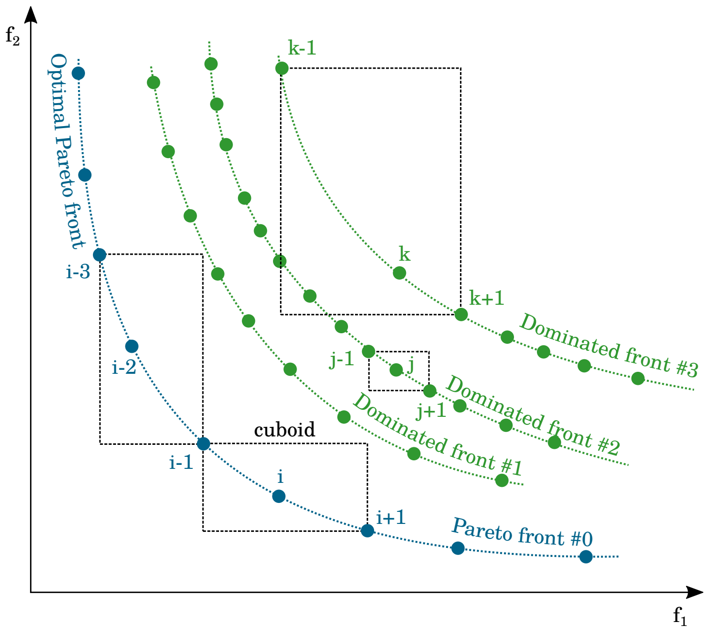

FIGURE 4.13: Crowding distance cuboid example. This parameter is represented by the average side length of such cuboid formed by the closest neighbors of a point sharing the same non-dominated front.

5. **Crowding distance**. The individuals of the population are then sorted in terms of the crowded comparison operator.

6. **New improved population**. The new parent population P_{t+1} is comprised of the N best solutions of R_t, starting off picking individuals from the first front (the non-dominated) until completing the

population size, based on crowding distance comparison.

7. **Test**. If the end condition is satisfied (generation limit), the algorithm stops and returns the optimum solutions in the current population. If not, $t = t + 1$ and former P_{t+1} becomes the new parent population P_t and a new offspring population Q_t is created from genetic operations on parent population. The process continues running from step 4.

4.5.3 Genetic operators

Selection

Mechanisms involving the selection process are inherent to the basis of the NSGA-II algorithm and were described in previous section.

Crossover

The crossover used in these studies applied the *uniform* crossover operator. In this case, as shown in Figure 4.14, offspring is the result of a random selection of bits from both parents according a random *crossover mask* (a binary string with the same size of chromosome) with each bit featuring a probability of 50% to be 0 or 1.

Mutation

The studies performed in this document apply the *bit-flipping* mutation, in which a single bit in the string is flipped to form a new offspring string (see Figure 4.8).

The considered mutation rate is $1/\mathrm{n_{ch}}$, with $\mathrm{n_{ch}}$ being the chromosome length of the barrier under study depending, as seen before, on both the number of design variables and the precision of the binary bits codification (see Figure 4.4).

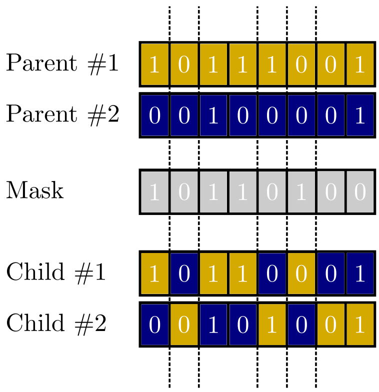

FIGURE 4.14: Scheme of the uniform crossover operator used in the multi-objective optimization of barrier models presented in this document.

5. METHODOLOGY APPLIED TO THE STUDY OF VERY THIN BARRIERS

Results derived of the implementation of the methodology briefly introduced in Chapter 1 for the search of the the best shielding designs of very thin barriers are presented in this chapter. As already mentioned, the procedure deals with the shape design optimization of noise barriers by coupling a Dual BEM formulation with an evolutionary algorithm.

The key aspect of this approach lies in the fact that a proper Dual BEM formulation is applied in the study of noise barriers featuring very thin boundaries, idealized as null section models (the section of the barrier is neglected). This simplification of reality greatly facilitates the geometric definition of barrier profiles, having no major influence on the acoustic performance [47]. The special nature of these types of barriers makes every node of the discretization hold both the pressure and the flux value at each side of it, i.e., $2n$ unknowns per n nodes. The inclusion of an additional BEM formulation (based on the hyper-singular boundary integral equation) combined with the classical one (singular) provides a compatible system of equations that allows the problem to be solved. The coupling of an evolutionary algorithm with the Dual BEM code allows us to obtain interesting acoustic solutions avoiding the complexity associated with the geometric generation of volumetric structures. To the researcher's knowledge, this approach is the first joint implementation of evolutionary algorithms and a Dual BEM formulation concerning this issue. Figure 5.1 shows the usefulness of representing complex volumetric structures as *single-wire* configurations.

As an application, two studies addressing issues of interest in sound attenuation are performed. In all of them, two-dimensional sound propagation problems concerning an infinite, coherent mono-frequency source of sound, placed parallel to an infinite noise barrier that stands on a flat plane (ground) of uniform admittance are considered. The sound propagation analysis is performed in the frequency domain with the usual assumptions: the medium (air) is modeled as homogeneous, elastic and isotropic with no viscosity, under small disturbances and initially at rest with no wind effects. Expression of the objective function to be maximized throughout the shape optimization process is written in terms of this response.

In one of the studies, different barrier configurations of practical interest, proposing more efficient designs in each case, are assessed. These profiles cover a wide range of designs, from complex straight boundary configurations to curve-shaped profiles, featuring rigid and noise absorbing surface treatments. While results are achieved by using a specific receivers' scheme, the influence of the receivers' location on the acoustic performance is also addressed.

The second study aims at estimating the influence of the screening performance through distance. Two different receivers configurations for three clearly distinguishable regions in terms of closeness to the barrier are considered in this analysis.

A numerical model validation of the proposed methodology on the basis of experimental results from a scale model test present in the bibliography [12] is also performed. Finally, this chapter concludes with the analysis drawn from the results disclosed.

5.1 Description of the shape optimization framework

Before disclosing the results of the analysis mentioned above, the bases of the methodology used in the numerical simulations need to be introduced. As is well known at this stage, the systematic improvement of the sound attenuation in the shadow region requires a versatile, robust procedure that includes incremental geometric changes on barrier topologies previously defined. Along the process, road barriers with ever-increasing shielding performance are found to finally lead to the desired optimum solution, within the frame of the conducted analysis.

Shape design optimization analyses are conducted by the combined use of an evolutionary algorithm and a code that implements a Dual BEM formulation. A detail description of this Dual approach of the Method for the proper assessment of the very thin barriers is found in Chapter 3. The evolutionary algorithm software used in the studies applies the GAlib package [112]. This library is a collection of C++ genetic algorithm (GA) components from which it is possible to quickly construct GA's to deal with a wide variety of problems. Additional information of the GA implemented in this code refers to Chapter 4.

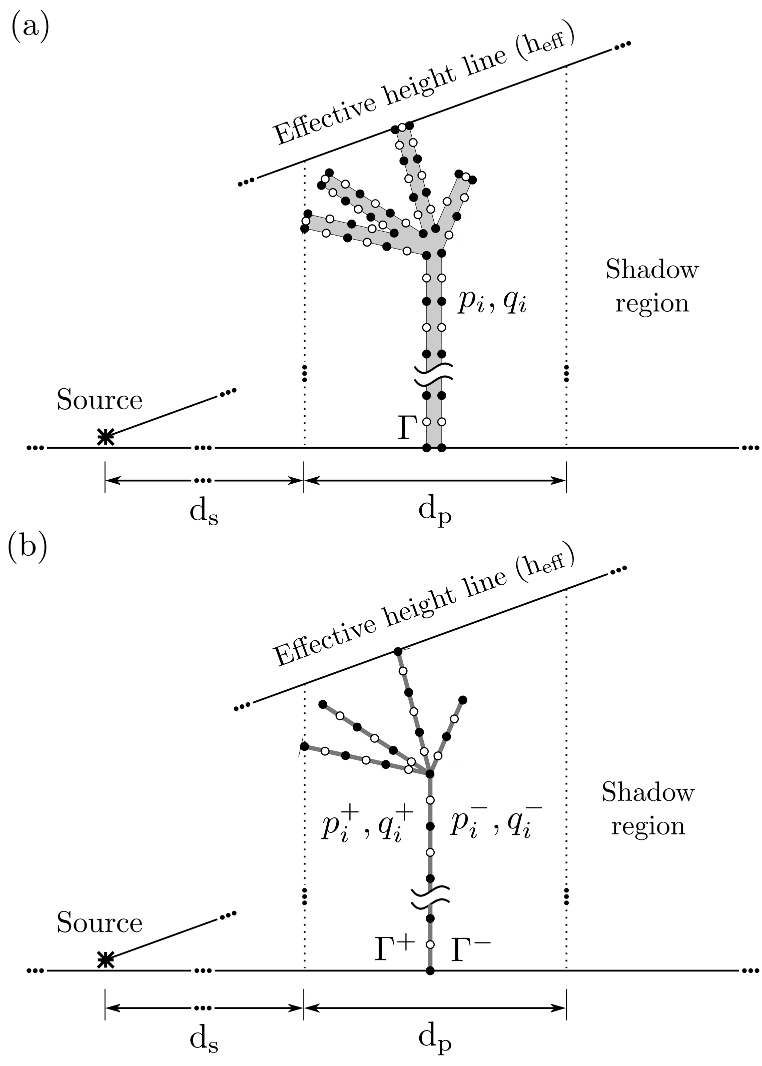

FIGURE 5.1: (a) Generic thin barrier modeled as a volumetric structure. (b) Idealization of the former barrier as a null section profile.

5.1.1 Determination of the acoustic efficiency of the barrier

As underlined in Chapter 2, the determination of the shielding efficiency of a barrier is well defined by means of the *insertion loss* coefficient (IL) that in the harmonic problem, for every frequency from the analyzed noise source, is defined as:

$$\mathrm{IL} = -20 \cdot \log_{10}\left(\frac{\mathrm{P_B}}{\mathrm{P_{HS}}}\right) [\mathrm{dB}] \tag{5.1}$$

on every frequency of the band spectrum. As can be seen, this coefficient represents the difference of sound pressure levels at the receiver points in the situation with ($\mathrm{P_B}$) and without ($\mathrm{P_{HS}}$) considering the barrier.

With the purpose of conducting an optimization process where the excitation is represented by a noise source pulsing at every frequency of the band spectrum, the efficiency of the barrier for a specific receiver can be written in terms of the *broadband insertion loss* ($\mathrm{IL_{total}}$):

$$\mathrm{IL_{total}} = -10 \cdot \log_{10}\left(\frac{\sum_{i=1}^{\mathrm{NF}} 10^{(\mathrm{A_i}-\mathrm{IL_i})/10}}{\sum_{i=1}^{\mathrm{NF}} 10^{\mathrm{A_i}/10}}\right) [\mathrm{dB(A)}] \tag{5.2}$$

being NF the studied spectrum number of frequencies (in the analyses conducted here, NF = 14), $\mathrm{A_i}$ the spectrum A-weighted noise level and $\mathrm{IL_i}$ the insertion loss value for sources pulsing at every frequency of the spectrum, according to (6.1).

Concerning the estimator taken into account along the shape optimization processes, it is worth noting that it is based on the overall IL mean value of all receiver points:

$$\mathrm{OF} = \sum_{j=1}^{\mathrm{NR}} \mathrm{IL_{total_j}}/\mathrm{NR} \tag{5.3}$$

being $\mathrm{IL_{total_j}}$ the broadband IL for each receiver - see (5.2) - and NR the total number of receivers. This value corresponds to the so-called *objective function* (OF) to be maximized, according to the proper terminology used in the field of evolutionary algorithms.

5.1.2 Applied spectrum

In all the studies performed in this chapter, the noise source is characterized by using the UNE-EN 1793 [117] normalized traffic noise spectrum for third-octave band center frequencies, ranging from 100 to 2 000 Hz, the same used by the Spanish Technical Building Code (CTE) [143].

5.1.3 Representation of the barrier models

Following [71, 72], a simple procedure to mathematically represent the geometry of barriers is proposed. The design points of the screen model are defined in a systematic, simple way in a reference domain as a previous step to the barrier profile generation in the real space. In short, the transformed domain holds the set of design variables of the model under study, denoted by (ξ_i, η_i), and represents the rectangular search space for the GA - see Figure 5.2(a) -. Every (ξ_i, η_i) point in the transformed domain has its image ($\mathrm{x_i}$, $\mathrm{y_i}$) in the Cartesian space, that is the real domain where the barrier operates.

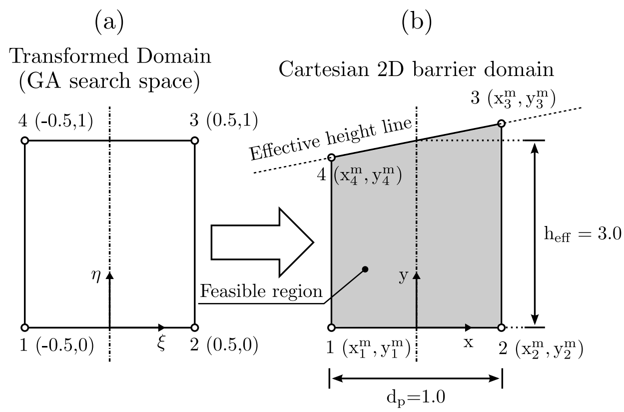

FIGURE 5.2: Bi-dimensional coordinate systems. Dimensions expressed in meters.

The transformation of Figure 5.2 can be expressed as follows:

$$\begin{Bmatrix} x_i \\ y_i \end{Bmatrix} = \gamma_1 \begin{Bmatrix} x_1^m \\ y_1^m \end{Bmatrix} + \gamma_2 \begin{Bmatrix} x_2^m \\ y_2^m \end{Bmatrix} + \gamma_3 \begin{Bmatrix} x_3^m \\ y_3^m \end{Bmatrix} + \gamma_4 \begin{Bmatrix} x_4^m \\ y_4^m \end{Bmatrix} \tag{5.4}$$

where:

$$\begin{gathered} \gamma_1 = \left(\frac{1}{2} - \xi\right)\left(1 - \eta\right) \; ; \; \gamma_2 = \left(\frac{1}{2} + \xi\right)\left(1 - \eta\right) \\ \gamma_3 = \eta\left(\frac{1}{2} + \xi\right) \; ; \; \gamma_4 = \eta\left(\frac{1}{2} - \xi\right) \end{gathered} \tag{5.5}$$

and:

$$\begin{gathered} x_1^m = x_4^m = -\frac{d_p}{2} \; ; \; x_2^m = x_3^m = \frac{d_p}{2} \\ y_1^m = y_2^m = 0 \; ; \; y_3^m = h_{eff}\left(\frac{d_s + d_p}{d_s + (d_p/2)}\right) \; ; \; y_4^m = h_{eff}\left(\frac{d_s}{d_s + (d_p/2)}\right) \end{gathered} \tag{5.6}$$

The maximum effective height of all barrier models is limited to $h_{eff} = 3$ m in the studies here presented. This value and the maximum barrier projection to the ground d_p have been chosen according to the geometric dimensions of the barriers studied herein and present in the bibliography. Both latter parameters define the feasible region by generating a trapezoidal search space in the Cartesian barrier domain - see Figure 5.2(b) -. Its final dimensions are dependent, logically, on the placement of the noise source d_s (see Figure 5.1).

5.1.4 Overview of the process

To facilitate understanding of the methodology, Figure 5.3 shows a flow diagram concerning the evolutionary process on the search of the best acoustic solutions of two barrier models, by way of example, in a generic bi-dimensional scenario. The procedure makes use, for a good equilibrium between exploration and exploitation, of a *steady state* GA [144, 145] that starts off with an initial population of 100 individuals initially based on a proposal on random design variables of the model under assessment. Such design variables form the chromosome of the individual proposed by the GA (see bottom part of models in Figure 5.5) shaping, therefore, the geometry of the barrier. At this point the screening behavior of each individual is performed using the aforementioned Dual BEM code. This requires a proper discretization of the barrier boundary with ever-increasing number of elements along the frequency spectrum. In this work, parabolic elements are coded with a maximum length of half the wavelength of the frequency under study for adequate convergence of the results (see Chapter 3). The initial population is then ranked in terms of acoustic performance, here represented by the objective function value (OF) characterized, in turn, by the broadband insertion loss (IL_{total}) - see (5.2) -. In this way, each individual is more likely to be selected according to its screening behavior (OF). Therefore, by using the *tournament selection* operator, two individuals are chosen (*parents* in proper terminology of evolutionary algorithms) and are to be crossed with a probability of 90% by the *single-point crossover* operator, leading to an offspring comprised of two new individuals (*children*) whose chromosomes are eligible for mutation according to probabilistic criteria. After mutation, offspring individuals replace the two worst in the parent population (in case of better value of OF, that is, improvement of the acoustic behavior). This iterative process continues until reaching the stopping criterion, which is met after a certain number of evaluations of the objective function.

5.2 Numerical shape optimization

All numerical optimization analyses presented in this chapter are based entirely on the GA parameters mentioned above and can be consulted in the flow diagram of Figure 5.3. Bi-dimensional configurations, barrier models and source-receivers schemes differ from one study to another, though.

The procedure previously described is applied to the study of different barrier designs in this section. The diversity of the models chosen has been intended to highlight the robustness and flexibility of the methodology, as well as the wide range of possible geometric designs to be assessed.

Five independent runs of the optimization process featuring 20 000 evaluations of the objective function (OF) are considered for each model of the following studies.

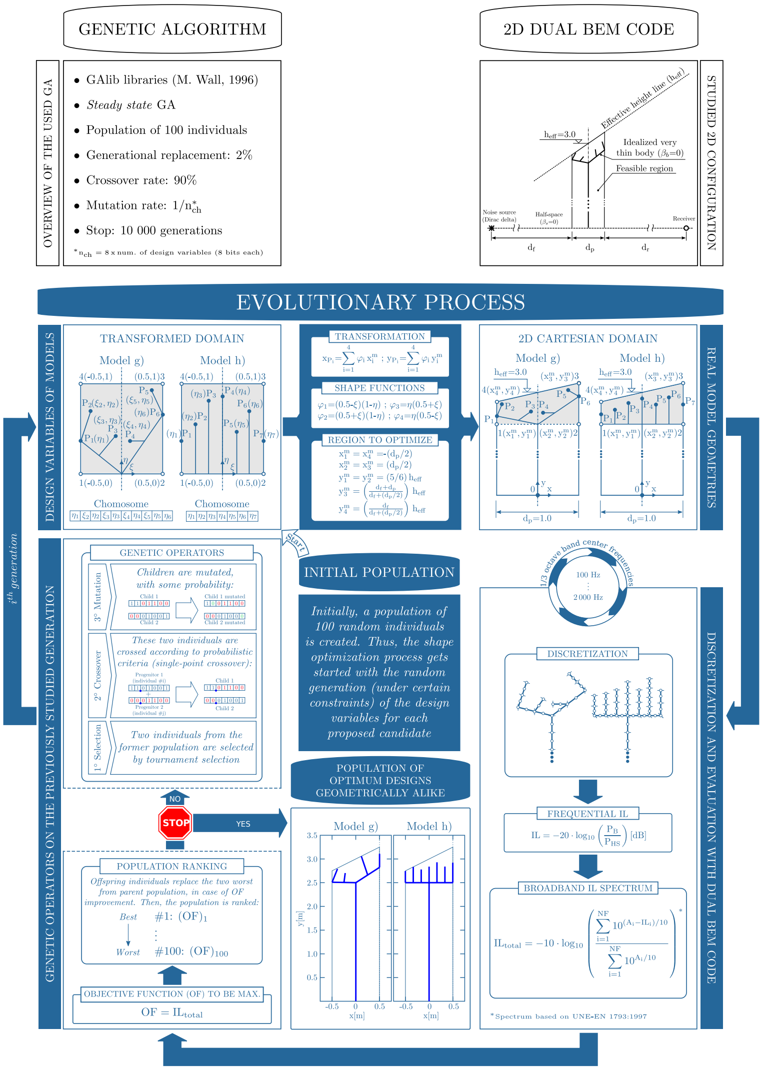

FIGURE 5.3: Overview of the GA used, layout of a generic bi-dimensional configuration and optimization flow diagram.

5.2.1 Study #1. Noise barriers with improved performance

The vertical screen is the simplest form of protection against noise. However, its simplicity implies some drawbacks in terms of sound attenuation when compared with other barrier designs with the same effective height. Increasing the height of a screen can increase its effect but brings other problems so, in many cases, the implementation of alternative, more complex designs appear to be suitable solutions to improve the shielding efficiency.

This study intends to outline the most common and effective geometric patterns, acoustically speaking, present in noise barriers. To do this and to expose the scope and features of the method, eight different designs are studied (see Figure 5.5), based either on an overall shape or in a top edge optimization of the barrier model, depending on the case.

Figure 7.1 represents the general configuration of the study. It deals with a source of sound placed on a ground with a perfectly reflecting surface ($\beta_g = 0$) at $d_s = 9.5\,m$ from the feasible region, parallel to an infinite thin cross-section noise barrier. A trapezoidal section holds the area for feasible profiles, defined by the limited barrier projection to the ground, that is $d_p = 1.0\,m$, and the maximum effective height to be achieved, that is $h_{eff} = 3.0\,m$ at the median of the rectangle trapezium.

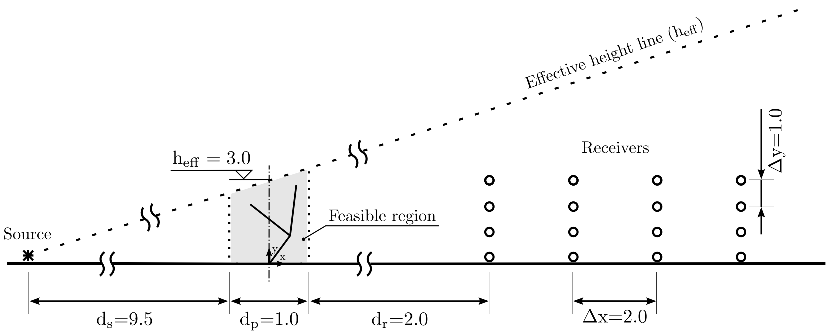

FIGURE 5.4: Bi-dimensional configuration for the shape optimization of noise barriers with improved performance. Dimensions expressed in meters.

A grid of 4x4 receivers is considered. The first line of receivers lays on the ground and the remaining ones are placed at different heights, vertically separated by $\Delta y = 1.0\,\mathrm{m}$. A horizontal distance of $\Delta x = 2.0\,\mathrm{m}$ among them is considered. The nearest receivers to the side limit of the feasible region are $d_r = 2.0\,\mathrm{m}$ away. The proximity of the receivers to the barrier is motivated by the fact that the barrier performance in near regions is more affected by the shape design rather than by the effective height, as occurs in non-near regions.

As for the overall shape design optimization, five barrier models are proposed: models a) and b) (**polygonal**-shaped designs), models c) and d) (**splines**-based models) and model e) (**Y**-shaped barrier) (see left part of Figure 5.5). As for the optimization of the top edge of the barrier, model f) (**tree**-shaped barrier), model g) (**Y-variant** model) and model h) (**fork**-shaped model) are studied (right part of Figure 5.5). Such models are based on a set of points defined by design variables in a transformed domain proposed by the evolutionary algorithm, according to the geometric model definition. It is worth stressing that contrary to the general approach (Figure 5.2), the feasible space is constrained to the barrier top in the Cartesian domain for models f), g) and h). The models previously cited will be referred as their corresponding names in brackets hereinafter. At this stage, it is not hard to reach the conclusion that some of the optimum designs obtained clearly lack of practical implementation. Considering the strong theoretical nature of these configurations, this study should be understood as an attempt to find acoustic principles of interest underlying such models that leads to easier-to-build barrier designs, as proposed in some of the models studied. The considered configurations depicted in Figure 5.5 are described in more detail below.

Polygonal-shaped barrier

This design is based on a set of points through which straight boundaries are consecutively connected. These points feature a completely free movement inside the feasible region with the exception of the first and the last one, placed on the ground and at the effective height line, respectively.

Two different configurations of this design are studied. The first one is a 3-sided polygonal-shaped barrier - model a) -; the second is a 5-sided polygonal-shaped one - model b) -.

The geometric feasibility of the individuals is constrained to the condition of non-cut-off points among boundaries.

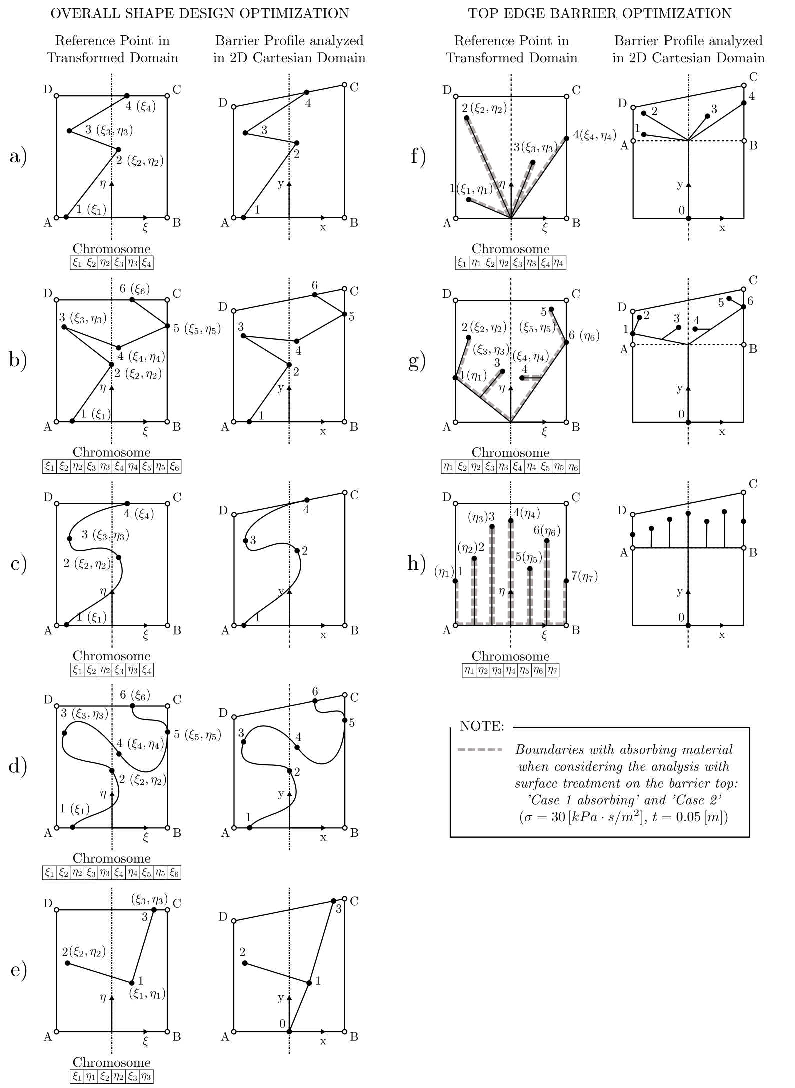

FIGURE 5.5: Proposed models for the shape optimization of noise barriers with improved performance.

Splines-based-shaped barrier

A set of splines-based curves is proposed as barrier model. The points through which the curves pass are proposed by the evolutionary algorithm to generate the cubic segmental interpolation that leads to the desired profile. These points feature a completely free movement inside the feasible region with the exception of the first and the last one, placed on the ground and at the effective height line, respectively.

These continuous, differentiable curves are defined as *natural* cubic splines, meaning that the second derivative is null at both the starting and the ending point of the overall resulting curve.

For the sake of convenience, the splines expressions are written in parametric form. This choice is in the interest of the geometric feasibility of the individuals proposed by the evolutionary algorithm, by ensuring that the tangent vectors to the curve at both sides of the common points between splines have the same sense (see Figure 5.6).

The sharp changes in direction that frequently arise when dealing with this sort of curves require some considerations. For both faithfully representing complex configurations and guaranteeing a good convergence of numerical integrations, the implementation of mesh-related strategies is needed. These criteria are implemented in the meshing algorithm of the code. In this way, a more refined mesh around critical points of the splines is generated for each frequency to perfectly fit the geometric discretization to the barrier profile (see Chapter 3). As parabolic elements are used for the boundary discretization, the placement of, at least, one element is considered around critical points (with the central node of such elements located at these points , i.e., at maximums and minimums).

Two different configurations of this design are studied: a 3 and a 5 cubic splines-shaped barrier - model c) and d), respectively -.

The geometry feasibility of the designs is also constrained to the condition of non-cut-off points among boundaries, obviously.

Y-shaped barrier

A commonly used Y-shaped barrier is studied - model e) -. This model is based on three points (1, 2 and 3) that feature a completely free movement inside the feasible region. Point 0 lays on the ground and is fixed at the median of the feasible region.

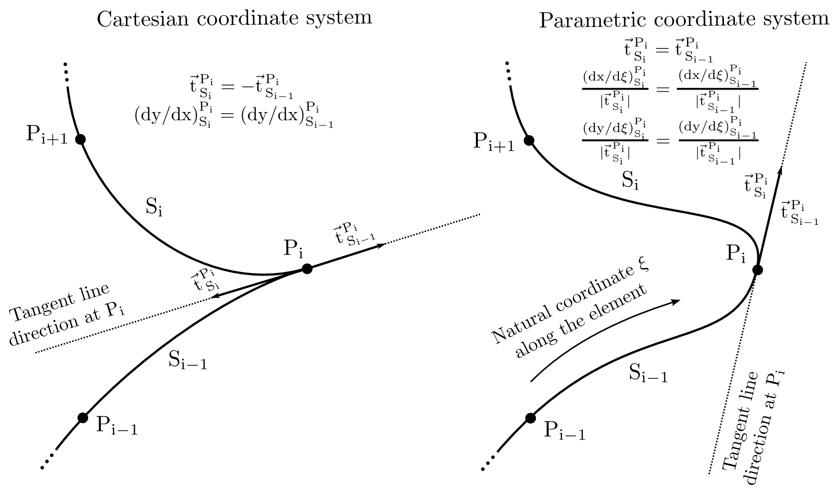

FIGURE 5.6: Convenience of the choice of a parametric representation to generate a multiple splines-based curve.

Tree-shaped barrier

This design is a tree-shaped model with four arms on its top - model f) -. Points from 1 to 4 can be placed anywhere inside the domain. This enables the tilt of the arms to cover a free range of angles.

The barrier model stands on a vertical, fix bar of 2.5 m height placed on the median of the feasible region from which the four arms are born.

Y-variant-shaped barrier

This model - model g) - can be understood as an evolution of the Y-shaped design - model e) - by adding two branches at each arm of such design. Two of the branches are born from the ending points of the main arms (points 1 and 6) while the remaining ones do it from the middle. The design variables responsible for the inclination of the main arms are constrained to vertical movements (η_1 and η_6) through the left- and right-side limits of the feasible region. The barrier model stands on a vertical, fix bar of 2.5 m height placed on the median of the feasible region.

The geometry feasibility of the model is constrained to both the condition of non-cut-off points among boundaries and the fact that points from 2 to 5 are always in the upper region enclosed by the main arms in the search domain.

Fork-shaped barrier

This model - model h) - represents a barrier with seven vertical branches that are born from a horizontal tray. The distance among branches remains constant ($d_p/6$) while their lengths vary throughout the optimization process. As in the previous cases, this barrier model stands on a vertical bar of 2.5 m height.

Considered surface treatments

In relation to the surface treatment of the barrier models to be analyzed, two different cases are proposed. In one of them (*Case 1*), a shape optimization considering perfectly rigid boundaries ($\beta_\Gamma = 0$) for all models is performed. As a reference comparing design, *Case 1 absorbing* deals with the assessment of the acoustic efficiency of the best profiles of models tree-, Y-variant- and fork-shaped from *Case 1*, on whose top edge boundaries a specific sound absorbing treatment is considered (marked with a grey line in the right part of Figure 5.5). The airflow resistivity and the thickness of the absorbing material are $\sigma = 30\,\mathrm{kPa}\cdot\mathrm{s/m^2}$, which corresponds to mineral wool, and $\mathrm{t} = 0.05\,\mathrm{m}$, respectively. In *Case 2*, a top edge optimization of barriers tree-, Y-variant- and fork-shaped with the same surface treatment on crowning boundaries than in *Case 1 absorbing* is conducted. These research cases aim at determining whether or not absorbing boundary conditions are needed to be considered within the optimization process in order to find the best affordable design solutions in terms of acoustic efficiency.

Acoustic performance of the introduced models

Results are shown for the best individuals from the optimization processes. The left part of Figures 5.7-5.10 illustrates the best optimum design found along the five optimization runs for each model. The objective function and the standard deviation with respect to the broadband IL distribution values of the receivers configuration (SD) are on the upper side of their corresponding barrier profiles. The rightmost graphs show the results concerning the acoustic efficiency of the aforementioned models. One of them displays the average frequency-related IL - from (6.1) - of the grid of receivers. The other graph shows the broadband IL spectrum - from (5.2) - mean value for the set of receivers at the same height. This latter assessment is conducted considering a set of four groups of ten receivers each for Figures 5.9 and 5.10. The first group lays on the ground and the remaining ones are placed at different heights, vertically separated by $\Delta y = 1.0\,\mathrm{m}$. A horizontal distance of $\Delta x = 1.0\,\mathrm{m}$ among them is considered, being the nearest ones at $d_r = 0.5\,\mathrm{m}$ from the feasible region. In the case of Figures 5.7 and 5.8, this analysis is restricted to the consideration of just a set of receivers placed at 2 m over the ground.

Figures 5.7, 5.8 and 5.9 show the results concerning the optimization of the models under the consideration of perfectly rigid boundaries (*Case 1*). Figure 5.10 shows the results concerning the top edge optimization of models featuring boundaries with absorbing surface (*Case 2*).

Table 5.1 shows both the shielding efficiency of the best optimums and their acoustic efficiency gain with respect to a 3 m height straight barrier with rigid boundaries. Finally, Table 5.2 collects the coordinates in the transformed domain of the design variables of the best optimum designs featuring rigid and absorbing treatment surfaces (*Case* 1 and *Case 2*, respectively).

Table 5.1: Acoustic performance of the best optimum designs, in dB(A).

Model	*Case 1*		*Case 1 absorbing*		*Case 2*	
	OF	ΔOF*	OF	ΔOF*	OF	ΔOF*
a) 3-sided polygonal	19.27	+4.73	-	-	-	-
b) 5-sided polygonal	20.54	+6.00	-	-	-	-
c) 3-cubic splines	19.03	+4.49	-	-	-	-
d) 5-cubic splines	19.32	+4.78	-	-	-	-
e) Y-shaped	19.29	+4.75	-	-	-	-
f) Tree-shaped	20.52	+5.98	20.94	+6.40	21.41	+6.87
g) Y-variant-shaped	21.29	+6.75	21.13	+6.59	22.00	+7.46
h) Fork-shaped	21.20	+6.66	20.82	+6.28	21.78	+7.24

$^{*}\Delta\mathrm{OF} = \mathrm{OF}_{\mathrm{Model}} - \mathrm{OF}_{\mathrm{Straight\ Rigid\ Barrier}}$

Table 5.2: Design variables of the best optimums for each model and case.

	Case 1								*Case 2*		
	a)	b)	c)	d)	e)	f)	g)	h)	f)	g)	h)
ξ_1	0.1784	-0.5000	0.1039	0.1588	-0.1235	-0.1118	-	-	0.3078	-	-
η_1	-	-	-	-	0.0588	0.8784	0.0431	0.9882	1.0000	1.0000	1.0000
ξ_2	0.5000	-0.3431	0.4647	0.1471	-0.3078	-0.4726	-0.4532	-	-0.5000	-0.3024	-
η_2	0.9451	0.6980	0.9647	0.6314	1.0000	1.0000	1.0000	0.4863	1.0000	1.0000	1.0000
ξ_3	-0.4608	0.4647	-0.1706	0.4765	0.5000	0.5000	-0.2250	-	0.5000	-0.0878	-
η_3	0.0628	0.9529	0.5647	0.7843	0.9647	0.7294	0.7686	1.0000	0.8353	1.0000	0.9255
ξ_4	-0.3314	0.1235	-0.4922	0.3078	-	0.2177	0.1081	-	0.0608	0.1552	-
η_4	-	0.8902	-	0.8980	-	0.8824	1.0000	0.2549	1.0000	0.9686	0.8353
ξ_5	-	-0.3941	-	-0.2098	-	-	0.3315	-	-	0.3827	-
η_5	-	1.0000	-	0.2392	-	-	0.9255	0.8353	-	0.8667	0.7412
ξ_6	-	-0.0608	-	-0.4569	-	-	-	-	-	0.7490	-
η_6	-	-	-	-	-	-	0.8039	0.8471	-	-	0.5686
η_7	-	-	-	-	-	-	-	0.7255	-	-	0.2431

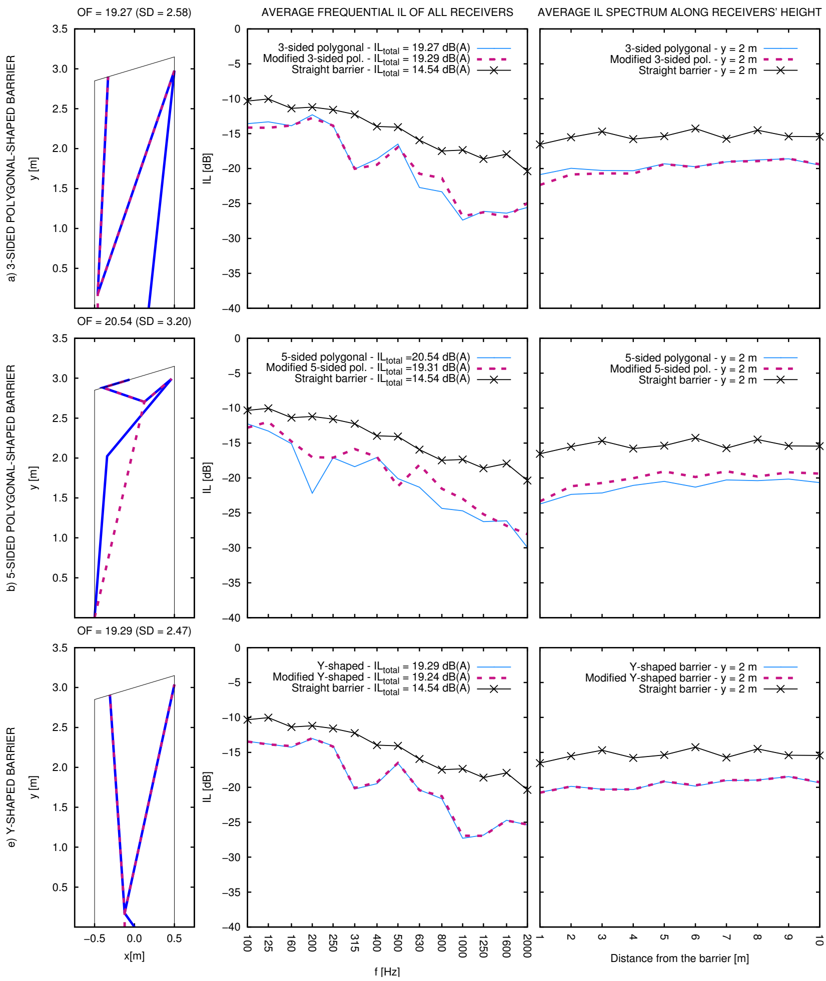

FIGURE 5.7: Overall shape design optimization for polygonal- and Y-shaped models - model a), b) and e), respectively -. *Case 1* (rigid boundaries).

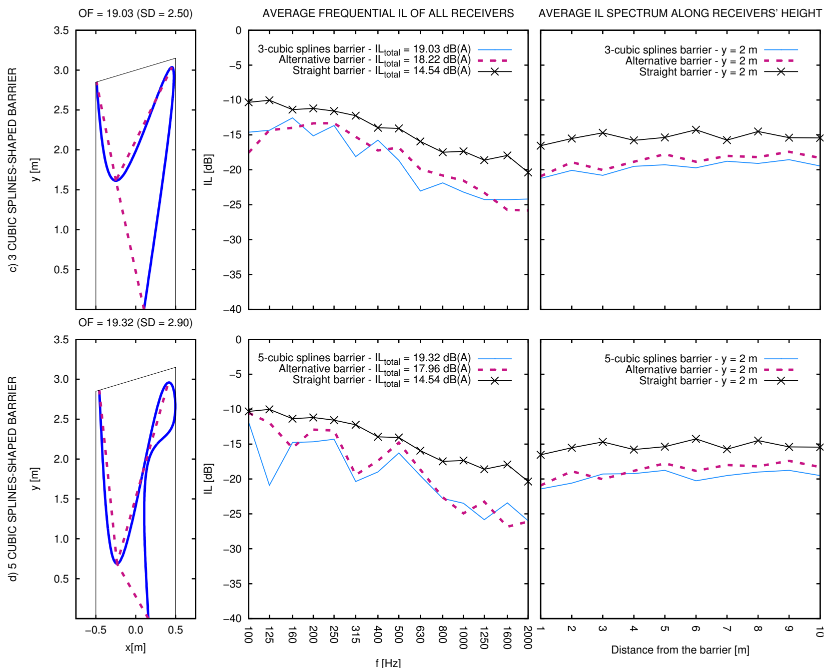

FIGURE 5.8: Overall shape design optimization for multiple cubic splines-based models - model c) and d) -. *Case 1* (rigid boundaries).

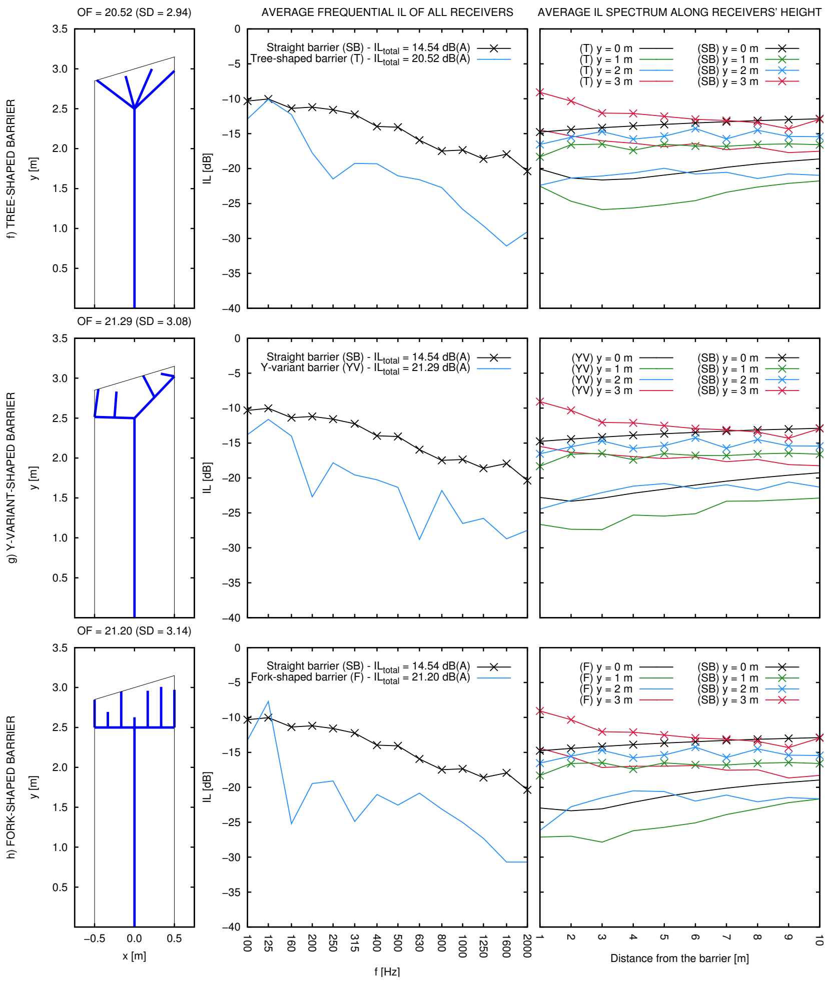

FIGURE 5.9: Top edge optimization for f) tree-, g) Y-variant- and h) fork-shaped model. *Case 1* (rigid boundaries).

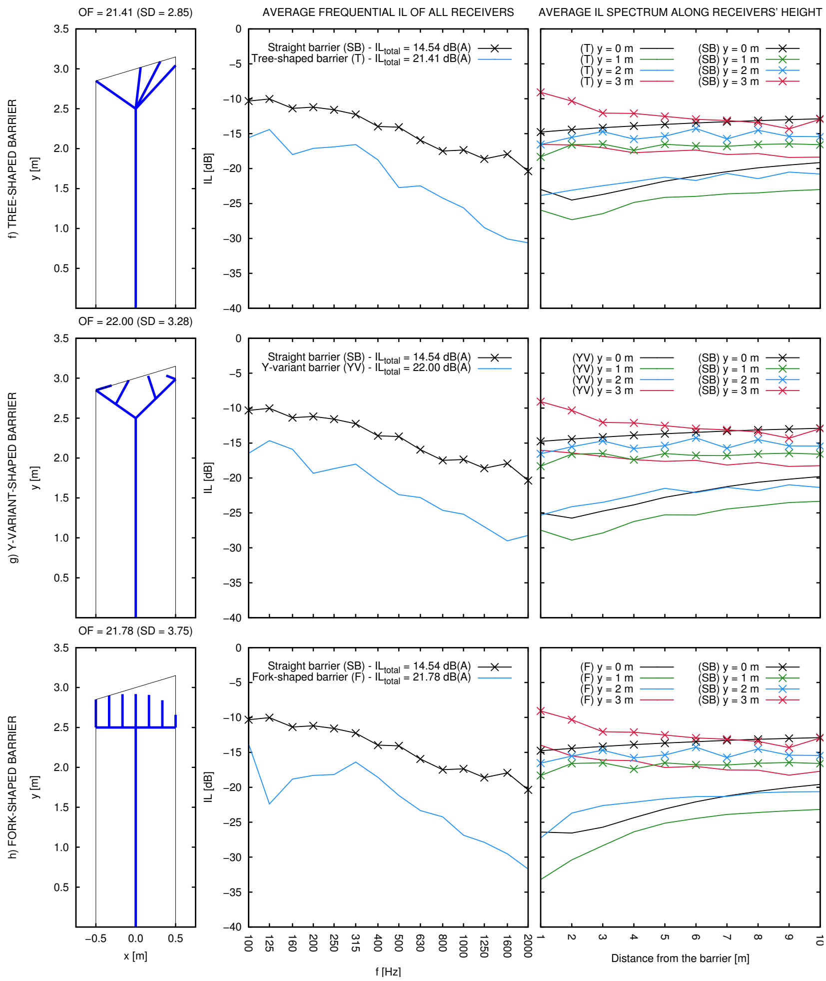

Figure 5.10: Top edge optimization for f) tree-, g) Y-variant- and h) fork-shaped model. *Case 2* (absorbing boundaries).

Sensitivity of the acoustic performance to receivers' location

The influence of the receivers' placement on the barrier performance is a widely known fact. However, the search of profiles with low sensitivity to this condition is a desirable aim. In this line, a study concerning the shape design optimization of model h) is conducted for 20 different receivers configurations. These sets have been chosen randomly, with a scope of application defined by enclosed regions of dimensions 1.0 m x 0.5 m around each original receiver point over the ground. The scope of application for receivers on the ground is restricted to a horizontal range of ± 0.5 m from their positions in the original configuration (see an example of a random-enclosed receivers configuration in the upper graph of Figure 5.11).

The results obtained from this sensitivity analysis disclose a good agreement between the sound performance of optimized profiles when considering random set of receivers configurations and that from the original receivers scheme. The bottom bar graphs of Figure 5.11 show the objective function values under each optimum profile. The geometric similarities of many of them with the optimum barrier for the original receivers configurations, and the homogeneity in the acoustic performance (less than a decibel in difference among them) highlight the suitability of this latter receivers scheme in the shape design optimization.

Discussion

From the analysis of the results obtained some conclusions on the response of the models studied and, most importantly, on the procedure described in this study are drawn:

- In line with other authors (e.g., [13–15, 66, 70]), acting on the top of the barrier is found to be an appropriate strategy to minimize the acoustic impact. This is illustrated by the fact that, on the whole, models based on their top edge optimization feature a better acoustic performance than those whose overall shape has been optimized. Furthermore, the latter models equally display a tendency towards the modification of their top edge in the search for the best acoustic performance.

- Roughly speaking, the overall shape optimization of models with a strong theoretical nature reveals a geometric convergence to the commonly used and largely studied Y-shaped barrier. Its importance lies in the fact that such complex designs can be simplified as easier-to-build configurations without having major influence on the acoustic performance (see Figure. 5.7 and 5.8).

- The barrier performance when applying sound-absorbing materials to some boundaries of its optimized reflecting profile (*Case 1 absorbing*) may lead to unexpected results, as the configuration of the top of sound reflecting barriers plays an important role by producing reflected waves that help partly offset the incident ones. The incidence of this effect largely depends on the crowning configuration of the models studied here, ranging from a gain of 0.4 dB(A) for the tree-shaped barrier - model f) - to a loss of the same value for the fork-shaped barrier - model h) - when compared to their respective performance for rigid boundaries condition (*Case 1*).

- Considering absorbing boundaries condition within the optimization process (*Case 2*) is necessary to give assurance that the search leads to the best affordable profiles in terms of acoustic efficiency. This is supported by the fact that the performance of the best individuals from the top edge optimization of f) tree-, g) Y-variant- and h) fork-shaped barrier under this consideration clearly outperforms the acoustic efficiency of such models from *Case 1 absorbing* - between 0.5 and 1.0 dB(A) -.

- The average IL spectrum values tend to remain roughly regular with the receiver distance to the barrier for the range studied. The fork-shaped barrier - model h) - shows a far better acoustic behavior for close receiver points - between 5 and 10 dB(A) -, though.

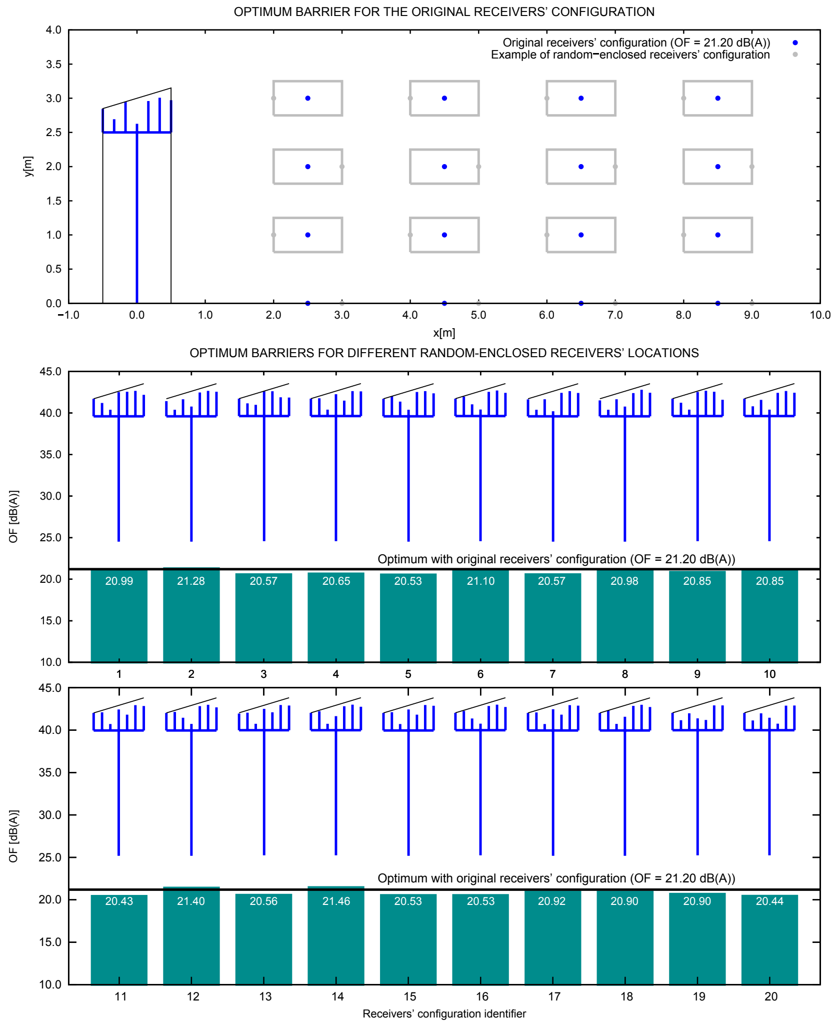

FIGURE 5.11: Up: optimum barrier profile for the original receivers scheme and example of random-enclosed receivers configurations. Bottom: best model h) profile found along the optimization process for each receivers configuration.

5.2.2 Study #2. Influence of the barrier location on the screening performance

To achieve optimal performance a general rule is to place the barrier as close as possible to the road. Unfortunately, however, in many cases this is just an aspirational target as it is not always possible place it as close as desired. One solution is to increase the height of the screen but this may cause great dissatisfaction due to visual obstruction.

The aim of this study is to asses the influence of the barrier placement on the shielding efficiency and minimize its negative effects in far locations. Following this objective, two barrier models (one of them topologically similar to one already studied in a different scenario in previous section) are studied in different locations and with different source-receivers schemes.

Figure 5.12 represents the general 2D configuration applied in this study. It deals with a source of sound, placed parallel to an infinite noise barrier of thin cross-section that stands on a flat plane (ground) of uniform admittance at $\mathrm{d_s} = 9.5\,\mathrm{m}$. Both the ground and the barrier feature a perfectly reflective surface in this analysis ($\beta_g = \beta_b = 0$). A trapezoidal section holds the area for feasible profiles, defined by the barrier projection to the ground, that is constant and $\mathrm{d_p} = 1\,\mathrm{m}$, and the maximum effective height to be achieved, that is $\mathrm{h_{eff}} = 3\,\mathrm{m}$ at the median of the rectangle trapezium.

Two different receivers configurations are studied. In one configuration (Ca) a group of four receivers placed on the ground and separated $\Delta\mathrm{x}$ from one another is considered. In the other configuration (Cb), four groups of four receivers are studied. The first group is laid on the ground and the remaining ones are placed at different heights, separated among them by a distance of $\Delta\mathrm{y}$. In accordance with the former configuration, the horizontal distance among the receivers of a group is $\Delta\mathrm{x}$.

In addition to this, three clearly distinguishable regions in terms of closeness to the median of the feasible region ($\mathrm{d_{r_1}}$) are proposed for both receiver configurations. Table 5.3 holds the data concerning these regions.

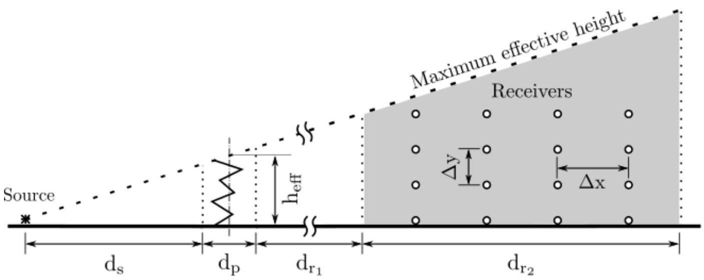

FIGURE 5.12: Bi-dimensional configuration used in the assessment of the influence of barrier location on the acoustic performance.

TABLE 5.3: Data concerning regions under study. Dimensions expressed in meters.

Region	d_s [m]	d_p [m]	d_{r_1} [m]	d_{r_2} [m]	Δx [m]	Δy [m]
1			0.0	10.0	2.0	1.0
2	10.0	1.0	10.0	40.0	8.0	2.0
3			50.0	50.0	10.0	5.0

As stated above, two acoustic barrier designs are proposed in this study (see Figure 5.13). One of them (Model A) is similar to one of the designs already study in previous section but based on six straight boundaries with articulated connections (*6-sided polygonal-shaped* model). Model B is based on a configuration created from patterns governing a 6^{th} degree Bézier curve (*Bézier-curve-shaped* model). The horizontal projection (d_p) and the effective height (h_{eff}) are identical for each design. Both models are built from seven points, being the first and the last one on the ground and on the effective height line respectively. The vertical distance among the points is $d_i = 1/6$ in the search space (transformed domain) and they are just allowed to feature horizontal movements. The polygonal model is built from points through which straight slopes pass. Similarly, the Bézier curve model is built from seven control points of which only the first (0) and the last (7) belong to it.

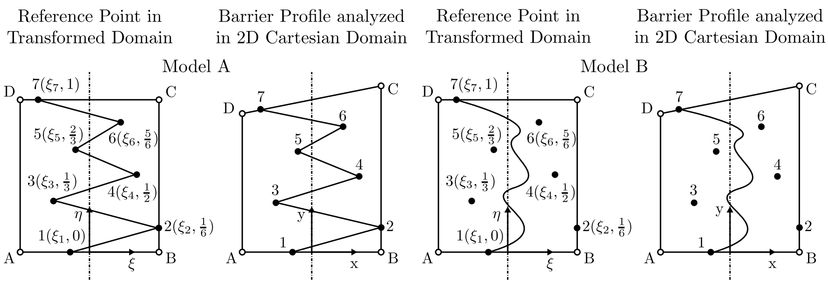

FIGURE 5.13: Design variables and models under study.

Results and discussion

Tables 5.4 collects the results of the best optimum designs found along the five optimization runs. More specifically, the total boundary length (L_b) and the overall screening performance of such optimums (OF_{best}) as well as their efficiency gain with respect a 3 m height vertical screen (ΔOF) are shown for each receiver configuration (RC in the table), region and model. The values of the design variables of these optimums can be consulted in Table 5.5.

Figures 5.14 and 5.15 show the barrier profile of the best optimums in terms of its acoustic efficiency, as well as the average frequential IL evolution of the receivers for each region and model. In addition, Figures 5.14 and 5.15 shows the acoustic performance evolution of the presented models along the optimization process for Ca and Cb receivers configuration, respectively. Solid lines represent the evolution graphs of Model A while dotted lines involve the evolution graphs of Model B. The upper graph represents the evolution of the OF mean value ($OF_{Average}$) considering the best individual of each run (5 individuals in all) at each generation. The graph in the middle involves the evolution of the shielding efficiency of the best individual found at each generation (OF_{Best}), in terms of the objective function (OF), within the 5 runs considered. Finally, the standard deviation mean value (considering just the best individual of each run) is represented at the bottom. As observed, the graphs are shown in an adjusted range in the ordinate coordinate. This facilitates viewing of the results with no loss of relevant details.

TABLE 5.4: Acoustic performance of the best optimum designs.

RC	Region	Model	L_b [m]	ΔL_b [m]	OF_{best} [dB(A)]	ΔOF^* [dB(A)]
Ca	1	A	4.08177	+1.08177	17.92628	+4.32966
		B	3.60547	+1.60547	16.77495	+3.17833
	2	A	3.97839	+0.97839	12.93384	+1.02711
		B	3.51863	+0.51863	14.08611	+2.17938
	3	A	3.52785	+0.52785	12.46634	+1.04716
		B	3.84417	+0.84417	13.57048	+2.15130
Cb	1	A	4.10065	+1.10065	16.95941	+2.41822
		B	3.41333	+0.41333	16.83553	+2.29434
	2	A	3.63842	+0.63842	14.36767	+0.92615
		B	3.71865	+0.71865	14.87088	+1.42936
	3	A	3.60034	+0.60034	13.64344	+0.88584
		B	3.68994	+0.68994	13.75215	+0.99450

$^*\Delta OF = OF_{best} - OF_{\text{Straight Barrier}}$

TABLE 5.5: Design variable values of the best optimums.

			Design variables						
RC	Region	Model	ξ_1	ξ_2	ξ_3	ξ_4	ξ_5	ξ_6	ξ_7
Ca	1	A	-0.48824	0.06078	0 .01765	0.35098	0.02941	0.49608	-0.31961
		B	-0.01373	0.05882	-0.48235	-0.57647	0.17647	-1.23529	0.50000
	2	A	-0.39412	-0.02549	0.39020	0.08824	0.04902	0.48039	0.34314
		B	-0.50000	0.36471	-1.44706	-0.01176	0.38823	-1.02353	0.40980
	3	A	-0.44902	-0.08039	-0.22549	0.35490	0.44510	0.26078	0.32353
		B	0.43726	-0.95294	0.15294	-1.30588	0.38824	-1.23529	0.31177
Cb	1	A	0.50000	0.22941	-0.15882	0.32745	-0.03333	0.37843	-0.44118
		B	-0.06078	-0.17647	0.10588	-0.92941	0.74118	-0.90588	0.50000
	2	A	-0.22156	-0.50000	0.29216	0.37451	0.50000	0.50000	0.31569
		B	-0.46470	-0.67059	2.05882	-0.95294	1.37647	-0.90588	0.50000
	3	A	-0.25294	-0.50000	0.24902	0.37843	0.50000	0.50000	0.29608
		B	-0.48039	-0.62353	2.01176	-1.04706	1.49412	-0.88235	0.50000

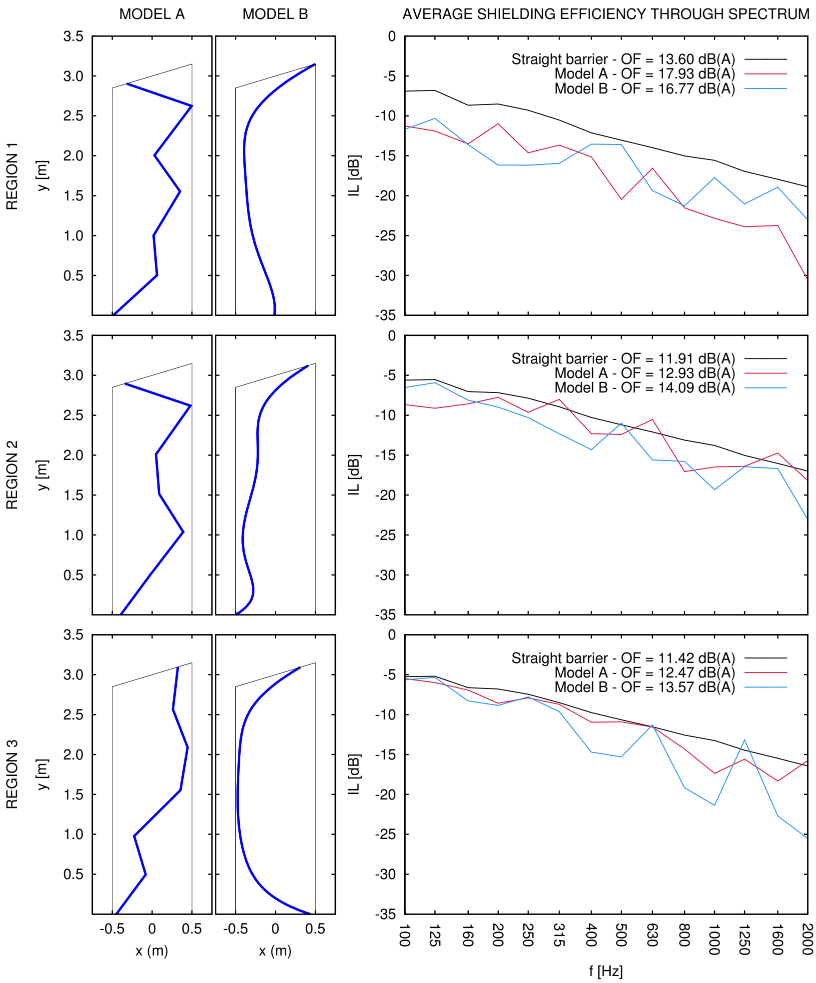

FIGURE 5.14: Ca receivers configuration. Left, barrier profile of the best individuals for each region and model. Right, average frequential IL evolution for both models and for the 3 m straight barrier.

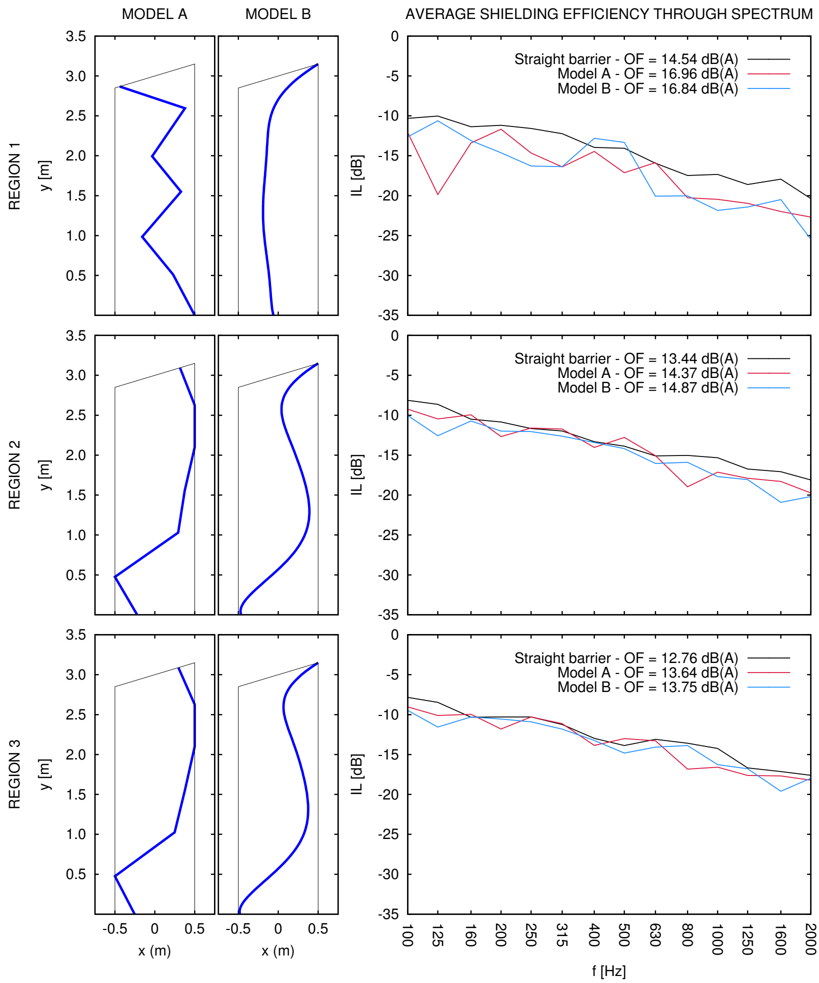

FIGURE 5.15: Cb receivers configuration. Left, barrier profile of the best individuals for each region and model. Right, average frequential IL evolution for both models and for the 3 m straight barrier.

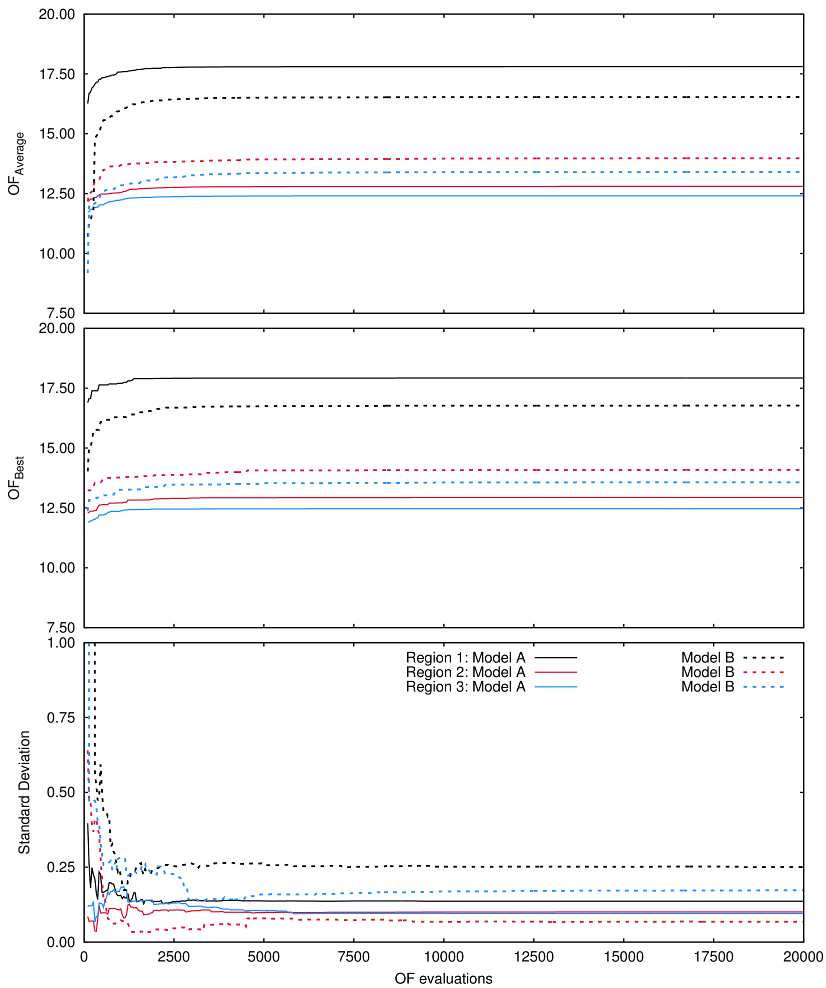

FIGURE 5.16: Evolution graphs of models for Ca receivers configuration.

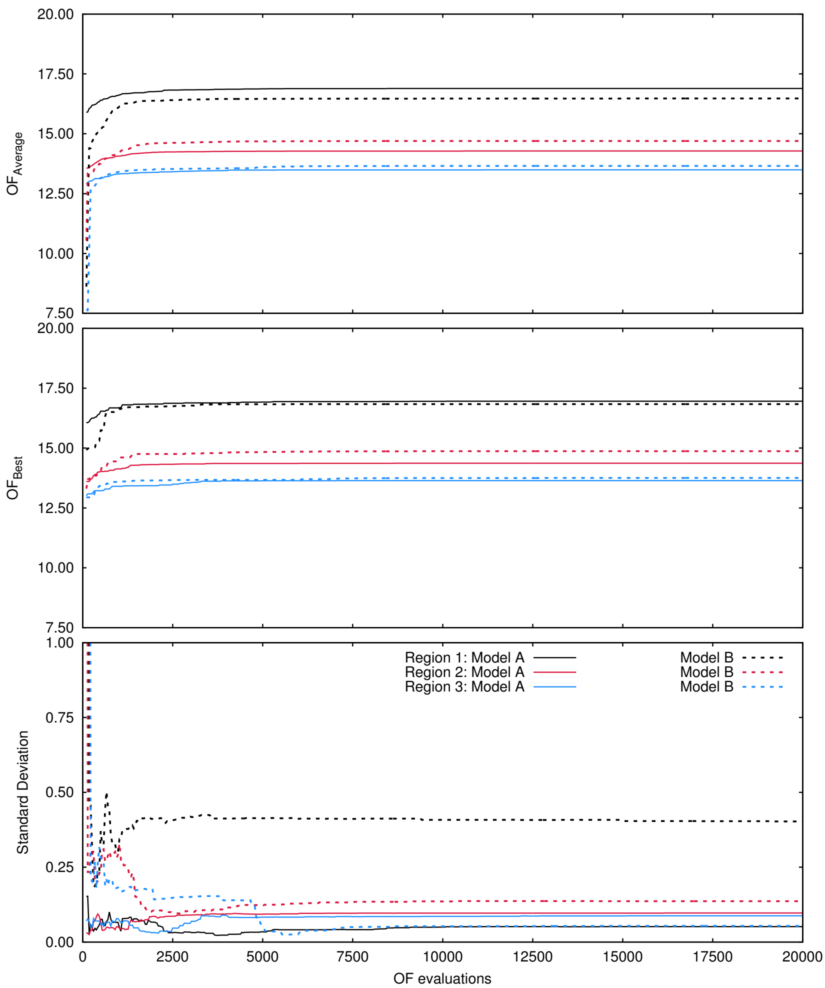

FIGURE 5.17: Evolution graphs of models for Cb receivers configuration.

In the light of the results the following analysis is drawn:

- The polygonal-shaped barrier outperforms the acoustic efficiency of the 6th degree Bézier curve-shaped model for the near region when the receivers are placed on the ground (Ca configuration). However, the latter model performs a better acoustic behaviour for non-near regions - over 1 dB(A) -.
- Both models under study display similar acoustic performances when a grid of receivers is considered in the shadow region of the barrier, with the exception of the intermediate region in which the Bézier model outperforms the polygonal design in half a decibel.
- According to the comparative analysis between the optimized models and the straight barrier the need to study designs alternative to the latter is suggested, even for far regions.
- Model B displays a wider variety among best individuals of the population when compared with Model A according to the evolution of the highest standard deviation (Figure 5.16 and 5.17), meaning that the convergence of the optimization process turns out to be more cumbersome in Model B (optimization process is easier in Model A).

5.3 Validation and application of the methodology on the basis of an scale model test from Fujiwara et al. [12]

This chapter concludes with a numerical model validation of the introduced methodology, on the basis of results present in the bibliography concerning experimental scale tests featuring top devices similar than those from the previously studied models. This analysis is conducted by using the same code that implements the Dual BEM formulation applied in the previous studies, with the purpose of both 1) validating the results here presented and 2) improving the acoustic performance of the selected experimental scale model by slightly modifying its top geometry.

Some works concerning acoustic measurements of full scale and scale-model of barriers can be found in the literature (e.g., [11, 12, 66, 146]). Regardless the fact that any of these works are of evident concern in terms of validation, the test conducted here aims at comparing both the experimental and numerical results from Fujiwara et al. [12] for a specific scale model. For the sake of homogenization with the configurations analyzed so far, the scale model in [12] has been adapted to a full-scale model in this analysis. The barrier under testing deals with a 3 m height fork-like shaped barrier featured with two types of wells, of depth 0.2 m and 0.4 m (see upper part of Figure 5.18). For guaranteeing the acoustic intensity along the spectrum to be the same, the 1/3-octave band center frequencies used so far is adapted to fit the 1/15-octave spectrum applied in [12], ranging from 200 to 630 Hz.

Figure 5.19 shows the good agreement in results between the Dual BEM formulation and both the experimental and numerical results (using the classical BEM formulation) from the aforementioned work. It can be proved that the thickness of the models plays an important role in the small differences observed in the numerical results depicted. In addition, results concerning the shape optimization of the tested barrier are displayed. The bottom part of Figure 5.18 represents the best individual found after five independent runs. As observed from this configuration, the top boundaries have been allowed, at most, to be as large as those from the original configuration (upper part of Figure 5.18), without taking advantage of the maximum effective height established for the feasible region. In conclusion, the optimum design clearly outperforms the acoustic behavior of the reference scale model, illustrated by a difference in objective function values of over 3 decibels (19.73 dB(A) for the profile under testing versus 23.41 dB(A) for the optimum profile) in the graph within the frequency range analyzed.

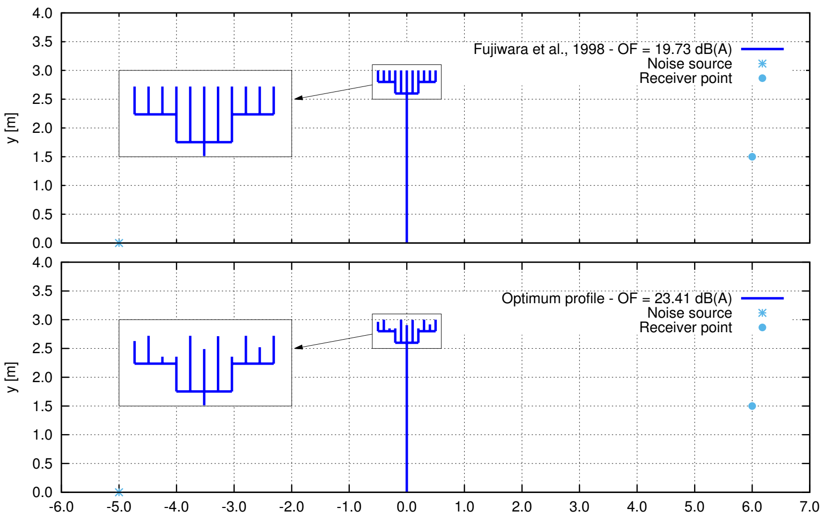

FIGURE 5.18: Up: barrier profile under testing (Fujiwara et al. [12]). Bottom: best design profile found along the shape optimization of the tested barrier.

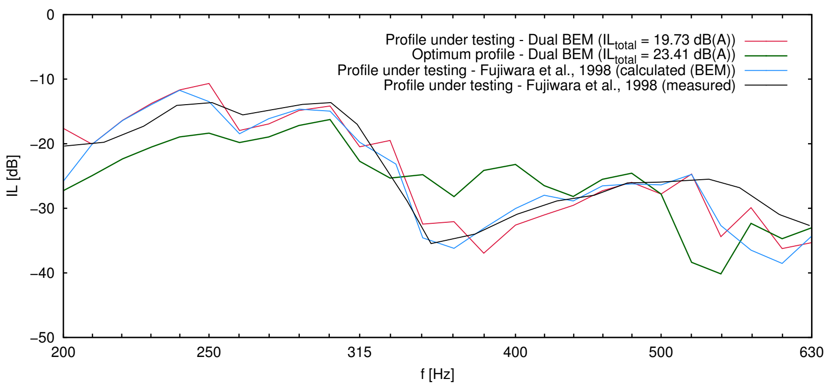

FIGURE 5.19: Validation of the results. Insertion loss evolution of both the tested and the optimized barrier compared with the results obtained by Fujiwara et al. [12].

6. METHODOLOGY APPLIED TO THE STUDY OF DIFFUSER-BASED BARRIERS

The approach of this study intends to broaden the versatility and adaptability of the methodology presented in the previous chapter. In this line, a more general Boundary Elements (BE) formulation is developed and implemented in a computer code that allows a procedure with a broader scope, allowing us to deal with any type of 2D acoustic optimization problem involving noise barriers in a more systematic, robust and flexible way.

The introduced procedure makes use of a Dual BE approach coupled with an evolutionary algorithm in the optimization of noise attenuation of barriers with reactive surfaces. More specifically, numerical results on the basis of three topological designs featuring wells with different depths on their top are performed. Based on complex geometries, these designs combine a general volumetric structure with very thin elements that can be idealized as null-thickness bodies. In this respect, the Dual formulation presented in this study arises as the most appropriate strategy from BEM to address the problem, by allowing us 1) to assume such an idealization of reality with no substantial influence on the acoustic performance for the considered thickness of very thin sections [47] and 2) to mitigate the fictitious eigenfrequencies associated with the inner domain of the volumetric structure. To the researcher's knowledge, there are no works in the bibliography that address the issue under the framework followed in this study.

Two-dimensional sound propagation hypotheses are considered, i.e., an infinite, coherent mono-frequency source of sound and a noise barrier with no geometric variation that stands on a flat plane (ground) of uniform admittance. The problem is performed in the frequency domain with the usual assumptions (Helmholtz equation): the medium (air) is modeled as homogeneous, elastic and isotropic with no viscosity, under small disturbances and initially at rest with no wind effects. Expression of the objective function to be maximized throughout the shape optimization process is written in terms of this response.

A study on the basis of leading to easier-to-build, more practical configurations from barrier designs obtained after optimization is also performed. In addition, a comparative study between the shielding efficiency associated with one of the optimum designs and a same topological design previously studied in the literature is conducted. Finally, this chapter ends with the insights derived from the analysis of the results obtained.

6.1 Diffuser-based top designs for sound attenuation in exterior acoustic problems

For their unquestioned benefits for scattering sound field, the use of diffusers has been the subject of many reviews and studies in indoor acoustic projects. Among them, those based on sequence number series (such as maximum length sequence, quadratic residue diffuser, primitive roots diffuser, etc.) have gained prominence for their excellent scattering properties, characterized by an approximately flat power spectral density. As the power spectrum and surface scattering are closely related [147–149], the far field scattering can be approximately predicted by taking the Fourier transform of the surface reflection coefficients (in this case, a series of wells with different depths that could be modeled as a flat surface of varying impedance). In short, any numerical sequence featuring good auto-correlation properties (in other words, the auto-correlation function of the reflection coefficients of the surface is a delta function) presents a Fourier transform with a flat power spectral density, meaning that such a surface exhibits an even scattering distribution of sound.

With the purpose of raising the acoustic performance, numerous and innovative designs have been proposed and studied in the literature for compensating the limitations normally associated with the parameter with greatest influence on the barrier efficiency: the effective height. In this way, despite the indoor-oriented application of well-based designs, the use of such devices on noise barriers in exterior acoustic problems has evidenced a better performance when compared with both a vertical screen and other classic top configurations. Some noteworthy works concerning the use of diffusers installed on the barrier top can be found in the literature. Such is the case of Quadratic Residue Diffusers (QRDs) [13, 29, 30, 33] and Primitive Roots Difussers (PRDs) [32]. Other designs featuring elaborated configurations eligible for either some kind of scattering or screening behavior can be found in [15, 21] (see Figure 6.1).

All the aforementioned works address the problem with the standard BEM formulation, considering the real geometry of the barrier comprised of thick and very thin elements. Despite their remarkable contribution, no shape design optimizations are performed in the referenced works. In this regard, the methodology here presented proposes a general procedure that aims at optimizing the shape design of edge-modified road acoustic barriers using BEM. This methodology offers an appropriate, ideal solution for complex configurations eligible for some sort of geometric simplification. Under this proposal, the overall barrier configuration can be modeled considering both thickness and null-thickness bodies as representatives of very thin elements (the thickness of these elements is neglected). Based on a frame of free geometric constraints, the definition of the barrier profile is then easily accomplished. This approach results in faster computational times within a cumbersome process where every possible design is assessed along the whole spectrum of frequencies.

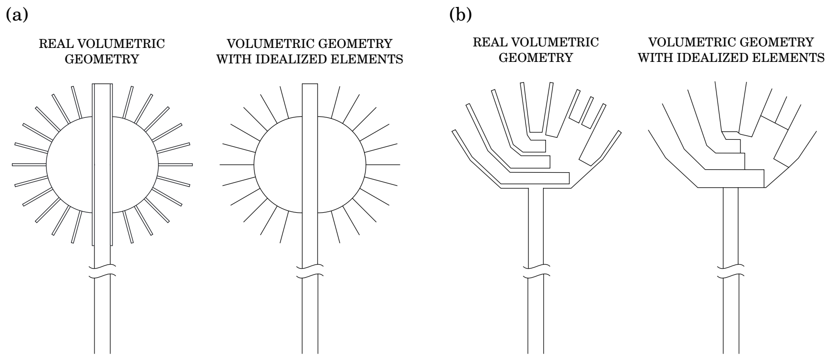

Figure 6.1: Examples of complex designs with elements eligible for geometric idealizations. (a) Waterwheel-top barrier from Okubo and Fujiwara [15]. (b) Complex barrier-top featuring wells with different lengths and paths [21].

The need of the implementation of the Dual BEM formulation in this work is clarified in Figure 6.2. The strategy of the application of both formulations varies depending on the nature of the element under consideration. This way, with the purpose of mitigating the effects of the fictitious eigenfrequencies when dealing with non-thin bodies, a Dual BEM formulation based on the combined use of the standard boundary integral equation (SBIE) and the hyper-singular boundary integral equation (HBIE) coupled by means of a frequency-related complex value is proposed [109]. The nature of the issue is different when dealing with very thin bodies. In this case, numerical integration problems may appear affecting, equally, to the barrier performance. The idealization of such elements as non-thickness bodies not only solves the problem but also contributes to ease their geometric representation, which greatly simplifies the optimization process. With this aim, the SBIE and the HBIE are applied simultaneously but separately. Such a simplification of reality is a real asset, specially when compared with the case of the faithful, detailed definition of real complex volumetric designs.

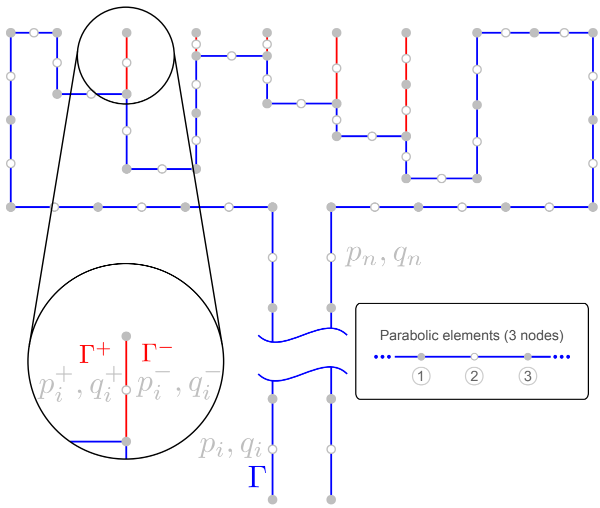

FIGURE 6.2: Example of barrier discretization, after idealization of very thin bodies as null-width elements, with parabolic elements (3 nodes) for f=500 Hz of a QRD-based design. For the ease of viewing, non-thin elements are represented in blue, while very thin bodies are idealized as null-thickness type and depicted in red.

6.2 Description of the shape optimization framework

Shape design optimization is performed by the combined use of an evolutionary algorithm and the mentioned Dual BEM formulation. A detail description of the Dual approach used in this study is found in Chapter

3. The evolutionary algorithm software used in this work applies the GAlib package [112]. Additional information of the GA implemented in this methodology refers to Chapter 4.

In the work presented in the previous chapter, a Dual BEM approach coupled with a GA for the analysis and optimization of very thin noise barriers was introduced. Concerning the work here presented, the scope of the Dual code is broaden to cope with the analysis of generic volumetric barriers featuring, in addition, very thin elements. Under the framework of the coupled use of this code and GAs, improved designs of top edge devices are proposed in a way, to the researcher's knowledge, not covered so far in the bibliography concerning the issue. As an application, numerical results on the basis of three models with complex top designs featuring both thick and very thin bodies (idealized as null-thickness type) are performed. The use of the Dual BEM formulation is justified in the sense that is the most appropriate strategy to address the proposed problems numerically, as reported by Hong and Chen [40], Krishnasamy et al. [42], de Lacerda et al. [47], Chen and Chen [43], Chen and Hong [45], Wu [44], Chen et al. [150] and Tadeu et al. [48]. Above all, the null-thickness idealization greatly eases the geometric definition of configurations with no substantial influence on the acoustic performance for the considered thickness of very thin bodies [47].

6.2.1 Bi-dimensional configuration

Figure 6.3 represents the general configuration for just one of the models under study - model (a) -. It deals with, as previously stated, a two-dimensional model concerning an infinite, coherent mono-frequency source of sound, generating pure tones within the considered frequency spectrum, parallel to an infinite barrier with no geometric variation that stands on a flat plane (ground) of uniform admittance. Both the ground and the barrier boundary feature a perfectly reflecting surface ($\beta_b = \beta_g = 0$). Just one receiver in the shadow region is considered in assessing the overall acoustic efficiency (to be maximized along the optimization process). Both the noise source and the receiver are located on the ground at a horizontal distance of 5.0 and 25.0 m of the barrier, respectively. The maximum effective height to be achieved is $\mathrm{h_{eff}} = 3.0$ m at the median vertical axis of the barrier.

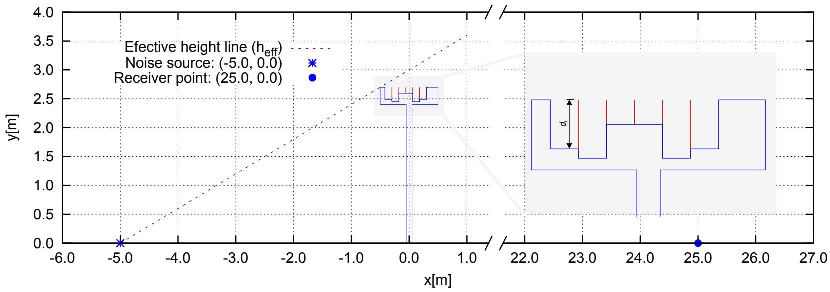

FIGURE 6.3: Bi-dimensional configuration to be used in the optimization process of the models presented in this work. Example of a QRD-inspired top design (model (a) in this study) with different well depths d_i.

6.2.2 Determination of the acoustic efficiency of the barrier

As is well known, the shielding efficiency of the barrier is measured for every frequency from the analyzed noise source by means of the insertion loss (IL), defined as usual:

$$\mathrm{IL} = -20 \cdot \log_{10}\left(\frac{\mathrm{P_B}}{\mathrm{P_{HS}}}\right) \text{[dB]} \tag{6.1}$$

with its measure being representative of the difference of sound pressure levels at the receiver point in the situation with ($\mathrm{P_B}$) and without ($\mathrm{P_{HS}}$) considering the barrier.

With the purpose of conducting an optimization process where the excitation is represented by a noise source pulsing at every frequency of the band spectrum, the efficiency of the barrier for the considered receiver can be written in terms of the broadband insertion loss as:

$$\mathrm{IL_{total}} = -10 \cdot \log_{10}\left(\frac{\sum_{\mathrm{i=1}}^{\mathrm{NF}} 10^{(\mathrm{A_i}-\mathrm{IL_i})/10}}{\sum_{\mathrm{i=1}}^{\mathrm{NF}} 10^{\mathrm{A_i}/10}}\right) \text{[dB(A)]} \tag{6.2}$$

being NF the studied spectrum number of frequencies, here NF = 86, A_i the spectrum A-weighted noise level and IL_i the insertion loss value for sources pulsing at every frequency of the spectrum, according to (6.1).

6.2.3 Road traffic noise spectrum applied

In this study, the noise source has been characterized by using the UNE-EN 1793 [117] standard involving the normalized traffic noise spectrum, generating pure tones ranging from 100 to 5 000 Hz corresponding to one-third center band frequencies. Given the high frequency dependence of the studied designs and to assess as accurately as possible the broadband IL, the 1/3-octave bands are expanded to 1/15 octave intervals, represented by band center frequencies. The normalized levels for 1/15 octave frequency bands in this corrected spectrum are calculated in such a way that the total acoustic intensity is the same than that of the original (Chapter 2). The estimator taken into account along the shape optimization process, that is, the objective function, is entirely based on the broadband IL value at the considered receiver point ($OF = IL_{total}$). The maximization of this latter parameter through the optimization process is intended.

6.2.4 Used GA parameters

As each objective function evaluation requires the execution of a high cost CPU for BEM, a high exploitative strategy with high selection pressure has been taken into account: a *steady-state* genetic algorithm [144, 145] is used replacing the two worst individuals (in terms of their objective function) at each generation. A population size of 100 individuals, with a *two-point* crossover operator (crossover rate equal to 0.9) is used in this study. The considered mutation rate is $1/n_{ch}$, where n_{ch} is the chromosome length with design variables coded with different binary bit precision, depending on the model, according to the Gray code (see Table 6.1). The stopping criterion condition is met for 1 000 generations.

6.2.5 Overview of the process

To facilitate understanding of the methodology, Figure 6.4 shows a flow diagram concerning the evolutionary process on the search of the best

Table 6.1: Description of the design variables (well length, coded with binary bits) of each topological model to be optimized and of the corresponding chromosome.

Model	Chromosome length (n_{ch})	Bit precision per variable	Design variable range [m]	Discrete values per variable
(a)	Symmetric: 15 Non-symmetric: 30	5 (each well)	0.000-0.250	32
(b)	Symmetric: 60 Non-Symmetric: 120			
(c)	Symmetric: 21	Well #1: 5 Well #2: 5 Well #3: 5	0.000-0.808 0.000-0.643 0.000-0.350	32
	Non-symmetric: 42	Well #4: 3 Well #5: 3	0.000-0.185	8

acoustic solutions. The procedure makes use of a steady state GA with individuals initially based on a proposal on random design variables of the topological model intended to be optimized, featured by discrete values of well length. A detailed description concerning the definition of both the design variables and the chromosome of each model is collected in Table 6.1. Such design variables form the chromosome of the individual proposed by the GA shaping, therefore, the geometry of the top device of the barrier. At this point, the screening behavior of each individual is performed using the aforementioned Dual BEM code. This requires a proper discretization of the barrier boundary with ever-increasing number of elements along the frequency spectrum. In this work, parabolic elements are coded with a maximum length of half the wavelength of the frequency under study for adequate convergence of the results (see Chapter 3). The initial population is then ranked in terms of acoustic performance, here represented by the objective function value (OF) characterized, in turn, by the broadband insertion loss (IL_{total}) - see (6.2) -. In this way, each individual is more likely to be selected according to its screening behavior (OF). Therefore, by using the *tournament selection* operator, two individuals are chosen (*parents* in proper terminology of evolutionary algorithms) and are to be crossed with a probability of 90% by the *two-point crossover* operator, leading to an offspring comprised of two new individuals (*children*)

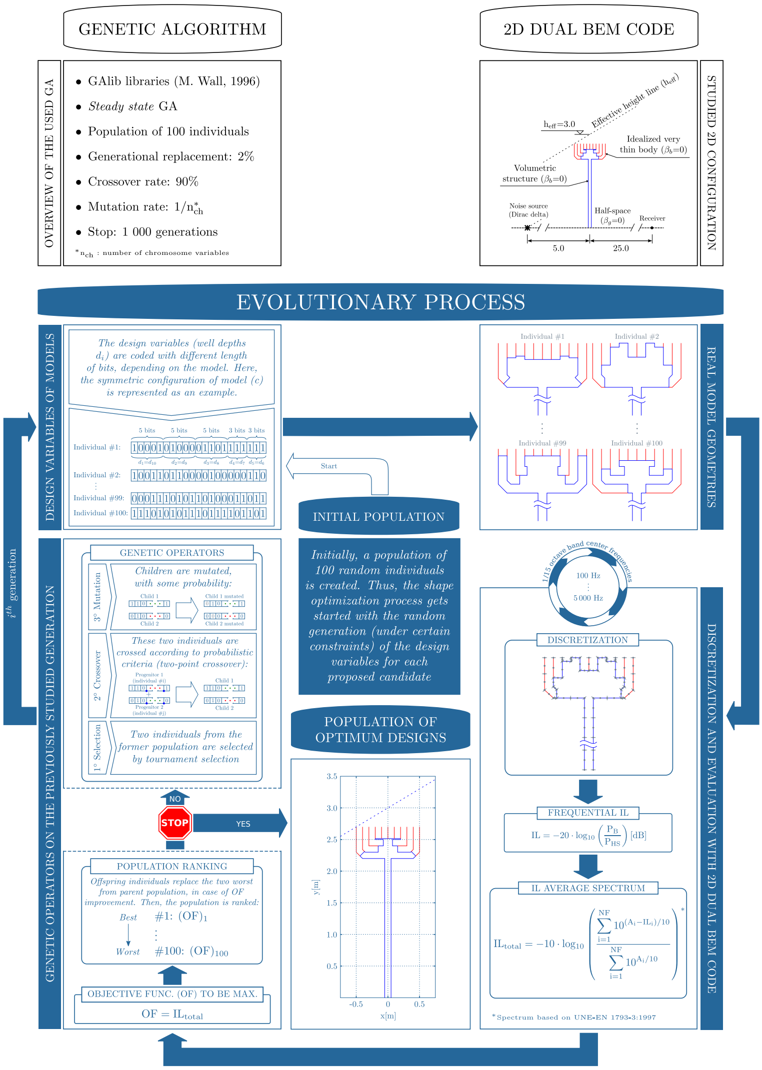

FIGURE 6.4: Overview of the GA used, layout of the considered bi-dimensional configuration and optimization flow diagram.

whose chromosomes are eligible for mutation according to probabilistic criteria. After mutation, offspring individuals replace the two worst in the parent population (in case of better value of OF, that is, improvement of the acoustic behavior). This iterative process continues until reaching the stopping criterion, which is set at 1 000 generations due to balancing an acceptable convergence of the results with invested computational resources. Five independent runs of the optimization process are considered for each model.

6.3 Numerical shape optimization

The shape optimization process aims at searching for series of wells that maximizes the screening performance at the considered receiver point, for both symmetric and non-symmetric configurations of the topological models described below.

6.3.1 Description of the topological models

The models proposed in this work have been conveniently designed with the intention of taking advantage of the potential screening properties underlying well-based top geometries (some of them inspired on configurations previously studied in the literature). Figure 6.5 shows the models under study. The upper model - model (a) - is a QRD-inspired top configuration derived from that studied by Monazzam et al. [13]. Installed on the top of a 0.10 m width vertical stem, it deals with a 1.00 m width, 0.30 m height box comprised of six wells of 0.12 m width and different depths (d_i) separated by very thin elements. The model in the middle - model (b) - is inspired on the so-called *waterwheel* cylinder studied by Okubo et al. [15]. It is based on a constant-radial top, over a 0.03 m width vertical stem, comprised of two semi-circular cores with an outer diameter of 0.59 m from which a uniform distribution of very thin elements are born that separate wells with different depths d_i. The model at the bottom - model (c) - is a novel design. It deals with a top configuration featuring a series of straight and crooked-type wells separated by very thin elements over a 0.10 m width vertical stem. With the purpose of easing the geometric definition, the very thin elements featuring the top of the models are mathematically considered as null bodies. As in the line of other works

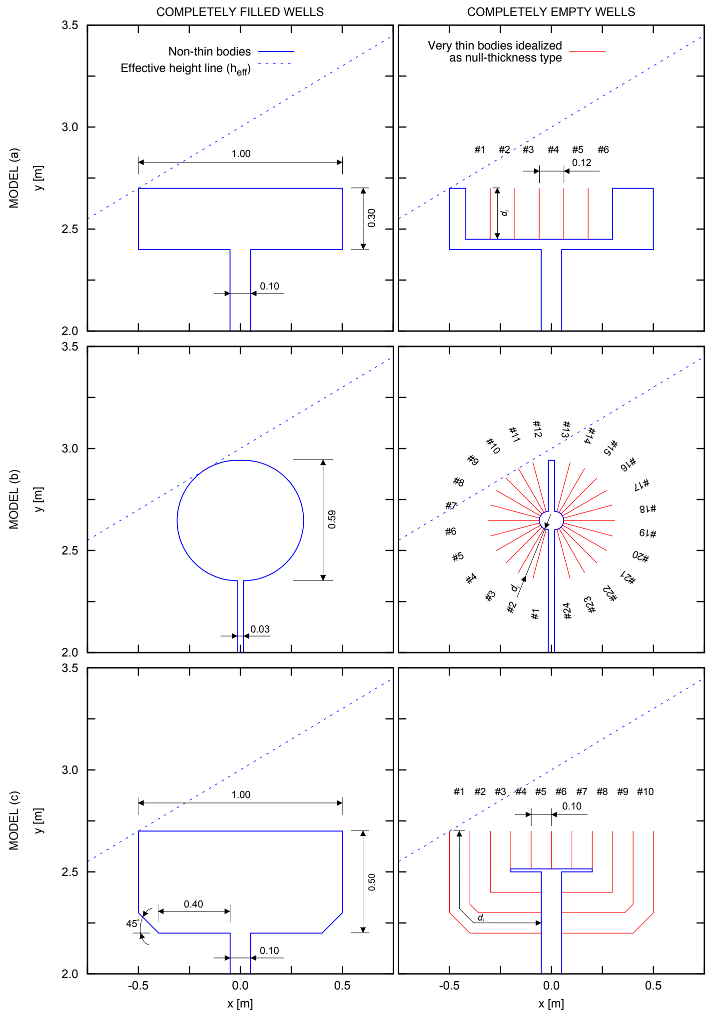

FIGURE 6.5: Top designs of the models under study. Left, models featuring just non-thin elements after filling the set of wells. Right, models featuring both non-thin and very thin bodies in the scenario in which every well is completely empty (for models (a) and (b): d_i=0.250 m; for model (c): d_1=d_{10}=0.808 m, d_2=d_9=0.643 m, d_3=d_8=0.350 m and d_4=d_5=d_6=d_7=0.185 m). Dimensions in meters.

(e.g., [71–73]), the effective height of these models is set to h_{eff}=3.0 m at the median axis. For this reason, despite models (a) and (b) are based on models already studied in the literature, their effective height has been modified to this value. As can be seen in 6.5, models (a) and (b) are comprised of wells with the same potential depth, while model (c) has been designed with the purpose of featuring wells with different lengths. A detailed description of the design variables of each model can be consulted in Table 6.1.

Generally speaking, the models presented can be categorized as edge-modified barriers, that is, barriers whose top edge has been conveniently shaped with the aim of raising the screening performance of the reference vertical screen. Based on different acoustic mechanisms, such as interference and resonance, the adequate shaping of these devices can lead to significantly high noise reduction when compared with the reference barrier for a specific source-receiver scheme [14]. Consequently, despite the apparent design complexity, models similar to those introduced here are designed for practical use [15, 21]. Other interesting devices for practical applications and distributed as commercial products in Japan can be consulted in [151].

6.3.2 Designs after optimization

Figure 6.6 illustrates the results concerning the best optimum individuals from the optimization processes. In the left part, the top geometries of each model for symmetric and non-symmetric configurations are shown. The right part depicts the IL spectrum evolution of such optimum designs along the considered frequency range, in comparison with their corresponding model for both completely filled and completely empty wells (see Figure 6.5) and with a 3 m vertical screen, for the given noise source-receiver scheme. The overall acoustic performance of the optimum designs, according to (6.2), is also included in the figure (see graphic legend). In addition, Figure 6.7 shows the acoustic performance evolution of the presented models along the optimization process. Red lines represent the shielding efficiency of the best individual found at each generation, in terms of the objective function (OF), within the 5 runs considered. Blue lines depict the OF mean value considering the best individual of each run (5 individuals in all) at each generation. As observed, the graphs are shown in an adjusted range in the ordinate coordinate. This facilitates viewing of the results with no loss of relevant details. The results achieved suggest that further evolution is needed for a proper convergence, specially in the case of non-symmetric configurations and, in particular, for model (b).

Table 6.2 presents the well depths (d_i) of the best optimum designs for each model, configuration and run. As an example, the corresponding computing time for model (a) cases is 97 hours on average, run in a CPU Intel© Xeon© 2.60 GHz processor (RAM is not significant here). Row $\mathrm{IL}_{\mathrm{total}}^{\mathrm{3\,m\,vert.}}$ collects the acoustic efficiency gain of such optimums in comparison with the reference 3 m vertical barrier.

Finally, with the intention of illustrating the effects of the best optimum designs of non-symmetric configurations, Figure 6.8 shows in colormaps the broadband sound pressure level ($\mathrm{SPL}_{\mathrm{total}}$) in a domain with a noise source intensity of 90 dB(A) (measured 1 m away in the free field) pulsing at every frequency according to the spectrum considered so far [117]. Results are easily obtained through simple operations from the $\mathrm{IL}_{\mathrm{total}}$ values associated with such optimums.

6.3.3 Designs for practical use

With the intention of both determining how important the role of wells at the top is in the shielding behavior and leading to easier-to-build, more practical barrier designs, Figure 6.9 shows some geometric modifications on the basis of the optimum symmetric and non-symmetric configuration of model (b). Starting off from such designs after the GA optimization, slight modifications, in terms of emptying-filling patterns of some wells, are introduced (represented by Mod. #1 to Mod. #7). In brief, wells with approximately the same depth are grouped: those at the bottom (wells from #1 and #3, and symmetric ones), at the middle (wells from #4 and #9, and symmetric ones) and at the top of the device (wells from #10 and #12, and symmetric ones). In addition, a design previously studied in the literature by Okubo et al. [15] is included as reference. Results are presented in terms of the broadband sound pressure level ($\mathrm{SPL}_{\mathrm{total}}$) in the vicinity of a noise source pulsing with a sound intensity level of 90 dB(A) according to the used traffic noise spectrum [117] for the considered source-receiver scheme. This way, the lower the $\mathrm{SPL}_{\mathrm{global}}$, the better. As observed, the practical designs outperform the reference case over a decibel in most cases for the symmetric configuration.

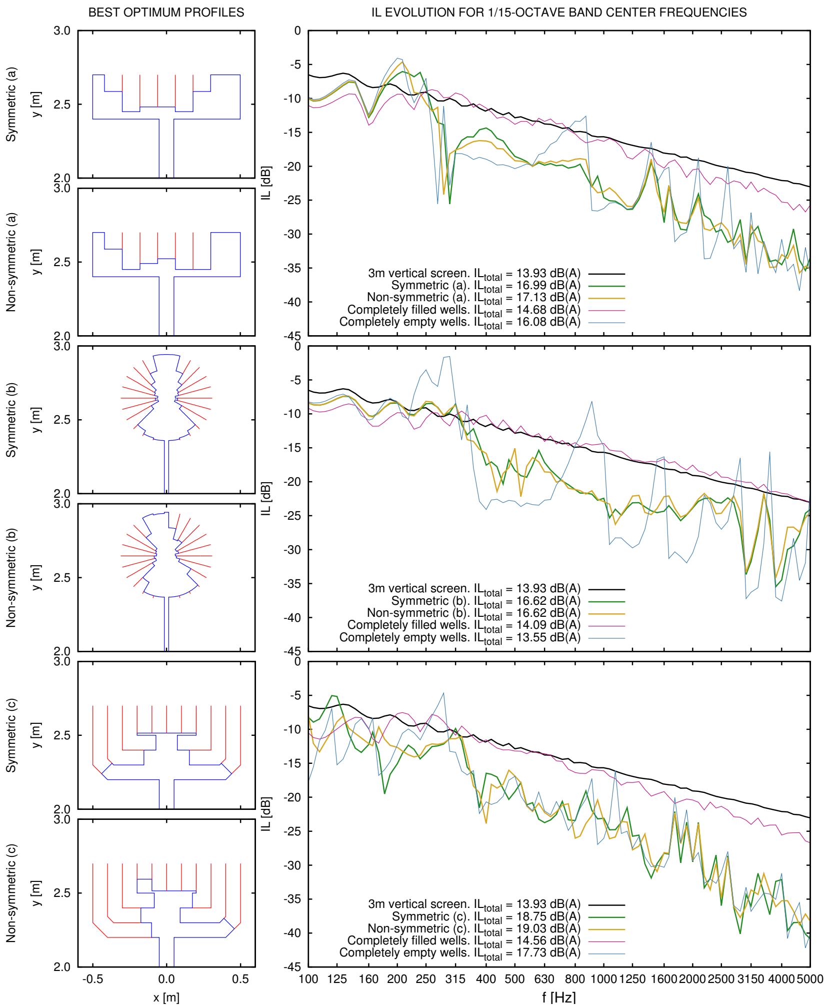

FIGURE 6.6: Results for the best individuals found along the optimization processes for each model and configuration. Left, best optimum profiles. Right, IL along the considered 1/15-octave band center frequencies for the aforementioned geometries and their corresponding model for both completely filled and completely empty wells (see Figure 6.5).

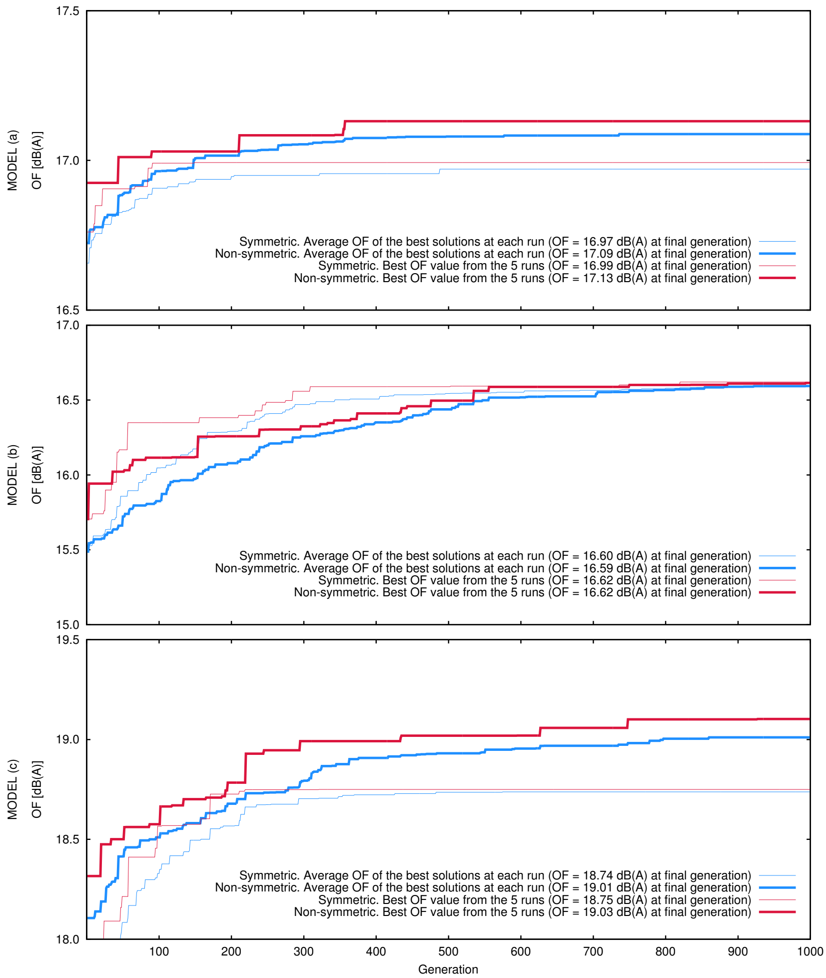

FIGURE 6.7: Objective function (OF) convergence charts for both symmetric and non-symmetric configurations of the studied models.

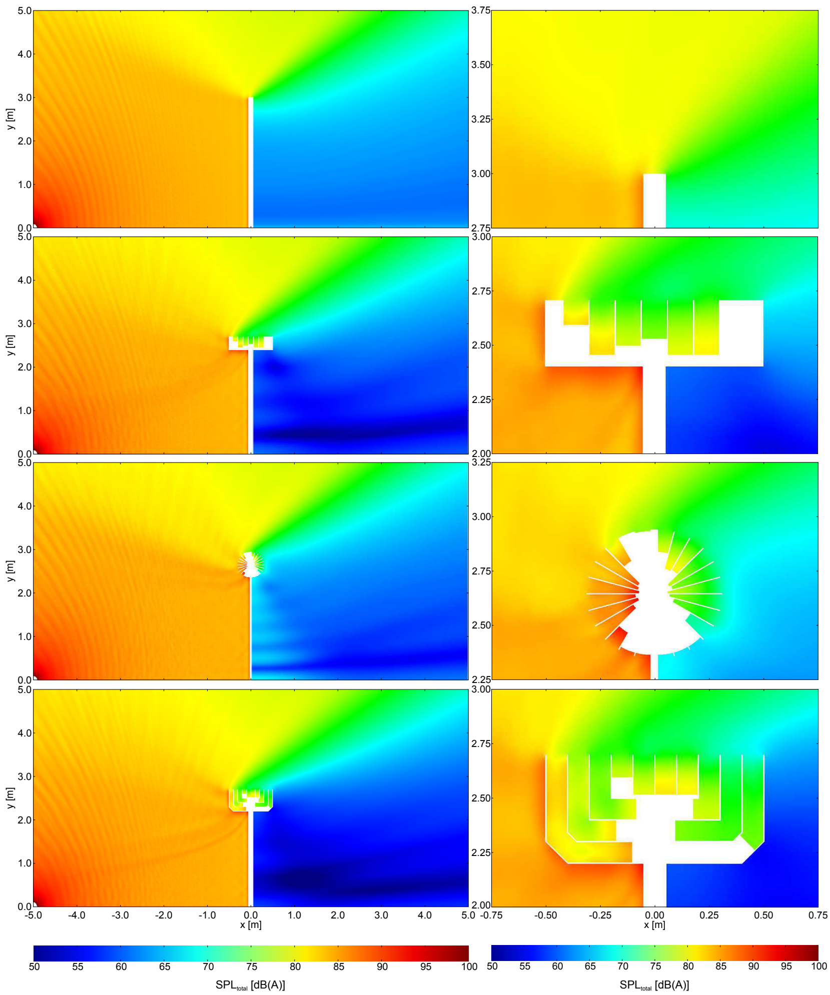

Figure 6.8: Broadband sound pressure level (SPL_{total}) colormaps for a sound intensity level of 90 dB(A) at 1 m from the noise source pulsing according to the considered traffic noise spectrum [117]. From top to bottom, results for a 3 m vertical screen and best optimum non-symmetric designs for models (a), (b) and (c). Noise source at (-5.0, 0.0).

Table 6.2: Design variables d_i (in centimeters) of the best optimum barrier profiles (see Figure 6.6) and shielding efficiency gain with respect to a 3 m vertical screen, in dB(A), for each model and configuration.

	Symmetric			Non-symmetric		
	Model (a)	Model (b)	Model (c)	Model (a)	Model (b)	Model (c)
d_1	11.29	0.00	44.34	11.29	1.61	75.64
d_2	25.00	1.61	53.92	25.00	1.61	51.85
d_3	21.77	5.65	32.74	20.97	8.87	31.61
d_4	21.77	17.74	18.50	17.74	20.16	10.57
d_5	25.00	25.00	18.50	25.00	23.39	18.50
d_6	11.29	23.39	18.50	25.00	22.58	18.50
d_7	-	24.19	32.74	-	24.19	18.50
d_8	-	22.58	53.92	-	23.39	22.58
d_9	-	18.55	44.34	-	22.58	60.14
d_{10}	-	15.32	-	-	12.10	41.73
d_{11}	-	12.10	-	-	0.00	-
d_{12}	-	0.00	-	-	0.81	-
d_{13}	-	0.00	-	-	10.48	-
d_{14}	-	12.10	-	-	17.74	-
d_{15}	-	15.32	-	-	16.94	-
d_{16}	-	18.55	-	-	23.39	-
d_{17}	-	22.58	-	-	22.58	-
d_{18}	-	24.19	-	-	25.00	-
d_{19}	-	23.39	-	-	24.19	-
d_{20}	-	25.00	-	-	21.77	-
d_{21}	-	17.74	-	-	12.10	-
d_{22}	-	5.65	-	-	1.61	-
d_{23}	-	1.61	-	-	1.61	-
d_{24}	-	0.00	-	-	1.61	-
$\mathrm{IL}_{\mathrm{total}}^{3\,\mathrm{m\,vert.}}$	+3.06	+2.67	+4.82	+3.20	+2.68	+5.10

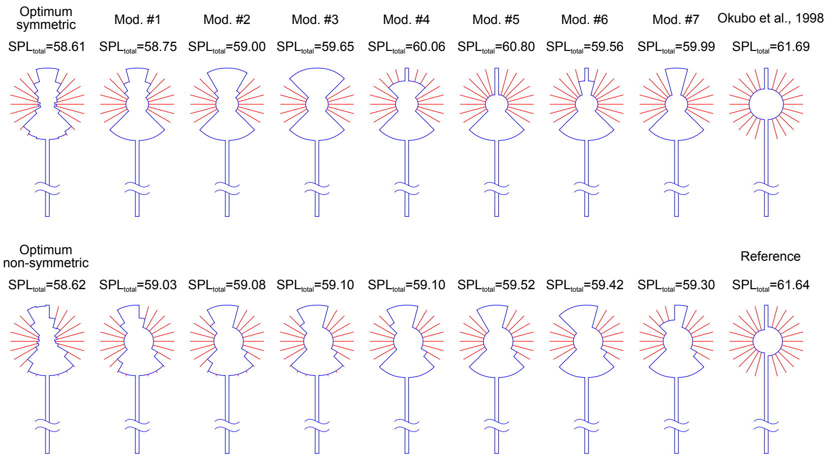

FIGURE 6.9: Slight geometric modifications on the basis of reference designs of model (b): up, modifications from the best optimum symmetric configuration; bottom, modifications from the best optimum non-symmetric configuration. Results expressed in terms of the broadband sound pressure level (SPL_{total}) measured in the considered receiver point, for a scheme featuring a noise source intensity of 90 dB(A) (measured 1 m away in the free field) pulsing at every frequency according to the considered spectrum [117].

On the other hand, the benefits of the methodology introduced in this work are shown in Figure 6.10. As observed, the acoustic performance of the best optimum designs for symmetric and non-symmetric configurations of model (a) are compared with a QRD of same topological design, previously studied in the literature by Monazzam et al. [13]. Results suggest the convenience of implementing procedures like that presented here for raising the acoustic performance of already existing barrier designs.

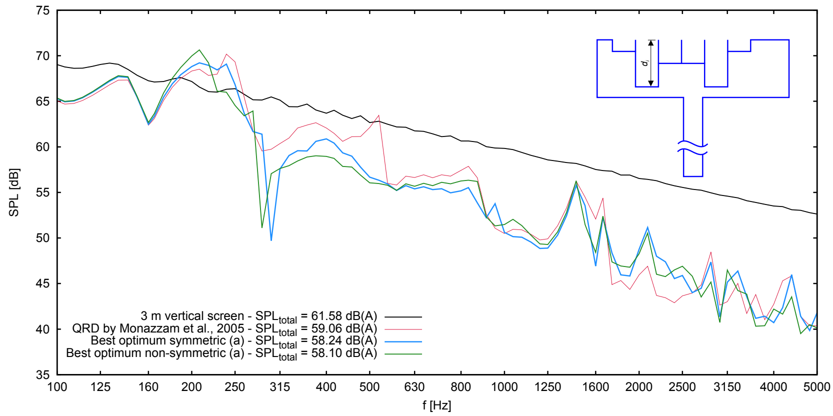

FIGURE 6.10: Sound pressure level (SPL) evolution. Graphs for a QRD (d_1=d_6=0.0600 m, d_2=d_5=0.24450 m, d_3=d_4=0.12225 m), the best optimum designs for symmetric and non-symmetric configurations of model (a) (d_i in Table 6.2) and a 3 m vertical screen.

6.3.4 Discussion of the results

From the analysis of the results obtained some conclusions on the response of the models studied in this work are drawn:

- The shielding efficiency of the optimal geometries here clearly outperform the acoustic behavior of the reference 3 m vertical screen for the considered noise source-receiver scheme. The non-so-near placement of the receiver point makes this issue more remarkable.

- The use of designs with longer wells raises the acoustic performance of the barrier. This is well illustrated by model (c) (Figure 6.6), where the IL curve performs far better than the 3 m vertical screen even for low frequencies.

- As expected, generally speaking, non-symmetric best designs are always better than symmetric ones, both in best OF values and average OF values. Even in the model (b) case, the non-symmetric optimum designs could have far outperformed the symmetric ones in a hypothetical scenario with higher number of generations (as seen in the convergence evolution of the search in Figure 6.7).

- Despite the well known strong frequency dependence-nature of these well-shaped devices (e.g., [15]), the optimum profiles present smoother IL curves than their corresponding model featuring completely empty wells (see Figure 6.6) but with considerably higher shielding efficiency.

- As shown in Figure 6.7 a slightly further convergence of the acoustic performance of the studied models, particularly of models (b) and (c), is still expected. Constraints regarding the considered spectrum (1/15-octave bands center frequencies) impose a high consuming CPU time per objective function evaluation, especially at high frequencies (the higher the frequency, the finer the required BEM mesh). However, the stopping criterion adopted in this work seems to have achieved reasonable convergence for the limited invested computational resources.

- The consideration of methodologies like the one here presented allows the search of interesting shielding solutions to be easily accomplished and can be considered as an adequate procedure to outperform the screening behavior of already existing barrier designs (see Figures 6.9 and 6.10).

7. MULTIOBJECTIVE OPTIMIZATION OF VERY THIN BARRIERS WITH IMPROVED PERFORMANCE

In real-world applications, the existence of problems with just a desired aim is a very rare scenario. Usually, multiple, often conflicting objectives arise naturally in most optimization problems. The task of solving multi-objective optimization problems is called multi-objective optimization (MO). Under this framework, optimizing involves establishing a set of design variables which satisfies constraints and simultaneously optimizes the set of objective functions that define the desired aims of our problem. The issue is further complicated when the intended goals are in conflict to each other, that is, when the fulfillment of one objective function mitigates against the fulfillment of the other. Therefore, using MO gives rise to a more comprehensive design scenario by providing a set of trade-off optimal solutions (not a single one, as in the case of mono-objective optimization), popularly known as Pareto-optimal solutions. Due to the multiplicity in solutions, these problems are proposed to be solved suitably using evolutionary algorithms which use a population approach in the search process.

The approach of this chapter is based on the evolutionary multi-objective optimization (EMO) of noise barrier models with improved performance. In this sense, results here presented are a step in the direction marked by previous works developed within the SIANI institute. As a brief background, in Maeso et al. [152] the simultaneous minimization of both noise attenuation level differences with respect a reference shielding curve and the effective height of Y-shaped barriers was conducted. Later on, the multi-objective optimization of the shielding efficiency and the cost of the barrier, represented by the overall boundary length, was addressed in Greiner et al. [73], on the basis of Y-shaped barriers with upper absorbing surface considering different receiver points' schemes. A comparative study between the strategy of introducing the optimal single-objective solution in the initial multi-objective population (seeded approach) and the standard approach was also presented. On the same line of this latter work, a single- and multi-objective optimization of Y models with different surface treatments was carried out in [72]. Finally, in Deb et al. [75] the multi-objective problem addressed in [152] was solved with increased performance by means of obtaining automatic design learnings through the use of the so-called *innovization* technique. All the aforementioned works addressed the issue implementing the standard BEM formulation for the sound attenuation prediction of Y-shaped barriers with real dimensions.

The EMO optimization here presented deals with very thin barriers whose topological designs were previously introduced in Chapter 5 (*Study*

#1). Similarly to the study carried out in the single-objective optimization of such models, the bi-dimensional sound propagation analysis is performed in the frequency domain with the usual assumptions: the medium (air) is modeled as homogeneous, elastic and isotropic with no viscosity, under small disturbances and initially at rest with no wind effects. The noise source is modeled as an infinite, coherent mono-frequency source of sound located parallel to an infinite very thin barrier idealized as a *single-wire* configuration that stands on a flat plane (ground) of uniform admittance. In this case, the study focuses on the simultaneous optimization of two objectives in conflict: the maximization of the shielding efficiency (represented, as known, by the broadband insertion loss for the considered spectrum) and the minimization of the cost of all barrier material used, represented by the overall length of the boundaries.

Two optimal sets of designs are obtained for each model after multi-objective optimization processes: when considering a random initial population and when including the best single-objective optimal design obtained in Chapter 5 in the initial population. The comparison of the optimal Pareto fronts derived from both processes, with equal number of fitness function evaluations, are performed by means of the *hypervolume* indicator. The insights derived from the analysis of the results disclosed are provided at the end of this chapter.

7.1 Description of the multi-objective optimization framework

As stated above, EMO algorithms are proper, efficient tools for the simultaneous optimization of two or more conflicting objectives. In this case, decreasing of barrier dimensions normally leads to reduction in sound attenuation. Thus, the intended maximization of the shielding efficiency of the barrier does not match well with the minimization of the total length of the barrier.

The study here presented deals with optimization problems performed by the combined use of a multi-objective genetic algorithm (MOGA) and a code that implements a Dual BEM formulation for the assessment of road barriers featuring very thin sections. A detail description of this Dual approach is found in Chapter 3. The MOGA software used in this study applies the NSGA-II [114] algorithm, one of the references in the EMO field. A population size of 100 individuals and uniform mutation rate of 3%, as well as uniform crossover are used. Additional information of the MOGA implemented in this methodology is provided in Chapter 4.

7.1.1 Bi-dimensional configuration

Figure 7.1 represents the general configuration of the study and was previously introduced in Chapter 5 for the assessment of noise barriers with improved efficiency (*Study #1*). A more detailed description of this configuration, the applied spectrum and the procedure followed to represent the barrier geometry is provided in section 5.2.1 of the cited chapter.

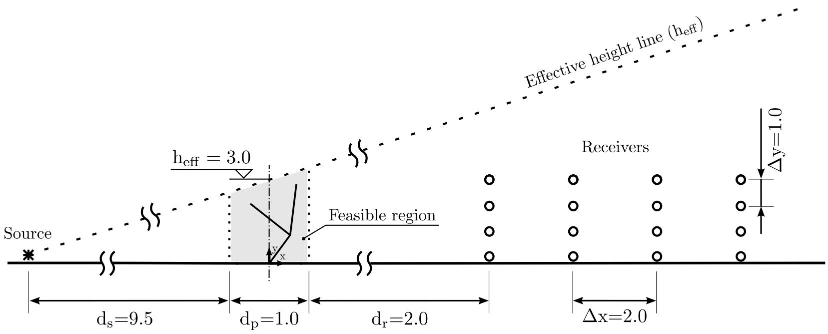

FIGURE 7.1: Bi-dimensional configuration for the multi-objective optimization of noise barriers with improved performance. Dimensions expressed in meters.

7.1.2 Definition of the conflicting objectives

One of the aims of the multi-objective optimization presented in this chapter is the search of barrier designs with ever-increasing screening performance (maximization of the shielding efficiency). This criterion has been the basis of shape optimizations presented so far and can be properly determined, as is well known, by the broadband insertion loss. Its representation in terms of the objective function can be expressed as follows:

$$\mathrm{OF}_1 = \sum_{j=1}^{\mathrm{NR}} \mathrm{IL}_{\mathrm{total}_j} / \mathrm{NR}\,[\mathrm{dB(A)}] \tag{7.1}$$

being $\mathrm{IL}_{\mathrm{total}_j}$ the broadband IL for each receiver and NR the total number of receivers considered in the study.

Additionally, the minimization of the manufacturing costs of the barrier profile is intended. This second objective can be expressed in terms of the sum of the boundary lengths (see Figure 7.2), as follows:

$$\mathrm{OF}_2 = \sum_{k=1}^{\mathrm{NB}} \mathrm{L}_k = \sum_{k=1}^{\mathrm{NB}} \sqrt{(\mathrm{x}_k^f - \mathrm{x}_k^i)^2 + (\mathrm{y}_k^f - \mathrm{y}_k^i)^2}\,[\mathrm{m}] \tag{7.2}$$

with L_k being the length of each boundary and NB the overall number of boundaries of the considered barrier.

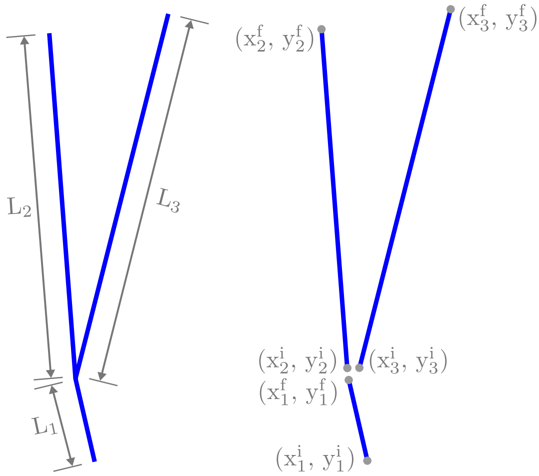

Figure 7.2: Total length of the barrier as a factor to be minimized along the multi-objective optimization. Example of a Y-shaped barrier model.

It is not difficult to understand at this stage that both criteria are in conflict: reducing the barrier length affects adversely, in the large majority of cases, the acoustic efficiency.

7.2 Numerical simulations

Five MO optimization runs of each single-wire topological model (as representative of their corresponding very thin profile) are conducted. To ensure a fair comparison among the optimal solutions of a particular model both after including the best single-objective solution (*Case B*) of such model (see section 5.2.1 of Chapter 5) in the initial population and after considering random initial individuals (*Case R*), different stop criteria are considered for each MO case. According to this, the stop condition is met for 400 and 600 generations of the MO optimization process for *Case B* and *Case R*, respectively. Recalling that the best optimal barriers after mono-objective optimizations were obtained for 20 000 objective functions evaluations, both cases performed the same number of assessments of the objective functions (60 000).

7.2.1 Description of the models

As stated above, the models to be optimized in this study are those presented and described in detail in section 5.2.1 of Chapter 5 (Figure 7.3). Unlike this latter, the analysis performed in this chapter just consider perfectly reflecting barrier surfaces.

7.2.2 Designs after optimization

Figures 7.4-7.11 collect the results after the multi-objective optimizations of each model. The upper graphs show the accumulated non-dominated front solutions of the five runs for both after starting off with a random initial population (*Case R*) and when including the best mono-objective solution in the initial population (*Case B*). Some of these solutions are labeled from 1 to 7 in both cases and represented within a grey box by their objective functions: the overall shielding efficiency considering all receiver points (OF_1) and the total length of the barrier (OF_2). The corresponding geometric representation of these solutions are shown at the bottom of such graphs.

In order to determine whether the inclusion of the best single-objective solutions (*Case B*) is a real asset in the improvement of the models studied, the comparison between the optimal Pareto front of this case and that from *Case R* is conducted by applying the hypervolume measure (HV). Data concerning this value for each optimization run are collected in Table 7.1 for both cases. Additionally, some information from this table is represented graphically in Figures 7.12 and 7.13 by vertical lines, whose extremes correspond to the lowest and the highest HV value found along the optimization runs of each model, while the dot spot represents the mean value

Table 7.1: Hypervolume measure (HV), mean value ($\overline{\mathrm{HV}}$) and standard deviation (σ) of the optimal Pareto fronts of barrier models when considering a random initial population (R) and when including the best single-objective solution (B) in the optimization runs. Reference point: (OF_1, OF_2) = (0, 20).

		Run 1	Run 2	Run 3	Run 4	Run 5	$\overline{\mathrm{HV}}$	σ
a) 3-sided polygonal	R	316.63	315.96	316.34	316.27	316.13	316.27	0.25
	B	324.77	325.03	324.85	324.49	324.62	324.75	0.21
b) 5-sided polygonal	R	316.41	321.63	330.68	315.88	315.63	320.05	6.44
	B	346.44	346.22	346.53	346.53	345.88	346.32	0.28
c) 3-cubic splines	R	332.42	331.47	291.56	329.35	322.54	321.47	17.16
	B	325.14	329.41	330.15	324.66	324.75	326.82	2.72
d) 5-cubic splines	R	312.09	325.40	326.31	318.33	330.27	322.48	7.23
	B	327.86	328.83	325.53	330.22	328.21	328.13	1.71
e) Y-shaped	R	327.97	324.20	334.71	332.93	324.42	328.85	4.82
	B	335.89	335.87	335.38	335.80	335.88	335.76	0.22
f) Tree-shaped	R	338.20	338.53	338.72	332.40	337.41	337.05	2.65
	B	339.08	339.12	338.85	338.60	339.00	338.93	0.21
g) Y-variant-shaped	R	325.62	328.87	326.89	339.64	343.80	332.96	8.21
	B	337.04	336.24	336.90	333.89	338.46	336.51	1.67
h) Fork-shaped	R	325.81	319.80	325.44	325.09	325.51	324.33	2.55
	B	332.50	332.27	332.24	332.43	332.52	332.39	0.13

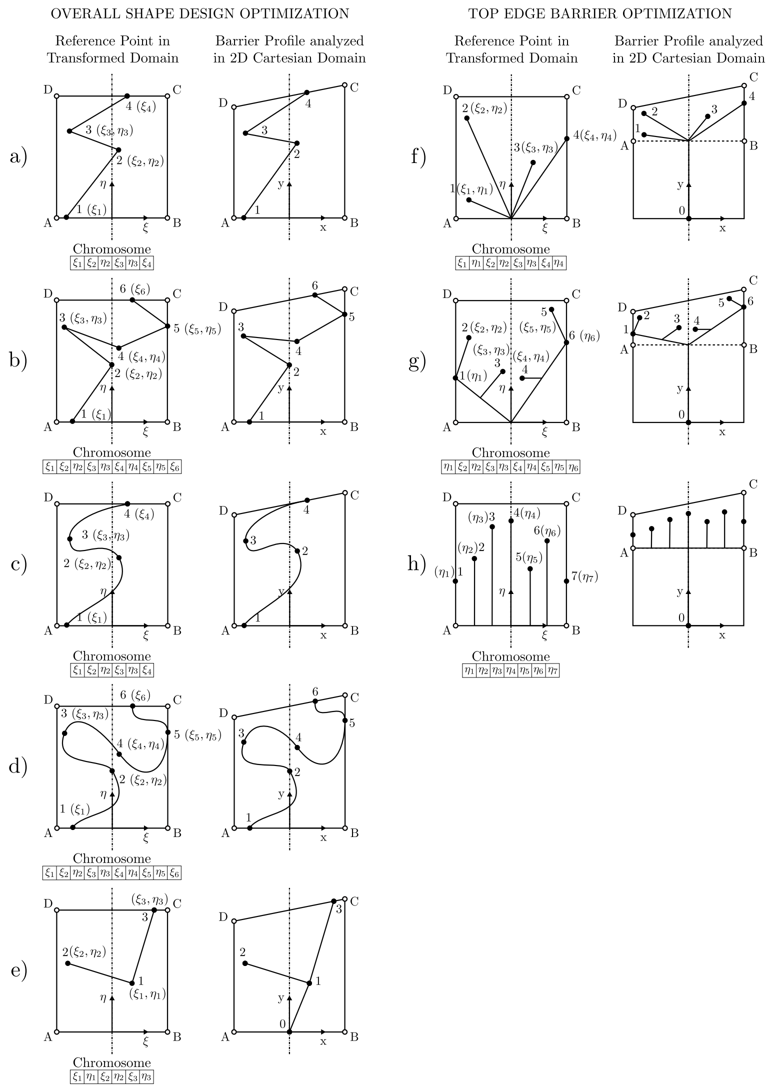

Figure 7.3: Models under study for the multi-objective optimization.

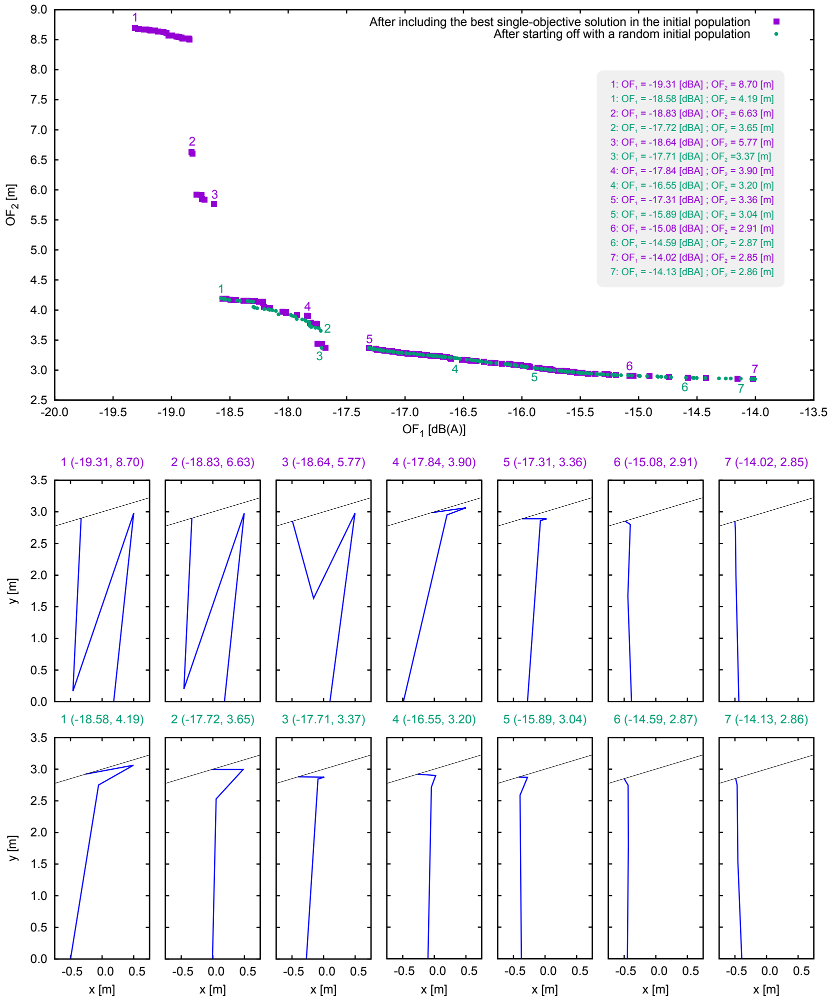

FIGURE 7.4: Model a): 3-sided polygonal shaped barrier results. Non-dominated solutions for *Case B* and *Case R*.

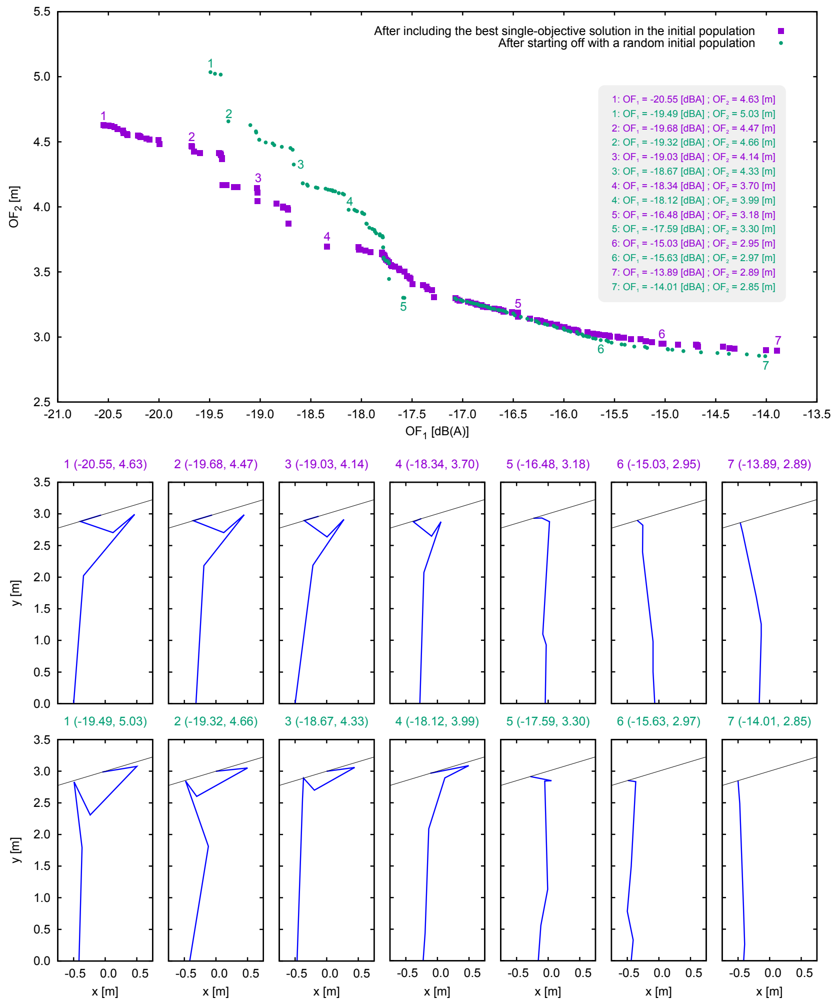

FIGURE 7.5: Model b): 5-sided polygonal-shaped barrier results. Non-dominated solutions for *Case B* and *Case R*.

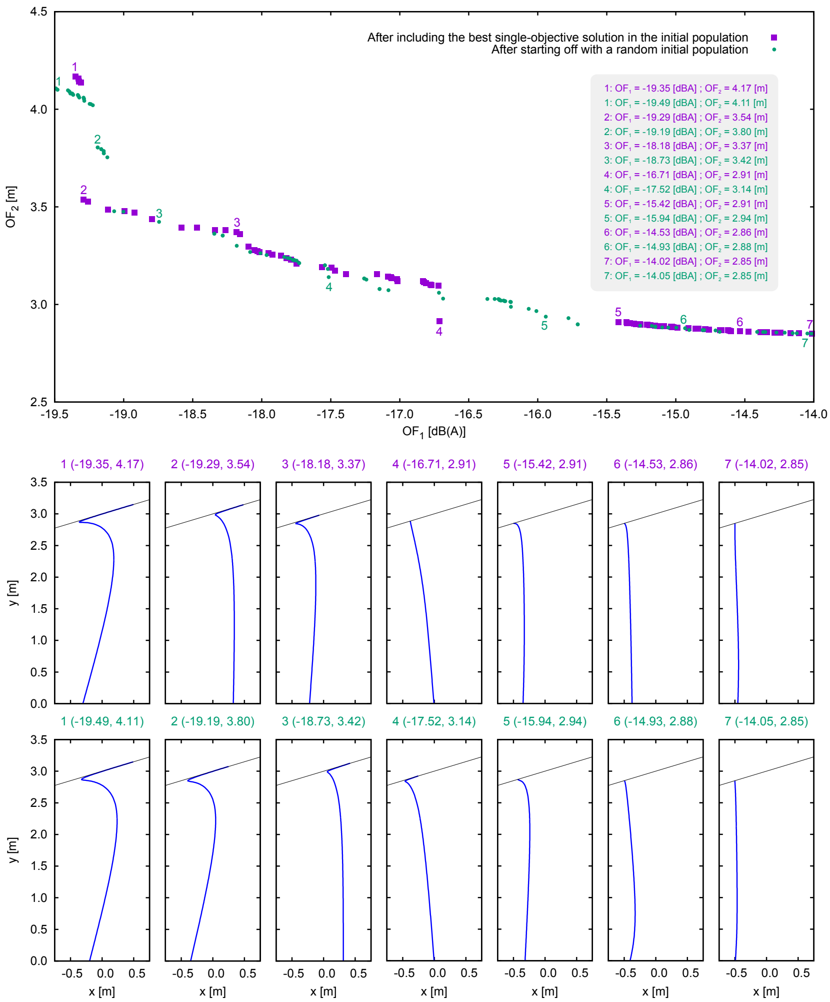

FIGURE 7.6: Model c): 3-cubic splines-shaped barrier results. Non-dominated solutions for *Case B* and *Case R*.

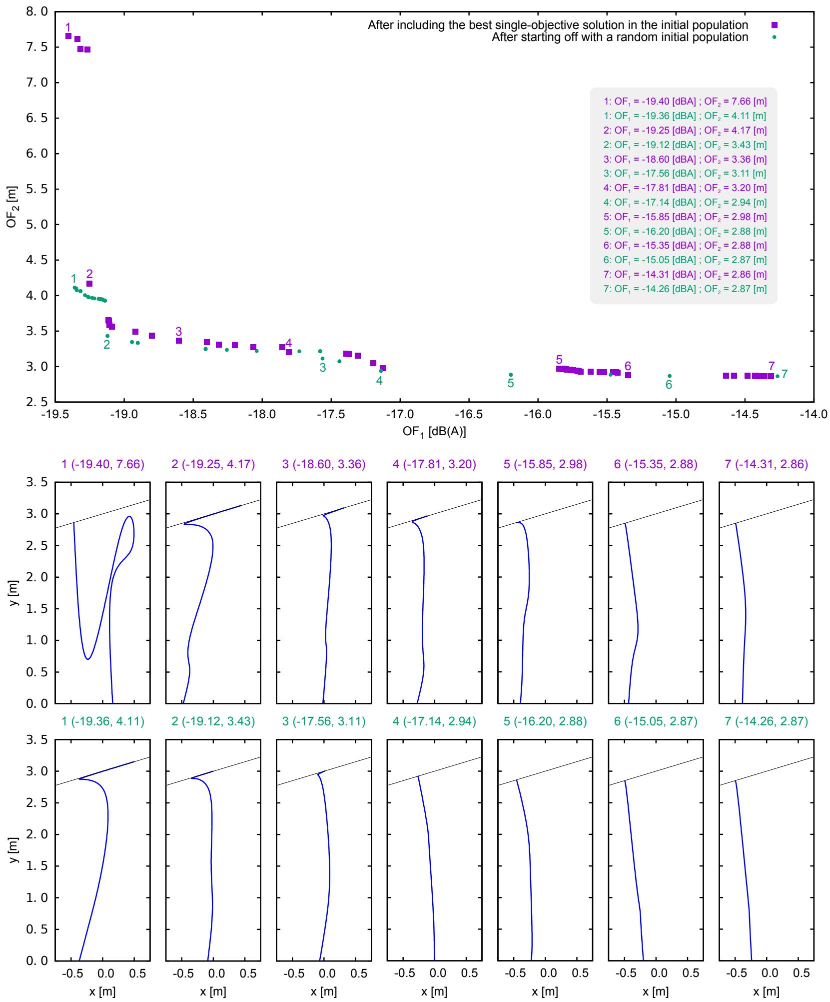

FIGURE 7.7: Model d): 5-cubic splines-shaped barrier results. Non-dominated solutions for *Case B* and *Case R*.

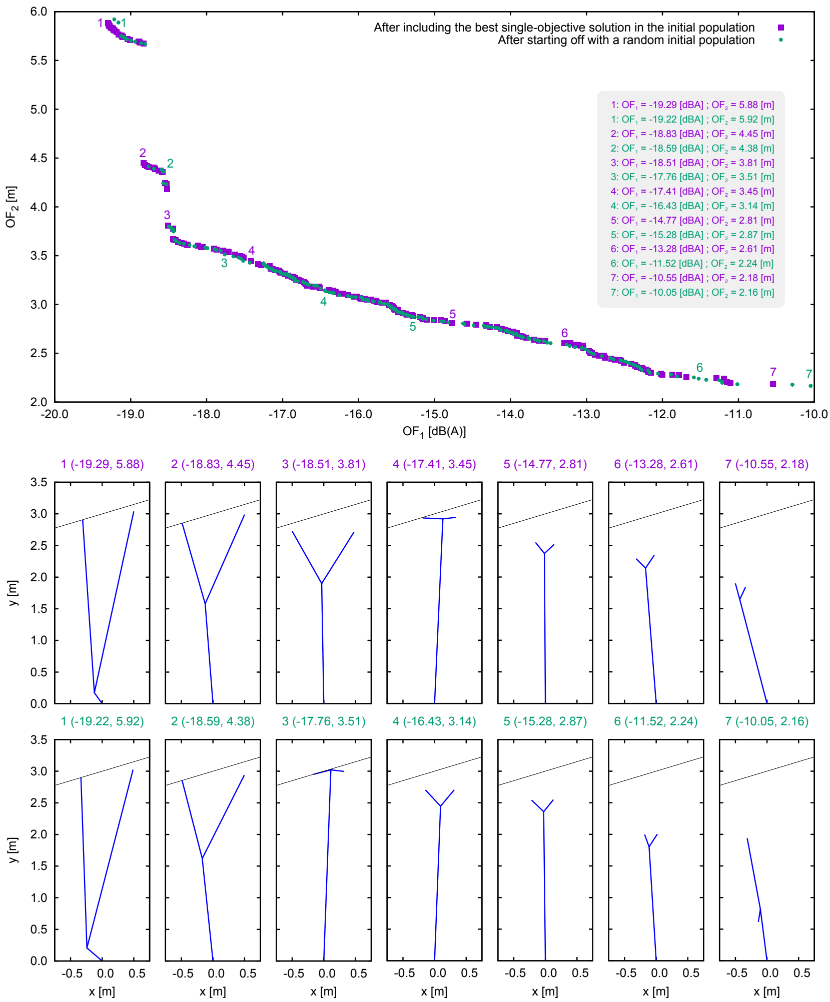

Figure 7.8: Model e): Y-shaped barrier results. Non-dominated solutions for *Case B* and *Case R*.

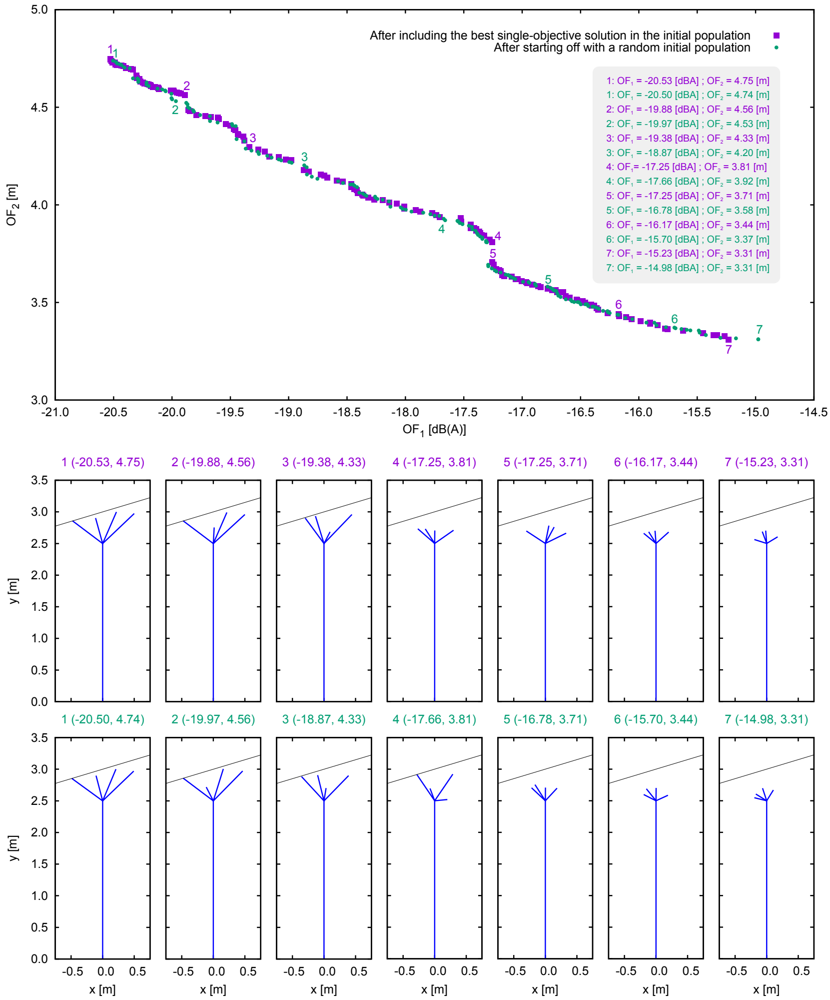

FIGURE 7.9: Model f): Tree-shaped barrier results. Non-dominated solutions for *Case B* and *Case R*.

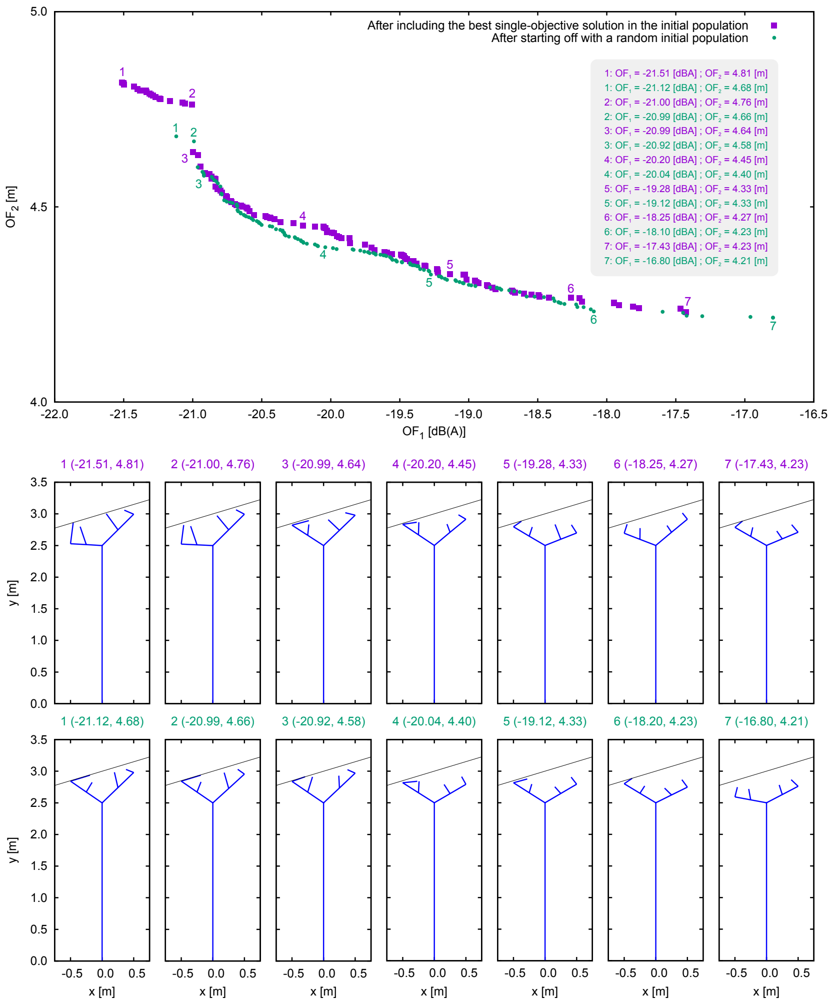

FIGURE 7.10: Model g): Y-variant-shaped barrier results. Non-dominated solutions for *Case B* and *Case R*.

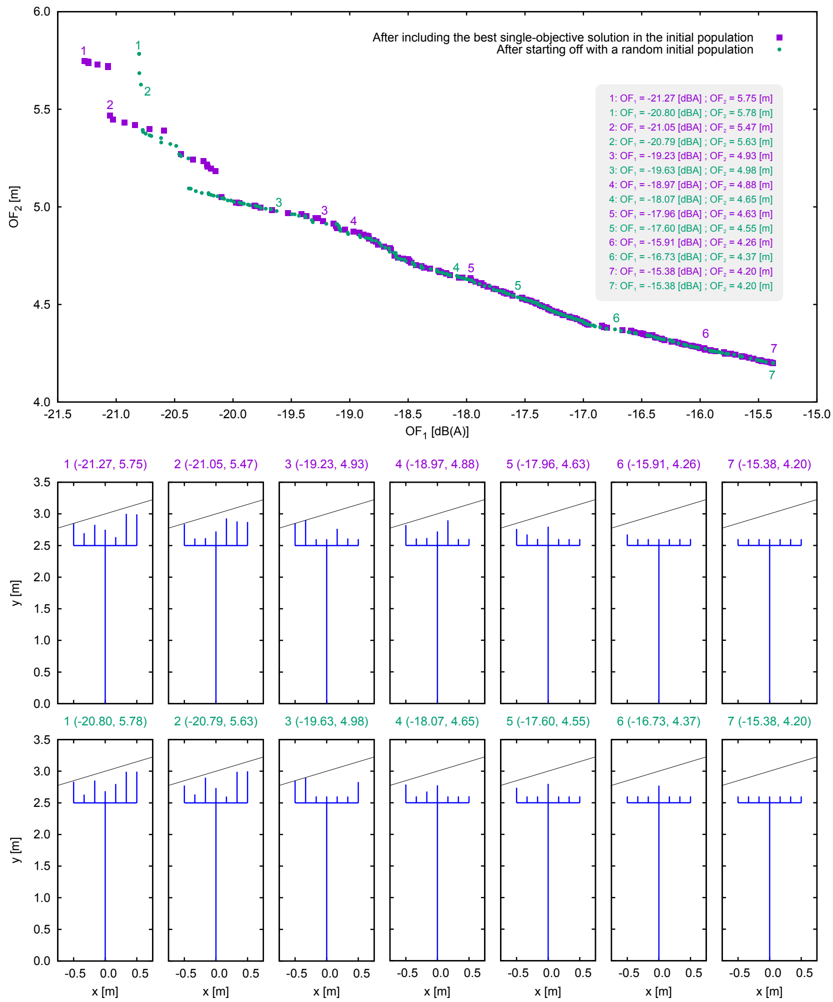

FIGURE 7.11: Model h): Fork-shaped barrier results. Non-dominated solutions for *Case B* and *Case R*.

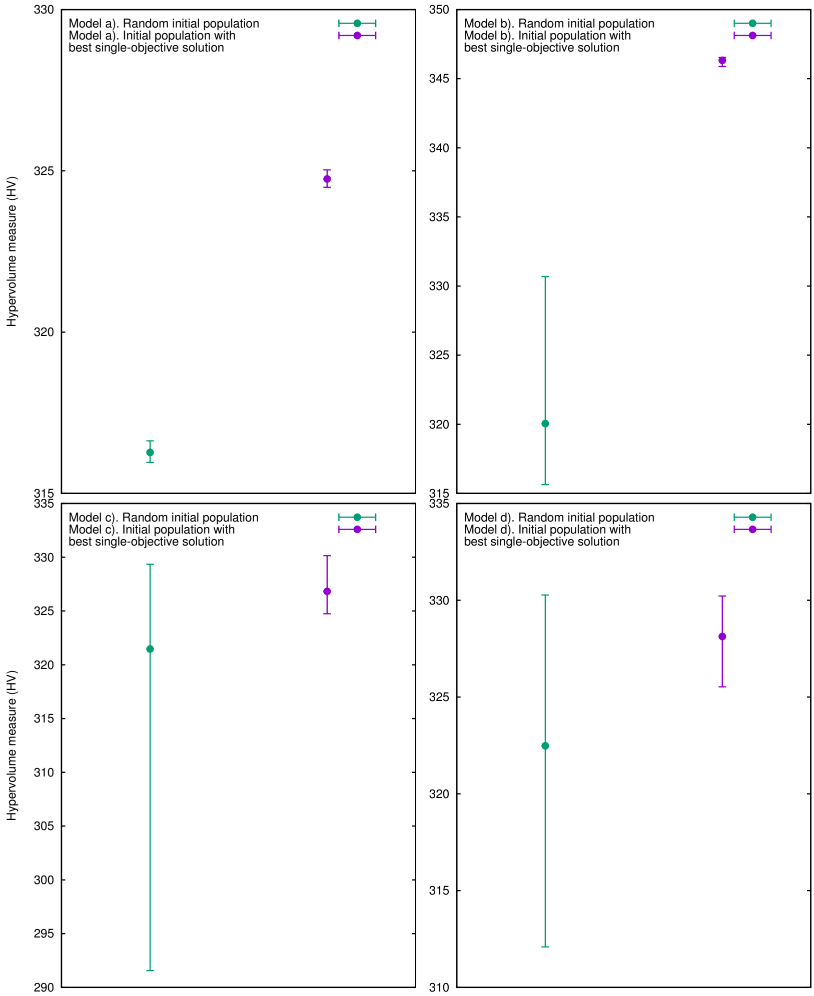

FIGURE 7.12: Hypervolume measures of the optimization runs for *Case B* and *Case R*. Models a) to d).

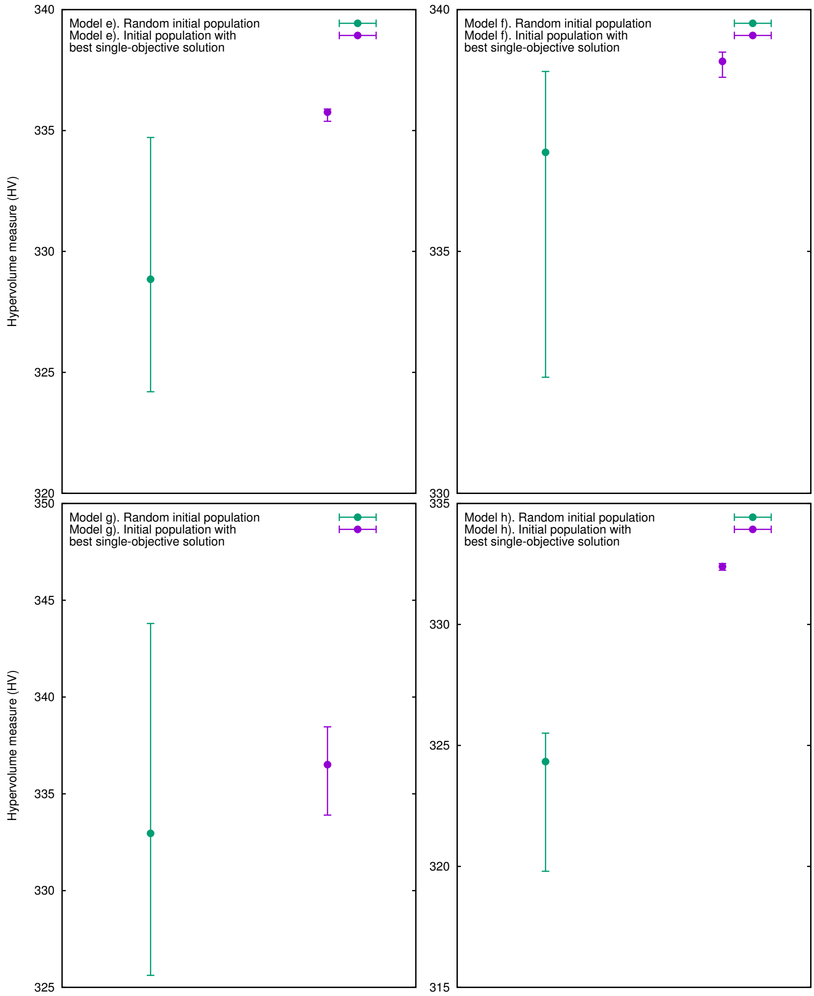

FIGURE 7.13: Hypervolume measures of the optimization runs for *Case B* and *Case R*. Models e) to h).

7.2.3 Discussion

According to the disclosed results, the following analysis is drawn:

- In all models, the value of the average hypervolume measures is always better (higher) in *Case B* than in *Case R*.
- In all models, the value of the standard deviation of the hypervolume measures is always better (lower) in *Case B* than in *Case R*.
- In four out of the eight models studied, the distribution of the hypervolume measures is not overlapped, meaning a complete outperformance of *Case B* over *Case R* in those cases - models a), b), e) and h) -.
- Including the best single-objective solution in the initial population confers a considerable advantage over the case in which the multi-objective optimization starts off with a random initial population, for the criteria involved in this study. This is explicitly reflected both in Table 7.1 and Figures 7.12 and 7.13, where it can be seen that the hypervolume measures of *Case B* perform significantly higher than *Case R* in all models. The low values of the standard deviation of *Case B* optimums make this issue more remarkable.
- The multi-objective optimization has performed well to find, generally speaking, wide and uniformly spread-out Pareto-optimal fronts (non-dominated solutions) for the presented barrier models. This is illustrated by the geometric diversity of noise barriers depicted in Figures 7.4-7.11, being most noticeable, logically, in barrier models featuring overall shape optimizations - models a) to e) -.

8. SUMMARY, CONCLUSIONS AND FUTURE RESEARCH DIRECTIONS

8.1 Summary and conclusions

The presented work proposes a systematic improvement of the shielding efficiency of road barriers by a general, robust procedure to address the study of 2D acoustic problems. Such a procedure uses Genetic Algorithms (GAs) for the guided search, within a space of feasible solutions according to the problem constraints, of geometries (based on topological designs previously defined) that coupled with Boundary Elements (BE) leads to ever-increasing acoustic performance solutions.

This study is a significant step forward regarding the numerical model for the realistic simulation of outdoor sound propagation problems induced by any type of noise source that has been continuously developed and improved over the past years, framed in an ongoing research line within the Institute of Intelligent Systems and Numerical Applications in Engineering (SIANI Institute), involving the shape design optimization of road acoustic barriers by coupling Boundary Elements with Evolutionary Algorithms (EAs).

As a background, the initial bi-dimensional model arose as a result of the research works by Prof. Orlando Maeso and Prof. Juan J. Aznárez (both supervisors of this document), who had been working in the previous years on the development and application of numerical methods for solving wave propagation problems in elastic media. The first code implementation for outdoor sound propagation prediction was based entirely on the standard boundary integral equation and allowed the study of various volumetric barrier designs in different scenarios [18, 98]. Later on, the scope of this research was extended to the systematic improvement of the screening performance of commonly used barrier configurations by benefiting from the expertise of Prof. David Greiner (one of the supervisors of this document) in the field of Evolutionary Algorithms. This fruitful collaboration resulted in the development and implementation of a more general procedure involving the coupled use of BE and EA for the shape design optimization of road barriers. The first joint implementation of both numerical approaches within the Research Group where this thesis is developed can be found in [71], followed by other notably works [72, 73, 108].

Despite the fact that the procedures developed until that moment had been successful in reducing sound attenuation systematically, the consideration of certain types of barrier geometries were challenging and, in most cases, just seen as unaffordable in terms of 1) the evaluation of the feasibility of complex designs proposed by the optimizer 2) the faithful representation of the shielding behavior. In this regard, the development of this thesis must be seen as a response to the lack of versatility and adaptability of previous procedures by implementing a broader, more robust, general methodology that may cover any type of 2D acoustic optimization problem.

Though the Boundary Element Method (BEM) is the most suitable technique in the study of outdoor sound propagation prediction, the implementation of its standard formulation may lead to insurmountable obstacles when dealing with certain type of barriers yielding, depending on the geometry nature, either numerical drawbacks or a singular equation system. In this respect, the procedure implemented in the studies presented in this thesis makes use of the so-called Dual BEM approach, the most appropriate strategy involving BE to overcome these difficulties. Such a formulation combines the standard boundary integral equation (SBIE) of the Method with a hyper-singular variant (HBIE) which is obtained by derivation of the former. The coupled use of both approaches in this Dual BEM formulation allows us to avoid drawbacks associated with the exclusive implementation of the standard formulation by 1) assuming the idealization of very thin elements as *single-wire* bodies, greatly facilitating the geometric definition of complex configurations with no substantial influence on the acoustic performance for the considered thickness of very thin sections [47], and 2) mitigating the fictitious eigenfrequencies associated with the inner domain of barriers or elements featuring real dimensions, that may adversely affect to the assessment of the screening efficiency. The accomplishment of such objectives, mainly the geometric idealization of very thin elements, gives rise to a more general and robust methodology for the systematic search of barrier designs that often feature complete geometric freedom according to their topological patterns. In addition, this approach enables us to tackle the shape design optimization of complex road barriers in a way, to the researcher's knowledge, not covered so far in the bibliography concerning the issue.

The strategy of the application of both formulations varies depending of the nature of the element under consideration. This way, both SBIE and HBIE are coupled by means of a frequency-related complex value [109] to mitigate the fictitious eigenfrequencies when dealing with volumetric structures (structures with real dimensions). Generally speaking, this issue affects the treatment of any type of element, regardless the thickness of the body. However, the problem is further aggravated when dealing with very thin sections. In this case, numerical integration problems may appear affecting, equally, to the barrier performance. The convenient application of the Dual BEM approach offers a proper solution to this issue by idealizing very thin elements as single-wire bodies. In this case, the SBIE and the HBIE are then applied separately on every node of the discretization of a boundary representing the fusion of the two opposite boundaries of the real section. Such a simplification of reality not only results in faster computational times but also is a real asset, especially when compared with the case of the faithful, detailed definition of real complex volumetric.

Different studies based on the aforementioned methodology have been performed and the corresponding results have been presented in the last chapters of this document. Numerical 2D simulations involving different scenarios have been conducted on the basis of two-dimensional sound propagation hypotheses, i.e., the source of sound is modeled as infinite, coherent and mono-frequency-type and placed parallel to an infinite noise barrier with no geometric variation that stands on a flat plane (ground) of uniform admittance. These simulations have been performed in the frequency domain with the usual assumptions (Helmholtz equation): the medium (air) is modeled as homogeneous, elastic and isotropic with no viscosity, under small disturbances and initially at rest with no wind effects.

Results concerning single- and multi-objective optimizations of different noise barriers have been included in this document. The most outstanding conclusions and insights drawn from these studies are exposed below.

On the overall and top edge shape optimization of very thin barriers

The single-objective optimization of very thin noise barriers idealized as single-wire bodies has been performed, on the basis of numerical simulations of barriers' performance implementing a 2D Dual BEM code in different scenarios.

In one study, shape optimizations of designs featuring overall shaped and top edge configurations (covering straight and curved models) with rigid and noise absorbing boundaries materials have been conducted. While simulations have been conducted for a specific receivers' scheme, the influence of the receivers' distribution on the acoustic performance has also been addressed. Results presented are in line with other authors' works [13–15, 66, 70] in the sense that higher sound attenuation levels are obtained when acting, geometrically speaking, on the barrier top instead of on the overall profile. The strong theoretical nature of many of the designs proposed in this study has not been an obstacle to find optimum designs that can be approximated to easier-to-build barrier configurations, with no major influence on the acoustic performance. As for the surface treatments, it was found that not always providing some boundaries with sound-absorbing treatments leads to the improvement of the shielding efficiency of edge-modified barriers, as the top configuration plays an important role by producing reflected waves that help partly offset the incident ones. In this respect, the consideration of absorbing surfaces in the optimization process was found necessary in the pursuit of barrier designs with highest sound attenuation levels. Finally, the introduced models showed, generally speaking, a regular, slight loss of shielding efficiency through distance.

This latter aspect was analyzed in further detail in the second study. The influence of the screening performance through distance was presented, considering two sets of receivers located at three clearly distinguishable regions in terms of closeness to the barrier. Simulations were performed on the basis of a 6-sided polygonal shaped barrier and a 6^{th} degree Bézier curve model, concluding that former model performed better for near regions when receivers are located on the ground. The Bézier curve-shaped barrier showed a better screening behavior for non-near regions, though. Under the analysis with a grid of receivers both models performed roughly the same.

On shape optimization of diffuser-based barriers

Results concerning the single-objective optimization of noise barriers with top-edge devices were presented. More specificially, topological designs with complex diffuser-type tops were studied. Based on complex geometries, these designs combine a general volumetric structure with very thin elements that can be idealized as null-thickness bodies. The Dual BEM approach implemented addressed properly the assessment of these designs through a robust, versatile procedure by mitigating the fictitious eigenfrequencies of the volumetric structures and by idealizing very thin sections as single-wire bodies.

As an application, numerical results on the basis of three well-based models (some of them inspired on configurations previously studied in the literature) were performed. As expected, the screening performance of the presented models after optimization significantly exceeded that from the reference 3 m simple screen, even for far location of receivers. As for the models themselves, in accordance with other authors (e.g., [15]), these designs showed a strong frequency-dependence. However, optimum models presented smoother shielding curves than that from the corresponding design with completely empty wells. In addition, it was found that the potential depth of wells is a real asset for raising the screening behavior, as the number of frequencies with high IL values is widen within the considered frequency spectrum. With a marked practical approach, easier-to-build designs were proposed inspired from optimum models, with no major influence on the acoustic performance. Finally, a comparative sound attenuation analysis between a QRD previously studied in the literature [13] and the topologically identical optimal model was conducted, justifying the need of considering procedures as the one presented in this study to improve the performance of already existing designs.

On multi-objective optimization of very thin road barriers

Lastly, results derived of the multi-objective optimzation of very thin noise barriers with perfectly rigid surface were presented. Based on barrier models previously introduced in the first study of Chapter 5, numerical optimizations were conducted in the pursuit of both the maximization of the shielding efficiency and the minimization of the cost of all barrier material used, represented by the overall length of the boundaries. Optimal sets of designs were obtained for each model after running processes with equal number of fitness function evaluations both when considering a random initial population (*Case R*) and when including the best single-objective optimal design obtained in Chapter 5 in the initial population (*Case B*). The comparison of the optimal Pareto fronts of each proposed designs (by means of the hypervolume measure) revealed the outperformance of *Case B* over *Cases R* in all models, meaning that including the best single-objective solution in the optimization run is a real asset. Futhermore, multi-objective optimizations led to wide and uniformly spread-out Pareto fronts, which was reflected in the geometric diversity featured by optimal designs.

8.2 Future research directions

The procedure presented in this document has successfully addressed shape design optimization problems, considered as intractable prior this thesis within the Research Group where it has has been developed. Despite its undoubted contribution, this work is eligible for improvement in the aspects detailed below.

i **On the efficiency of the optimizer.** Genetic Algorithms belong to the paradigm of Evolutionary Algorithms and Metaheuristics. Among their advantages are their global optimizer capabilities due to their stochastic population based search. However, one of their main drawbacks is the high number of evaluations of the fitness function required to obtain a proper convergence, which is specially critical when solving engineering problems (where each evaluation implies a high computational cost). Such is the case of solving Boundary Element problems. In this respect, the efficiency of the approach is a critical issue in obtaining solutions of acceptable quality with the allowable computational resources invested. Among the field of evolutionary algorithm applications for the computational simulation of engineering problems (fluid dynamics, structural engineering, etc.), recent advances in enhancing the efficiency are mainly based on the use of parallel evolutionary algorithms, game strategies and surrogate models. All the aforementioned strategies, separately or simultaneously used (e.g., [153–155]), are state of the art tools advisable to be taken into consideration in prospective works to enhance efficiency of the procedure implemented here.

ii **On the efficiency of the evaluator**. The computing times of the overall methodology can be improved by just considering the parallelization of the highest time-consuming task within BEM: the assembly of the matrices of the integration cores of the Method involving both the SBIE and the HBIE. As the assembly of each row of the aforementioned matrices are independent from one another, the accomplishment of this aim is simple and straightforward.

iii **On the scope of application of the evaluator**. Finally and with a more ambitious purpose, another future research direction that may emerge from this study is that involving the combined use of Fast Multipole Methods (FMM) with BEM for solving one of the main drawbacks of this latter numerical technique in any physical problem: the high computational cost both in terms of run times and memory resources when dealing with very large-scale problems, such as those involving 3D spaces. In addition, in harmonic dynamic problems (frequency domain) the issue is further aggravated as the application of the Method results in systems of equations which grow exponentially with the excitation frequency. The key point of the coupled FMM-BEM approach (see, e.g., [156–159]) is the significant reduction in computational costs of dense-matrix storage of $\mathcal{O}\left(n^2\right)$ and evaluation of $\mathcal{O}\left(n^3\right)$ (in case of direct resolution algorithms) to a quasilinear problem. In this way, the prediction of the noise attenuation of three-dimensional noise barriers featuring several million degrees of freedom can be easily addressed on a desktop computer within hours. Among the fast multipole methods, the generalized minimal residual [160–163] (GMRES) iterative method arises as one of the application in this context, as does not require that the coefficients matrix is stored in memory. The array-vector product is performed by using multipole expansions of the fundamental solution stored on a cells structure that group the elements of the boundary discretization. With this, the node-node interaction (collocation-integration) of the conventional BEM turns into a cell-cell interaction.

A. NUMERICAL ASPECTS OF THE HYPER-SINGULAR FORMULATION OF BEM

This appendix deals with the numerical treatment of the integration cores involved in the Dual BEM formulation presented in this dissertation. Following, the numerical aspects of the integrals involving the hyper-singular boundary integral equation (HBIE) are addressed.

The HBIE for the boundary point i, once the strategy to avoid singularity around i is considered (see Figure A.1), can be written as follows:

$$\begin{gathered}\frac{\partial p_i}{\partial n_i} + \int_{\Gamma-\Gamma_\varepsilon} M(i,j)\, p\, d\Gamma + \int_{\Gamma_\varepsilon} M(i,j)\, p\, d\Gamma_\varepsilon = \\ \int_{\Gamma-\Gamma_\varepsilon} L(i,j) \frac{\partial p}{\partial n_j}\, d\Gamma + \int_{\Gamma_\varepsilon} L(i,j) \frac{\partial p}{\partial n_j}\, d\Gamma_\varepsilon + L(0,i)\end{gathered} \qquad \textbf{(A.1)}$$

with:

$$\begin{aligned} M(i,j) &= \frac{\partial^2 G(k,r)}{\partial n_i n_j} \\ L(i,j) &= \frac{\partial G(k,r)}{\partial n_i} \\ L(0,i) &= \frac{\partial G_0(k,r)}{\partial n_i} \\ i &= \text{collocation point} \\ j &= \text{integration point} \\ k &= \text{wave number} \\ r &= \text{distance from } i \text{ to } j \end{aligned}$$

The integrals involving the infinitesimal boundary Γ_ε must be studied in the limit. In this way, by expressing p as a Taylor series in Γ_ε and after some operations the integrals around the singularity can be expressed as follows:

$$\begin{aligned}\lim_{\varepsilon\to 0} \int_{\Gamma_\varepsilon} M(i,j)\, p\, d\Gamma_\varepsilon &= \lim_{\varepsilon\to 0} -\frac{1}{2\pi\varepsilon} \int_0^\pi \sin\theta\, p\, d\theta = \\ &= -\frac{1}{4}\left(\frac{\partial p}{\partial n_i}\right) - \underbrace{\frac{p_i}{\pi} \lim_{\varepsilon\to 0}\left(\frac{1}{\varepsilon}\right)}_{\textit{improper term}}\end{aligned} \qquad \textbf{(A.2)}$$

$$\lim_{\varepsilon\to 0} \int_{\Gamma_\varepsilon} L(i,j)\, \frac{\partial p}{\partial n_j}\, d\Gamma_\varepsilon = \lim_{\varepsilon\to 0} \frac{1}{2\pi} \int_0^\pi \sin\theta\, \frac{\partial p}{\partial n_j}\, d\theta = \frac{1}{4}\left(\frac{\partial p}{\partial n_i}\right) \qquad \textbf{(A.3)}$$

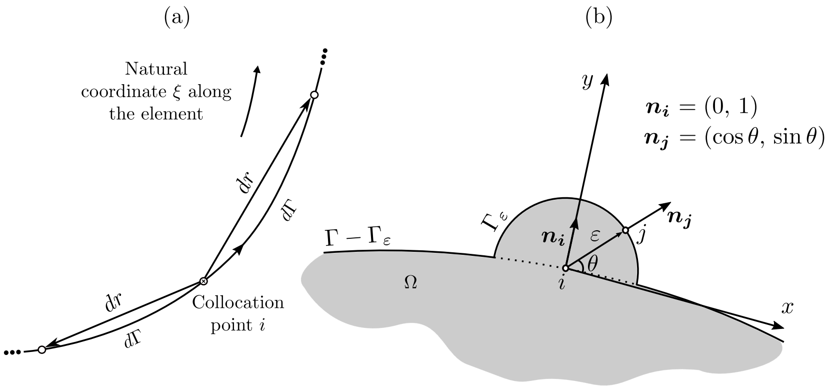

FIGURE A.1: (a) Element geometry around the collocation point i [119]. (b) Integral equality around the singularity on the barrier boundary.

As will be seen later, integral $\int_{\Gamma-\Gamma_\varepsilon} M(i,j)\,p\,d\Gamma$ from (A.1) leads to a term of the same order of singularity that enables the improper term from (A.2). Therefore, the only relevant subintegral of such expression is that involving just the finite part. This way and once the singularity around the collocation point has been extracted, expression (A.1) can be rewritten as follows:

$$0.5\left(\frac{\partial p_i}{\partial n_i}\right) + \fint\!\!\!\!\!\!-_{\Gamma} M(i,j)\,p\,d\Gamma = \fint_{\Gamma} L(i,j)\frac{\partial p}{\partial n_j}d\Gamma + L(0,i) \tag{A.4}$$

where $\fint\!\!\!\!\!\!-_{\Gamma}$ and $\fint_{\Gamma}$ represent the Hadamard finite-part and Cauchy principal integrals, respectively.

On the other hand, integrals extended to the boundary $\Gamma - \Gamma_\varepsilon$ are still to study. As a reminder, the integration cores of the hyper-singular BEM formulation are:

$$\begin{aligned}
\text{MW} &= \int_{\Gamma-\Gamma_\varepsilon} \phi \, \frac{\partial^2 G(k,r)}{\partial n_i \partial n_j} \, d\Gamma \qquad \text{(A.5)} \\
&= \int_{\Gamma-\Gamma_\varepsilon} \phi \left(\frac{ik}{2\pi} \left[ik\, K_2(ikr) \, \frac{\partial r}{\partial n_i} \frac{\partial r}{\partial n_j} + \frac{1}{r} \, K_1(ikr) \, (\boldsymbol{n_i} \cdot \boldsymbol{n_j}) \right] \right) d\Gamma \\
\text{LW} &= \int_{\Gamma-\Gamma_\varepsilon} \phi \, \frac{\partial G(k,r)}{\partial n_i} \, d\Gamma_\varepsilon = \int_{\Gamma-\Gamma_\varepsilon} \phi \left(-\frac{ik}{2\pi} \, K_1(ikr) \frac{\partial r}{\partial n_i} \right) d\Gamma \qquad \text{(A.6)}
\end{aligned}$$

The integral from (A.6) presents a term of $\mathcal{O}(1/r) = K_1(ikr)$ (here i corresponds to the imaginary unit) and other of $\mathcal{O}(r) = \partial r/\partial n$, so it is a regular integral to be solved by Gaussian quadrature. Integral (A.5) demands a special treatment. This can be split into two subintegrals to lead to a regular integral expression (I_R) and a hyper-singular one (I_H):

$$\begin{aligned}
\text{MW} &= \frac{1}{2\pi} \left(\text{I}_\text{R} + \text{I}_\text{H} \right) \qquad \text{(A.7)} \\
\text{I}_\text{R} &= \int_{\Gamma-\Gamma_\varepsilon} (ik)^2 \, K_2(ikr) \, \frac{\partial r}{\partial n_i} \frac{\partial r}{\partial n_j} \, \phi \, d\Gamma \qquad \text{(A.8)} \\
\text{I}_\text{H} &= \int_{\Gamma-\Gamma_\varepsilon} \frac{ik}{r} \, K_1(ikr) \, (\boldsymbol{n_i} \cdot \boldsymbol{n_j}) \, \phi \, d\Gamma \qquad \text{(A.9)}
\end{aligned}$$

Expression (A.8) presents terms of $\mathcal{O}(1/r^2) = K_2(ikr)$, $\mathcal{O}(r) = \partial r/n_i$ and $\mathcal{O}(r) = \partial r/n_j$, so it is a regular expression of $\mathcal{O}(r^0)$ to be solved by means of Gaussian quadrature. Integral (A.9) demands a particular consideration. Operating conveniently, the expression can be divided into three subintegrals:

$$\begin{aligned}
\text{I}_\text{H} &= \text{I}_\text{H1} + \text{I}_\text{H2} + \text{I}_\text{H3} \\
\text{I}_\text{H1} &= (ik)^2 \int_{\Gamma-\Gamma_\varepsilon} \left[\frac{K_1(ikr)}{ikr} - \frac{1}{(ikr)^2} - \left(\frac{1}{2} \right) ln(r) \right] (\boldsymbol{n_i} \cdot \boldsymbol{n_j}) \, \phi \, d\Gamma \qquad \text{(A.10)} \\
\text{I}_\text{H2} &= (ik)^2 \int_{\Gamma-\Gamma_\varepsilon} \frac{1}{(ikr)^2} \, (\boldsymbol{n_i} \cdot \boldsymbol{n_j}) \, \phi \, d\Gamma \qquad \text{(A.11)} \\
\text{I}_\text{H3} &= \frac{1}{2} \, (ik)^2 \int_{\Gamma-\Gamma_\varepsilon} ln(r) \, (\boldsymbol{n_i} \cdot \boldsymbol{n_j}) \, \phi \, d\Gamma \qquad \text{(A.12)}
\end{aligned}$$

with (A.11) being a regular integral. After operating conveniently on expression (A.10) the following is obtained:

$$
\begin{aligned}
\mathrm{I_{H1}} =& \mathrm{I_{H11}} + \mathrm{I_{H12}} \\
\mathrm{I_{H11}} =& \int_{\Gamma-\Gamma_\varepsilon} \frac{1}{r^2} \cdot \left(\boldsymbol{n_i} \cdot \boldsymbol{n_j} - \left| \frac{dr}{d\Gamma} \right| \right) \cdot \phi \cdot d\Gamma & \text{(A.13)} \\
\mathrm{I_{H12}} =& \left(\frac{1}{2}\right) \left(\frac{d^2\phi}{d\xi^2}\right)^i \left(\frac{1}{(J^i)^2}\right) (R_1 + R_3) + \left(\frac{d\phi}{d\xi}\right)^i \left(\frac{1}{J^i}\right) ln \left(\frac{R_3}{R_1}\right) + & \text{(A.14)} \\
& \phi_i \left[\left(\frac{1}{R_1} - \frac{1}{R_3} \right) - \underbrace{\frac{c}{\pi} \lim_{\varepsilon \to 0} \left(\frac{1}{\varepsilon} \right)}_{improper\, term} \right]
\end{aligned}
$$

As can be seen, expression (A.13) is a regular expression of $\mathcal{O}(r^0)$ to be solved by means of Gaussian quadrature. Furthermore, the improper term of expression (A.14) is canceled with that from expression (A.2) for free terms values of $c = 1$, that is to say, for non-nodal collocation within the element. Hyper-singular BEM formulation, as stated in Chapter 3 of this document, demands p to be continuous in the sense of Hölder continuity (C1 continuity) so the cancellation of this improper term and that from expression (A.3) is then assured in the HBIE integral equality (A.1). The term J^i refers to the Jacobian of the element, while R_1 and R_3 represent the distances from the inner collocation point to the extremes of the element (see Figure A.2).

On the other hand, after some operations on expression (A.12) the following is obtained:

$$
\begin{aligned}
\mathrm{I_{H3}} &= \mathrm{I_{H31}} + \mathrm{I_{H32}} \\
\mathrm{I_{H31}} &= \frac{1}{2} (ik)^2 \int_{\Gamma-\Gamma_\varepsilon} ln(r) \left(\boldsymbol{n_i} \cdot \boldsymbol{n_j} - 1 \right) \phi \, d\Gamma & \text{(A.15)} \\
\mathrm{I_{H32}} &= \frac{1}{2} (ik)^2 \int_{\Gamma-\Gamma_\varepsilon} ln(r) \left[\phi - \phi^i \left| \frac{dr}{d\Gamma} \right| \right] d\Gamma & \text{(A.16)} \\
&+ \frac{1}{2} (ik)^2 \phi^i \left[R_1 \left(ln(R_1) - 1 \right) + R_3 \left(ln(R_3) - 1 \right) \right]
\end{aligned}
$$

with $(\boldsymbol{n_i} \cdot \boldsymbol{n_j} - 1)$ from (A.15) and $\left[\phi - \phi^i \cdot \left| \frac{dr}{d\Gamma} \right| \right]$ from (A.16) terms of $\mathcal{O}(r^2)$ and $\mathcal{O}(r)$, respectively.

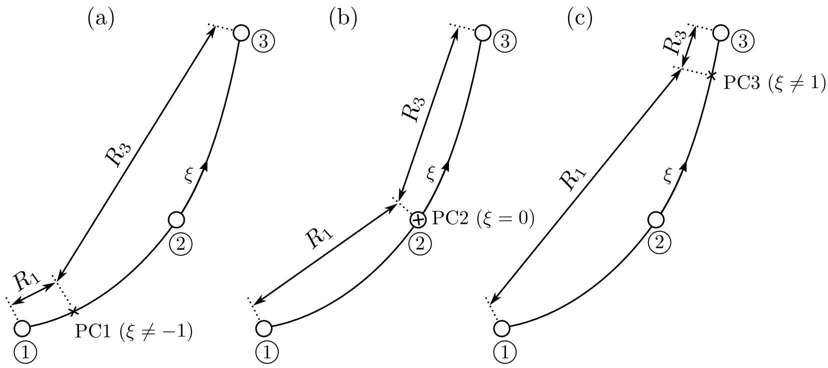

FIGURE A.2: Distances from the collocation point i to the extremes of the quadratic element. (a) Collocation point PC1. (b) Collocation point PC2. (c) Collocation point PC3.

The numerical strategies employed in the regularization of both the singular and the hyper-singular BEM integrals have been developed and implemented in a computer code by following the patterns proposed by Sáez et al. [119].

Summary of the dissertation in Spanish

Contenidos

Índice de Figuras

Índice de Tablas

B. DISSERTATION SUMMARY IN SPANISH

B.1 INTRODUCCIÓN Y ANTECEDENTES

De entre los subproductos más negativos derivados de la actividad industrial y el desarrollo tecnológico de la sociedad moderna la degradación ambiental es, indudablemente, uno de los asuntos de mayor preocupación. Desafortunadamente, esta problemática se ha agravado considerablemente a lo largo de los últimos años con el rápido crecimiento de la ciudades y de las actividades de las áreas urbanas. Los efectos perjudiciales derivados de estas actividades pueden afectar seriamente a la salud de las personas tanto física como psicológicamente [1, 2], lo que ha contribuido a despertar la conciencia del compromiso ciudadano.

Pese a ser una forma omnipresente de contaminación el ruido es, a día de hoy, una problemática a la que no se le presta toda la atención que merece. Según la Organización para la Cooperación y el Desarrollo Económico (OCDE), la contaminación acústica se trata de un *nivel excesivo de sonido que puede resultar perjudicial para la salud humana*. En otras palabras, toda clase de ruido excesivo o sonido desagradable que altera provisionalmente el equilibrio natural entra dentro de esta definición, la cual se aplica tanto a sonidos como a ruidos artificiales (bien en volumen o en su origen).

El tráfico urbano es, con mucha diferencia, la fuente más común de contaminación acústica in la ciudades y áreas urbanas, llegando a representar el 80% del total de la contaminación por ruido. Se estima que alrededor de 80 millones de personas están expuestas a niveles inaceptables de contaminación acústica continua derivada del uso del transporte exterior dentro de la Unión Europea (UE). Es por ello que el ruido asociado a los vehículos de motor es uno de los problemas sobre los que más se quejan los ciudadanos en las encuestas de opinión.

La gestión del ruido urbano se trata de un asunto que preocupa indistintamente a políticos, planificadores urbanísticos y gestores municipales. Es por ello que tareas como que el correcto tratamiento de las quejas ciudadanas, la elaboración de mapas de ruido, la restricción y/o disminución de sus niveles y la zonificación o creación de áreas urbanas para el desarrollo de determinadas actividades vertebran las líneas maestras de la correcta gestión de la contaminación acústica. Asimismo, esto ha sido un asunto prioritario para distintas Organizaciones Internacionales, tales como la ya citada OCDE, la EU y la Organización Mundial de la Salud (OMS), entre otras, las cuales han establecido y promovido en los últimos años distintas directivas, pautas y recomendaciones orientadas a la disminución del ruido, especialmente para la minimización del impacto acústico derivado de infraestructuras de transporte existentes y de nueva creación.

Afortunadamente, se están adoptando medidas proactivas encaminadas a la eliminación de problemas acústicos y a la prevención de aquellos potencialmente perjudiciales antes de que supongan un problema para los ciudadanos. Conocidos los niveles de ruido (bien sea por predicción o mediante medición directa) los diseñadores urbanos pueden minimizar sus efectos en los zonas colindantes mediante la implementación, siempre que sea posible, de medidas correctoras. En este sentido cabe destacar que en la fase de diseño a menudo los planificadores son advertidos de los requisitos de espacio que deben contemplar para la posterior inclusión de pantallas acústicas en el paisaje urbano. No es de extrañar, por tanto, el papel destacado que las pantallas acústicas han tenido a lo largo de los últimos años, especialmente en situaciones donde la implemetación de medidas correctoras en el foco emisor resultan inabordables. En estos casos, las pantallas acústicas se erigen como una de las medidas más efectivas en la protección contra el ruido.

La función principal de una pantalla acústica es ofrecer una correcta protección a los receptores (ciudadanos o animales) del ruido excesivo (el ruido de tráfico en el caso tratado en esta tesis) mediante la creación de una zona de *sombra* en el área que se pretende proteger. Un buen diseño debe contemplar aspectos de diversa naturaleza. La elección del material de la superficie de la pantalla, su localización así como su forma y dimensiones forman parte de las consideraciones a tener en cuenta en el correcto diseño acústico. Existen otros requerimientos, sin embargo, a tener en cuenta. Como suele ser el caso, un buen diseño centrado únicamente en aspectos acústicos puede afectar negativamente a otros aspectos de igual importancia. En este sentido, el diseño obtenido puede resultar inseguro para las personas (podría deslumbrar a los conductores por una mala elección del tratamiento superficial, producir lesiones en los viandantes por disponer de elementos inseguros, etc.) o de difícil acceso para su correcto mantenimiento, entre otros. La consideración de estos aspectos es igualmente importante para la construcción de la barrera. Es por ello que la investigación y desarrollo de todo tipo de pantallas acústicas se encuentra actualmente en auge. El continuo desarrollo de patentes de diseños comerciales y de tratamientos superficiales demuestra este hecho.

Desafortunadamente, la naturaleza del sonido es muy distinta a la de la luz. Debido al fenómeno de la difracción el ruido puede superar con cierto facilidad los obstáculos que se encuentra a su paso (cuanto menor sea la frecuencia a la que se propaga, mayor facilidad), tales como el borde superior de la barrera, de manera que la mencionada región de sombra dista, generalmente, de ser perfecta. Pese al progreso experimentado en los últimos años una de las direcciones de investigación que suponen un mayor reto es la que se centra en el estudio y desarrollo de diseños de borde, el punto débil de la eficacia a apantallamiento debido a la difracción. Es precisamente en la reducción de los efectos negativos de este fenómeno donde se deben centrar los esfuerzos, con miras a conseguir niveles aceptables de contaminación acústica.

B.1.1 Estado del arte

De entre todas las técnicas numéricas disponibles para el correcto tratamiento del problema que se presenta, el Método de los Elementos de Contorno (MEC) es una de las más empleadas. Hasta la fecha, se han llevado a cabo algunos trabajos interesantes relativos al estudio del apantallamiento acústico de barreras mediante el uso de esta técnica. A modo de antecedentes, Seznec [3] implementa esta técnica en el análisis de la difracción del sonido detrás la barrera. Hothresall et al. [4] llevan a cabo un estudio bidimensioal con el propósito de determinar los niveles de presión sonora en las inmediaciones de las terrazas de un edificio alto cercano a la carretera, concluyendo que las reflexiones producidas tanto por el techo como por las paredes frontales de estas terrazas afectan negativamente a la eficacia de apantallamiento. Sin embargo, la aplicación de materiales absorbentes en dichas paredes resulta ser la mejor estrategia en términos de reducción de niveles de ruido. Watts et al. [5] hacen uso del Método para evaluar las fugas de sonido que se producen en pantallas dispuestas en lamas con distintas configuraciones de ángulos, separación y tratamientos absorbentes. Martin and Hothersall [6] realizan un estudio en el que evalúan los efectos que el suelo produce en la atenuación del sonido mediante la simulación con modelos de fuentes de ruido coherentes e incoherentes, ante la presencia única y simultánea de pantallas de distintas alturas. Hothersall et al. [7, 8] emplean esta técnica en el estudio de pantallas simples para comparar sus efectos con los de otras tipologías de pantallas que presentan elementos difusivos en el borde superior. Siguiendo la misma línea de investigación, Ishizuka et al. [9] estudian el comportamiento de elementos reflectores de sonido instalados en la terrazas de edificios altos, concluyendo que la atenuación del ruido puede ser de hasta 10 dB(A) respecto de la situación original. Este estudio se complementa con experimentos basados en modelos tridimensionales a escala. Watts y Morgan [10] simulan el comportamiento acústico de un dispositivo que interfiere el recorrido normal de propagación del sonido instalado en el borde superior de una pantalla simple ya existente en una localización real. Los resultados obtenidos muestran mejoras significativas en la eficacia de apantallamiento del nuevo diseño. Crombie et al. [11] analizan el comportamiento de pantallas acústicas con múltiples bordes, concluyendo que la inclusión de paneles laterales a ambos lados de una pantalla simple mejora considerablemente su eficacia acústica. Fujiwara et al. [12] evalúan el apantallamiento de barreras muy delgadas, volumétricas, en forma de T y con bordes cilíndricos dotados de tratamientos superficiales rígidos, absorbentes y tipo *soft* (una superficie con valores de presión sonora casi nulos). Éstos últimos se modelan como una superficie plana con distintos valores de impedancia acústica, lo que idealmente representa el caso de una superficie con pozos de distintas profundidades dispuestos en la parte superior de dicha superficie. Monazzam y Lam [13] llevan a cabo un estudio comparativo entre pantallas acústicas en T, en Y, cilíndricas y en forma de flecha y los mismos diseños simulados con distintas secuencias de difusores de residuo cuadrático (QRD por sus siglas en inglés) en su parte superior, tanto para superficies reflejantes como para superficies absorbentes. En la misma línea, Ishizuka y Fujiwara [14] determinan que disponer de superficies tipo *soft* en el borde superior de las pantallas mejora significativamente su eficacia acústica. Las modificaciones geométricas que se realizan sobre la configuración general de la pantalla producen, sin embargo, mejoras poco destacables. Okubo y Fujiwara [15] estudian el comportamiento acústico de los denominados *waterwheel cylinder*, unas estructuras con forma de rueda de molinos de agua (de ahí su nombre en ingles) que instalado en el borde superior de las pantallas consiguen producir una superficie tipo *soft*. En este estudio se destaca finalmente que la eficacia de estos dispositivos depende en gran medida de la frecuencia analizada. Jean et al. [16] realizan un estudio sobre la influencia tanto del tipo suelo como de fuente de sonido en la evaluación de la eficacia de una pantalla simple, en forma de T y de borde cilíndrico. Jean y Gabillet [17] estudian la interacción del paso del tren y pantallas delgadas de escasa altura situadas en el interior de las vías. Adicionalmente a la configuración anterior el estudio contempla la presencia de una pantalla acústica de 2 m de altura situada en el borde de la carretera. Para el esquema fuente-receptor considerado, los mayores niveles de reducción sonora se dieron para el caso en el que tanto las pantallas como la parte inferior del tren fueron estudiados con tratamientos absorbentes. Para completar este compendio bibliográfico, Maeso y Aznárez han realizado en los últimos años algunos estudios interesantes en relación con la evaluación de la eficacia de distintas configuraciones de pantallas acústicas. Dichos trabajos se pueden consultar en [18]. Otros trabajos de importancia que emplean el MEC en problemas de acústica exterior son los presentados en [19–39].

Desde una perspectiva más general, existen trabajos interesantes en la bibliografía que tratan la formulación Dual del MEC con distintos enfoques. Esta formulacion ha sido empleada por Hong y Chen [40] y Portela et al. [41] en el estudio de grietas en problemas de elasticidad. Enfoques distintos de esta estrategia del Método se han presentado con posterioridad por Khrishnasamy et al. [42], Chen y Chen [43] y Wu [44]. Una completa y detallada revisión bibliográfica del uso de esta formulación y, en especial, de las distintas técnicas numéricas utilizadas en la regularización de las integrales hipersingulares del Método se puede consultar en Chen y Hong [45]. Más recientemente, Chen et al. [46] hacen uso de esta técnica en problemas de ondas marinas con el propósito de evitar las frecuencias espurias que se revelan asociadas al tratamiento de elementos con volumen. En lo que se refiere a problemas de acústica exterior, de Lacerda et al. [47] desarrollan una formulación 2D Dual del MEC para el correcto tratamiento de pantallas con volumen. Esta formulación se aplica en la evaluación del comportamiento acústico de una pantalla simple y una pantalla en T, modeladas como pantallas delgadas sobre un suelo absorbente. Tadeu et al. [48] proponen una formulación BEM-TBEM (denominación en inglés del Método conjunto al denominado *Traction BEM*) para modelar la propagación del sonido en presencia de elementos de sección muy delgada. Otros estudios de interés relativos al empleo la fomurlación Dual del MEC se pueden consultar en [49–56].

Por otro lado, existe abundante bibliografía relativa a modelos experimentales. En este sentido, May y Osman [57] realizan un estudio basado en la medición acústica de modelos a escala de barreras en distintas situaciones. En ellas se reproducen las condiciones del entorno de autopista destacando, dependiendo del caso, las ventajas de instalar pantallas en T y la idoneidad de emplear tratamientos superficiales absorbentes. En [58–60] se aborda el análisis del impacto acústico del ruido de tráfico sobre edificios próximos a carreteras. De nuevo May y Osman [61] testean la eficacia de una pantalla simple de 4 m, primero con tratamiento absorbente en una de sus caras y luego con tratamiento perfectamente reflejante. Del análisis comparativo de los resultados obtenidos con los derivados del test realizado a una pantalla en T de la misma altura se concluye que ésta última posee una mejor eficacia de apantallamiento. Jung et al. [62] llevan a cabo experimentos a escala reducida para determinar la eficacia de pantallas simple y en forma de T, éstas últimas con superficies de borde reactivas, en las proximidades de las vías de un tren de alta velocidad. Watts et al. [63] experimentan con modelos a escala real de pantallas en T, de múltiple borde y dobles de 2 m de altura de distintas dimensiones y con diferentes tipos de tratamientos superficiales, concluyendo que los diseños estudiados superan en eficacia acústica a la de la pantalla simple de misma altura. Hothersall et al. [64] reproducen distintos experimentos a escala de barreras en vías de tren en escenarios con diferentes tratamientos superficiales, tanto para la pantalla como para el suelo. Los resultados del experimento revelan la importancia de dotar al suelo con un tratamiento reflejante y a la pantalla de materiales absorbentes, especialmente el lateral de cara a la vía, para conseguir mejores niveles de apantallamiento. En Watts [65, 66] se analiza el comportamiento de pantallas paralelas y de múltiples bordes. Con la intención de reproducir lo más fielmente posible la influencia que los tratamientos superficiales tienen en la reducción del ruido, Watts y Godfrey [67] experimentan en dos localizaciones reales con pantallas acústicas existentes. Las conclusiones del estudio determinan que se alcanzan reducciones de niveles de ruido de hasta medio decibelio a favor de pantallas con materiales absorbentes respecto del caso perfectamente reflejante.

De entre los diferentes métodos metaheurísticos / bioinspirados / de optimización basada en técnicas de inteligencia de enjambre (tales como Estrategias Evolutivas, Optimización de Enjambres de Partículas, etc.), los Algoritmos Genéticos (AGs) son escogidos en esta tesis como representativos del paradigma de los Algoritmos Evolutivos. En general, cualquiera de las técnicas de optimización anteriormente mencionadas puede proporcionar una solución adecuada en el ámbito de aplicación de este trabajo. Sin embargo, la demostrada idoneidad de los algoritmos genéticos en aplicaciones similares para estos fines justifica su uso en los estudios que se presentan en este documento. Existen trabajos destacables en la literatura relativos al uso combinado del MEC y AG aplicado a la optimización de forma de pantallas acústicas. En este sentido, Duhamel [68] propone la optimización de forma de una barrera partiendo de una estructura volumétrica prismática dividida en bloques de idéntico tamaño, cuya forma final optimizada está conformada por una estructura sin huecos internos en la que algunos de los bloques de la configuración inicial permanecen y otros desaparecen, de acuerdo con los patrones marcados por el proceso evolutivo. Baulac et al. [69] llevan a cabo una optimización multicriterio sobre pantallas de múltiples bordes. Posteriormente, los mismos autores [70] realizan la optimización de pantallas en T con superficie de borde reactiva. Los parámetros a optimizar en este estudio se corresponden con las profundidades de los pozos y las características de sus tratamientos superficiales. Greiner et al. [71, 72] proponen una optimización mono- y multio-bjetivo de pantallas en Y; la consideración de incertidumbres en los diseños óptimos se estudia en [73]. Grubeša et al. [74] realizan una optimización tridimensional tanto de la eficacia acústica como de la viabilidad económica de pantallas acústicas constituidas de diferentes módulos de sección variable. En un estudio más reciente, Deb et al. [75] realizan una optimización multiobjetivo mediante el denominado proceso de *innovización*.

B.1.2 Antecedentes

El enfoque de esta Tesis se enmarca dentro de una línea de investigación ya en curso en el Instituto de Sistemas Inteligentes y Aplicaciones Numéricas en Ingeniería (Instituto SIANI) sobre el diseño óptimo de pantallas acústicas mediante el uso acoplado de Elementos de Contorno y Algoritmos Evolutivos.

A modo de antecedentes, el Prof. Orlando Maeso y el Prof. Juan J. Aznárez (ambos directores de esta tesis) han trabajado en los años previos en el desarrollo y la aplicación de métodos numéricos que permiten el tratamiento apropiado de problemas de propagación de ondas en medios elásticos. Los códigos desarrollados hasta la fecha, basados principalmente en el Método de los Elementos de Contorno (MEC), se han aplicado con éxito en diversos campos. En este sentido, merece destacar los trabajos de investigación llevados a cabo mediante la implementación tanto del MEC multi-dominio como de la aplicación conjunta de esta técnica y los Elementos Finitos (MEC-MEF) en el ámbito de la dinámica estructural (en la respuesta sísmica de cimentaciones pilotadas y superficiales [76–83], de presas bóveda [84–90], en problemas de interacción suelo - estructura por el método de subestructuración [91, 92], de interacción suelo -cimentación - estructura [93, 94], de interacción fluido - estructura [95], de fluido - suelo - estructura [96] y de estructura - suelo - estructura [97]). Previo al trabajo de investigación presentado en esta tesis se había desarrollado y mejorado un modelo numérico basado en la Ecuación Integral Estándar (SBIE por sus siglas en inglés) del Método para la simulación realista del fenómeno de propagación acústica exterior 2D inducida por cualquier tipo de fuente sonora. Basado en este código, en [18] se encuentra una recopilación de distintos estudios sobre la predicción de la eficacia acústica en situaciones diversas y sobre distintos diseños de pantallas anti-ruido. Muchos de estos trabajos se centran en la aplicabilidad y posibilidades de la formulación estándar del MEC para este problema. En otros se aborda la incorporación de algunos cambios sobre geometrías clásicas (en forma de Y, de T, de M, de flecha, de múltiples bordes, etc.) y el análisis de su influencia en la eficacia de esta medida. Otro trabajo de interés derivado del desarrollo de este código se puede consultar en [98].

Con posterioridad, el ámbito de desarrollo de esta línea de investigación se amplió a la búsqueda y mejora sistemática de la eficacia de apantallamiento de diseños de barrera habitualmente empleados en el entorno de carreteras. De este modo, los estudios anteriormente mencionados fueron complementados con los conocimientos y la experiencia en el ámbito aportados por el Prof. David Greiner (también director de esta tesis), firmante de algunos trabajos previos basados en la aplicación de Algoritmos Evolutivos (AEs) y, en particular, de Algoritmos Genéticos (AGs) en distintos problemas de optimización. Algunos de estos trabajos se han desarrollado en el ámbito del diseño óptimo estructural [99–104], mientras que en otros esta técnica se ha aplicado en distintos campos de la ingeniería [105–107]. En este sentido, en los años previos a este documento, los directores de la tesis habían desarrollado, y aplicado con éxito en distintos trabajos de investigación, un procedimiento general para la mejora sistemática de la eficacia acústica de pantallas anti-ruido a través de la optimización de forma de topologías previamente definidas, mediante el uso acoplado del MEC y AEs. Así, los resultados derivados de la primera implementación conjunta de ambas técnicas numéricas en el seno del Grupo de Investigación donde se enmarca este trabajo se pueden consultar en [71]. En este trabajo se lleva a cabo la maximización del comportamiento acústico de pantallas en Y con respecto a la de una barrera de referencia topológicamente idéntica. Posteriormente, en [108] se aborda la optimización de forma de pantallas volumétricas en M de altura efectiva prefijada. A diferencia del trabajo anterior, en este caso se busca minimizar las diferencias entre la eficacia de apantallamiento de un diseño en M a optimizar y la de pantallas simples de referencia con mayores alturas efectivas. En [73] se presenta un estudio basado en la optimización robusta y multiobjetivo de pantallas en Y. Más concretamente, el procedimiento se centra en la búsqueda de diseños, dotados de tratamientos absorbentes en su borde superior, que mejor se adaptan al comportamiento acústico de una pantalla en Y de referencia para cada longitud de barrera propuesta, considerando por primera vez esquemas de varios receptores. La minimización simultánea de ambos objetivos en conflicto es el aspecto central de este trabajo. Por último, en la misma línea de los anteriores trabajos, en [72] se aborda la optimización mono- y multi-objetivo de diseños en Y dotados de diferentes tratamientos superficiales.

B.1.3 Objetivos de esta tesis

La metodología desarrollada hasta la fecha había permitido abordar con éxito problemas de optimización basados en la mejora sistemática de la eficacia de apantallamiento de barreras anti-ruido. Sin embargo, la consideración de determinadas tipologías de pantallas suponían un reto importante, cuando no un problema inabordable, en términos de 1) la determinación de la validez geométrica de los diseños, a menudo complejos, propuestos por el optimizador y 2) la representación fiel del comportamiento acústico asociado al diseño de pantalla que se propone. Con el propósito de suplir estas carencias, se propone en este trabajo un procedimiento más general y robusto que permite llevar cualquier problema de optimización acústica en 2D. En este sentido, el objetivo de esta tesis es doble:

- Desarrollar e implementar formulaciones de Elementos de Contornos más adecuadas que nos permitan abordar la optimización de forma de cualquier tipo de pantalla anti-ruido bidimensional en un modo más robusto y flexible que en las formulaciones desarrolladas hasta la fecha.

- Diseñar e implementar una metodología basada en el uso acoplado del MEC y AE que permita obtener, de manera general y sistemática, diseños de pantallas que sean acústicamente cada vez más eficientes.

Para ser más precisos, este trabajo se centra en la búsqueda de las mejores soluciones acústicas, en términos de apantallamiento, que permitan minimizar el ruido de tráfico en las inmediaciones de zonas residenciales. La metodología presentada conduce a soluciones óptimas de topologías de pantallas acústicas previamente definidas y que, en general, superan significativamente la eficacia de apantallamiento de diseños clásicos que habitualmente se erigen en el entorno de carreteras.

A lo largo de este documento, se propone el estudio tanto de diseños novedosos como de diseños existentes y ampliamente estudiados en la literatura que, mediante modificaciones sistemáticas de su geometría, permiten obtener diseños mejorados. La complejidad inherente a muchos de estos diseños aconseja realizar algún tipo de simplificación que facilite el proceso de optimización. En este sentido, existen elementos integrados en el propio diseño de la barrera (cuando no el propio diseño de la barrera en su totalidad) susceptibles de simplificación matemática y geométrica que permita idealizar secciones muy delgadas como elementos de sección nula, para mediciones de la eficacia alejadas del contorno. Bajo este marco, las tipologías de barreras que se pueden abordar con la metodología que se presenta se pueden clasificar de las siguiente forma: i) pantallas volumétricas de dimensiones reales. Este sería el caso, por ejemplo de una pantalla en M; ii) pantallas de sección muy delgada en su totalidad. Su análisis se realiza mediante la idealización de su contorno como un elemento unifilar; iii) pantallas volumétricas con elementos muy delgados. Se trata de un caso mixto, en el que la configuración general conserva su geometría mientras que los elementos muy delgados se idealizan y estudian como elementos de sección nula.

B.1.4 Enfoques numéricos implementados

Las leyes que gobiernan los fenómenos naturales se expresan normalmente en términos de ecuaciones diferenciales. Desafortunadamente, la inmensa mayoría de los problemas a los que se enfrenta la ingeniería no se pueden resolver de manera directa, pues sólo se conoce la solución exacta de contada ecuaciones diferenciales en términos de funciones elementales (las ecuaciones diferenciales que se podían resolver de manera explícita hasta la segunda mitad del siglo XX eran escasas) o, simplemente, los sistemas descritos por estas ecuaciones son tan complejos o grandes, que la solución analítica no resulta viable. Es precisamente en estos sistemas complejos donde las simulaciones por ordenador y los métodos numéricos son de gran ayuda.

Las soluciones numéricas de estos fenómenos tan dispares nos permiten obtener con facilidad la solución aproximada en los casos en los que no se conoce la solución exacta y, por tanto, reducir los costes derivados de la experimentación. Pese a que estas técnicas se desarrollaron con anterioridad a los primeros ordenadores programables, el auge y desarrollo significativo que han experimentado los computadores en las últimas décadas ha posibilitado la rápida integración de estos métodos basados en aproximaciones numéricas de la solución real.

El Método de los Elementos de Contorno (MEC), también conocido como Método de la Ecuación Integral de Contorno o Método Integral de Contorno, es una técnica numérica que permite resolver ecuaciones lineales en derivadas parciales que han sido formuladas como ecuaciones integrales. En las últimas décadas, el MEC ha ido evolucionando paulatinamente hasta convertirse en una de las pocas técnicas numéricas ampliamente utilizadas en problemas de condición de frontera, tanto en el ámbito de la ingeniería como en el de las ciencias físicas. Por su inherente capacidad para abordar problemas de dominio infinito o de campo libre (la implementación del método requiere sólo discretizar el contorno del dominio de soluciones. La solución en cualquier punto del dominio se puede obtener una vez se conocidos los valores de la solución en el contorno), el MEC se trata de una de las técnicas más adecuadas para el estudio de la predicción de la propagación exterior de ondas acústicas. Sin embargo, la implementación de la formulación clásica del Método conduce a problemas inabordables en muchos de los casos estudiados en este trabajo.

Para poder cumplir con los objetivos marcados en esta tesis (mencionados en la sección anterior) se requiere de una formulación específica de Elementos de Contorno (EC) que permita el tratamiento correcto de los problemas planteados. Este nuevo planteamiento combina la formulación estándar del Método con una variante hipersingular, obtenida por derivación de la anterior, para finalmente obtener la denominada formulación Dual del MEC. El uso conjunto de ambos enfoques en esta formulación Dual nos permite sortear los inconvenientes asociados con la implementación exclusiva de la formulación estándar. En este sentido, este enfoque Dual es la estrategia más apropiada desde los EC para abordar los problemas numéricos que se proponen en este trabajo, permitiéndonos 1) adoptar idealizaciones geométricas sobre el diseño real de la pantalla, facilitando enormemente la representación geométrica y el tratamiento numérico de configuraciones complejas sin que ello introduzca errores apreciables para los espesores de pantalla tratados [47] y 2) evitar las frecuencias espurias asociadas al dominio interior de la barrera que pueden falsear la evaluación de la eficacia real de la pantalla. El tratamiento de estos problemas con EC a menudo deriva, según el caso, en problemas numéricos cuando no en un sistema de ecuaciones singular. Se trata por tanto de dos aspectos fundamentales a resolver en la metodología que se presenta. La solución a estos planteamientos, sobre todo la idealización geométrica de elementos muy delgados como cuerpos sin espesor, permite un procedimiento más general y sencillo en la búsqueda sistemática de diseños que, a menudo, gozan de completa libertad geométrica de acuerdo a su patrón topológico.

Bajo esta perspectiva, el diseño real de la barrera puede ser modelado, según el caso, como un elemento *unifilar*, como representativo de la sección de una pantalla muy delgada - Figura B.1(a) -, o como una estructura volumétrica que presenta elementos de sección muy delgada idealizados como cuerpos sin espesor - Figura B.1(b) -. Así, en un escenario libre de restricciones geométricas la representación de la pantalla se consigue de un modo más sencillo. Esta simplificación se traduce en menores tiempos de computación comparados con la representación real de la barrera, especialmente dentro de un proceso donde cada diseño que se propone se evalúa dentro de un espectro completo de frecuencias.

La necesidad de la formulación Dual del MEC en este trabajo se entiende a partir de la Figura B.10. La estrategia de aplicación de ambas formulaciones varía en función de la naturaleza del elemento que se estudia. Así, con el propósito de evitar las frecuencias espurias que pueden aparecer cuando tratamos con elementos de espesor considerable, el enfoque Dual del Método se basa en la aplicación conjunta y combinada de la ecuación integral estándar (SBIE) y de su variante hipersingular (HBIE por sus siglas en inglés), relacionadas a través de un valor complejo dependiente de la frecuencia [109]. La naturaleza del problema es distinta en el caso de elementos muy delgados. En este caso, el tratamiento directo

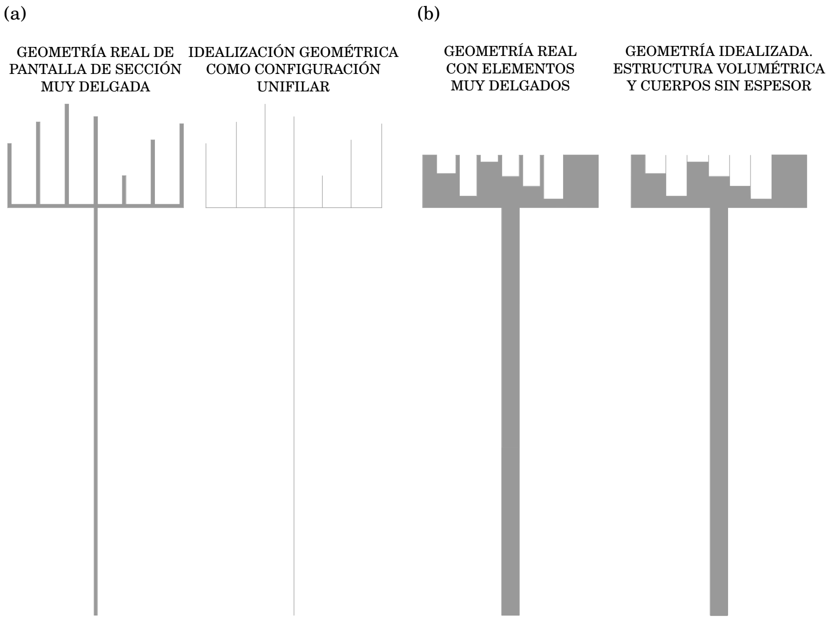

FIGURA B.1: Ejemplos de diseños de pantallas susceptibles de simplificación geométrica. (a) Diseño en forma de tenedor. La sección tan delgada de la pantalla sugiere su idealización como configuración unifilar. (b) Diseño inspirado en un difusor de residuo cuadrático (QRD por sus siglas en inglés) que presenta elementos muy delgados idealizados como cuerpos sin espesor.

de estos elementos puede dar lugar a problemas de integración numérica, afectando al comportamiento acústico de la pantalla. Tal y como muestra la Figura B.10(b), los contornos a ambos lados de los elementos sin espesor (con valores diferentes de presión acústica y flujo) están representados por la propia discretización. La aplicación de la SBIE sobre cada nodo a ambos lados de la pantalla conduce a un sistema de ecuaciones singular que no permite obtener la solución del problema. Sin embargo, la utilización simultánea, aunque por separado, de esta ecuación y su derivada en el nodo de colocación (HBIE) proporciona un sistema de ecuaciones compatible que permite obtener los valores de presión a cada lado de la barrera. Como resultado, este enfoque de la formulación Dual del MEC permite tratar elementos de sección muy delgadas como cuerpos de cuerpos sin espesor (elementos unifilares). Esta idealización geométrica proporciona una ventaja significativa respecto del caso en el que se analiza la pantalla, a menudo compleja en su diseño, con dimensiones reales.

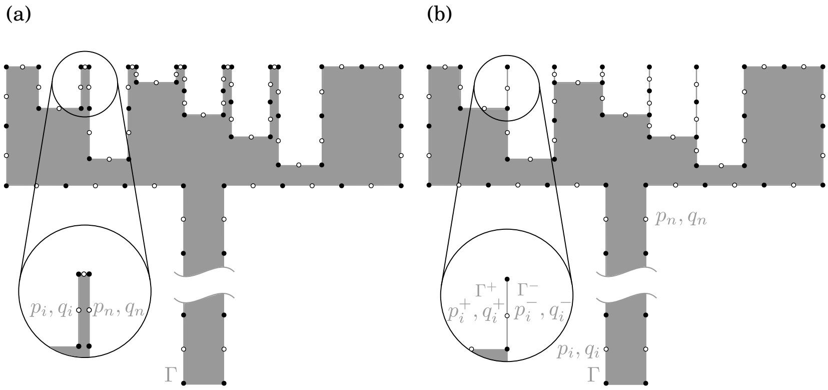

Figura B.2: Ejemplo de discretización con elementos parabólicos (3 nodos) para f=500 Hz en un diseño de pantalla inspirado en un QRD. (a) Discretización de la geometría real. (b) Discretización tras la idealización de los elementos de sección muy delgada como cuerpos unifilares.

Los métodos de optimización son herramientas de ayuda en la toma de decisiones que nos ayudan a alcanzar los objetivos propuestos. Para el caso que nos ocupa, en general, cualquiera de los métodos de optimización existentes puede proporcionar una solución satisfactoria en los términos planteados. Sin embargo, tal y como se ha comentado previamente, los Algoritmos Evolutivos han sido escogidos en este trabajo para la búsqueda de diseños de pantallas acústicas cada vez más eficientes. Los AEs, aunque relativamente nuevos, han destacado por ser unas herramientas muy potentes para encontrar soluciones en multitud de problemas de optimización de aplicación real. Muchos de estos problemas se definen a partir de más de un objetivo, lo que conduce a un conjunto de soluciones óptimas conocidas como soluciones *no dominadas*. En esta línea, la implementación de AEs se ha mostrado efectiva en la búsqueda de múltiples soluciones en una sola simulación numérica [110, 111].

Con el propósito de continuar con la línea de investigación ya abierta desde hace unos años en el Grupo donde se desarrolla esta tesis, se escogen los Algoritmos Genéticos como representativos del paradigma de los algoritmos evolutivos para la optimización de forma de pantallas acústicas. De entre los AEs, los AGs han demostrado su idoneidad para el tratamiento de problemas y metodologías similares a los que aquí se presentan [68–75].

Se presentan en este documento resultados relativos a la optimización mono- y multi-objetivo de pantallas acústicas. El algoritmo evolutivo empleado en la optimización mono-objetivo de la eficacia de apantallamiento hace uso del software libre GAlib [112], una colección de componentes de AGs escritos en lenguaje C++ que permite abordar diversos problemas con una implementación rápida y sencilla.

Por otro lado, la creciente importancia que la optimización evolutiva multi-objetivo (EMO por sus siglas en inglés) [110, 111] ha adquirido en los últimos años se debe al éxito que éstos métodos han tenido en la resolución de innumerables problemas en el campo de la ingeniería y de las ciencias en general [113]. Los algoritmos EMO son herramientas muy válidas cuando nos encontramos ante la optimización de dos o más objetivos en conflicto. Es lo que sucede en la optimización multi-objetvio llevada a cabo en este trabajo. Uno de los objetivos se centra en la maximización de la atenuación del sonido en la zona de sombra de la barrera, mientras que el otro trata de minimizar la longitud total del contorno de la pantalla, representativo del coste de manufacturación. Se deduce fácilmente que no se puede ir en favor de uno de los objetivos sin ir en perjuicio del otro. Dicho de otro modo, para el caso que nos ocupa, aumentar la eficacia de apantallamiento conduce, por lo general, a pantallas con contornos más largos (más caras de fabricar). El código empleado en la optimización multi-objetivo se trata de una implementación propia del conocido algoritmo NSGA-II [114], ampliamente utilizado en distintos trabajos de investagación en el seno del Instituto SIANI (ver [72, 73, 103, 108]).

B.1.5 Estructura del documento

Tal y como ha quedado de manifiesto, el contenido íntegro de esta tesis ha sido redactado en inglés. Sin embargo, y siguiendo lo establecido en el *reglamento para la elaboración, tribunal, defensa y evaluación* *de tesis doctorales de la Universidad de Las Palmas de Gran Canaria* del año 2005, se incluye este apartado, redactado en castellano, que recoge los antecedentes y objetivos de la investigación, la metodología utilizada, aportaciones originales, las conclusiones obtenidas y las futuras líneas de investigación.

Dado que este anexo recoge tan solo una parte del material presentado en la tesis doctoral, se ha optado por comentar a continuación la estructura y contenidos de la parte principal del documento original con el objetivo de ofrecer al lector una visión completa de los temas tratados en esta tesis.

Luego de las breves notas introductorias, el Capítulo 2 recoge los aspectos más fundamentales de la acústica. En primer término se presenta una breve introducción relativa a la física del problema y se detallan las variables acústicas más comunes utilizadas a lo largo del capítulo, seguido de una descripción detallada acerca de las hipótesis de partida tomadas en consideración y la presentación de las ecuaciones de gobierno. Asimismo, se definen las condiciones de contorno aplicable en problemas de propagación de ondas acústicas, haciendo especial hincapié en contornos que presentan cierta capacidad absorbente (condición tipo Robin) y la determinación de la impedancia acústica asociada por medio del modelo de Daleny y Bazley [115]. El capítulo concluye con la presentación y definición de las magnitudes acústicas más comunes, así como con la caracterización del sonido a través de su contenido en frecuencias y la información asociada.

La formulación Dual del MEC configura el contenido principal de este trabajo. El Capítulo 3 está dedicado a este enfoque de EC. En primer lugar, se introducen las bases de la formulación clásica (SBIE) así como de la ecuación integral hipersingular (HBIE) del Método como paso previo a la presentación de la formulación Dual en sus distintas variantes. En este sentido, se realiza una descripción detallada de los distintos planteamientos duales que permiten, dependiendo del caso, 1) evitar las frecuencias espurias que pueden revelarse en la evaluación de pantallas con sus dimensiones reales, 2) idealizar elementos muy delgados como cuerpos unifilares y 3) estudiar pantallas de dimensiones reales que presentan simultáneamente elementos muy delgados idealizados como elementos de espesor nulo. Por último, los ejemplos de validación de los distintos enfoques duales se encuentran al final de este capítulo.

El Capítulo 4 se centra en las bases teóricas de los Algoritmos Evolutivos y, en particular, de los Algoritmos Genéticos y la conveniencia de esta técnica de búsqueda en el marco de esta tesis. Tras una visión general de estos paradigmas, se realiza una descripción contextualizada del AG empleado en la optimización mono-objetivo presentada en este trabajo. Tras una breve introducción a la optimización evolutiva multi-objetivo, el capítulo cierra con una descripción del algoritmo EMO escogido.

Los Capítulos del 5 al 7 están dedicados a los resultados. Concretamente, el Capítulo 5 recoge los resultados numéricos de dos casos de estudio basados en la optimización de forma de pantallas acústicas de sección muy delgada que se idealizan como configuraciones unifilares. En el primer estudio se presentan diferentes topologías de pantallas de interés práctico. Éstos incluyen diseños basados en contornos rectos o curvos en su totalidad, cuya forma general o de borde, dependiendo del diseño topológico, se pretende optimizar considerando distintos tratamientos superficiales sobre determinados contornos. Dada la marcada naturaleza teórica de muchas de las topologías que se presentan, se realizan algunas modificaciones geométricas sobre algunos diseños optimizados que permiten obtener pantallas acústicas más prácticas desde el punto de vista de su construcción y posterior mantenimiento. Pese a que los resultados se han obtenido para un esquema específico de receptores, este estudio cierra con la evaluación de la influencia que la disposición de los receptores tiene sobre el comportamiento acústico. Es precisamente en este último punto donde se centra el segundo estudio, aunque desde una perspectiva más amplia: la influencia de la eficacia de apantallamiento con la distancia. Para ello se proponen dos modelos de pantallas evaluados con dos esquemas de receptores en tres regiones distintas en términos de cercanía a la barrera. Los análisis derivados de los resultados de ambos estudios se incluyen asimismo en este capítulo.

Continuando con la optimización mono-objetivo, el Capítulo 6 muestra el estudio numérico de pantallas con configuraciones de borde que presentan pozos con distintas profundidades, que combinan una estructura volumétrica general con elementos muy delgados que sugieren una idealización geométrica como cuerpos sin espesor. Con el propósito de determinar la importancia que el patrón de llenado de los pozos tiene en el comportamiento acústico, se modifica leve e incrementalmente la geometría óptima de uno de los diseños propuestos. Así se consiguen, al mismo tiempo, diseños modificados más prácticos y sencillos de construir que el original optimizado. Este capítulo finaliza con las conclusiones parciales obtenidas tras el análisis de los resultados mostrados.

Los resultados de la optimización multi-objetivo se recogen en el Capítulo 7. El análisis presentado en este capítulo plantea la optimization simultánea de dos objetivos en conflicto: la maximización de la atenuación del ruido y la minimización del coste derivado del material empleado para la pantalla, representado por la longitud total de los contornos. Las topologías que se optimizan fueron presentadas y definidas con anterioridad en el primer estudio llevado a cabo en el Capítulo 5. Aquí el escenario bidimensional es idéntico al de este último estudio, si bien sólo se contempla el caso de pantallas con superficies perfectamente reflejantes. Bajo estas consideraciones, la optimización multi-objetivo se realiza con dos escenarios de simulación: 1) partiendo de una población inicial completamente aleatoria y 2) incluyendo la mejor solución mono-objetivo del Capítulo 5 en la población inicial. En el análisis de los resultados se discute si este último caso supone una ventaja significativa en la mejora de las soluciones encontradas en los términos que se estudian.

En el Capítulo 8 se mencionan los logros más significativos y se resumen las conclusiones más destacables derivadas de este trabajo de investigación. Asimismo, se indican las futuras líneas de investigación que se pueden llevar a cabo a corto plazo enlanzando con los resultados de esta tesis.

Tras el contenido principal de este documento, el Apéndice A incluye los aspectos numéricos relativos a la regularización de las integrales hipersingulares de la formulación Dual del MEC presentada en el Capítulo 3.

Finalmente se cierra este documento con las referencias bibliográficas citadas a lo largo del texto, presentadas por orden de aparición.

B.1.6 Trabajos publicados derivados de esta tesis

Los logros obtenidos en los cuatro últimos años como consecuencia del desarrollo de esta tesis han sido publicados y presentados en distintos eventos siguiendo distintos formatos. Para finalizar este capítulo, se presentan a continuación los detalles de esta producción científica.

Contribuciones en congresos

- R. Toledo, J. J. Aznárez, O. Maeso and D. Greiner (2013). Optimización de diseños de pantallas acústicas de pequeño espesor mediante la implementación de la formulación dual del MEC. *Congreso de Métodos Numéricos en Ingeniería, SEMNI, Bilbao, España*.

- R. Toledo, J. J. Aznárez, O. Maeso and D. Greiner (2013). A comparative study in design optimization of polygonal and Bézier curve shaped-thin noise barriers using dual BEM formulation. *International Conference on Evolutionary and Deterministic Methods for Design, Optimization and Control with Applications to Industrial and Societal Problems, EUROGEN, Las Palmas de G. C., España*.

- R. Toledo, J. J. Aznárez, O. Maeso and D. Greiner (2014). Une méthodologie por l'optimisation d'écrans anti-bruit routiers de faible épaisseur et forme géométrique complexe en utilizant des algorithmes évolutionnaires et la méthode des éléments de frontière. *12éme Congrès Français d'Acoustique, CFA, Poitiers, Francia,* pp. 337-343.

- R. Toledo, J. J. Aznárez, O. Maeso and D. Greiner. A procedure for the top geometry optimization of thin acoustic barriers (2014). *E. Oñate et al. (Eds.), 11th World Congress on Computational Methods, WCCM XI, Barcelona, Spain*. ISBN.: 978-84-942844-7-2.

- R. Toledo, J. J. Aznárez, O. Maeso and D. Greiner (2015). Procedimiento para la optimización de forma de dispositivos de coronación para mejora de la eficacia de pantallas acústicas. *Congress on Numerical Methods in Engineering, Lisboa, Portugal*.

Contribuciones en capítulos de libro

- R. Toledo, J. J. Aznárez, O. Maeso and D. Greiner (2015). *Advances in Evolutionary and Deterministic Methods for Design, Optimization and Control in Engineering and Sciences, Computational Methods in Applied Sciences,* vol. 36, chap. A comparative study on design optimization of polygonal and Bézier curve-shaped thin noise barriers using Dual BEM formulation, pp. 335-349. Springer International Publishing Switzerland.

- R. Toledo, J. J. Aznárez, O. Maeso and D. Greiner (2015). *Evolutionary Algorithms and Metaheuristics in Civil Engineering and Construction Management, Computational Methods in Applied Sciences,* chap. A procedure for improving the acoustic efficiency of top-edge devices on noise barriers: an application of genetic algorithms and boundary elements, pp. 105-125. Springer.

Contribuciones en revistas inexadas (ISI-JCR)

- R. Toledo, J. J. Aznárez, O. Maeso and D. Greiner (2015). Optimization of thin noise barrier designs using Evolutionary Algorithms and a Dual BEM formulation. *Journal of Sound and Vibration,* **334**, 219-238.

- R. Toledo, J. J. Aznárez, D. Greiner and O. Maeso (2015). Shape design optimization of road acoustic barriers featuring top-edge devices by using Genetic Algorithms and Boundary Elements. *Engineering Analysis with Boundary Elements*. Aceptado para publicación.

Contribución en otras revistas

- R. Toledo, J. J. Aznárez, O. Maeso and D. Greiner (2015). Un procedimiento basado en el uso de algoritmos genéticos y elementos de contorno para el diseño óptimo de la geometría de pantallas acústicas de pequeño espesor. *Revista de Acústica, SEA,* **46(1,2)**, 13-21.

B.2 FORMULACIÓN DUAL DE ELEMENTOS DE CONTORNO

La mejora del comportamiento acústico de diseños topológicos clásicos de pantallas anti-ruido sin aumentar su altura efectiva es un reto difícil de abordar. Estos diseños, basados en las formas más simples, están representados en la gran mayoría de los casos por pantallas rectas o variantes de ésta. Si bien existen configuraciones de este estilo que presentan un buen comportamiento bajo ciertas condiciones, lo cierto es que los niveles de reducción de ruido por difracción asociados a estos diseños es prácticamente despreciable, pues su principio de funcionamiento se basa casi en exclusividad en la reflexión del sonido en su geometría. Existe por tanto una necesidad real de estudiar diseños alternativos que se comporten mejor acústicamente. En este sentido, a lo largo de los últimos años se han propuesto y estudiado distintos diseños de pantallas que han gozado de distinto éxito. En general, se ha constatado que las configuraciones que consiguen mayores reducciones de ruido son aquellas que presentan algún tipo de modificación geométrica en su borde superior (denominadas pantallas de borde modificado). De entre ellas cabe destacar el papel predominante que las pantallas de múltiples bordes, pantallas en forma de T, de Y, de M, de flecha, pantallas de borde cilíndrico, etc., han tenido en estos estudios. Siguiendo la misma estrategia, otros diseños más complejos hacen uso de dispositivos de borde con pozos de distintas profundidades cuya configuración se basa en una serie numérica matemática concreta. Tal es el caso, por ejemplo de los diseños basados en la secuencia de longitud máxima, en los difusores de residuo cuadrático o de raíces primitivas, etc.

La naturaleza geométrica de los diseños mencionados es diversa. Por ejemplo, algunos de ellos poseen una sección muy delgada que se mantiene constante a lo largo de toda su geometría. En este caso, la configuración general de la pantalla se puede idealizar como una estructura unifilar en casos en los que esta simplificación de la realidad no afecte significativamente a la medida de la eficacia de la pantalla. En otros casos, el diseño de la barrera se basa en una estructura general volumétrica que presenta simultáneamente elementos muy delgados que se pueden idealizar como cuerpos sin espesor.

El correcto tratamiento de estas geometrías requiere de un planteamiento de los Elementos de Contorno (EC) que permita sortear los principales inconvenientes que surgen de la aplicación exclusiva de la formulación estándar del Método de los Elementos de Contorno (MEC). Al respecto, la denominada formulación Dual del Método es la estrategia más apropiada, desde los EC, para abordar los problemas numéricos que se proponen en este trabajo, permitiéndonos 1) evitar las frecuencias espurias asociadas al dominio interior de la barrera y 2) adoptar idealizaciones geométricas sobre el diseño real de la pantalla, situaciones aplicables en las topologías que se estudian en este Trabajo.

Dependiendo de la problemática a tratar, la aplicación de la formulación Dual presenta un enfoque distinto. Las bases de la formulación clásica, hipersingular y Dual del MEC en sus distintas enfoques se presentan en detalle en las siguientes secciones.

B.2.1 Ecuación integral en el contorno singular (SBIE). Formulación clásica del MEC

La ecuación integral en el contorno singular (SBIE por sus siglas en inglés) para el punto del contorno i a ser resuelta mediante el MEC se puede expresar como:

$$c_i p_i + \fint_\Gamma p \frac{\partial G(k,r)}{\partial n_j}\, d\Gamma = G_0(k,r) + \int_\Gamma \frac{\partial p}{\partial n_j} G(k,r)\, d\Gamma \tag{B.1}$$

Esta igualdad integral implica sólo a puntos del contorno de la pantalla que se estudia. El símbolo $\fint$ representa la integral a lo largo del contorno entendida en el sentido del valor principal de Cauchy, una vez se ha extraído la singularidad en torno al punto de colocación i, tal y como se muestra gráficamente en la Figura B.3. En (B.1), p es el campo de presiones acústica en la superficie de la barrera y $G(k,r)$ es la solución fundamental del semiespacio (el campo de presión acústica cuando la fuente se sitúa en el punto de colocación i sobre un plano con admitancia β_g - admitancia del suelo -) y c_i es el término libre. Como norma general: $c_i = \theta/2\pi$, donde θ representa el ángulo interno al contorno medido en radianes. Se deduce fácilmente que $c_i = 0.5$ para contornos suaves.

Para un suelo reflejante ($\beta_g = 0$), las expresiones de la solución fundamental y su derivada para problemas armónicos bidimensionales son:

$$G(k,r) = \frac{1}{2\pi}\left[K_0(ikr) + K_0(ik\bar{r})\right] \tag{B.2}$$

$$\frac{\partial G(k,r)}{\partial n_j} = -\frac{ik}{2\pi}\left[K_1(ikr)\frac{\partial r}{\partial n_j} + K_1(ik\overline{r})\frac{\partial \overline{r}}{\partial n_j}\right] \tag{B.3}$$

donde i es la unidad imaginaria, k el número de onda, y r, $\overline{r}$ las distancias al punto de observación desde el punto de colocación y su punto simétrico respecto del plano formado por el suelo, respectivamente (ver Figura B.3). K_0 y K_1 son las funciones modificadas de Bessel de orden 0 y 1, respectivamente.

Aplicando la ecuación (B.1) sobre un nodo i de las discretización e interpolando la variables con elementos cuadráticos se obtiene:

$$c_i \cdot p_i + \sum_{k=1}^{NE}\sum_{l=1}^{3} p_l^k \cdot h_l^{ik} = p_0^* + \sum_{k=1}^{NE}\sum_{l=1}^{3} q_l^k \cdot g_l^{ik} \tag{B.4}$$

siendo NE el número total de elementos de la discretización. Finalmente, la aplicación sucesiva de (B.1) sobre cada nodo del contorno da lugar al siguiente sistema de ecuaciones:

$$(\mathbf{C}^s + \mathbf{H}) \cdot \mathbf{P} = \mathbf{G} \cdot \mathbf{Q} + \mathbf{G_0} \tag{B.5}$$

donde $\mathbf{C}^s$ es una matriz diagonal que alberga los valores del término libre en los nodos de la discretización, $\mathbf{P}$, $\mathbf{Q}$ son vectores que contienen los valores de presión y flujo (la derivada de la presión respecto de la normal en cada nodo del contorno), el vector $\mathbf{G_0}$ almacena los valores de la solución fundamental de la fuente de ruido y $\mathbf{H}$, $\mathbf{G}$ son matrices asociadas a los núcleos de integración de la formulación del MEC que implican únicamente a las variables del problema a lo largo del contorno:

$$h_l^{ik} = \int_{\Gamma_k} \frac{\partial G(k,r)}{\partial n_k}\, \phi_l \, d\Gamma_k \quad ; \quad g_l^{ik} = \int_{\Gamma_k} G(k,r)\, \phi_l \, d\Gamma_k \tag{B.6}$$

siendo i, en este caso, el punto de colocación, j el punto de observación y ϕ_l las funciones de forma con aproximación cuadrática de la variable local ξ a lo largo del elemento que se integra. En los estudios presentados en este trabajo, este tipo de aproximación se emplea para interpolar tanto el valor de la presión como la geometría del contorno de la barrera(elementos isoparamétricos). De este modo, la presión acústica en el elemento k se puede expresar como sigue:

$$p^k = \sum_{l=1}^{3} \phi_l \, p_l^k = \phi_1 \, p_1^k + \phi_2 \, p_2^k + \phi_3 \, p_3^k \tag{B.7}$$

siendo:

$$\begin{aligned} \phi_1(\xi) &= \frac{1}{2} \xi \, (\xi - 1) \\ \phi_2(\xi) &= 1 - \xi^2 \\ \phi_3(\xi) &= \frac{1}{2} \xi \, (\xi + 1) \end{aligned} \tag{B.8}$$

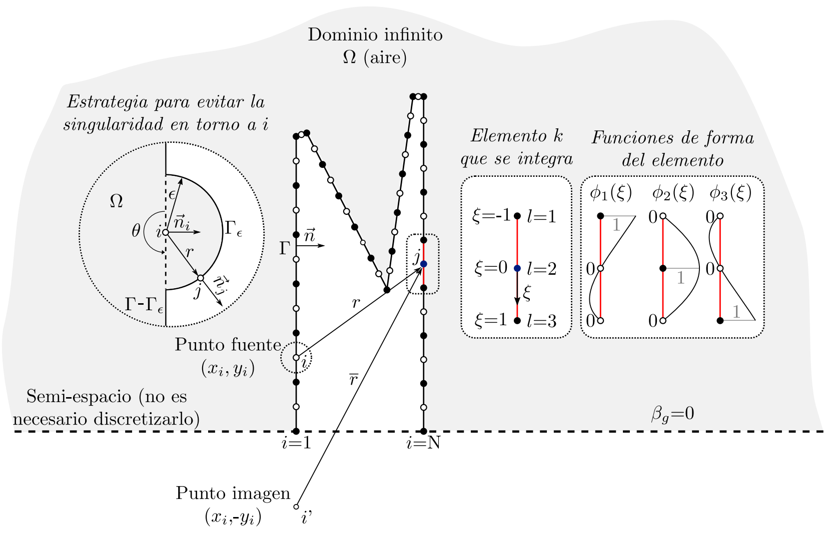

FIGURA B.3: Colocación fuente-imagen tras la discretización de una pantalla en M con elementos cuadráticos (3 nodos). Integración sobre un elemento genérico k. El punto de colocación se denota por medio de i mientras que el punto de observación en el elemento bajo integración se denota por j (tras la discretización del propio elemento con puntos de Gauss).

B.2.2 Ecuación integral en el contorno hipersingular (HBIE)

La ecuación integral en el contorno hipersingular (HBIE por sus siglas en inglés) para el punto del contorno i a ser resuelta mediante el MEC puede escribirse como:

$$c_i \left(\frac{\partial p_i}{\partial n_i} \right) + \fint_{\Gamma} p \frac{\partial^2 G(k,r)}{\partial n_i \partial n_j} d\Gamma = \fint_{\Gamma} \frac{\partial G(k,r)}{\partial n_i} \frac{\partial p}{\partial n_j} d\Gamma + \frac{\partial G_0(k,r)}{\partial n_i} \tag{B.9}$$

donde los símbolos $\fint$ y $\fint$ representan las integrales a lo largo del contorno entendidas según la parte finita de Hadamard y en el sentido del principal de Cauchy, respectivamente. Dado que la condición de Hölder [118] se debe satisfacer en el punto de colocación i, el tratamiento numérico de la formulación hipersingular se puede abordar bien 1) mediante el uso de elementos discontinuos o bien 2) mediante la colocación no nodal de la fuente dentro del elemento. De este modo, en ambas estrategias y para todos los casos se cumple que $c_i = 0.5$ en (B.9).

Las expresiones (B.10) y (B.11) muestran los valores de la solución fundamental implicadas en la ecuación integral hipersingular (B.9):

$$\frac{\partial G(k,r)}{\partial n_i} = -\frac{ik}{2\pi} \left[K_1(ikr) \frac{\partial r}{\partial n_i} + K_1(ik\overline{r}) \frac{\partial \overline{r}}{\partial n_I} \right] \tag{B.10}$$

$$\begin{aligned}\frac{\partial^2 G(k,r)}{\partial n_i \partial n_j} = \frac{(ik)^2}{2\pi} \Bigg[& \left(K_2(ikr) \frac{\partial r}{\partial n_i} \frac{\partial r}{\partial n_j} + \frac{1}{r} K_1(ikr)\, n_i \cdot n_j \right) + \\ & \left(K_2\,(ik\overline{r}) \frac{\partial \overline{r}}{\partial n_I} \frac{\partial \overline{r}}{\partial n_j} + \frac{1}{\overline{r}} K_1(ik\overline{r})\, n_I \cdot n_j \right) \Bigg]\end{aligned} \tag{B.11}$$

Similarmente a (B.1), i es la unidad imaginaria, k el número de onda y r, $\overline{r}$ as distancias al punto de observación desde el punto de colocación y su punto simétrico respecto del plano formado por el suelo, respectivamente. Cabe hacer una distinción relativa a los vectores normales implicados en las expresiones anteriores. En este caso, n_j representa un vector con dirección normal al contorno en el punto de integración, mientras que $n_i\,(n_x^i, n_y^i)$, $n_I\,(n_x^i,\text{-}n_y^i)$ representan los vectores normales al contorno real en el punto de colocación (i) y su punto simétrico (I) localizado sobre un contorno simétrico ficticio con respecto del suelo, respectivamente. K_1 y

K_2 representan las funciones modificadas de Bessel de orden 1 y 2, respectivamente.

Aplicando (B.9) sobre un nodo i del contorno discretizado e interpolando la variable con elementos cuadráticos se obtiene:

$$c_i \cdot q_i + \sum_{k=1}^{NE} \sum_{l=1}^{3} p_l^k \cdot m_l^{ik} = \frac{\partial G_0(k,r)}{\partial n_i} + \sum_{k=1}^{NE} \sum_{l=1}^{3} q_l^k \cdot l_l^{ik} \tag{B.12}$$

donde NE representa el número total de elementos de la discretización. La aplicación sucesiva de (B.9) sobre cada nodo de la discretización, similarmente a la formulación clásica, conduce al siguiente sistema de ecuaciones:

$$\mathbf{M} \cdot \mathbf{P} = \left(\mathbf{L} - \mathbf{C}^h\right) \cdot \mathbf{Q} + \frac{\partial \mathbf{G_0}}{\partial n_i} \tag{B.13}$$

donde $\mathbf{C}^h$ es una matriz diagonal con valores iguales a 0.5, $\mathbf{P}$, $\mathbf{Q}$ son vectores que contienen los valores de presión y flujo (la derivada de la presión respecto de la normal en cada punto del contorno), $\frac{\partial \mathbf{G_0}}{\partial n_i}$ es un vector que almacena los valores de la derivada de la solución fundamental relativa a la fuente externa de ruido y $\mathbf{M}$, $\mathbf{L}$ son matrices cuyas entradas están asociadas a los núcleos de integración de la formulación hipersingular del MEC que implican sólo a las variables del problema en el contorno de la pantalla:

$$m_l^{ik} = \int_{\Gamma_k} \frac{\partial^2 G(k,r)}{\partial n_i \, n_k} \, \phi_l \, d\Gamma_k \quad ; \quad l_l^{ik} = \int_{\Gamma_k} \frac{\partial G(k,r)}{\partial n_i} \, \phi_l \, d\Gamma_k \tag{B.14}$$

Las estrategias numéricas empleadas en la evaluación de las integrales singulares e hipersingulares del Método han sido desarrolladas e implementadas en un código de ordenador siguiendo las estrategias propuestas por Sáez et al. [119].

B.2.3 Formulación Dual del MEC

Una vez que las formulaciones de la SBIE y la HBIE han sido presentadas, los siguientes apartados se centran en las distintas variantes del uso conjunto de estas formulaciones para dar lugar a la denominada formulación Dual del MEC. Tal y como se ha comentado previamente, esta variante del MEC es la estrategia más apropiada del Método para el tratamiento correcto de las pantallas acústicas que se estudian en este trabajo.

Enfoque Dual para evitar las frecuencias espurias

La aplicación de la formulación estándar del MEC en el análisis de barreras que presentan contornos con espesores no despreciables puede conducir a una interpretación incorrecta de los resultados, al asociar valores picos de IL a determinadas frecuencias con un comportamiento acústico propio de la pantalla estudiada. Pese a que los problemas que se estudian en este documento son probelmas de acústica exterior, estos efectos de naturaleza puramente matemática representan las frecuencias propias (frecuencias naturales) del problema de acústica interior (los autovalores de las matrices de la formulación clásica del Método) y no representan en ningún modo la calidad del apantallamiento en dichas frecuencias. Una solución libre de frecuencias espurias y, por lo tanto, apropiada para sortear esta problemática se halla en la formulación propuesta por Burton y Miller [109]. Esta formulación se basa en la aplicación conjunta y combinada de la SBIE y la HBIE, relacionadas mediante un valor complejo dependiente de la frecuencia (α). En este caso, la expresión para un punto del contorno i para ser calculado mediante el MEC puede expresarse como sigue:

$$0.5\ (p_i + \alpha\, q_i) + \sum_{j=1}^{N} (h_j + \alpha\, m_j)\ p_j = \sum_{j=1}^{N} (g_j + \alpha\, l_j)\ q_j + \left(G_0 + \alpha\, \frac{\partial G_0}{\partial n_i} \right) \tag{B.15}$$

En (B.15), p es la presión acústica del campo de presiones sobre la superficie de la pantalla, q es el flujo (la derivada de la presión respecto de la normal en cada nodo de la discretización) y G_0, $\frac{\partial G_0}{\partial n_i}$ la solución fundamental del semi-espacio y su derivada relativa a la fuente de ruido externa, respectivamente. Por último, h y g son los núcleos de integración de la formulación clásica del MEC, mientras que l y m son los propios de la formulación hipersingular y que implican, como ya es sabido, sólo a las variables del problema en el contorno discretizado de la barrera con N nodos. El valor más ampliamente utilizado en la bibliografía para relacionar ambas ecuaciones integrales del Método se corresponde con $\alpha = i/k$ [120, 121], donde i se corresponde con la unidad imaginaria y k con el número de onda.

Además, tal y como se justificó con anterioridad, la formulación hipersingular del Método requiere que el punto de colocación j se encuentre en el interior del elemento. De esta manera, el término libre se asume igual a 0.5 en todos los casos.

Por otro lado, la capacidad de absorción del contorno queda determinada normalmente a través de la condición de Robin, de manera que el valor de la presión y el de su derivada en cada nodo del contorno quedan relacionados de la siguiente manera:

$$q_j = -i\,k\,\beta_\Gamma\,p_j \tag{B.16}$$

De este modo, (B.15) se puede expresar matricialmente como sigue:

$$[0.5\ (1+\beta)\ \mathbf{I} + \mathbf{H} + (i/k)\,\mathbf{M}\ + (i\,k\,\mathbf{G} - \mathbf{L})\ \beta] \cdot \mathbf{P} = \mathbf{G_0} - (i/k)\,\frac{\partial \mathbf{G_0}}{\partial n_i} \tag{B.17}$$

donde $\mathbf{I}$ es la matriz identidad.

Enfoque Dual para la idealización de elementos muy delgados como elementos unifilares

La naturaleza del problema es distinta cuando nos encontramos ante elementos de sección muy delgada. El tratamiento de estos elementos exclusivamente mediante la formulación clásica del MEC puede dar lugar a problemas numéricos relativos a los núcleos de integración de las matrices, afectando, de igual modo, a la correcta interpretación del comportamiento acústico de la pantalla. La idealización matemática de estos elementos como elementos unifilares (elementos de espesor nulo) no sólo resuelve esta problemática sino que además facilita la generación geométrica del perfil a estudiar. Con este fin, la SBIE y la HBIE se aplican simultáneamente y por separado en todo el contorno de la barrera ([47, 54]). La Figura B.4 facilita la comprensión de este asunto. Los contornos a ambos lados de los elementos idealizados quedan representados por la propia discretización, con valores distintos de presión y flujo. La aplicación de la SBIE a ambos lados de estos elementos sin espesor conduce a un sistema de ecuaciones singular que no permite obtener la solución del problema. Sin embargo, la aplicación adicional de la HBIE da lugar a la variante de la formulación Dual que proporciona un sistema de ecuaciones compatible que permite obtener los valores de presión a cada lado de la barrera.

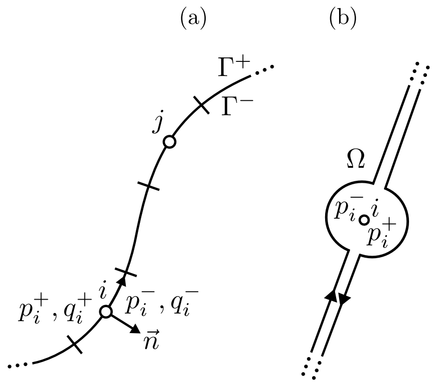

FIGURA B.4: (a) Idealización geométrica como cuerpo unifilar de una pantalla de sección muy delgada. (b) Estrategia empleada para sortear la singularidad alrededor del punto de colocación en el enfoque Dual para el tratamiento de elementos idealizados como cuerpos sin espesor (ver e.g. [95, 122]).

Tras la discretización del contorno idealizado - ver Figura B.4(a) - cada nodo contiene los valores de presión y flujo respecto a la normal al contorno (p^+, q^+, p^-, q^- en adelante). La Figura B.4(b) representa la estrategia empleada para evitar la singularidad del Método en este tipo de dominios [95, 122]. De este modo, la expresión de la formulación del MEC para este tipo de contornos puede ser expresada como sigue:

$$0.5\left(p_i^+ + p_i^-\right) + \sum_{j=1}^{N}\left(H_j^+ p_j^+ + H_j^- p_j^-\right) = \sum_{j=1}^{N}\left(G_j^+ q_j^+ + G_j^- q_j^-\right) + G_0(k,r) \tag{B.18}$$

siendo N el número total de nodos de la discretización. Asumiendo que $n^+ = -n^-$, se demuestra fácilmente que:

$$H_j^+ = -H_j^- \quad ; \quad G_j^+ = G_j^- \tag{B.19}$$

Considerando la condición de contorno tipo Robin (B.16), se puede expresar matricialmente:

$$(0.5\,\mathbf{I}^* + \mathbf{H} + i\,k\,\beta\,\mathbf{G}) \cdot \mathbf{P} = \mathbf{G}_0 \tag{B.20}$$

siendo $\mathbf{I}^*$ una matriz que contiene la contribución del término libre a ambos lados de los nodos de la discretización:

$$\mathbf{I}^* = \begin{bmatrix} 1 & 1 & 0 & 0 & 0 & 0 & \cdots & 0 & 0 \\ 0 & 0 & 1 & 1 & 0 & 0 & \cdots & 0 & 0 \\ \vdots & \vdots & \vdots & \vdots & \vdots & \vdots & & \vdots & \vdots \\ 0 & 0 & 0 & 0 & 0 & 0 & \cdots & 1 & 1 \end{bmatrix} \tag{B.21}$$

Tal y como se observa, la aplicación de la SBIE en cada nodo de la discretización conduce a un sistema de ecuaciones incompatibles (el número de incógnitas dobla al número de ecuaciones planteadas) que hace que el problema sea inabordable desde la implementación exclusiva de esta formulación. Sin embargo, la aplicación adicional de la HBIE permite plantear las ecuaciones restantes y abordar el problema con éxito. Así, la expresión de la formulación hipersingular para este tipo de geometrías puede expresarse como:

$$0.5\left(\frac{\partial p_i^+}{\partial n_i^+} + \frac{\partial p_i^-}{\partial n_i^+}\right) + \sum_{j=1}^{N}\left(M_j^+ p_j^+ + M_j^- p_j^-\right) = \sum_{j=1}^{N}\left(L_j^+ q_j^+ + L_j^- q_j^-\right) \tag{B.22}$$

donde:

$$\frac{\partial p_i^-}{\partial n_i^+} = -q_i \quad ; \quad M_j^+ = -M_j^- \quad ; \quad L_j^+ = L_j^- \tag{B.23}$$

Considerando la condición de contorno tipo Robin (B.16), se puede expresar matricialmente:

$$[i\,k\,\beta\,(0.5\,\mathbf{I}^* + \mathbf{L}) + \mathbf{M}] \cdot \mathbf{P} = \frac{\partial \mathbf{G_0}}{\partial n_i} \tag{B.24}$$

Finalmente, recopilando las expresiones (B.20) y (B.24) se obtiene el siguiente sistema matricial que permite el análisis adecuado de configuraciones de pantallas acústicas idealizadas como cuerpos de sección nula:

$$\begin{bmatrix} 0.5\,\mathbf{I}^* \; + \mathbf{H} + i\,k\,\beta\,\mathbf{G} \\ \\ i\,k\,\beta\,(0.5\,\mathbf{I}^* + \mathbf{L}) + \mathbf{M} \end{bmatrix} \cdot \left\{ \mathbf{P} \right\} = \left\{ \begin{matrix} \mathbf{G_0} \\ \\ \dfrac{\partial \mathbf{G_0}}{\partial n_i} \end{matrix} \right\} \tag{B.25}$$

Enfoque Dual para el análisis de configuraciones volumétricas con elementos muy delgados

Este planteamiento general incorpora ambas variantes de la formulación Dual del MEC, permitiendo la correcta evaluación del comportamiento acústico de pantallas que presentan una estructura general volumétrica simultáneamente con elementos muy delgados que se pueden idealizar como cuerpos sin espesor. De acuerdo a algunas de las expresiones obtenidas en este capítulo y denotando:

$$\mathbf{A_1} = 0.5\;(1+\beta)\;\mathbf{I} + \mathbf{H} + (i/k)\,\mathbf{M} + (i\,k\,\mathbf{G} - \mathbf{L})\;\beta \tag{B.26}$$

$$\mathbf{A_2} = 0.5\,\mathbf{I}^* \; + \mathbf{H} + i\,k\,\beta\,\mathbf{G} \;\;;\;\; \mathbf{A_3} = i\,k\,\beta\,(0.5\,\mathbf{I}^* + \mathbf{L}) + \mathbf{M} \tag{B.27}$$

$$\mathbf{B_1} = \mathbf{G}_0 - (i/k)\,\frac{\partial \mathbf{G_0}}{\partial n_i} \;\;;\;\; \mathbf{B_2} = \mathbf{G}_0 \;\;;\;\; \mathbf{B_3} = \frac{\partial \mathbf{G_0}}{\partial n_i} \tag{B.28}$$

la expresión final de la variante Dual del MEC para este tipo de pantallas se puede expresar como sigue:

$$\begin{bmatrix} \mathbf{A_1} \\ \mathbf{A_2} \\ \mathbf{A_3} \end{bmatrix} \cdot \left\{ \mathbf{P} \right\} = \left\{ \begin{matrix} \mathbf{B_1} \\ \mathbf{B_2} \\ \mathbf{B_3} \end{matrix} \right\} \tag{B.29}$$

En (B.29), $\mathbf{A_1}$ es una matriz de dimensiones $N_{Thick}\,x\,N_{Unk}$ y $\mathbf{A_2}$, $\mathbf{A_3}$ de dimensiones $N_{Thin}\,x\,N_{Unk}$. En este caso, N_{Thick} y N_{Thin} representan el número de nodos de la discretización propios de elementos con sección real y de elementos idealizados, respectivamente, mientras que N_{Unk} es el número de incógnitas del problema ($N_{Thick} + 2xN_{Thin}$). De acuerdo a esta nomenclatura, $\mathbf{P}$ se trata de un vector de dimensión N_{Unk} que contiene los valores de presión relativo a cada nodo de la discretización. Por último, $\mathbf{B_1}$ es un vector de dimensión N_{Thick}, mientras que $\mathbf{B_2}$, $\mathbf{B_3}$ son de dimensión N_{Thin}.

B.2.4 Presión acústica en el dominio

Conocidos los valores de la variable en el contorno, la presión acústica en cualquier punto del dominio interno (posición del receptor) se puede obtener fácilmente sin más que aplicar la expresión discretizada de la formulación clásica del MEC:

$$p^i = G_0(k,r) - \sum_{j=1}^{N_{Unk}} (h_j + i\,k\,\beta\,g_j)\;p_j \tag{B.30}$$

B.2.5 Criterio de discretización aplicado

Llegados a este punto es necesario destacar que la discretización del contorno de la barrera es dependiente de la frecuencia que se estudia. En este sentido, todos las simulaciones llevadas a cabo en este documento asumen una discretización con al menos cuatro elementos por longitud de onda. Estudios numéricos previos llevados a cabo por el investigador de este trabajo han demostrado que la consideración de este criterio conduce a una convergencia adecuada de los resultados. Asimismo, la estrategia adoptada está en consonancia con otros trabajos de investigación presentes en la literatura [7, 123].

Por otro lado se llevan a cabo algunos procedimientos para el correcto tratamiento numérico de contornos angulosos o que presentan cambios bruscos de dirección en su unión con otros contornos. Con el propósito de asegurar la convergencia numérica de las integrales cuasi-singulares, el código empleado en los estudios que aquí se presentan considera dos estrategias. Una de ellas está basada en el procedimiento propuesto por Telles [124], en el cual se realiza una redistribución y concentración de los puntos de Gauss en torno al punto de mínima distancia r dentro del elemento bajo integración. La otra estrategia consiste en la subdivisión del elemento que se integra, resultado de la discretización del contorno, en múltiples subintervalos en función de la distancia mínima r al punto cuasi-singular. El valor final resulta de la suma de cada integración numérica aplicada a cada subintervalo del elemento.

B.2.6 Estrategia de colocación empleada

Tal y como se ha comentado a lo largo de este capítulo, la estrategia de colocación empleada depende de la formulación que se aplica. De este modo, el código que implementa la formulación estándar del Método (SBIE) hace uso de la colocación nodal a excepción de los nodos situados en los extremos de los contornos no conectados, donde se adopta en este caso la estrategia de colocación no nodal.

La Figura B.5 representa la estrategia de colocación empleada en la implementación de la formulación hipersingular del MEC (HBIE) para los casos estudiados en este documento. Como ya es sabido, esta formulación requiere una estrategia de colocación no nodal en los extremos de los elementos. Un mayor nivel de detalle relativo a la elección del valor de δ en elementos discontinuos se puede consultar en [123, 125].

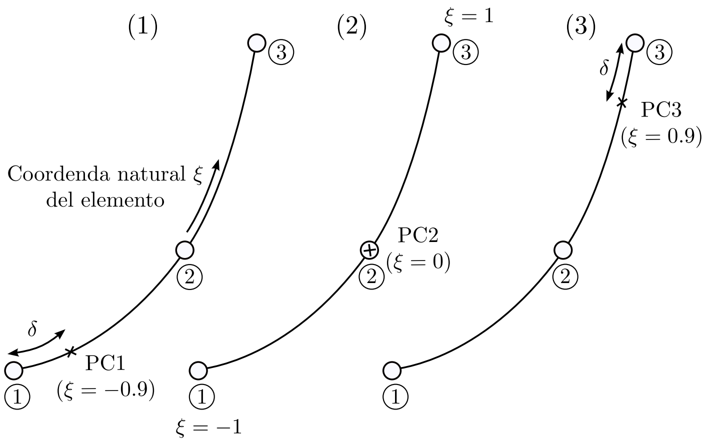

Figura B.5: Colocación no nodal en los extremos de los elementos cuando se aplica la formulación hipersingular del MEC. (1) punto de colocación PC1; (2) punto de colocación PC2; (3) punto de colocación PC3.

Para los casos aquí presentados, el punto de colocación se mueve una distancia de $\delta = 5\%$ de la longitud del elemento hacia su interior. La elección de este valor está avalada por estudios numéricos previos realizados por el investigador. Con todo, las diferencias observadas relativas a la elección de δ (dentro del ámbito de los rangos empleados en otros trabajos en la bibliografía) no son significativos, especialmente si se tiene en cuenta que los niveles de presión sonora que de interés en los estudios realizados no se corresponden ni con los de los contornos ni con los de los extremos de los mismos, sino con los de puntos concretos del dominio donde se encuentra la pantalla.

B.2.7 Estudios de validación

En este apartado se muestran los casos de validación de los distintos enfoques de la formulación Dual presentados. Los resultados se muestran en términos comparativos del comportamiento acústico de diseños de pantalla anti-ruido evaluados con la formulación clásica del MEC y con el correspondiente enfoque Dual.

La necesidad de implementar la formulación de Dual del MEC en el análisis de pantallas de dimensiones reales queda clarificada en la Figura B.6. Como se observa, este enfoque Dual del Método resuelve con éxito la problemática asociada a esta tipología de pantallas al evitar la frecuencias de resonancia (espurias) asociadas al dominio interior del diseño, pese a que el problema que se estudia es el de propagación exterior. En el análisis con la formulación clásica del Método, la aparición de éstos valores ficticios (valores pico de IL en la gráfica) en dichas frecuencias pueden a llegar a distorsionar en gran medida la calidad del apantallamiento. Este aspecto adquiere aún más relevancia dentro un proceso de optimización donde las mejores soluciones candidatas se seleccionan de acuerdo a diseños que no se ajustan a su comportamiento acústico real.

La idoneidad de representar pantallas de sección muy delgada como configuraciones unifilares se justifica con los resultados mostrados en la Figura B.7. El enfoque Dual del MEC implementado permite representar con mayor facilidad la geometría del diseño que se estudia. En este sentido, la definición en detalle de diseños con sus dimensiones reales daría lugar a un proceso más complejo y, muy posiblemente, menos general. Las ventajas de este tipo de representación, por tanto, aumentan a medida que el diseño se complica geométricamente. Simultáneamente, esta idealización ayuda a solucionar los problemas de integración numérica que a menudo se dan en la integración sobre puntos cuasi-singulares de estos elementos con espesores muy pequeños. Tal y como se observa en el gráfico esta problemática, sin embargo, no se manifiesta en el caso aquí presentado.

Finalmente, la Figura B.8 representa la evolución del comportamiento acústico de un diseño de borde basado en un Difusor de Residuo Cuadrático (QRD por sus siglas en inglés), previamente estudiado en la literatura por Monazzam et al. [13]. Al presentar una estructura general volumétrica con ciertos elementos que se pueden idealizar como cuerpos sin espesor, estas tipologías de pantallas resultan idóneas para validar el planteamiento Dual más general del MEC. Para facilitar la visualización, la estructura que conserva sus dimensiones reales está representada en azul en el gráfico, mientras que los elementos idealizados se representan en rojo. De acuerdo al análisis del trabajo original, el estudio se realiza en este caso para frecuencias centrales de bandas de 1/15 de octava. De los gráficos de evolución se concluye que los resultados derivados de la aplicación de la formulación Dual del MEC están en la línea de los presentados en el trabajo original con la formulación clásica del MEC.

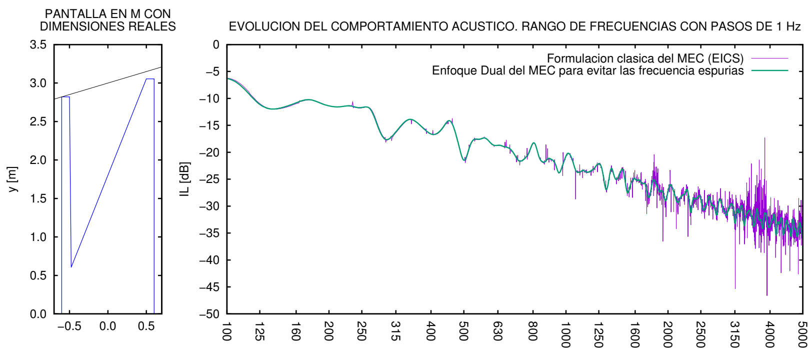

Figura B.6: Validación del enfoque Dual del MEC en una pantalla en M. La fuente de ruido y el receptor se encuentran en (-10.0, 0.0) y en (50.0, 0.0), respectivamente.

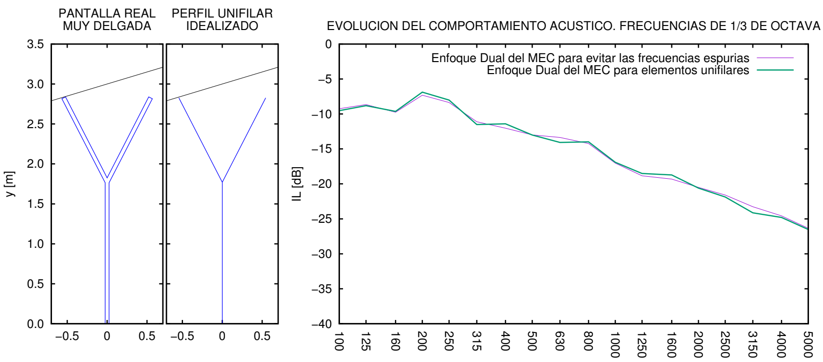

Figura B.7: Validación del enfoque Dual del MEC en una pantalla en Y de referencia de sección muy delgada. La fuente de ruido y el receptor se encuentran en (-10.0, 0.0) y en (50.0, 0.0), respectivamente.

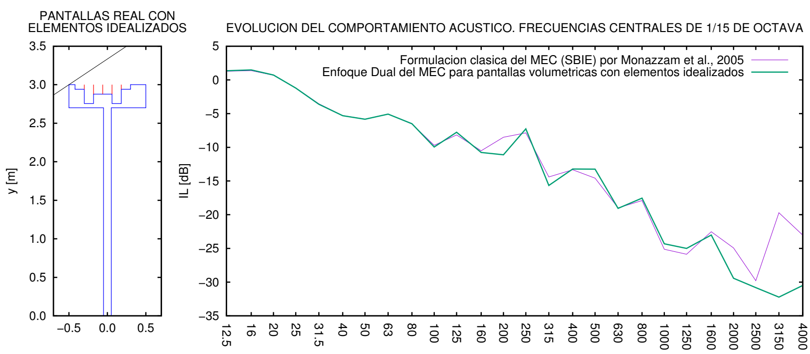

Figura B.8: Validación del enfoque Dual del MEC para pantallas volumétricas con elementos muy delgados. Estudio comparativo con los resultados presentados en Monazzam et al. [13] con la formulación clásica del MEC. La fuente de ruido y el receptor se encuentran en (-5.0, 0.0) y en (50.0, 0.0), respectivamente.

B.3 METODOLOGÍA APLICADA A LA OPTIMIZACIÓN DE PANTALLAS CON DISPOSITIVOS DIFUSORES

El estudio que se presenta tiene como objetivo ampliar la versatilidad y robustez de la metodología desarrollada e implementada hasta este momento en la optimización de forma de diseños topológicos de pantallas anti-ruido. Con este propósito se presenta una formulación de Elementos de Contorno (EC) más general que, implementada en un código de ordenador, permite un procedimiento con un alcance más amplio, posibilitando el estudio de cualquier tipo de problema de optimización de pantallas acústicas en 2D en una manera más sistemática, robusta y flexible.

El procedimiento propuesto hace uso de un enfoque de la formulación Dual del MEC combinado con un algoritmo evolutivo en la optimización del comportamiento acústico de pantallas con superficies reactivas. Más concretamente, se llevan a cabo estudios numéricos sobre tres diseños topológicos de pantallas con dispositivos de borde que presentan configuraciones de pozos de distintas profundidades. Basados en geometrías complejas, estos diseños combinan estructuras volumétricas con elementos muy delgados que sugieren una simplificación geométrica apropiada, mediante su consideración matemática como elementos de espesor nulo, a efectos de facilitar el proceso de optimización. En este sentido, debe verse la necesidad de la formulación Dual del MEC como la estrategia más apropiada desde los EC que nos permite 1) adoptar esta simplificación de la realidad sin que ello introduzca errores apreciables para los espesores de pantalla tratados [47] y 2) evitar las frecuencias espurias asociadas al dominio interior de la estructura volumétrica. Hasta donde conoce el investigador de esta tesis, no existen trabajos en la bibliografía que aborden el problema bajo las consideraciones que aquí se presentan.

El análisis presentado aborda el fenómeno como un problema de propagación bidimensional y en el dominio de la frecuencia, esto es, el ruido es causado por una fuente mono-frecuencia e infinita que discurre paralelamente a una pantalla que presenta una estructura volumétrica combinada con elementos de sección muy delgada y longitud igualmente infinita que yace sobre un semiespacio de admitancia uniforme. A partir de la respuesta en frecuencia y un espectro de ruido que caracterice la fuente, puede expresarse la función de optimización de forma sencilla.

Tras la optimización, sobre la base de los perfiles óptimos de uno de los diseños topológicos propuestos se realizan modificaciones geométricas incrementales que ayudan a entender cómo influye el patrón de llenado de los pozos en el comportamiento acústico. A partir de este análisis se consiguen diseños de pantallas más prácticos y sencillos de construir que los diseños optimizados. Asimismo, se realiza un estudio comparativo entre la eficacia de apantallamiento de una de las geometrías óptimas y un diseño de pantalla topológicamente idéntico previamente estudiado en la literatura. Finalmente, el capítulo concluye con la discusión de los resultados obtenidos.

B.3.1 Dispositivos de borde basados en difusores para la atenuación del sonido en problemas de acústica exterior

Debido a sus incuestionables beneficios para dispersar el sonido, el uso de difusores en proyectos de acústica interior ha sido objeto de numerosos exámenes y estudios. De entre ellos, los diseños basados en series matemáticas numéricas (como por ejemplo los difusores de secuencia de máxima longitud, de residuo cuadrático, de raíces primitivas, etc.) han ganado importancia por sus excelentes propiedades de difusión, caracterizados por presentar un espectro de densidad de potencia aproximadamente plano. Debido a que el espectro de potencia y la capacidad difusiva de una determinada superficie están relacionados [147–149], se puede predecir de manera aproximada la dispersión del sonido en el campo lejano sin más que aplicar la transformada de Fourier sobre los coeficientes de reflección de dicha superficie (en el caso tratado, un conjunto de pozos con distintas profundidades modelados como una superficie plana con distintos valores de impedancia). En resumen, cualquier secuencia numérica que presente buenas propiedades auto-correlación (la función auto-correlación de los coeficientes de reflección de una superficie es una función delta) posee una transformada de Fourier con una densidad espectral de potencia plana, lo que implica que la superficie estudiada asegura una distribución homogénea de la dispersión del sonido.

Con el propósito de mejorar la calidad del apantallamiento, en los últimos años se han propuesto y he estudiado numerosos e innovadores diseños en la literatura con la intención de compensar las limitaciones asociadas con el parámetro con mayor influencia en el comportamiento acústico: la altura efectiva. En este sentido, a pesar de que inicialmente fueron concebidos para proyectos de acústica interior, el uso de difusores como dispotivos instalados en el borde superior de pantallas ha puesto de manifiesto la idoneidad de estos diseños en problemas de acústica exterior, presentando un buen comportamiento acústico no sólo respecto al de la pantalla simple de referencia sino incluso al de otros diseños de borde clásicos. Existen algunos trabajos notables en la bibliografía relativos al uso de difusores en problemas de acústica exterior. Tal es el caso de los Difusores de Residuo Cuadrático [13, 29, 30, 33] o de los Difusores de Raíces Primitivas [32] (QRDs y PRDs, por sus siglas en inglés respectivamente). Otros diseños de geometría más compleja han sido estudiados en [15, 21] (ver Figura B.9).

Los trabajos mencionados abordan el problema con la formulación estándar del MEC, considerando la geometría real de la pantallas constituida por elementos de espesor considerable y, simultáneamente, elementos de sección muy delgada. Sin desmerecer la contribución de estos trabajos, ninguno de los estudios llevados a cabo propone la optimización de forma de estos diseños de borde. En este sentido, la metodología que se presenta en este capítulo propone un procedimiento de carácter general que permite optimizar la forma de pantallas acústicas con diseños de borde mediante la formulación Dual del MEC. Dicha metodología ofrece una solución apropiada para la evaluación de diseños complejos que son susceptibles de simplificación geométrica. Bajo esta consideración, la configuración general de la pantalla se puede modelar considerando una estructura general volumétrica (que conserva sus dimensiones reales) con elementos unifilares (sin espesor) representativos de elementos de sección muy delgada. En un marco libre de restricciones geométricas, la definición de la pantalla se convierte, de este modo, un proceso sencillo. Además, este enfoque geométrico permite reducir los tiempos de computación en el marco de un proceso costoso donde cada diseño ha de ser evaluado en todo el espectro de frecuencias.

La necesidad de la formulación Dual del MEC en este estudio se entiende a partir de la Figura B.10. La estrategia de aplicación de ambas formulaciones varía en función de la naturaleza del elemento que se estudia. Así, con el propósito de evitar las frecuencias espurias que pueden aparecer cuando tratamos con elementos de espesor considerable, el enfoque Dual del Método se basa en la aplicación conjunta y combinada de la ecuación integral estándar (SBIE) y de su variante hipersingular (HBIE), relacionadas a través de un valor complejo dependiente de la frecuencia [109]. La naturaleza del problema es distinta en el caso de elemen-

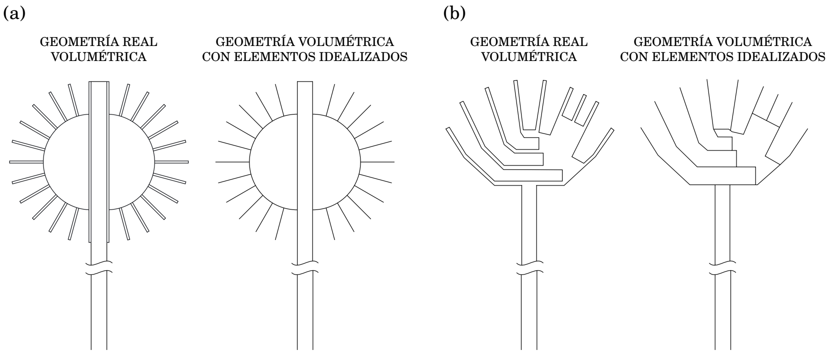

FIGURA B.9: Ejemplos de diseños de pantallas con elementos susceptibles de idealización geométrica. (a) Diseño de borde estudiado por Okubo y Fujiwara [15]. (b) Diseño de geometría compleja con pozos de distintos trayectos y profundidades [21].

tos muy delgados. En este caso, el tratamiento directo de estos elementos puede dar lugar a problemas de integración numérica que pueden afectar al comportamiento acústico de la pantalla. La idealización de estos elementos como cuerpos sin espesor no sólo resuelve esta problemática sino que además facilita la representación geométrica de la pantalla, simplificando en gran medida el proceso de optimización. Con este fin, la SBIE y la HBIE se aplican simultáneamente, aunque por separado, sobre cada nodo de la discretización de la pantalla. Esta simplificación de la realidad proporciona una ventaja significativa respecto del caso en el que se analiza la pantalla con dimensiones reales.

B.3.2 Descripción del proceso de optimización

La optimización de forma se realiza, tal y como se ha comentado, mediante el uso combinado de un algoritmo evolutivo y la mencionada formulación Dual del MEC. Para más nivel de detalle acerca de los aspectos del enfoque Dual empleado en este estudio se puede consultar el Capítulo II de este Resumen. Respecto al algoritmo evolutivo en la optimización se utiliza el software libre GAlib [112], una colección de componentes de

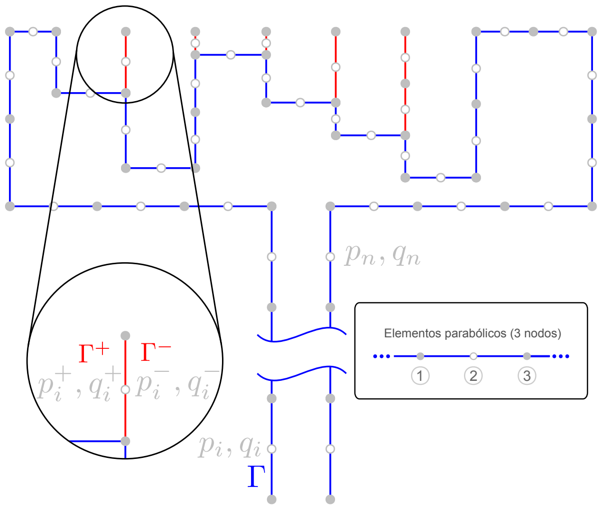

Figura B.10: Ejemplo de la discretización de una pantalla, tras la idealización de los elementos muy delgados como cuerpos sin espesor, con elementos parabólicos (3 nodos) para f=500 Hz de un diseño inspirado en un QRD. Para facilitar la visualización, la estructura volumétrica se representa en azul mientras que los elementos idealizados se representan en rojo.

algoritmos genéticos (AG) escritos en lenguaje C++.

La metodología que se aplica en este proceso permite la optimización de forma de cualquier tipología de pantalla anti-ruido bidimensional. En este contexto, el procedimiento aquí utilizado aborda la mejora de la eficacia de dispositivos de borde de una manera, hasta donde conoce el investigador de este estudio, no tratada hasta la fecha en la bibliografía. Dicha metodología se aplica al estudio numérico de tres diseños topológicos de pantallas con dispositivos de borde que presentan una estructura volumétrica con elementos muy delgados idealizados como elementos de espesor nulo. El uso de la formulación Dual del MEC se justifica en el sentido de que se trata de la estrategia más adecuada desde los EC para abordar numéricamente los problemas que aquí se presentan, tal y como han puesto de manifiesto Hong and Chen [40], Krishnasamy et al. [42], de Lacerda et al. [47], Chen and Chen [43], Chen y Hong [45], Wu [44], Chen et al. [150] y Tadeu et al. [48]. Su justificación se hace extensiva, principalmente, a la idealización de los elementos muy delgados. Esta simplificación facilita en gran medida la representación geométrica de la pantalla sin influir sustancialmente en el comportamiento acústico para los espesores considerados en este estudio.

Configuración bidimensional estudiada

La Figura B.11 muestra la configuración general objeto de estudio. Como ya se ha adelantado, se trata de un problema de propagación 2D asociado a una fuente de sonido monofrecuencia e infinita (matemáticamente representada por la función delta de Dirac) situada paralelamente a una barrera acústica que combina estructuras volumétricas con elementos muy delgados y que se encuentra sobre un plano (suelo) de admitancia uniforme. En los análisis realizados, tanto el suelo como la barrera presentan una superficie perfectamente reflejante ($\beta_b = \beta_g = 0$). La función objetivo (FO) se evalúa en un único receptor situado en el lado de sombra. Tanto la fuente de ruido como el receptor se sitúan sobre el suelo separados 5.0 m y 25.0 m del eje central de la pantalla, respectivamente. Asimismo, la máxima altura efectiva que se permite alcanzar es $\mathrm{h_{ef}} = 3.0$ m en el eje medio de la barrera.

Determinación de la eficacia acústica de la pantalla

Tal y como se conoce, la calidad de apantallamiento a cada frecuencia a la que emite la fuente de ruido considerada se determina por medio del coeficiente de pérdida por inserción (IL por sus siglas en inglés) definido, como es sabido:

$$\mathrm{IL} = -20 \cdot \log_{10}\left(\frac{\mathrm{P_B}}{\mathrm{P_{HS}}}\right)[\mathrm{dB}] \tag{B.31}$$

siendo su medida representativa de la diferencia de niveles de presión sonora en el punto del dominio considerado (donde se encuentra el receptor) en la situación con ($\mathrm{P_B}$) y sin pantalla ($\mathrm{P_{HS}}$).

Con el propósito de llevar a cabo un proceso de optimización donde la excitación esté representada por una fuente de ruido pulsando a cada

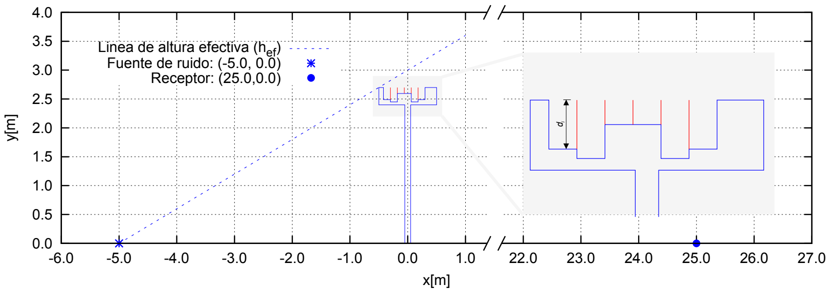

FIGURA B.11: Configuración bidimensional empleada en el proceso de optimización. Ejemplo de diseño de borde inspirado en un QRD (modelo (a) en este estudio), compuesto por pozos de distintas profundidades (d_i). Para facilitar la visualización de la geometría, los elementos de espesor no despreciable se representan en azul mientras que los elementos muy delgados se idealizan como elementos sin espesor y se representan en rojo.

frecuencia del espectro, la eficacia global de la barrera para el receptor considerado se puede expresar en términos del coeficiente de pérdida por inserción de todo el espectro:

$$\mathrm{IL_{total}} = -10 \cdot \log_{10} \left(\frac{\sum_{\mathrm{i=1}}^{\mathrm{NF}} 10^{(\mathrm{A_i - IL_i})/10}}{\sum_{\mathrm{i=1}}^{\mathrm{NF}} 10^{\mathrm{A_i}/10}} \right) [\mathrm{dB(A)}] \qquad \text{(B.32)}$$

siendo NF el número de frecuencias centrales de banda de octava del espectro considerado, aquí NF $= 86$, $\mathrm{A_i}$ el nivel de ruido ponderado del espectro e $\mathrm{IL_i}$ el coeficiente de pérdida por inserción de la barrera para cada una de estas frecuencias, según (B.31).

Espectro de ruido de tráfico utilizado

En este estudio, la fuente de ruido se caracteriza de acuerdo al espectro normalizado de ruido de automóviles, ponderado A, definido por la norma UNE-EN 1793 [117] para frecuencias centrales de tercio de octava en el rango de 100 a 5 000 Hz. Dada la alta variabilidad en el comportamiento acústico que los diseños que se estudian presentan con la frecuencia, así como con la intención de determinar la eficacia global de la pantalla de una manera más precisa, las bandas de 1/3 de octava se expanden a intervalos de 1/15. En este espectro corregido, los valores normalizados para las bandas de frecuencias centrales de 1/15 de octava han sido calculados de manera tal que la intensidad acústica total asociada a cada banda se conserva con respecto a la correspondiente banda de 1/3 de octava. El estimador considerado en el proceso de optimización, es decir, la función objetivo, se basa exclusivamente en el valor del IL espectral en la localización del receptor propuesto ($\mathrm{OF} = \mathrm{IL}_{\mathrm{total}}$). Como es de esperar, a lo largo del proceso se intenta maximizar el valor de este parámetro.

Parámetros usados en el AG

Debido a que la evaluación de la función objetivo para cada diseño candidato exige un coste computacional alto para el MEC, se implementa un algoritmo genético de *estado estacionario* [144, 145] el cual trata de compensar estos inconvenientes a través de una estrategia con una elevada capacidad de explotación combinada con una gran presión de selección. El algoritmo evoluciona a partir de una población inicial de 100 individuos, utilizando el operador de *cruce en dos puntos* con una probabilidad de reproducción del 90%. Asimismo, se emplea una tasa de mutación igual a $1/\mathrm{n}_{\mathrm{ch}}$, siendo n_{ch} la longitud total del cromosoma codificado con variables binarias de distinta precisión, según el diseño topológico que se optimiza, de acuerdo a la codificación Gray (ver Tabla B.1). El reemplazo generacional empleado es del 2%, lo que significa que los dos peores individuos de cada generación son susceptibles de ser reemplazados si los nuevos individuos tras las operaciones de selección, cruce y mutación son mejores en términos de la función objetivo. Finalmente, el criterio de parada se establece tras 1 000 generaciones o iteraciones del proceso evolutivo.

Descripción general del proceso

Con el propósito de facilitar la comprensión de la metodología, la Figura B.12 muestra en un diagrama de flujo el proceso evolutivo que tiene lugar en la búsqueda de los mejores diseños acústicos. Dicho proceso hace uso de un AG de estado estacionario que parte de una población inicial

TABLA B.1: Descripción de las variables de diseño (profundidades de pozo, codificadas con variables binarias) de los modelos topológicos a optimizar y de los cromosomas correspondientes.

Modelo	Longitud del cromosoma (n_{ch})	Bits por cada variable	Rango de la variable [m]	Valores discretos por variable
(a)	Simétrico: 15 No simétrico: 30	5 (cada pozo)	0.000-0.250	32
(b)	Simétrico: 60 No simétrico: 120			
(c)	Simétrico: 21	Well #1: 5 Pozo #2: 5 Pozo #3: 5	0.000-0.808 0.000-0.643 0.000-0.350	32
	No simétrico: 42	Pozo #4: 3 Pozo #5: 3	0.000-0.185	8

de individuos obtenidos mediante la propuesta aleatoria de las variables de diseño del modelo topológico que se pretende optimiza, representadas en este caso por valores discretos de profundidades de pozos. Una descripción detallada relativa a la definición de las variables de diseño y del cromosoma de cada modelo se puede consultar en la Tabla B.1. Las geometrías a estudiar se definen a partir de dichas variables, que conforman el cromosoma del individuo propuesto por el AG, y que caracterizan de este modo su diseño topológico. Ya en este punto se analiza la eficacia acústica de cada uno de estos individuos a partir de los resultados obtenidos tras la aplicación del código MEC Dual mencionado. Para ello es necesaria la discretización de la geometría con un número de elementos creciente con la frecuencia. En este trabajo se hace uso de elementos parabólicos (elementos de 3 nodos) cuya longitud máxima, para obtener una adecuada convergencia en los resultados, debe ser inferior a la mitad de la longitud de onda correspondiente a la frecuencia analizada. La población inicial se ordena entonces en términos de la eficacia de apantallamiento de los individuos, representada por el valor de la función objetivo (FO) caracterizada, a su vez, por el IL espectral (IL_{total}) (B.32). A cada individuo se le confiere entonces mayor probabilidad de ser seleccionado en base a su comportamiento acústico (FO). Así, haciendo uso del operador de *selección por torneo*, se escogen dos individuos (*progenitores*

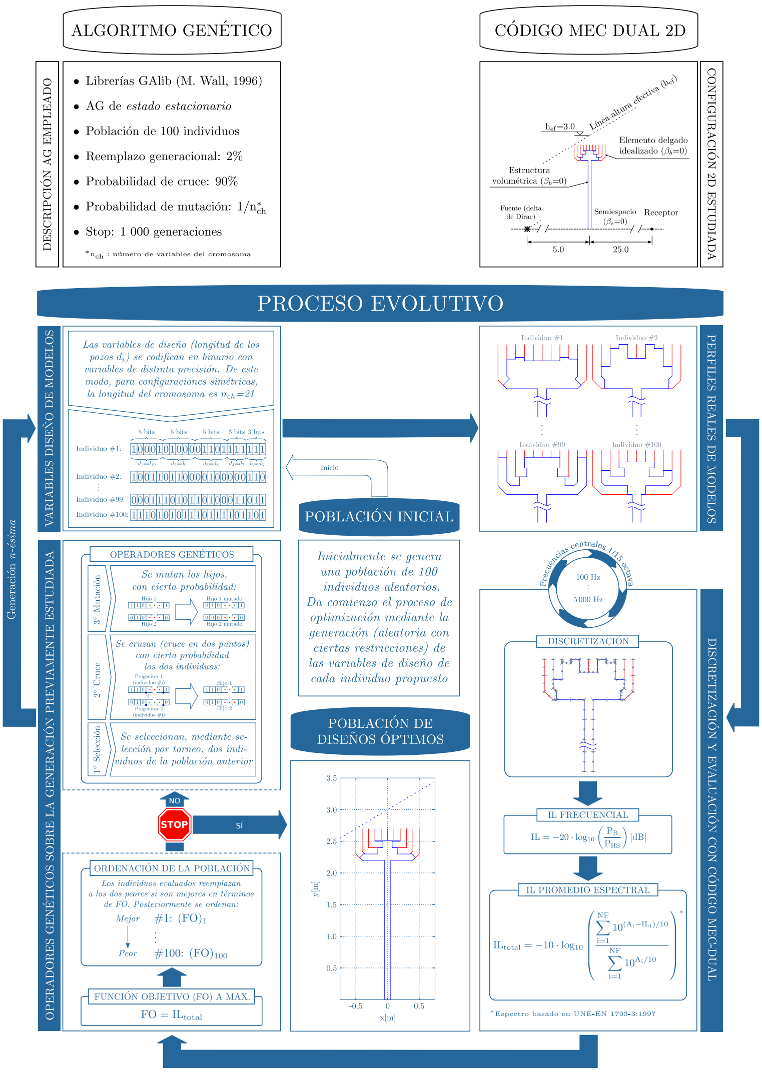

Figura B.12: Descripción general del AG empleado, configuración bidimensional estudiada diagrama de flujo de la optimización.

en terminología propia de algoritmos genéticos) que se cruzarán con un 90% de probabilidad mediante el operador de *cruce en dos puntos*, dando lugar a dos individuos distintos (*hijos*) cuyo genoma puede ser mutado, igualmente, atendiendo a criterios probabilistas. Estos dos nuevos individuos son evaluados y reemplazarán a los dos peores de la población precedente si mejoran su comportamiento acústico dando lugar, de este modo, a sucesivas poblaciones con individuos más eficientes en los términos que se estudian. Este proceso iterativo continúa hasta alcanzar las 1 000 generaciones, condición de parada impuesta ante la necesidad de encontrar una solución de compromiso entre los recursos computacionales disponibles y una aceptable convergencia acústica y geométrica de los individuos de la población final. Se llevan a cabo cinco ejecuciones independientes del proceso de optimización para cada diseño topológico propuesto.

B.3.3 Optimización numérica

A través de la maximización de la eficacia de apantallamiento en el receptor, el proceso se centra en la búsqueda de diseños cuyas profundidades de pozos se seleccionan dentro de un rango discreto de valores, tanto para configuraciones simétricas como no simétricas de los modelos que se describen a continuación.

Descripción de los modelos topológicos

La Figura B.13 muestra los diseños topológicos que se estudian. El modelo superior - modelo (a) - está inspirado en un difusor QRD previamente estudiado por Monazzam et al. [13]. Instalado sobre el borde superior de una pantalla con un eje vertical de 0.10 m de espesor, se trata de una configuración de 1.00 m de ancho y 0.30 m de alto compuesta de seis pozos de 0.12 m de ancho y diferentes profundidades (d_i) separadas por elementos muy delgados. El modelo central - modelo (b) - se inspira en la denominada *rueda de molino* estudiada por Okubo et al. [15]. Ésta se basa en una estructura radial de borde dispuesta sobre una pantalla de eje vertical de 0.03 m, compuesto de dos núcleos semi-circulares con un diámetro de 0.59 m sobre el que se disponen elementos muy delgados que separan pozos de distintas profundidades d_i. El modelo inferior - modelo (c) - se trata de un diseño novedoso. Está basado en una topología definida por un

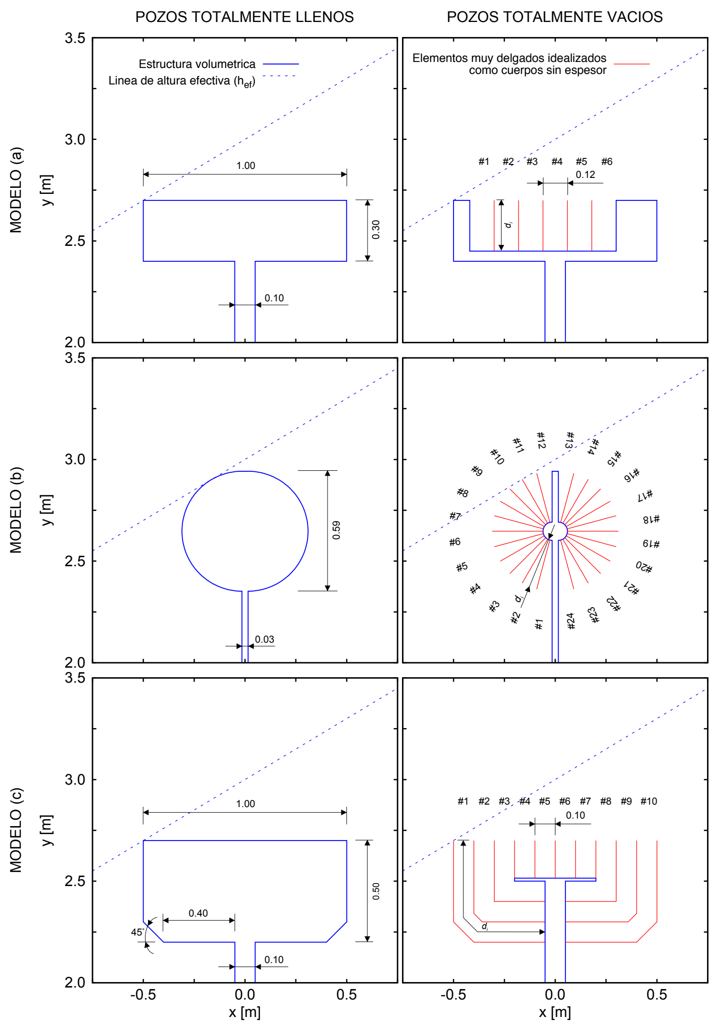

Figura B.13: Modelos a optimizar. Izquierda, modelos que presentan exclusivamente una estructura volumétrica por disponer todos sus pozos llenos. Derecha, modelos con una estructura general volumétrica con elementos de sección muy delgada con pozos completamente vacíos (para los modelos (a) y (b): d_i=0.250 m; para el modelo (c): d_1=d_{10}=0.808 m, d_2=d_9=0.643 m, d_3=d_8=0.350 m and d_4=d_5=d_6=d_7=0.185 m). Dimensiones expresadas en metros.

conjunto de pozos de distintas profundidades y trayectorias, separados por elementos muy delgados situados sobre el pie de una barrera de 0.10 m de espesor. Con el propósito de evitar la problemática relativa a los aspectos numéricos de los núcleos de integración de las matrices de la formulación así como de facilitar la definición geométrica de los modelos se considera, a efectos matemáticos, la idealización de los elementos muy delgados como elementos de sección nula (elementos unifilares). En la línea de otros trabajos ([71–73]), la altura efectiva de estos diseños medida en su eje central se fija en h_{ef}=3.0 m. Por esta razón, a pesar de que los modelos (a) y (b) están inspirados en diseños ya estudiados en la bibliografía, su altura efectiva se ha ajustado a este valor. Tal y como se observa en la Figura B.13, los modelos (a) y (b) están diseñados sobre la base de profundidades de pozo potencialmente idénticas, mientras que el modelo (c) presenta pozos con trayectos y profundidades potencialmente distintas. Una descripción detallada de las variables de diseño de cada modelo topológico se puede consultar en la Tabla B.1.

En general, los modelos presentados se pueden clasificar como pantallas de borde modificado, es decir, pantallas cuyo borde superior ha sido convenientemente diseñado con la intención de mejorar la calidad del apantallamiento de la pantalla simple de referencia. Basado en distintos mecanismos acústicos, tales como la interferencia y la resonancia, el adecuado diseño de estos dispositivos puede contribuir significativamente a la mejora de la atenuación del sonido en comparación con la pantalla recta de referencia, para un esquema específico fuente-receptor [14]. Por consiguiente, a pesar de la complejidad aparente de estos diseños, en la bibliografía se pueden encontrar modelos similares concebidos para un uso práctico [15, 21]. Otros dispositivos interesantes con el mismo enfoque práctico y distribuidos comercialmente en Japón se pueden consultar en [151].

Diseños obtenidos tras la optimización

La Figura B.15 recoge los resultados de los mejores perfiles tras la optimización. Concretamente, en la parte izquierda se muestran las mejores geometrías óptimas de la configuración simétrica y de la no simétrica para cada modelo. En la parte derecha se representa la evolución del IL frecuencial para el espectro considerado de las geometrías anteriormente mencionadas en comparación con las geometrías de los modelos en la situación con los pozos totalmente llenos y totalmente vacíos (ver Figura B.13) y con la pantalla simple de 3.0 m, para el mismo esquema fuente-receptor. El valor de la eficacia acústica global asociado a cada diseño óptimo, de acuerdo a (B.32), se muestra en la leyenda de estos gráficos. Asimismo, la Figura B.15 muestra la evolución de la calidad de apantallamiento de los modelos estudiados a lo largo de las generaciones. Las curvas rojas representan la eficacia del mejor individuo encontrado, en términos del valor de la función objetivo (FO), en las 5 ejecuciones llevadas a cabo para cada ejemplo. Las curvas azules muestran el valor promedio de FO considerando los 5 mejores individuos (tomando al mejor de cada ejecución) en cada generación. Tal y como se observa, la evolución se representa en un rango ajustado en el eje de ordenadas. Esto permite una observación más cómoda de los resultados sin perder información relevante. Las curvas de evolución sugieren ampliar el proceso de optimización para una convergencia más adecuada, especialmente en los casos no simétricos y, en particular, para el modelo (b). Los resultados de la configuración simétrica del modelo (c) y ambas configuraciones del modelo (a) presentan, sin embargo, curvas de convergencia aceptables.

La Tabla B.2 muestra los valores de las longitudes de pozos d_i de las mejores geometrías óptimas para cada configuración. A modo de ejemplo, el coste computacional asociado a los procesos de optimización del modelo (a) es de aproximadamente 97 horas de media, ejecutados en una CPU Intel© Xeon© con una velocidad de procesador de 2.60 GHz processor (la memoria RAM requerida no es significativa en estos estudios). La fila $\mathrm{IL}_{\mathrm{total}}^{3\,\mathrm{m\,vert.}}$ representa la ganancia de eficacia acústica de dichas geometrías con respecto a la de la pantalla recta de 3.0 m evaluada con el mismo esquema fuente-receptor.

Por último, con el propósito de facilitar la interpretación de las estrategias de apantallamiento más exitosas de las configuraciones no simétricas, la Figura 8 representa en diversos mapas de color los valores de los niveles de presión sonora espectral ($\mathrm{SPL}_{\mathrm{total}}$, por sus siglas en inglés) en un dominio en el que se encuentra una fuente de ruido que pulsa a cada frecuencia del espectro considerado con una intensidad de 90 dB(A) (medida a 1 m de distancia en campo libre). Los resultados se obtienen mediante simples operaciones a partir de los valores del IL espectral asociados a dichos óptimos.

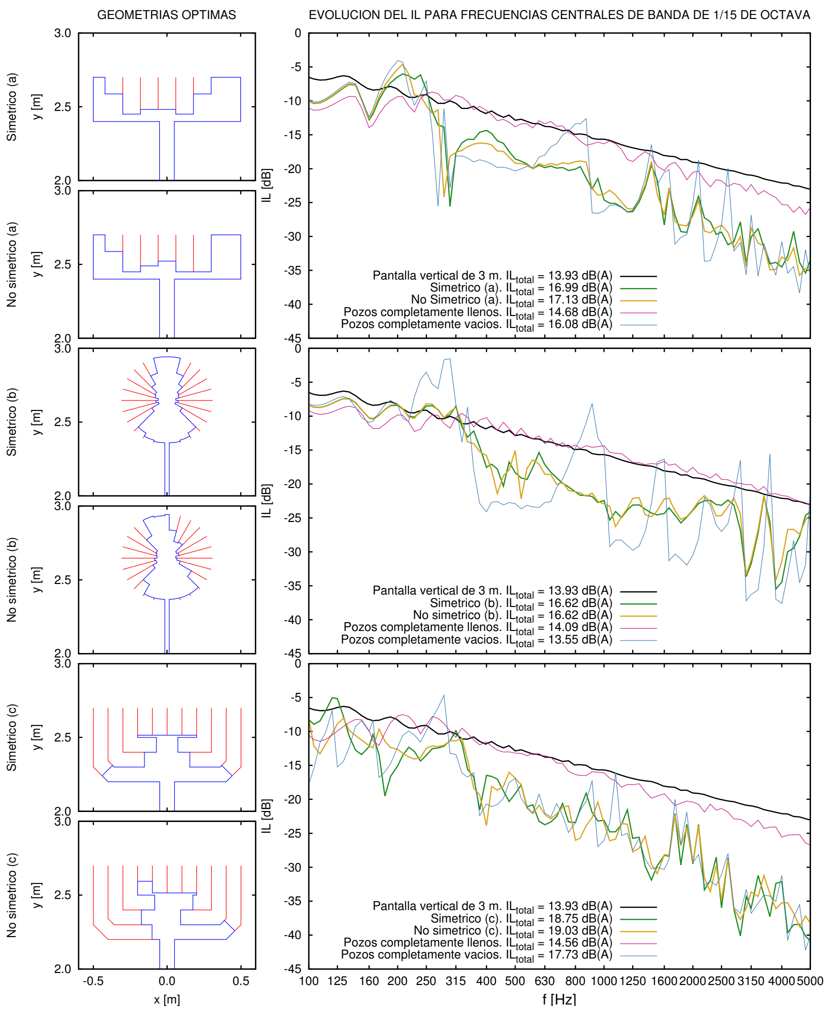

FIGURA B.14: Resultados de las mejores geometrías tras el proceso de optimización para cada modelo topológico y configuración. Izquierda, representación geométrica de los mejores diseños. Derecha, curvas de IL para frecuencias centrales de bandas de 1/15 de octava para las geometrías anteriores y las correspondientes con pozos completamente llenos y vacíos (ver Figura B.13).

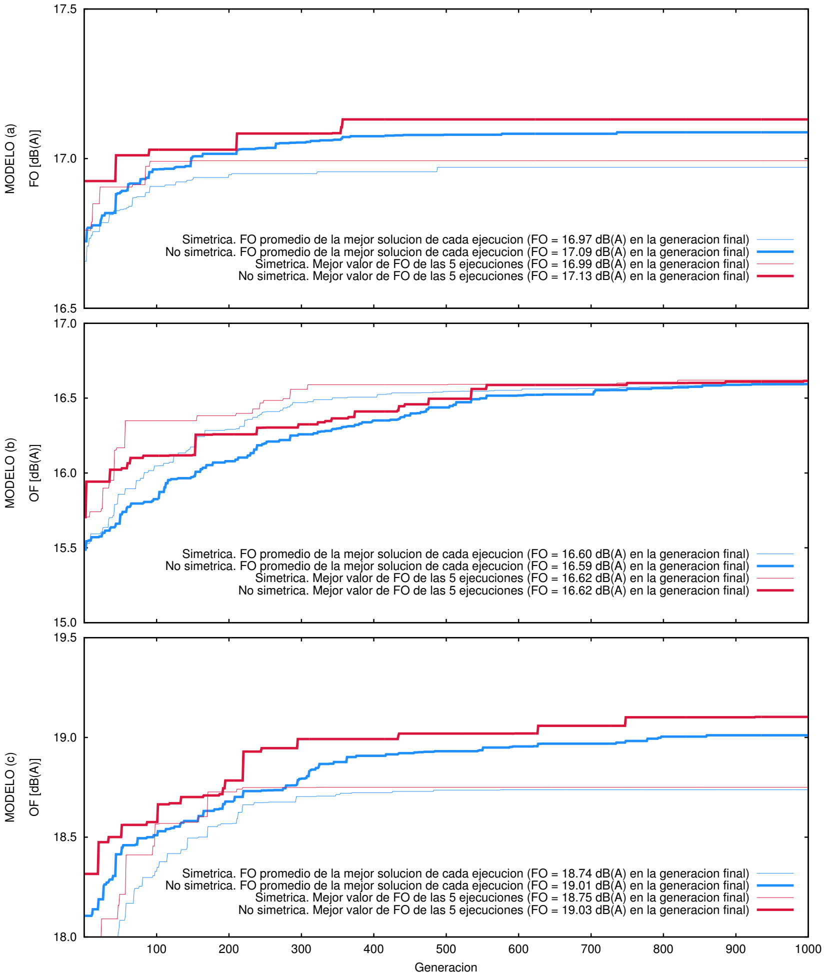

Figura B.15: Gráficos de convergencia de la función objetivo (FO) para las configuraciones simétricas y no simétricas de los modelos presentados.

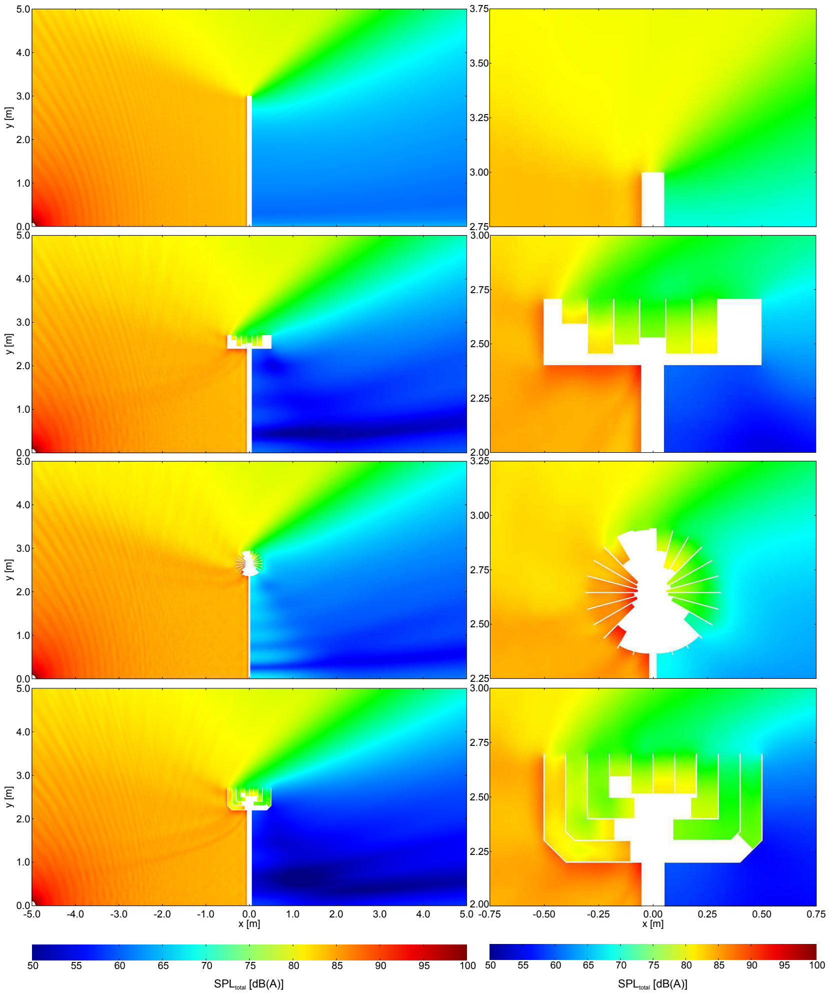

Figura B.16: Mapas de color de los niveles de presión acústica espectral (SPL_{total}) para una fuente de ruido con una intensidad 90 dB(A), medida a 1 m, pulsando de acuerdo al espectro de frecuencias propuesto [117]. De arriba a abajo, resultados para la pantalla vertical de 3 m y las mejores geometrías óptimas no simétricas de los modelos (a), (b) y (c). La fuente de ruido se sitúa en (-5.0, 0.0).

Tabla B.2: Variables de diseño d_i (en centímetros) de las mejores geometrías óptimas (ver Figura B.14) y ganancia de eficacia acústica con respecto a la pantalla simple de 3 m, en dB(A), para cada modelo y configuración.

	Simétrico			No simétrico		
	Mod. (a)	Mod. (b)	Mod. (c)	Mod. (a)	Mod. (b)	Mod. (c)
d_1	11.29	0.00	44.34	11.29	1.61	75.64
d_2	25.00	1.61	53.92	25.00	1.61	51.85
d_3	21.77	5.65	32.74	20.97	8.87	31.61
d_4	21.77	17.74	18.50	17.74	20.16	10.57
d_5	25.00	25.00	18.50	25.00	23.39	18.50
d_6	11.29	23.39	18.50	25.00	22.58	18.50
d_7	-	24.19	32.74	-	24.19	18.50
d_8	-	22.58	53.92	-	23.39	22.58
d_9	-	18.55	44.34	-	22.58	60.14
d_{10}	-	15.32	-	-	12.10	41.73
d_{11}	-	12.10	-	-	0.00	-
d_{12}	-	0.00	-	-	0.81	-
d_{13}	-	0.00	-	-	10.48	-
d_{14}	-	12.10	-	-	17.74	-
d_{15}	-	15.32	-	-	16.94	-
d_{16}	-	18.55	-	-	23.39	-
d_{17}	-	22.58	-	-	22.58	-
d_{18}	-	24.19	-	-	25.00	-
d_{19}	-	23.39	-	-	24.19	-
d_{20}	-	25.00	-	-	21.77	-
d_{21}	-	17.74	-	-	12.10	-
d_{22}	-	5.65	-	-	1.61	-
d_{23}	-	1.61	-	-	1.61	-
d_{24}	-	0.00	-	-	1.61	-
$\mathrm{IL}_{\mathrm{total}}^{3\,\mathrm{m\,vert.}}$	+3.06	+2.67	+4.82	+3.20	+2.68	+5.10

Diseños de uso práctico

Con la intención de determinar la importancia que el patrón de llenado de los pozos tiene en la calidad de apantallamiento y, al mismo tiempo, conseguir diseños de pantallas más prácticos en términos de su construcción y posterior mantenimiento, la FiguraB.17 muestra las modificaciones geométricas realizadas sobre los mejores diseños óptimos del modelo (b), tanto en su configuración simétrica como en la no simétrica. A partir de los diseños derivados de la optimización, se realizan ligeras variaciones incrementales en términos de patrones de llenado/vaciado de algunos pozos (representados en la figura por Mod. #1 a Mod. #7). En definitiva, se agrupan los pozos que presentan aproximadamente la misma profundidad de la siguiente forma: los que se encuentran en la parte inferior del dispositivos (pozos del #1 al #3, y simétricos), en la zona media (pozos del #4 al #9, y simétricos) y los de la parte superior (pozos del #10 al #12, y simétricos). Adicionalmente se incluye un diseño previamente estudiado en la bibliografía por Okubo et al. [15] a modo de caso de referencia. Los resultados se presentan en términos de los niveles de presión acústica espectral (SPL_{total}), considerando una fuente de ruido que presenta una intensidad de 90 dB(A) medida a 1 m de distancia, de acuerdo al espectro aplicado [117], para el esquema fuente-receptor empleado hasta ahora.

Por otro lado, en la Figura B.18 se muestran las ventajas de la metodología presentada en la búsqueda de óptimos. Como se puede observar, el comportamiento acústico de los mejores diseños óptimos del modelo (a), tanto de la configuración simétrica como de la no simétrica, se comparan con un modelo QRD de topología idéntica a la de dichos diseños, estudiado con anterioridad por Monazzam et al. [13]. Los resultados mostrados sugieren la conveniencia de aplicar procedimientos similares al que se ha presentado en este estudio en la mejora de la calidad de apantallamiento de diseños clásicos de pantallas y de aquellos ya existentes.

Discusión de los resultados

A la luz de los resultados obtenidos se realiza el siguiente análisis en relación a los modelos estudiados en este trabajo:

- La eficacia de apantallamiento de las geometrías optimizadas supera con claridad el comportamiento acústico presentado por la pantalla recta de referencia de 3.0 m, para el mismo esquema fuente-receptor.

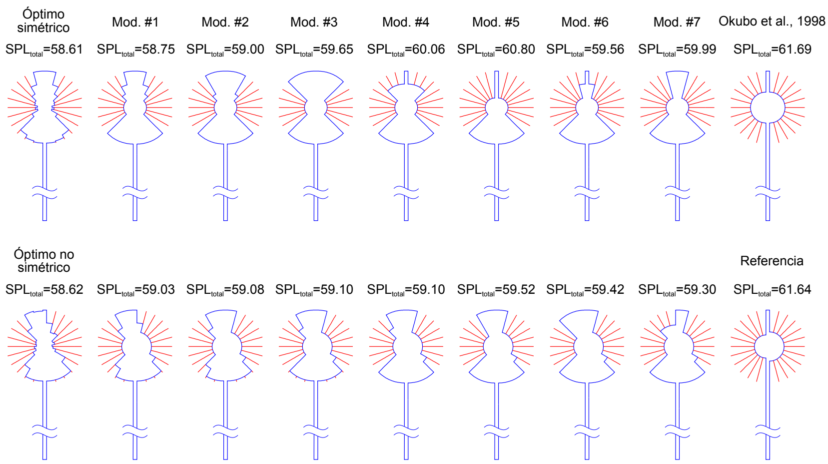

FIGURA B.17: Variaciones geométricas incrementales sobre la base del modelo (b): arriba, modificaciones sobre el mejor óptimo simétrico; abajo, modificaciones sobre el mejor óptimo no simétrico. Resultados expresados en términos de los niveles de presión sonora espectral (SPL_{total}) en el receptor considerado, para una fuente de ruido pulsando con una intensidad de 90 dB(A) (medido a 1 m en campo libre) en cada frecuencia del espectro [117].

La localización lejana del receptor y el buen comportamiento incluso a bajas frecuencias hace que este hecho adquiera aun mas relevancia.

- El uso de diseños topológicos que presentan longitudes de pozo potencialmente mayores permite diseños con mejor comportamiento acústico. Esto hecho queda bien reflejado en la Figura B.14 por el modelo (c), donde se observa que la atenuación del sonido es claramente mejor con este tipo de pantallas en relación a la de la pantalla recta de referencia, incluso a bajas frecuencias.

- Como cabía esperar, las geometrías óptimas de las configuraciones no simétricas superan, en general, a las de las simétricas tanto en los mejores valores de FO como en la media de sus valores. Incluso en el caso del modelo (b), la geometría óptima no simétrica podría

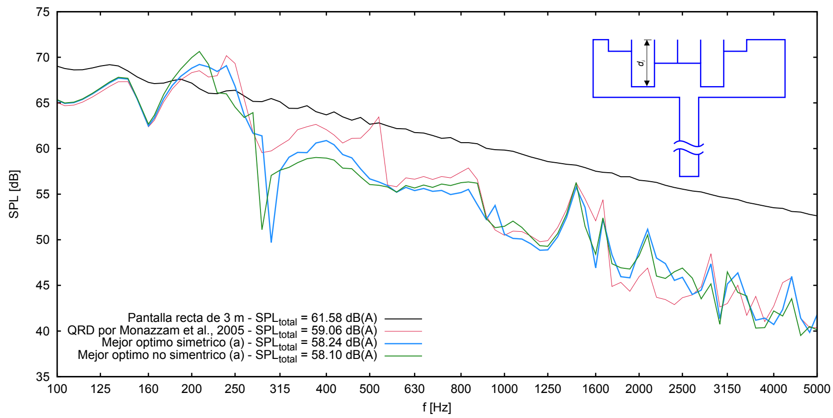

Figura B.18: Evolución de los niveles de presión sonora (SPL). Gráficos para para un QRD estudiado por Monazzam et al. [13] (d_1=d_6=0.0600 m, d_2=d_5=0.24450 m, d_3=d_4=0.12225 m), las mejores geometrías simétricas y no simétricas del modelo (a) (d_i en la Table B.2) y la pantalla simple de 3 m.

mejorar a la simétrica en el caso de haber permitido evolucionar el proceso de evolutivo un mayor número de generaciones (tal y como se desprende de los gráficos de convergencia de la Figura B.15).

- A pesar de la fuerte variabilidad en el comportamiento acústico que los dispositivos como los presentados en este trabajo muestran con la frecuencia, los diseños óptimos presentan curvas de IL más suaves que los correspondiente diseños con pozos completamente vacíos, aunque con una mejor calidad de apantallamiento (ver Figura B.14).

- Tal y como muestra la Figura B.15 es aconsejable una mejor convergencia de los resultados, particularmente para el modelo (b) y (c). El estudio en frecuencias a lo largo de todo un espectro refinado como el empleado en este trabajo tiene un coste computacional elevado en la evaluación de la función objetivo de cada geometría candidata, especialmente a altas frecuencias (el mallado del contorno se refina a medida que aumenta la frecuencia analizada). Con todo, el criterio de parada adoptado en este trabajo permite alcanzar una convergencia razonable de acuerdo a los recursos computacionales disponibles.

- La consideración de metodologías como las presentadas permiten encontrar de manera sencilla y sistemática estrategias de apantallamiento interesantes posibilitando, al mismo tiempo, la mejora de diseños clásicos y de aquellos ya existentes (ver Figuras B.17 and B.18).

B.4 RESUMEN, CONCLUSIONES Y DESARROLLOS FUTUROS

B.4.1 Resumen y conclusiones

El trabajo presentado aborda la mejora sistemática de la eficacia acústica de pantallas anti-ruido mediante un procedimiento numérico estable, robusto y flexible que permite abordar la optimización de un amplia gama de pantallas acústicas en problemas 2D. Sobre la base de la mejora de la atenuación del sonido (representada por el coeficiente de pérdida por inserción), el procedimiento hace uso de Algoritmos Genético (AGs) en la búsqueda guiada, en un espacio de soluciones factibles de acuerdo a las restricciones del problema, de pantallas acústicas que combinado con Elementos de Contorno (EC) conduce a diseños cada vez más eficientes.

Este estudio se enmarca dentro de una línea de investigación en curso dentro del Instituto de Sistemas Inteligentes y Aplicaciones Numéricas en Ingeniería (instituto SIANI) sobre el diseño óptimo de pantallas acústicas bidimensionales mediante el uso acoplado del Método de los Elementos de Contorno (MEC) y Algoritmos Evolutivos (AEs). En este sentido, el trabajo desarrollado supone un avance importante en el modelado numérico, desarrollado y mejorado en los años previos a este documento, para la simulación realista de este tipo de problemas de propagación de ondas acústicas en el medio exterior inducidas por cualquier tipo de fuente de ruido.

A modo de antecedentes, el modelo numérico 2D inicial surgió a partir de los trabajos de investigación llevados a cabo por el Prof. Orlando Maeso y el Prof. Juan J. Aznárez (ambos directores de esta tesis), quiénes habían trabajado en los años previos en el desarrollo y aplicación de métodos numéricos para la resolución de problemas de propagación de ondas en medios elásticos. La primera implementación del modelo en la predicción de la propagación acústica en el medio exterior se basaba en la ecuación integral del contorno singular (SBIE) y permitía el estudio de la eficacia acústica en situaciones diversas y sobre distintos diseños de pantallas anti-ruido [18, 98]. Con posterioridad, el ámbito de desarrollo de la investigación se amplió a la mejora sistemática del comportamiento acústico de configuraciones de pantallas clásicas a partir de los conocimientos y la experiencia del Prof. David Greiner, también director de este trabajo, en el campo de los Algoritmos Evolutivos. De los resultados de esta colaboración se desarrolló e implementó un procedimiento más general que hacía uso del MEC y AEs en la optimización de forma de pantallas que habitualmente se erigen en el entorno de carreteras. La primera implementacion conjunta de ambas técnicas numéricas en el Grupo de Investigación donde se desarrolla esta tesis se encuentra en [71]. Otros trabajos de interés al respecto se pueden consultar en [72, 73, 108].

Pese a que los procedimientos desarrollados hasta ese momento habían permitido abordar con éxito la reducción sistemática de la atenuación del sonido, la consideración de ciertas geometrías de pantallas suponían un reto importante, cuando no inabordable en muchos casos, en términos de 1) la determinación de la validez topológica de los diseños, a menudo complejos, propuestos por el optimizador y 2) la evaluación y representación fiel de la calidad del apantallamiento del diseño que se estudia. Con el propósito de suplir estas carencias, se propone en este trabajo una metodología más general, robusta y versátil que permite el estudio de cualquier problema de optimización acústica en 2D.

Si bien el MEC es la técnica numérica más apropiada en el estudio de la predicción de la propagación acústica exterior, la implementación de su formulación estándar puede conducir a dificultades insalvables en la evaluación de determinadas tipologías de pantallas. De este modo, el tratamiento de estos problemas con EC a menudo deriva, según el caso, en problemas numéricos cuando no en un sistema de ecuaciones singular. Por tanto, el análisis de cierta tipologías particulares de pantallas requiere de una formulación específica de EC que permita resolver estas dificultades. Este nuevo planteamiento combina la formulación clásica del Método (SBIE) con una variante hipersingular (HBIE), obtenida por derivación de la anterior, para dar lugar a la denominada formulación Dual del MEC que nos permite sortear los inconvenientes derivados de la implementación exclusiva de su formulación estándar. En este sentido, este enfoque Dual es la estrategia más apropiada, desde los EC, para abordar los problemas numéricos que se proponen en este trabajo, permitiendo: 1) adoptar idealizaciones geométricas de elementos muy delgados como cuerpos unifilares, facilitando enormemente la representación geométrica y el tratamiento numérico de configuraciones complejas sin que ello introduzca errores apreciables para los espesores de pantalla tratados [47] (muy presentes en los diseños estudiados) y 2) evitar las frecuencias espurias asociadas al dominio interior de las estructuras volumétricas de la barrera que pueden falsear la evaluación de su eficacia acústica real. La consecución de estos objetivos, sobre todo la idealización geométrica de elementos muy delgados, posibilita que el procedimiento sea más general y sencillo en la búsqueda sistemática de diseños que, a menudo, gozan de completa libertad geométrica de acuerdo a su patrón topológico. Asimismo, este planteamiento permite abordar la optimización de forma de pantallas anti-ruido 2D desde un enfoque, hasta donde conoce el investigador de este trabajo, no tratado hasta la fecha en la bibliografía.

La estrategia de aplicación de ambas formulaciones varía según la naturaleza del elemento que se evalúa. De este modo, la SBIE y la HBIE se aplican conjuntamente y combinadas por medio de un valor complejo dependiente de la frecuencia [109] para evitar las frecuencias ficticias asociadas al dominio interior de las estructuras volumétricas. En general, esta problemática afecta al tratamiento de cualquier tipo de elemento, con independencia de las dimensiones de su sección. Sin embargo, el asunto se agrava con el tratamiento de elementos muy delgados. Problemas de integración numérica se añaden en este caso al problema anterior, afectando igualmente a la correcta evaluación de la pantalla. La aplicación conveniente del enfoque Dual del MEC ofrece una solución adecuada a este problemática, por medio de la idealización de elementos de sección muy delgada como cuerpos unifilares. Así, la SBIE y la HBIE se aplican simultánemante y por separado sobre cada nodo de la discretización de un contorno que representa la fusión de los dos contornos opuestos de la sección real. Esta simplificación de la realidad se traduce no sólo en menores tiempos de computación sino que además supone una ventaja significativa respecto de la representación fiel y detallada de diseños complejos de pantallas acústicas de dimensiones reales.

Resultados derivados de diferentes estudios basados en la metodología anteriormente descrita se presentan en los últimos capítulos de este documento. Las simulaciones numéricas llevadas a cabo contemplan el análisis de distintas situaciones en las que el fenómeno de propagación se aborda como un problema bidimensional, esto es, el ruido es causado por una fuente mono-frecuencia e infinita (matemáticamente representada por la función delta de Dirac) que discurre paralelamente a una pantalla de geometría invariable y longitud igualmente infinita que yace sobre un semiespacio de admitancia uniforme. Las simulaciones se han realizado en el dominio de la frecuencia bajo las hipótesis habituales (de acuerdo a la ecuación de Helmholtz): el medio (el aire) se considera no viscoso, homogéneo, elástico e isotrópico, en un estado de pequeñas perturbaciones e inicialmente en reposo, despreciándose todos los posibles efectos del viento.

Se han presentado en este documento los resultados de la optimización mono- y multi-objetivo de distintos diseños topológicos de pantalla antiruido. Las conclusiones y análisis más destacables derivados de estos estudios se resumen a continuación.

Sobre la optimización de forma de pantallas muy delgadas

Se presentaron resultados derivados de la optimización mono-objetivo de pantallas muy delgadas, idealizadas como configuraciones unifilares, sobre la base de la formulación Dual del MEC correspondiente para predecir el comportamiento acústico en distintas situaciones.

Uno de los estudios se centró en la optimización de forma de la configuración total o de borde de pantallas con diseños topológicos basados en contornos rectos o curvos con distintos tratamientos superficiales. Pese a que las simulaciones se realizaron para un determinado esquema fuente-receptor, la influencia de la distribución de los receptores en la eficacia de la pantalla también fue objeto de análisis en este estudio. Los resultados obtenidos estuvieron en la línea de los trabajos de otros autores [13–15, 66, 70] en el sentido de que se observaron mayores niveles de atenuación del ruido al introducir variaciones en la zona de coronación de la pantalla (borde superior) que sobre la geometría general de la pantalla. El enfoque eminentemente teórico de muchos de los diseños topológicos optimizados se aproximó geométricamente a perfiles de pantallas acústicas más prácticos, tanto desde el punto de vista de su construcción como de su posterior mantenimiento, sin observar una disminución significativa en la eficacia de apantallamiento. En relación a los tratamientos superficiales se determinó que la consideración de materiales absorbentes sobre determinados contornos de la zona de coronación no siempre conduce a mejoras en el comportamiento acústico, pues la configuración de borde juega un papel importante al reflejar ondas que pueden contrarrestar los efectos de las ondas incidentes. En este sentido, se observó que la consideración de superficies absorbentes como variable de diseño dentro del proceso de optimización es imprescindible en la búsqueda de geometrías que presenten la mejor calidad de apantallamiento posible. Finalmente, los modelos estudiados presentaron, en general, una eficacia decreciente con la distancia.

Este último aspecto se trató con mayor profundidad en el segundo estudio. En el análisis de la influencia de la eficacia acústica con la distancia se consideraron dos configuraciones de receptores situados en tres regiones claramente distinguibles en términos de proximidad a la pantalla. Bajo estas consideraciones, se realizó un estudio comparativo entre una pantalla poligonal de seis tramos rectos y una pantalla basada en una curva Bézier de sexto grado. En regiones cercanas y para receptores situados en el suelo la pantalla poligonal mostró un mejor comportamiento, mientras que la pantalla basada en la curva Bézier lo hizo en regiones distantes. Sin embargo, ambos modelos mostraron eficacias similares para la malla de receptores.

Sobre la optimización de forma de pantallas con dispositivos difusores

Asimismo, se presentaron resultados de la optimización mono-objetivo de pantallas acústicas con dispositivos de bordes que combinan una estructura volumétrica general con elementos muy delgados. El enfoque Dual del MEC aplicado en estos estudios permitió evaluar correctamente esta tipología de pantallas, en el marco de un procedimiento robusto y versátil que posibilita el estudio de cualquier tipo de optimización acústica 2D al evitar las frecuencias espurias asociadas a las estructuras volumétricas y permitir, simultáneamente, la idealización de elementos de sección muy delgada como cuerpos sin espesor.

Se realizaron simulaciones numéricas sobre tres modelos topológicos con configuraciones de borde basadas en estructuras de pozos, algunos de ellos inspirados en configuraciones previamente estudiados en la bibliografía. Como era de esperar, la eficacia de apantallamiento de los modelos optimizados excedió claramente la de la pantalla simple de 3 m, incluso en mediciones alejadas de la barrera. En cuanto al comportamiento de los modelos se demostró que, tal y como ya habían apuntado otros autores (e.g., [15]), su eficacia depende en gran medida de la frecuencia analizada. Sin embargo, las geometrías óptimas presentaron curvas de IL más suaves que las de los correspondientes diseños con pozos completamente vacíos. Además, se determinó que las topologías que presentan longitudes de pozo potencialmente mayores dan lugar a geometrías con mejor comportamiento acústico debido a que se amplía el número de frecuencias, en el espectro considerado, en las que se producen la interferencia acústica entre la onda incidente y la reflejada (valores altos de IL). Con un enfoque práctico se propusieron diseños geométricamente más sencillos a partir de los modelos optimizados, sin observar una reducción significativa en la eficacia de apantallamiento. Finalmente se realizó un análisis comparativo entre el comportamiento acústico de un QRD previamente estudiado en la literatura y del modelo topológicamente idéntico optimizado, justificándose la necesidad de considerar procedimientos como el presentado en este estudio en la mejora de diseños ya existentes.

Sobre la optimización multi-objetivo de pantallas muy delgadas

Por último se mostraron los resultados derivados de la optimización multi-objetivo de pantallas muy delgadas con superficies perfectamente reflejantes. Basadas en los diseños presentados con anterioridad en el primer estudio del Capítulo 5, las simulaciones numéricas se llevaron cabo para la optimizacion simultánea de dos objetivos en conflicto: la maximización de la eficacia y la minimización de la longitud total del contorno de la pantalla, representativo del coste de manufacturación. Se obtuvieron conjuntos de soluciones óptimas para cada modelo topológico tras procesos de optimización en los que se partió por un lado de una población inicial aleatoria (*Caso R*) y en los que por otro se incluyó la mejor solución mono-objetivo del Capítulo 5 en la población inicial (*Caso B*). La comparación de los frentes óptimos de Pareto de ambos casos, por medio de la medida del hipervolumen, mostró la superioridad del *Caso B* sobre el *Caso R* en todos los modelos estudiados, lo que pone de manifiesto que incluir la mejor solución mono-objetivo en el proceso de optimización supone una ventaja significativa en la mejora de las soluciones encontradas. Además, se obtuvieron frentes de Pareto amplios y con soluciones uniformemente distribuidas. Este aspecto quedó reflejado en la diversidad geométrica de los diseños topológicos optimizados.

B.4.2 Desarrollos futuros

El procedimiento presentado ha permitido abordar con éxito problemas de optimización de forma de pantallas acústicas considerados inabordables hasta el desarrollo de este trabajo dentro del Grupo de Investigación donde se enmarca esta tesis. A pesar de la contribución de esta tesis, existen aspectos susceptibles de ser mejorados y ampliados que responden a los puntos que se detallan a continuación:

i **Sobre la eficiencia del optimizador.** Los Algoritmos Genéticos pertenecen al paradigma de los Algoritmos Evolutivos y la Metaheurística. De entre sus ventajas destacan su capacidad como optimizadores globales debido a que realizan una búsqueda estocástica basada en una población de posibles soluciones. Sin embargo, uno de sus principales inconvenientes se encuentra en el elevado número de evaluaciones de la función de ajuste que requiere para conseguir una correcta convergencia. Esta problemática está especialmente presente en la resolución de problemas de ingeniería, donde cada evaluación exige, a menudo, un gran coste computacional. Tal es el caso de la resolución de problemas de EC. En este sentido, la eficiencia del planteamiento numérico se convierte en un aspecto clave a la hora de obtener soluciones cualitativamente aceptables con los recursos computacionales comprometidos. Los avances más recientes en la eficiencia de las aplicaciones en el campo de los algoritmos evolutivos orientadas a la simulación computacional de problemas de ingeniería (dinámica de fluidos, ingeniería estructural, etc.) se basan, principalmente, en el uso de la computación paralela, la teoría de juegos y los modelos subrogados. Todas esta estrategias, usadas por separado o de manera simultánea (e.g., [153–155]), son herramientas convenientes de aplicación para la mejora de procedimientos como el presentado en esta tesis.

ii **Sobre la eficiencia del evaluador.** Asimismo se podría agilizar considerablemente la evaluación de cada pantalla acústica dentro de la metodología presentada, sin más que considerar la paralelización de la tarea que más recursos computacionales requiere en términos de tiempo de procesador: el ensamblaje de las matrices de los núcleos de integración del MEC, tanto de la SBIE como de la HBIE. En tanto que el ensamblaje de las filas de las mencionadas matrices no guarda dependencia entre sí, la implementación de esta estrategia se puede realizar de manera sencilla y directa.

iii **Sobre el ámbito de aplicación del evaluador.** Por último y con un propósito más ambicioso, otra línea de investigación interesante tiene que ver con la implementación de la formulación Dual del MEC aquí presentada combinada con el uso de Algoritmos Rápidos Multipolo (FMM por sus siglas en inglés) para dar solución al principal inconveniente que la aplicación del MEC tiene en cualquier problema físico: su elevado coste computacional tanto en tiempos de ejecución como en recursos de memoria, especialmente en problemas de grandes dimensiones (problemas tridimensionales). Este inconveniente se acentúa, además, en problemas dinámicos armónicos (dominio de la frecuencia), ya que la aplicación del Método conduce a sistemas de ecuaciones cuyo tamaño crece de forma exponencial con la frecuencia de excitación. La clave del modelo acoplado de ambas técnicas (ver, e.g., [156–159]) es la reducción del costo computacional del cálculo de los coeficientes de la matriz llena de EC de $\mathcal{O}\left(n^2\right)$ y su resolución de $\mathcal{O}\left(n^3\right)$ (en caso de algoritmos de resolución directa) a cuasi-lineal. De esta manera, la predicción de la eficacia de apantallamiento de pantallas 3D con millones de incógnitas se puede abordar en unas horas con cualquier ordenador personal. De entre los métodos multipolo, el método del residuo mínimo generalizado [160–163] (GMRES por sus siglas en inglés) se postula como una de las estrategias de aplicación en este contexto al no requerir que la matriz de coeficientes esté presente en memoria. Así, el producto matriz por vector se realiza haciendo uso de expansiones multipolo de la solución fundamental que se construyen sobre una estructura de celdas (hojas) que agrupan a los elementos en que se discretiza el contorno. Con ello, se convierte la interacción nodo-nodo del BEM convencional (colocación-integración) en interacción celda-celda.

Bibliography

[1] Bond, M. (1996) Plagued by noise. *New Scientist*, pp. 14-15.

[2] Kiernan, V. (1997) Noise pollution robs kids of language skills. *New Scientist*, p. 5.

[3] Seznec, R. (1980) Diffraction of sound barrires: use of the boundary element technique. *Journal of Sound and Vibration*, **73**, 195-209.

[4] Hothersall, D. C., Horoshenkov, K. V., and Mercy, S. E. (1996) Numerical modelling of the sound field near a tall building with balconies near a road. *Journal of Sound and Vibration*, **186(4)**, 507-515.

[5] Watts, G. R., Hothersall, D. C., and Horoshenkov, K. V. (2001) Measured and predicted acoustic performance of vertically louvred noise barriers. *Applied Acoustics*, **62**, 1287-1311.

[6] Martin, S. J. and Hothersall, H. C. (2002) Numerical modelling of median road traffic noise barriers. *Journal of Sound and Vibration*, **251(4)**, 671-681.

[7] Hothersall, D. C., Chandler-Wilde, S. N., and Hajmirzae, M. N. (1991) Efficiency of single noise barriers. *Journal of Sound and Vibration*, **146**, 303-322.

[8] Hothersall, D. C., Crombie, D. H., and Chandler-Wilde, S. N. (1991) The performance of T-profile and associated noise barriers. *Applied Acoustics*, **32(4)**, 269-287.

[9] Ishizuka, T. and Fujiwara, K. (2012) Traffic noise reduction at balconies on a high-rise building façade. *Journal of the Acoustical Society of America*, **131**, 2110-2117.

[10] Watts, G. R. and Morgan, P. A. (1996) Acoustic performance of an interference type noise-barrier profile. *Applied Acoustics*, **49 (1)**, 1-16.

[11] Crombie, D. H., Hothersall, D. C., and Chandler-Wilde, S. N. (1995) Multiple-edge noise barriers. *Applied Acoustics*, **44**, 353-367.

[12] Fujiwara, K., Hothersall, D. C., and Kim, C. (1998) Noise barriers with reactive surfaces. *Applied Acoustics*, **53**, 255-272.

[13] Monazzam, M. R. and Lam, Y. W. (2005) Performance of profiled single noise barriers covered with quadratic residue diffusers. *Applied Acoustics*, **66**, 709-730.

[14] Ishizuka, T. and Fujiwara, K. (2004) Performance of noise barriers with various edge shapes and acoustical conditions. *Applied Acoustics*, **65**, 125-141.

[15] Okubo, T. and Fujiwara, K. (1998) Efficiency of a noise barrier on the ground with an acoustical soft cylindrical edge. *Journal of Sound and Vibration*, **216**, 771-790.

[16] Jean, P., Defrance, J., and Gabillet, Y. (1999) The importance of source type on the assessment of noise barriers. *Journal of Sound and Vibration*, **226**, 201-216.

[17] Jean, P. and Gabillet, Y. (2000) Using boundary element approach to study small screens close to rails. *Journal of Sound and Vibration*, **231**, 673-679.

[18] Maeso, O. and Aznárez, J. J. (2005) *Estrategias para la reducción del impacto acústico en el entorno de carreteras. Una aplicación del Método de los Elementos de Contorno*. Universidad de Las Palmas de Gran Canaria, ISBN: 846890340X.

[19] Crombie, D. H. and Hothersall, D. C. (1994) The performance of multiple noise barriers. *Journal of Sound and Vibration*, **176**, 459-73.

[20] Watts, G. R., Chandler-Wilde, S. N., and Morgan, P. A. (1999) The combined effects of porous asphalt surfacing and barriers on traffic noise. *Applied Acoustics*, **58**, 351-377.

[21] Okubo, T. and Fujiwara, K. (1999) Efficiency of a noise barrier with an acoustically soft cylindrical edge for practical use. *Journal of the Acoustical Society of America*, **105**, 3326-3335.

[22] Defrance, J. and Gabillet, Y. (1999) A new analytical method for the calculation of outdoor noise propagation. *Applied Acoustics*, **57**, 109-127.

[23] Godinho, L., António, J., and Tadeu, A. (2001) 3D sound scattering by rigid barriers in the vicinity of tall buildings. *Applied Acoustics*, **62**, 1229-1248.

[24] Branco, F. J. F. G., Godinho, L., and Tadeu, A. (2003) Acoustic insertion loss provided by rigid acoustic barriers of different shapes. *Journal of Computational Acoustics*, **11**, 503-519.

[25] Thorsson, P. J. (2003) Combined effects of admittance optimisation on both barrier and ground. *Applied Acoustics*, **64**, 693-711.

[26] Defrance, J. and Jean, P. (2003) Integration of the efficiency of noise barrier caps in a 3D ray tracing method. Case of a T-shaped diffracting device. *Applied Acoustics*, **64**, 765-780.

[27] Peplow, A. T. (2006) On the efficiency of screens near roadside cuttings. *Journal of Sound and Vibration*, **298**, 982-1000.

[28] Okubo, T. and Yamamoto, K. (2006) Procedures for determining the acoustic efficiency of edge-modified noise barriers. *Applied Acoustics*, **68**, 797-819.

[29] Monazzam, M. R. and Lam, Y. W. (2008) Performance of T-shape barriers with top surface covered with absorptive quadratic residue diffusers. *Applied Acoustics*, **69**, 93-109.

[30] Monazzam, M. R. and Nassiri, P. (2009) Contribution of quadratic residue diffusers to efficiency of tilted profile parallel highway noise barriers. *Iranian Journal of Environmental Health Science & Engineering*, **6**, 271-284.

[31] Jean, P. (2009) Sound transmission through opened windows. *Applied Acoustics*, **70**, 41-49.

[32] Monazzam, M. R., Naderzadeh, M., Nassiri, P., and Fard, S. M. B. (2010) Performance of environmental T-shape noise barriers covered with primitive root diffusers. *Archives of Acoustics*, **35**, 565-578.

[33] Naderzadeh, M., Monazzam, M. R., Nassiri, P., and Fard, S. M. B. (2011) Application of perforated sheets to improve the efficiency of reactive profiled noise barriers. *Applied Acoustics*, **72**, 393-398.

[34] Oldham, D. J. and Egan, C. A. (2011) A parametric investigation of the performance of T-profiled highway noise barriers and the identification of a potential predicitive approach. *Applied Acoustics*, **72**, 803-813.

[35] Jolibois, A., Duhamel, D., Sparrow, V. W., Defrance, J., and Jean, P. (2012) Scattering by a cylinder covered with an arbitrary distribution of impedance and application to the optimization of a tramway noise abatement system. *Journal of Sound and Vibration*, **331**, 5597-5622.

[36] Koussa, F., Defrance, J., Jean, P., and Blanc-Benon, P. (2013) Acoustic peformance of gabions noise barriers: Numerical and experimental apporaches. *Applied Acoustics*, **74**, 189-197.

[37] António, J., Tadeu, A., and Castro, I. (2013) Performance of double three-dimensional rigid barriers used to create an acoustic space-A normal derivative integral equation approach. *Journal of Sound and Vibration*, **332**, 3258-3269.

[38] Fan, R., Su, Z., and Cheng, L. (2013) Modeling, analysis, and validation of an active T-shaped noise barrier. *Acoustical Society of America*, **134**, 1990-2003.

[39] Oldham, D. J. and Egan, C. A. (2015) A parametric investigation of the performance of multiple edge highway noise barriers and proposals design guidance. *Applied Acoustics*, **96**, 139-152.

[40] Hong, H.-K. and Chen, J. T. (1988) Derivations of Integral Equations of Elasticity. *Journal of Engineering Mechanics, ASCE*, **114**, 1028-1044.

[41] Portela, A., Aliabadi, M. H., and Rooke, D. P. (1992) The dual boundary element method: Effective implementation for crack problems. *International Journal for Numerical Methods in Engineering*, **33**, 1269-1287.

[42] Krishnasamy, G., Rizzo, F. J., and Lie, Y. (1994) Boundary integral-equations for thin bodies. *International Journal for Numerical Methods in Engineering*, **37**, 107-121.

[43] Chen, J. T. and Chen, K. H. (1998) Dual integral formulation for determining the acoustic modes of a two-dimensional cavity with a degenerate boundary. *Engineering Analysis with Boundary Elements*, **21**, 105-116.

[44] Wu, T. (ed.) (2000) *Boundary Element Acoustics*. WIT Press.

[45] Chen, J. T. and Hong, H.-K. (1999) Review of dual boundary element methods with emphasis on hypersingular integrals and divergent series. *Applied Mechanics Reviews, ASME*, **52**, 17-33.

[46] Chen, I. L., Lee, J. W., Hsiao, Y. C., and Chen, J. T. (2012) On physical and numerical resonances for water wave problems using the dual boundary element method. *Engineering Analysis with Boundary Elements*, **36**, 1571-1580.

[47] de Lacerda, L. A., Wrobel, L. C., and Mansur, W. J. (1997) A dual boundary element formulation for sound porpagation around barriers over an impedance plane. *Journal of Sound and Vibration*, **202(2)**, 235-247.

[48] Tadeu, A., António, J., Godinho, L., and Mendes, P. A. (2012) Simulation of sound absorption in 2D thin elements using a coupled BEM/TBEM formulation in the presence of fixed and movig 3D sources. *Journal of Sound and Vibration*, **331**, 2386-2403.

[49] de Lacerda, L. A., Wrobel, L. C., Power, H., and Mansur, W. J. (1998) A novel boundary integral formulation for three-dimensional analysis of thin acoustic barriers over an impedance plane. *Journal of the Acoustical Society of America*, **104**, 671-678.

[50] Tadeu, A. and António, J. (2000) Use of constant, linear and quadratic boundary elements in 3D wave diffraction analysis. *Engineering Analysis with Boundary Elements*, **24**, 131-144.

[51] Tadeu, A., Mendes, P. A., and António, J. (2006) The simulation of 3D elastic scattering produced by thin rigid inclusions using the traction boundary element method. *Computers & Structures*, **84**, 2244-2253.

[52] Tadeu, A., Mendes, P. A., and António, J. (2006) 3D elastic wave propagation modelling in the presence of 2D fluid-filled thin inclusions. *Engineering Analysis with Boundary Elements*, **30**, 176-193.

[53] Tadeu, A., Godinho, L., António, J., and Mendes, P. A. (2007) Wave propagation in cracked elastic slabs and half-space domains - TBEM and MFS approaches. *Engineering Analysis with Boundary Elements*, **31**, 819-835.

[54] Tadeu, A., António, J., Mendes, P. A., and Godinho, L. (2007) Sound pressure level attenuation provided by thin rigid screens coupled to tall buildings. *Journal of Sound and Vibration*, **304**, 479-496.

[55] Tadeu, A., António, J., and Castro, I. (2010) Coupling the BEM/TBEM and the MFS for the numerical simulation of acoustic wave propagation. *Engineering Analyis with Boundary Elements*, **34**, 405-416.

[56] Tadeu, A. and António, J. (2012) 3D acoustic wave simulation using BEM formulations: Closed form integration of singular and hypersingular integrals. *Engineering Analysis with Boundary Elements*, **36**, 1389-1396.

[57] May, D. N. and Osman, N. M. (1980) Highway noise barriers: new shapes. *Journal of Sound and Vibration*, **71**, 73-101.

[58] Mohsen, E. A. and Oldham, D. J. (1997) Traffic noise reduction due to the screen effect of balconies on a building façade. *Applied Acoustics*, **10(4)**, 243-257.

[59] Oldham, D. J. and Mohsen, E. A. (1979) A model investigation of the acoustical performace of courtyard houses with respect to noise from road traffic. *Applied Acoustics*, **12(3)**, 215-230.

[60] Hothersall, D. C. and Simpson, S. (1983) The reflection of road traffic noise. *Journal of Sound and Vibration*, **90(3)**, 399-405.

[61] May, D. N. and Osman, M. . M. (1980) The performance of sound absorptive, reflective, and T profile noise barriers in Toronto. *Journal of Sound and Vibration*, **71**, 65-71.

[62] Jung, S. S., Kim, Y. T., Cheong, C. U., Kim, H. C., and Lee, W. S. (2006) Noise barrier with top cylindrical tubes. *Journal of the Korean Physical Society*, **49**, 145-149.

[63] Watts, G. R., Crombie, D. H., and Hothersall, D. C. (1994) Acoustic performance of new desings of traffic noise barriers: full scale tests. *Journal of Sound and Vibration*, **177(3)**, 289-305.

[64] Hothersall, D. C., Horoshenkov, K. V., Morgan, P. A., and Swift, M. J. (2000) Scale modelling of railway noise barriers. *Journal of Sound and Vibration*, **234**, 207-223.

[65] Watts, G. R. (1996) Acoustic performance of parallel traffic noise barriers. *Applied Acoustics*, **47 (2)**, 95-119.

[66] Watts, G. R. (1996) Acoustic performance of a multiple edge noise barrier profile at motorway sites. *Applied Acoustics*, **47**, 47-66.

[67] Watts, G. R. and Godfrey, N. S. (1999) Effects on roadside noise llevel of sound absorptive materials in noise barriers. *Applied Acoustics*, **58**, 385-402.

[68] Duhamel, D. (2006) Shape optimization of noise barriers using genetic algorithms. *Journal of Sound and Vibration*, **297**, 432-443.

[69] Baulac, M., Defrance, J., and Jean, P. (2007) Optimization of multiple edge barriers with genetic algorithms coupled with a Nelder-Mead local search. *Journal of Sound and Vibration*, **300**, 71-87.

[70] Baulac, M., Defrance, J., and Jean, P. (2008) Optimisation with genetic algorithm of the acoustic performance of T-shaped noise barriers with a reactive top surface. *Applied Acoustics*, **69**, 332-342.

[71] Greiner, D., Aznárez, J. J., Maeso, O., and Winter, G. (2006) Shape design of noise barriers using Evolutionary optimization and Boundary Element. In: B. H. V. Topping, G. Montero, R. Montenegro (ed.), *Proceedings of the Fifth International Conference on Engineering Computational Technology*, Stirlingshire, UK, no. 43, Civil-Comp Press.

[72] Greiner, D., Aznárez, J. J., Maeso, O., and Winter, G. (2010) Single- and multi-objective shape design of Y-noise barriers using Evolutionary computation and Boundary Elements. *Advances in Engineering Software*, **41**, 368-378.

[73] Greiner, D., Galván, B., Aznárez, J. J., Maeso, O., and Winter, G. (2009) Robust design of noise attenuation barriers with Evolutionary multiobjective algorithms and the Boundary Element Method. M. Ehrgott et al. (ed.), *Lecture Notes in Computer Science*, vol. 5467, pp. 261-274.

[74] Grubeša, S., Jambrošić, K., and Domitrović, H. (2012) Noise barriers with varying cross-section optimized by genetic algorithms. *Applied Acoustics*, **73**, 1129-1137.

[75] Deb, K., Bandaru, S., Greiner, D., Gaspar-Cunha, A., and Tutum, C. C. (2014) An integrated approach to automated innovization for discovering useful design principles: Case studies from engineering. *Applied Soft Computing*, **15**, 42-56.

[76] Padrón, L. A., Aznárez, J. J., and Maeso, O. (2007) BEM-FEM coupling model for the dynamic analysis of piles and pile groups. *Engineering Analysis with Boundary Elements*, **31**, 473-484.

[77] Padrón, L. A., Aznárez, J. J., and Maeso, O. (2008) Dynamic analysis of piled foundations in stratified soils by a BEM-FEM model. *Soil Dynamics and Earthquake Engineering*, **28**, 333-346.

[78] Padrón, L. A., Mylonakis, G., and Beskos, D. (2009) Importance of footing-soil separation on dynamic stiffness of piled embedded footings. *International Journal for Numerical and Analytical Methods Geomechanics*, **33**, 1439-1448.

[79] Padrón, L. A., Aznárez, J. J., Maeso, O., and Santana, A. (2010) Dynamic stiffness of deep foundations with inclined piles. *Earthquake Engineering and Structural Dynamics*, **39**, 1343-1367.

[80] Padrón, L. A., Aznárez, J. J., Maeso, O., and Saitoh, M. (2012) Impedance functions of end-bearing inclined piles. *Soil Dynamics and Earthquake Engineering*, **38**, 97-108.

[81] Medina, C., Padrón, L. A., Aznárez, J. J., Santana, A., and Maeso, O. (2014) Kinematic interaction factors of deep foundations with inclined piles. *Earthquake Engineering and Structural Dynamics*, **43**, 2035-2050.

[82] Padrón, L. A., Suárez, A., Aznárez, J. J., and Maeso, O. (2015) Kinematic internal forces in deep foundations with inclined piles. *Earthquake Engineering and Structural Dynamics*, p. (Accepted for publication).

[83] Santana, A., Aznárez, J. J., Padrón, L. A., and Maeso, O. (2015) A BEM-FEM model for the dynamic analysis of building structures founded on viscoelastic or poroelastic soils. *Bulletin of Earthquake Engineering*, p. (In review).

[84] Maeso, O. and Domínguez, J. (1993) Earthquake analysis of arch dams I: Dam-foundation interaction. *Journal of Engineering Mechanics (ASCE)*, **119**, 496-512.

[85] Domínguez, J. (1993) Boundary elements in dynamics. *CMP-Elsevier*.

[86] Maeso, O., Aznárez, J. J., and Domínguez, J. (2002) Effects of the space distribution of the excitation on the seismic response of arch dams. *Journal of Engineering Mechanics (ASCE)*, **128**, 759-768.

[87] Maeso, O., Aznárez, J. J., and Domínguez, J. (2004) Three-dimensional models of reservoir sediment and effects on seismic response of arch dams. *Earthquake Engineering & Structural Dynamics*, **33**, 1103-1123.

[88] Maeso, O., Aznárez, J. J., and Domínguez, J. (2006) BE analysis of bottom sediments in dynamic fluid-structure interaction problems. *Engineering Analysis with Boundary Elements*, **30**, 124-136.

[89] García, F., Aznárez, J. J., and Maeso, O. (2011) Variabilidad de la respuesta sísmica de presas bóveda ante diferentes combinaciones de ondas P y S compatibles con un espectro de respuesta. Tadeu, A., Figuereido, I. N., Menezes, L. F., Mendes, P. A., Rodríguez-Ferrán, A., Arias, I., and Blanco, J. M. (eds.), *Métodos Numéricos em Engenharia*, Coimbra, Portugal.

[90] García, F., Aznárez, J. J., Cifuentes, H., Medina, F., and Maeso, O. (2014) Influence of reservoir geometry and conditions on the seismic response of arch dams. *Soil Dynamics and Earthquake Engineering*, **67**, 264-272.

[91] Medina, C., Aznárez, J. J., Padrón, L. A., and Maeso, O. (2013) Effects of soil–structure interaction on the dynamic properties and seismic response of piled structures. *Soil Dynamics and Earthquake Engineering*, **53**, 160-175.

[92] Medina, C., Padrón, L. A., Aznárez, J. J., and Maeso, O. (2015) Influence of pile inclination angle on the dynamic properties and seismic response of piled structures. *Soil Dynamics and Earthquake Engineering*, **69**, 196-206.

[93] Padrón, L. A., Aznárez, J. J., and Maeso, O. (2009) Dynamic structure-soil-structure interaction between nearby piled buildings under seismic excitation by BEM-FEM model. *Soil Dynamics and Earthquake Engineering*, **29**, 1084-1096.

[94] Padrón, L. A., Aznárez, J. J., and Maeso, O. (2011) 3-D boundary element-finite element method for the dynamic analysis of piled buildings. *Engineering Analysis with Boundary Elements*, **35**, 465-477.

[95] Bordón, J. D. R., Aznárez, J. J., and Maeso, O. (2014) A 2D BEM-FEM approach for time harmonic fluid-structure interaction analysis of thin elastic bodies. *Engineering Analysis with Boundary Elements*, **43**, 19-29.

[96] Bordón, J. D. R., Aznárez, J. J., and Maeso, O. (2014) A 2D BEM-FEM model of thin structures for time harmonic fluid-soil-structure interaction analysis including poroelastic media. Mallardo, V. and Aliabadi, M. H. (eds.), *Proceedings of the Conference on Boundary Element and Meshless Techniques XIV*, Florencia, Italia.

[97] Álamo, G. M., Padrón, L. A., Aznárez, J. J., and Maeso, O. (2015) Structure-Soil-Structure Interaction effects on the dynamic response of piled structures under obliquely- incident seismic shear waves. *Soil Dynamics and Earthquake Engineering*, p. (In review).

[98] Perdomo, F., Aznárez, J. J., and Maeso, O. (2002) Aplicación del MEC en la evaluación de medidas para reducir el impacto acústico en el entorno de carreteras. *Revista de Acústica*, **23**, 13-19.

[99] Greiner, D., Emperador, J. M., and Winter, G. (2000) Multiobjective Optimisation of Bar Structures by Pareto-GA. *European Congress on Computational Methods in Applied Sciences and Engineering*.

[100] Greiner, D., Winter, G., and Emperador, J. M. (2001) Optimising frame structures by different strategies of genetic algorithms. *Finite Elements in Analysis and Design*, **37**, 381-402.

[101] Greiner, D., Emperador, J. M., and Winter, G. (2004) Single and multiobjective frame optimization by evolutionary algorithms and the auto-adaptative rebirth operator. *Computer Methods in Applied Mechanics and Engineering*, **193**, 3711-3743.

[102] Greiner, D., Emperador, J. M., Winter, G., and Galván, B. (2007) Improving computational mechanics optimum design using helper objectives. *Lecture Notes in Computer Science*, pp. 575-589.

[103] Greiner, D. and Hajela, P. (2012) Truss topology optimization for mass and reliability considerations - co-evolutionary multiobjective formulations. *Structural and Multidisciplinary Optimization*, **45**, 589-613.

[104] Periaux, J. and Greiner, D. (2014) A Nash Genetic Algorithm for the Fully Stressed Design Problem in Structural Engineering Optimization. Repin, S., Neittaanmäki, P., and Tuovinen, T. (eds.), *International Conference for Mathematical Modeling and Optimization in Mechanics (MMOM)*, pp. 65-68.

[105] Galván, B., Winter, G., Greiner, D., Cruz, M., and Cabrera, S. (1999) Generator scheduling in power systems by genetic algorithm and expert system. John Wiley & Sons (ed.), *Evolutionary algorithms in engineering and computer science: recent advances in genetic algorithms, evolution strategies, evolutionary programming, genetic programming, and industrial applications*, pp. 411-424.

[106] Galván, B., Greiner, D., Periaux, J., and M Séfrioui, G. W. (2002) Parallel Evolutionary Computation for solving complex CFD Optimization problems: a review and some nozzle applications. *Parallel CFD'02 Conference Proceedings, Nara, Japan*.

[107] Greiner, D., Galván, B., and Winter, G. (2003) Safety systems optimum design by multicriteria evolutionary algorithms. *Evolutionary MultiCriterion Optimization, Lecture Notes in Computer Science*, pp. 722-736.

[108] Greiner, D., Aznárez, J. J., Maeso, O., and Winter, G. (2007) Improving the design of M-shape noise barriers using the Boundary Element Method and Evolutionary Algorithms. In: B. H. V. Topping (ed.), *Proceedings of the Ninth International Conference on the Application of Artificial Intelligence to Civil, Structural and Environmental Engineering*, Stirlingshire, UK, no. 14, Civil-Comp Press.

[109] Burton, A. J. and Miller, G. F. (1971) The application of integral equation methods to the numerical solution of some exterior boundaryvalue problems. *Proceedings of the Royal Society of London*, **323**, 201-210.

[110] Deb, K. (2001) *Multiobjective Optimization Using Evolutionary Algorithms*. Series in Systems and Optimization, John Wiley & Sons.

[111] C. A. Coello Coello and D. Van Veldhuizen and G. Lamont (2002) *Evolutionary algorithms for solving multi-objective problems*. GENA series, Kluwer Academic Publishers.

[112] Wall, M. (1996) *GAlib: A C++ Library of Genetic Algorithm Components (http://lancet.mit.edu/ga/)*. Mechanical Engineering Department, Massachusetts Institute of Technology.

[113] Coello, C. (2006) Evolutionary multiobjective optimization: a historical view of the field. *IEEE Computational Intelligence Magazine*, **1**, 28-36.

[114] Deb, K., Pratap, A., Agrawal, S., and Meyarivan, T. (2002) A fast and elitist multiobjective genetic algorithm: NSGA-II. *IEEE Transactions on Evolutionary Computation*, **6**, 182-197.

[115] Delany, M. E. and Bazley, E. N. (1970) Acoustical properties of fibrous absorbent materials. *Applied Acoustics*, **3**, 105-116.

[116] Rosing, T. D. (ed.) (2007) *Springer Handbook of Acoustics*. Springer.

[117] UNE-EN 1793 (1997), Road traffic noise reduction devices. Test method for determining the acoustic performance. Part 3: Normalized traffic noise spectrum.

[118] Martin, P. A., Rizzo, F. J., and Cruse, T. A. (1998) Smoothness-relaxation strategies for singular and hypersingular integral equations. *International Journal of Numerical Methods in Engineering*, **42**, 885-906.

[119] Sáez, A., Gallego, R., and Domínguez, J. (1995) Hypersingular quarter-point boundary elements for crack problems. *International Journal for Numerical Methods in Engineering*, **38**, 1681-1701.

[120] Kress, R. (1985) Minimizing the condition number of boundary integral operators in acoustic and electromagnetic scattering. *The Quarterly Journal of Mechanics & Applied Mathematics*, **38**, 323-341.

[121] Amini, S. (1990) On the choice of the coupling parameter in boundary integral formulations of the exterior acoustic problem. *Applicable Analysis. An International Journal*, **35**, 75–92.

[122] Luo, J. F., Liu, Y. J., and Berger, J. (1998) Analysis of two-dimensional thin structures (from micro- to nano-scales) using the boundary element method. *Computational Mechanics*, **22**, 404-412.

[123] Marburg, S. (2008) *Computational Acoustics of Noise propagation in Fluids-Finite and Boundary Elements Methods*, chap. Discretization requirements: how many elements are necessary?, pp. 309-332. Springer.

[124] Telles, J. C. F. (1987) A self-adaptative coordinate transformation for efficient numerical evaluation of general boundary element integrals. *International Journal for Numerical Methods in Engineering*, **24**, 959-973.

[125] Aliabadi, M. H. (2002) *The Boundary Element Method. Applications in solids and structures*, vol. 2. John Wiley & Sons.

[126] Simon, D. (2013) *Evolutionary Optimization Algorithms*. John Wiley & Sons.

[127] Holland, J. H. (1975) *Adaptation in Natural and Artificial Systems*. Ph.D. thesis, University of Michigan Press, Ann Arbor.

[128] Bäck, T., Hoffmeister, F., and Schwefel, H.-P. (1991) A Survey of Evolution Strategies. Booker, L. and Belew, R. (eds.), *Proceeding of the 4th International Conference on Genetic Algorithms. Morgan Kaufmann*, pp. 2-9.

[129] Goldberg, D. (1989) *Genetic Algorithms in Search, Optimization and Machine Learning*. Addison-Wesley Longman Publishing Co.

[130] Schwefel, H.-P. (1981) *Numerical Optimization of Computer Models*. John Wiley & Sons.

[131] Schwefel, H.-P. (1995) *Evolution and Optimum Seeking*. John Wiley & Sons.

[132] Bäck, T. (1996) *Evolutionary Algorithms in Theory and Practice*. Oxford University Press.

[133] Koza, J. (1990) Genetic programming: a paradigm for genetically breeding populations of computer programs to solve problems. Report, Stanford University, CA.

[134] J. Koza and D. Goldberg and D. Fogel and R. Riolo (1996) *Genetic Programming 1996: Proceedings of the First Annual Conference (Complex Adaptive Systems)*. MIT Press.

[135] L. J. Fogel and A. J. Owens and M. J. Walsh (1966) *Artificial Intelligence through Simulated Evolution*. John Wiley & Sons.

[136] Fogel, D. B. (1992) *Evolving Artifical Intelligence*. Ph.D. thesis, University of California, San Diego, CA.

[137] Coello, C. and amd D. Van Veldhuizen, G. L. (2007) *Evolutionary algorithms for solving multi-objective problems*. Springer, 2nd edn.

[138] Zitzler, E. and Thiele, L. (1998) Multiobjective optimization using Evolutionary Algorithms - A comparative case study. *Proc. 5th International Conference on Parallel Problem Solving from Nature (PPSN-V)*, Amsterdam, Netherlands, pp. 292-301.

[139] Zitzler, E. and Thiele, L. (1999) Multiobjective Evolutionary Algorithms: a comparative case study and the strength Pareto approach. *IEEE Transactions on Evolutionary Computation*, **3**, 257-271.

[140] Deb, K., Agrawal, S., Pratap, A., and Meyarivan, T. (2000) A fast elitist non-dominated sorting genetic algorithm for multiobjective optimization: NSGA-II. *Sixth International Conference on Parallel Problem Solving from Nature (PPSNVI), Paris*, pp. 849-858.

[141] Srinivas, N. and Deb, K. (1993) Multi-objective optimization using non-dominated sorting in genetic algorithms. Report, Department of Mechanical Engineering, Indian Institute of Techniology, Kanput, India.

[142] Srinivas, N. and Deb, K. (1995) Multi-objective optimisation using non-dominated sorting in genetic algorithms. *Evolutionary Computation*, **2**, 221-248.

[143] Código Técnico de la Edificación (2009), Documento Básico HR. Protección frente al ruido. Ministerio de Fomento de España.

[144] Whitley, D. and Kauth, J. (1988) GENITOR: A different genetic algorithm. Report CS88101, Colorado State University. Department of Computer Science, Fort Collins.

[145] Syswerda, G. (1991) A study of reproduction in generational and steady-state genetic algorithms. *Proceedings of the Foundations of Genetic Algorithms (FOGA)*, pp. 94-101, (Ed.) Gregory J. E. Rawling, Morgan Kaufmann Publishers, San Mateo, California.

[146] Watts, G. R., Morgan, P. A., and Surgand, M. (2004) Assessment of the diffraction efficiency of novel barrier profiles using an MLS-based approach. *Journal of Sound and Vibration*, **274**, 669-683.

[147] Schroeder, M. R. (1975) Diffuse sound reflection by maximum-length sequences. *Journal of the Acoustical Society of America*, **57(1)**, 149-150.

[148] Schroeder, M. R. (1979) Binaural dissimilarity and optimum ceilings for concert halls: More lateral sound diffusion. *Journal of the Acoustical Society of America*, **65(4)**, 958-963.

[149] T. J. Cox and P. D'Antonio (2009) *Acoustic Absorbers and Diffusers*. Abington, Oxfordshire: Taylor & Francis, 2nd edn.

[150] Chen, J. T., Chen, K. H., and Chen, C. T. (2002) Adaptive boundary element method of time-harmonic exterior acoustics in two dimensions. *Computer methods in applied mechanics and engineering*, **191**, 3331-3345.

[151] Okubo, T. (2004) Edge-modified noise barriers. *Journal of the Institute of Noise Control Engineering of Japan*, **28**, 317-322.

[152] Maeso, O., Greiner, D., Aznárez, J. J., and Winter, G. (2008) Design of noise barriers with boundary elements and genetic algorithms. *Advances in Boundary Element Techniques IX, Sevilla, Spain*, **Keynote Lecture**, 101-106.

[153] Andrés, E., Salcedo-Sanz, S., Monge, F., and Pérez-Bellido, A. M. (2012) Efficient aerodynamic design through evolutionary programming and support vector regression algorithms. *Expert Systems with Applications*, **39**, 10700-10708.

[154] Periaux, J., González, F., and Lee, D. S. C. (2015) *Evolutionary optimization and game strategies for advanced multi-disciplinary design: applications to aeronautics and UAV design*, vol. 75 of *Intelligent Systems, Control and Automation: Science and Engineering Series*. Springer.

[155] Periaux, J. and Greiner, D. (2016) An efficient parallel Nash - genetic algorithm for solving inverse problems in structural engineering. In: S. Repin, P. Neittaanmäki and T. Tuovinen (ed.), *Mathematical Modeling and Optimization of Complex Structures, Computational Methods in Applied Sciences*, vol. 40, pp. 205-228, Springer.

[156] Fujiwara, H. (2000) The fast multipole method for solving integral equations of threedimensional topography and basin problems. *Geophysical Journal International*, **140**, 198-210.

[157] Takahashi, T., Nishimura, N., and Kobayashi, S. (2003) A fast BIEM for three-dimensional elastodynamics in time domain. *Engineering Analysis with Boundary Elements*, **27**, 491-506.

[158] Sanz, J. A., Bonnet, M., and Domínguez, J. (2008) Fast multipole method applied to 3-D frequency domain elastodynamics. *Engineering Analysis with Boundary Elements*, **32**, 787-795.

[159] Liu, Y. (2014) *Fast Multipole Boundary Element Method. Theory and Applications in Engineering*. Cambridge University Press.

[160] Saad, Y. and Schultz, M. H. (1986) GMRES: A Generalized Minimal Residual Algorithm for Solving Nonsymmetric Linear Systems. *SIAM Journal on Scientific Computing*, **7**, 856-869.

[161] Golub, G. H. and van Loan, C. F. (1996) *Matrix Computations*. Johns Hopkins University Press, 3rd edn.

[162] Greenbaum, A. (1997) *Iterative Methods for Solving Linear Systems*. SIAM.

[163] Saad, Y. (2003) *Iterative Methods for Sparse Linear Systems*. SIAM, 2nd edn.

INSTITUTO UNIVERSITARIO

SIANI

INGENIERIA COMPUTACIONAL

Edificio Central del Parque Tecnológico
Campus Universitario de Tafira
35017 Las Palmas de Gran Canaria
e-mail: info@siani.es · www.siani.es

UNIVERSIDAD DE LAS PALMAS
DE GRAN CANARIA